# UNIVERSITY OF SOUTHAMPTON

FACULTY OF NATURAL AND ENVIRONMENTAL SCIENCE

Ocean and Earth Science

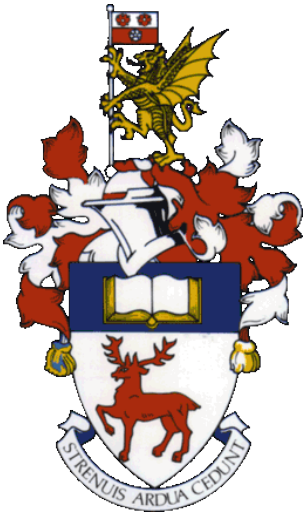


Volume 1 of 1

**Controls on the attenuation of sinking particulate organic carbon in the mesopelagic**

By

**Anna Christine Belcher**

Thesis for the degree of Doctor of Philosophy

October 2016

**UNIVERSITY OF SOUTHAMPTON**

# ABSTRACT

FACULTY OF NATURAL AND ENVIRONMENTAL SCIENCES

Ocean and Earth Science

Thesis for the degree of Doctor of Philosophy

## CONTROLS ON THE ATTENUATION OF SINKING PARTICULATE ORGANIC CARBON IN THE MESOPELAGIC

By Anna Christine Belcher

The biological carbon pump plays a key role in regulating the ocean-atmosphere balance of $CO_2$, without it atmospheric $CO_2$ would likely be 200ppm higher than it is today. The most rapid attenuation of downward particulate organic carbon (POC) flux typically occurs in the upper few hundred meters of the water column, yet the practical difficulties of making measurements in this dynamic region of the ocean mean that the processes controlling POC flux attenuation are still poorly understood.

In this thesis, Marine Snow Catchers were deployed in the Scotia Sea, Antarctica and the northeast Atlantic to obtain intact sinking particles and investigate the relationship between particle type and attenuation rate. Faecal pellets (FP) were a major component of the flux at all stations, yet total POC attenuation varied between sites in relation to zooplankton composition and bloom timing. A novel method was employed to characterise particle-associated microbial respiration on FP, which is currently a poorly understood term. Oxygen microsensors were used to measure small scale oxygen gradients through the boundary layer at the interface of FP. Rates of particle-associated microbial respiration were too low to account for the observed large decreases in FP flux over the upper 200 m, and evidence suggests that losses via zooplankton grazing and fragmentation are more important.

The importance of Antarctic krill for setting the export efficiency of POC in the marginal ice zone (MIZ) of the Scotia Sea is highlighted through unique comparisons between observed mesopelagic krill FP fluxes and predicted surface FP production. Krill FP are transferred through the upper mesopelagic much more efficiently than values of POC attenuation typically used in global biogeochemical models. I conclude that improved, regionally specific knowledge of the zooplankton community composition is vital to understand global variations in POC flux attenuation, and hence allow better predictions of ocean carbon sequestration.

Ultimately carbon is lost from the organic carbon pool as $CO_2$ via respiration, and hence in theory, at steady state, the attenuation of POC should be balanced by community respiration. In reality this balance is difficult to achieve, suggesting that our understanding is incomplete. Very low rates of both absolute and carbon specific particle-associated microbial respiration (a term missing from previous budget studies) were measured on marine snow particles collected in the northeast Atlantic and hence cannot resolve imbalances in the upper mesopelagic POC budget. Microbial disaggregation and solubilisation of POC as well as fragmentation of large particles into slowly sinking and non-sinking POC by zooplankton, may help to explain imbalances in the carbon budget, highlighting the need to measure respiration losses on both fast, slow and non-sinking pools of POC.

# Table of Contents

**Table of Contents** ..... **i**

**List of Tables** ..... **vii**

**List of Figures** ..... **ix**

**DECLARATION OF AUTHORSHIP** ..... **xvii**

**Acknowledgements** ..... **xix**

**Definitions and Abbreviations** ..... **xxi**

**Chapter 1. Introduction** ..... **1**

1.1 The ocean's role in the global carbon cycle ..... 1

1.2 The biological carbon pump ..... 2

1.2.1 Particle type ..... 3

1.3 Flux attenuation ..... 5

1.4 Transfer efficiency ..... 6

1.4.1 Remineralisation depth ..... 9

1.5 Mesopelagic carbon budget ..... 11

1.5.1 The role of zooplankton ..... 12

1.5.2 The role of microbes ..... 14

1.6 Measuring particle flux ..... 16

1.6.1 Sediment traps ..... 17

1.6.2 Thorium tracers ..... 18

1.6.3 Marine Snow Catchers ..... 19

1.6.4 Other methods ..... 20

1.7 Study sites ..... 20

1.7.1 The Southern Ocean ..... 20

1.7.2 The Porcupine Abyssal Plain observatory ..... 22

1.8 Research aims ..... 23

**Chapter 2. The role of particle-associated microbes in remineralisation of faecal pellets in the upper mesopelagic of the Scotia Sea, Antarctica** ..... **27**

2.1 Abstract ..... 27
2.2 Introduction ..... 28
2.3 Materials and methods ..... 29
2.3.1 Chlorophyll-a ..... 30
2.3.2 Particle flux and type ..... 30
2.3.3 Faecal pellet collection ..... 33
2.3.4 Oxygen fluxes and respiration rates ..... 34
2.3.5 Faecal pellet POC content ..... 35
2.3.6 Statistical analysis ..... 35
2.3.7 Ancillary zooplankton data ..... 36
2.4 Results ..... 36
2.4.1 Hydrography and surface chlorophyll-a ..... 36
2.4.2 Sinking material ..... 37
2.4.3 POC flux ..... 38
2.4.4 Faecal pellet flux ..... 40
2.4.5 Microbial respiration rates ..... 41
2.4.6 Zooplankton abundance ..... 43
2.5 Discussion ..... 43
2.5.1 Role of bloom timing in export flux ..... 43
2.5.2 Particle type and mesopelagic flux attenuation ..... 45
2.5.3 Role of zooplankton in mesopelagic flux attenuation ..... 46
2.5.4 Microbial respiration ..... 47
2.5.5 Limitations ..... 52
2.6 Conclusions ..... 53
**Chapter 3. Depth-resolved particle-associated microbial respiration in the northeast Atlantic ..... 55**
3.1 Abstract ..... 55
3.2 Introduction ..... 56
3.3 Methods ..... 58
3.3.1 Study site ..... 58
3.3.2 Chlorophyll-a ..... 58

3.3.3 Particle flux and particle type ..... 58
3.3.4 Oxygen gradients in marine snow aggregates ..... 61
3.3.5 Statistics and error analysis ..... 62
3.3.6 Zooplankton respiration ..... 63
3.4 Results ..... 64
3.4.1 Hydrography and surface chlorophyll-a ..... 64
3.4.2 Particle type ..... 64
3.4.3 Particle sinking velocities ..... 66
3.4.4 Particle flux ..... 68
3.4.5 Microbial respiration in phytodetrital aggregates ..... 68
3.4.6 Zooplankton respiration ..... 71
3.5 Discussion ..... 73
3.5.1 Rate of particle-associated microbial respiration ..... 73
3.5.2 Role of particle-associated microbes in mesopelagic POC flux attenuation 75
3.5.3 Mesopelagic carbon budget ..... 76
3.5.4 The missing piece of the mesopelagic carbon budget? ..... 79
3.6 Conclusions ..... 81
**Chapter 4. Antarctic krill facilitate efficient carbon export at the marginal ice zone in spring ..... 83**
4.1 Abstract ..... 83
4.2 Introduction ..... 84
4.3 Methods ..... 86
4.3.1 Study site ..... 86
4.3.2 Particle collection ..... 86
4.3.3 Particle type ..... 89
4.3.4 Faecal pellet flux ..... 90
4.3.5 Krill density ..... 90
4.3.6 Faecal pellet production ..... 91
4.3.7 Faecal pellet flux attenuation ..... 91
4.4 Results ..... 92

4.4.1 Oceanographic setting ..... 92
4.4.2 Particle flux and type ..... 94
4.4.3 Krill density and faecal pellet production ..... 96
4.4.4 Faecal pellet flux attenuation ..... 96
4.5 Discussion ..... 96
4.5.1 Faecal pellet flux ..... 96
4.5.2 Faecal pellet attenuation ..... 98
4.5.3 Sensitivity analysis ..... 100
4.5.4 Krill as an agent for carbon transfer in the Southern Ocean ..... 103
4.5.5 Incorporation of krill FP into global biogeochemical models ..... 104
**Chapter 5. Antarctic krill faecal pellets in the marginal ice zone: The hidden 'highway' for particulate organic carbon flux ..... 107**
5.1 Abstract ..... 107
5.2 Introduction ..... 108
5.3 Methods ..... 109
5.3.1 Krill faecal pellet production ..... 109
5.3.2 Faecal pellet fluxes ..... 110
5.3.3 Model comparisons ..... 111
5.4 Results and discussion ..... 113
5.4.1 Krill faecal pellet production ..... 113
5.4.2 Krill faecal pellet flux ..... 113
5.4.3 Seasonal krill faecal pellet flux- comparisons with model data ..... 115
5.4.4 Sensitivity analysis ..... 117
5.5 Conclusions ..... 120
**Chapter 6. Synthesis ..... 123**
6.1 Key findings ..... 123
6.2 Key processes identified as controlling attenuation ..... 124
6.2.1 Particle type ..... 124
6.2.2 Zooplankton community composition ..... 126
6.2.3 Particle-associated microbes ..... 127

6.3 Future directions ..... 131
6.4 Closing Statement ..... 133

**Appendix A Images of sinking phytoplankton cells..... 135**
**Appendix B Flow chamber experimental set up..... 136**
**Appendix C Krill faecal pellet production in the MIZ ..... 137**
**List of References ..... 139**

# List of Tables

Table 2-1: MSC deployments during cruise JR304 to the Scotia Sea, Antarctica .....31

Table 2-2: Size and respiration rates of FP measured in the Scotia Sea, Antarctica .....41

Table 3-1: Deployment table for cruise DY032 to the PAP site and details of particle flux composition (particle type) and sinking rates. .....65

Table 3-2: Rates of particle-associated microbial respiration rates in phytodetrital aggregates. Means are given for each depth with full range in brackets. Results are for experiments carried out at 10 °C. .....70

Table 3-3: Particulate organic carbon (POC) content of marine snow aggregates (PA). PA were grouped into size classes for bulk carbon measurement (see methods). ND=No Data.....70

Table 4-1: Marine Snow Catcher deployment data for cruises JR291, and JR304 to the South Orkneys, Antarctica, also showing total faecal pellet (FP), and krill FP POC fluxes. .....94

Table 4-2: Sensitivity analysis of attenuation rates ($b_{FPP}$) at ICE1 JR291, and ICE2 JR304. Attenuation rates were calculated based on the range of krill abundances (ind. $m^{-2}$) from KRILLBASE (mean ±1SE), the range of FPP rates (mg C $ind^{-1}$ $d^{-1}$) from Clarke et al. (1988), and krill FP carbon contents from Clarke et al. (1988) and Atkinson et al. (2012).....101

Table 5-1: Comparison of krill FP POC export at 100 m with model-derived total POC export for the period Oct- Mar .....116

Table 5-2: Estimated FP export flux at 100 m for various sensitivity runs for the period Oct-Mar. A is the standard run; the remaining runs are as of run A but with the following adjustments, B: minimum FPP rates, C: maximum FPP rates, D: minimum FP attenuation rates, E: maximum FP attenuation rates, F: only high krill density data, G: only KRILLBASE data collected post 1990, and H: MIZ climatology for 1980-1990 with only KRILLBASE data collected pre 1990. .....118

# List of Figures

Figure 1-1: The global carbon cycle illustrating the mass of carbon in each reservoir (Pg C) and the annual carbon exchange fluxes (Pg C $yr^{-1}$). Black numbers and arrows show reservoir sizes and fluxes for the pre-Industrial Period (pre 1750). Red numbers in the reservoirs indicate the change in anthropogenic carbon in the Industrial Period (1750-2011), and red arrows and numbers denote annual 'anthropogenic' fluxes averaged over the 2000-2009 period. Figure from Ciais et al. (2013). ..... 1

Figure 1-2: Simplified schematic of the biological carbon pump. ..... 2

Figure 1-3: Global maps of satellite-derived estimates of a) primary production, b) POC export at 100 m, and c) POC flux at 2000 m. Taken directly from Henson et al. (2012a). 3

Figure 1-4: Example of sinking particles collected from the bathypelagic ocean. ..... 5

Figure 1-5: Schematic defining the export efficiency out of the euphotic zone, the transfer efficiency ($T_{100}$) to 100 m below the euphotic depth (Ez), and the deep transfer efficiency to 2000 m used by Francois et al. (2002) and Henson et al. (2012a). A "Martin type" attenuation curve of particulate organic carbon (POC) is also shown (thick black line). ..... 7

Figure 1-6: Global maps of satellite-derived a) particle export efficiency and b) transfer efficiency to 2000 m. Taken directly from Henson et al. (2012a). ..... 8

Figure 1-7: Comparison of estimates of Martin's *b* value. Figure taken from Marsay et al. (2015) which compares their estimated values of *b* over the upper 500 m with *b* from Henson et al (2012) calculated over the upper 2000 m. ..... 9

Figure 1-8: Modelled relationship between remineralisation depth of POC and atmospheric $CO_2$. Redrawn from Kwon et al. (2009) ..... 10

Figure 1-9: Schematic to illustrate the loss of carbon from sinking aggregates. POM= Particulate organic matter. Taken directly from Simon et al. (2002). ..... 11

Figure 1-10: Example of measured imbalances in the mesopelagic carbon budget, taken from Steinberg et al. (2008). The carbon demand of bacteria (white bars) and

zooplankton (grey bars), far exceeds the POC supply (black bars) over the mesopelagic (150 – 1000 m) ..... 12

Figure 1-11: Methods employed to measure particle flux. A) PELAGRA neutrally buoyant sediment trap, B) Marine Snow Catcher, C) McClane sediment trap ..... 17

Figure 1-12: Diagram of Marine Snow Catcher. Adapted from Riley et al. (2012)..... 19

Figure 1-13: The Scotia Sea region in the Southern Ocean. Red dots show positions of stations sampled in this study. White lines indicate mean frontal positions. APF=Antarctic Polar Font (Orsi et al. 1995), SACCF = Southern Antarctic Circumpolar Current Front (Thorpe et al. 2002), SB-ACC-=Southern Boundary - Antarctic Circumpolar Current (Orsi et al. 1995). White dotted lines indicates the position of the ice edge on 3rd Dec 2013 (OSTIA Sea Ice satellite data)..... 21

Figure 1-14: Location of PAP observatory site in northeast Atlantic. ..... 23

Figure 2-1: Station locations (indicated by red circles and red square) overlain on MODIS Aqua satellite chlorophyll for December 2014. Position of ice edge on December 14th 2014 shown by black dotted line (OSTIA sea ice data). Inset displays vertical temperature profiles at ICE (blue), P2 (red) and P3 (green), lighter shades indicate standard deviations based on multiple deployments at each site.... 30

Figure 2-2: Microscope photos of sinking material collected in Marine Snow Catchers, A) faecal pellet from ICE station, B) marine snow aggregate from P2, C) diatom chain from P2, D) cylindrical faecal pellet from P2, E) radiolarian from P2, F) round faecal pellet from P2, G) *Euphausia superba* faecal pellet from Western Core Box site. Scale bar refers to all photos..... 37

Figure 2-3: Composition (particle type) of fast-sinking POC at A) ICE, B) P2, and C) P3 stations based on microscope analysis and calculated carbon content. Black = faecal pellets, hashed = phytodetrital aggregates, white = phytoplankton cells and grey = other. MLD+10 and MLD+110 represent measurements at 10 and 110 m below the base of the mixed layer depth (MLD) respectively. ..... 39

Figure 2-4: Flux of particulate organic carbon (POC mg C $m^{-2}$ $d^{-1}$) measured at a number of time points over the diel cycle at ICE (black diamonds), P2 (grey triangle) and P3 (open circle) in the Scotia Sea Antarctica. Exponential curves have been plotted for ICE (thick black dashed), P2 (solid black) and P3 (dotted) to illustrate flux attenuation, $p < 0.001$, 0.018 and 0.419 at P2, P3 and ICE respectively. Note the

break in the x axis scale for extreme value at P2 which has been excluded from the exponential fit. .....40

Figure 2-5: Sinking velocities and respiration rates of FP collected at the Western Core Box (open squares), ICE (filled squares) and P2 (filled triangles) stations. A) FP sinking velocity versus equivalent spherical diameter (ESD), B) FP respiration rate versus FP volume with linear fit (Y = 4.8208X -0.1497, $R^2$ = 0.56 (Pearson's correlation), $p < 0.001$), C) Carbon-specific respiration rates versus FP ESD (no significant relationship, $p > 0.05$). .....42

Figure 2-6: Zooplankton abundances (ind. $m^{-2}$ (0-200m)) measured in the Scotia Sea in December 2014 using a 100 µm mesh. A) Copepods (black), euphausiids (light grey), other (dark grey). B) Copepod abundances (excluding nauplii) divided into two groups; small microcopepods (black), and large calanoids (hashed) (see text for full details on groups). .....44

Figure 2-7: Comparison of FP fluxes measured at MLD+10 (black) and MLD+110 (grey), to those predicted at MLD+110 (white). MLD+10 and MLD+110 represent measurements at 10 and 110 m below the base of the mixed layer depth (MLD) respectively. Predicted fluxes are based on measured FP fluxes at MLD+10 and mean FP respiration rates (0.028 $d^{-1}$) derived during this study. Hence, the predicted fluxes only consider microbial degradation via respiration. Error bars show minimum predicted values using minimum literature values for euphausiid FP POC content (González 1992). FP POC contents measured in this study lie at the upper end of literature estimates and hence there is no upper error bar. ....50

Figure 2-8: Schematic to illustrate the mechanisms contributing to flux attenuation in the upper mesopelagic in the Scotia Sea, Antarctica, and the influence of bloom phase on these mechanisms. .....53

Figure 3-1: Surface chlorophyll concentration (mg $m^{-3}$) at the PAP site, (a) PAP study region (black box) overlain on 9 km Aqua MODIS satellite chlorophyll for 18/06/2015-25/06/2015. (b) Mean vertical temperature, salinity and chlorophyll profiles measured at the PAP site (red, blue and green lines respectively) and the standard deviation (light shading) of CTD deployments coinciding with MSC deployments. (c) Temporal change in surface chlorophyll (mg $m^{-3}$) over the PAP study region based on 8-day, 9 km Aqua MODIS satellite data. Gaps in data are due to cloud cover. Vertical red lines indicate start and end of sampling period,

and dark green squares are discrete measurements made from the CTD at depths of 5-10 m. ..... 59

Figure 3-2: Example light microscope image of a phytodetrital aggregate collected from depth. Scale bar=0.5 mm ..... 61

Figure 3-3: Composition (particle type) of fast-sinking POC at each measured depth horizon. The percent (%) contribution of faecal pellets (black), phytodetrital aggregates (hatched), and unidentified phytodetritus (grey) to the total mass of fast-sinking POC collected in Marine Snow Catchers at each depth horizon. See Table 3-1 for numbers of particles in each category. ..... 65

Figure 3-4: Relationship between sinking velocity (m $d^{-1}$) and equivalent spherical diameter (ESD, mm) of phytodetrital aggregates. The depth from which aggregates were sampled is shown by the colour of circles (36 m=yellow, 46 m=orange, 73 m=red, 113 m, light blue, 128 m=dark blue, 203 m=light green, 500 m=dark green). Note the log scale on the Y axis. A power-law fit between sinking velocity and aggregate ESD (dotted line $Y = 85.8X^{1.4}$) is applied. Six outliers (black open squares), defined as being outside 2 standard deviations from the mean, were excluded from the power-law fit..... 66

Figure 3-5: Flux of POC (mg C $m^{-2}$ $d^{-1}$) with depth at the PAP site. POC fluxes of fast-sinking particles measured in June 2015 at the PAP site via deployment of Marine Snow Catchers. Error bars relate to replicate filters per sample. A power-law curve was fitted to the data (black line), $Y=194.9 \cdot (X/MLD)^{-0.71}$ ($R^2$= 0.42, $p$=0.060, n=9), excluding the point at 500 m (triangle) which is likely due to non-steady state conditions. The grey shaded area indicates the mixed layer depth over the study period. ..... 67

Figure 3-6: Example oxygen profile (µM) through a phytodetrital aggregate collected at 46 m depth. Measurements were made with microsensors in steps of 50-100 µm, with negative values reflecting the distance into the aggregate from the surface. The solid black line shows the model fit used to calculate the oxygen flux in the diffusive boundary layer..... 69

Figure 3-7: Respiration rates of phytodetrital aggregates with depth. Oxygen fluxes to aggregates (nmol $O_2$ $mm^{-3}$ $d^{-1}$). For reference aggregate respiration rates are also shown in terms of carbon per aggregate volume (µg C $mm^{-3}$ $d^{-1}$). Data are for experiments carried out at 10 °C. Error bars represent ± one standard error of the mean. 71

Figure 3-8: Carbon-specific respiration rates ($d^{-1}$) for aggregates collected at depth. Rates adjusted to the *in situ* temperature (T) are shown by the dashed black line (open circles). Grey shading shows the range in mixed layer depth over the study period, and error bars represent ± one standard error of the mean. .....72

Figure 3-9: Carbon-specific respiration rates ($d^{-1}$) of phytodetrital aggregates collected at depth. Data have been adjusted for *in situ* temperatures.....73

Figure 3-10: Balance of processes controlling fast-sinking POC flux attenuation. (a) Comparison of observed POC loss (black bars) and estimated POC loss based on particle-associated microbial respiration (grey bars) over two depth horizons (36-128 m, and 128-500 m). (b) POC sources and sinks in the upper 200m. Additional losses ('sinks') via solubilisation of POC to DOC by particle-associated microbes (estimate based on respiration, see section 3.5.3), and zooplankton respiration (estimate based on zooplankton biomass and allometric equations). Error bars show uncertainties from sensitivity analysis. .....77

Figure 4-1: A) ICE station locations (indicated by red circles) overlain on MODIS Aqua satellite chlorophyll (mg $m^{-3}$) for December 2014. Position of ice edge on December 14$^{th}$ 2014 (thick black dashed line) and December 3$^{rd}$ 2013 (black dotted line) (OSTIA sea ice data). Black box shows region covered by Figure 3-1B. B) Location of krill density samples taken from KRILLBASE for ICE1 and ICE2 (red squares). ICE1 and ICE2 stations are shown by large black triangles.....87

Figure 4-2: Sea ice concentrations (%) (OSTIA sea ice data, averaged over 1 ° box centred on ICE1) during 2013 (blue solid line) and 2014 (green solid line). Sampling dates for JR291 (blue) and JR304 (green) are shown by vertical dotted lines.....88

Figure 4-3: Vertical profiles of temperature (blue lines) and chlorophyll (green lines) from CTD deployments at ICE1 (solid line), and ICE2 (dashed line) during JR291, and ICE2 during JR304 (dotted line). .....92

Figure 4-4: Composition (particle type) of fast-sinking POC at A) ICE1 JR291, B) ICE2 JR291, and C) ICE2 JR304 stations based on microscope analysis and calculated carbon content. Black=krill faecal pellets, dark grey=other faecal pellets, hashed=phytodetrital aggregates, white=phytoplankton cells and light grey=other phytodetritus. .....93

Figure 4-5: Histogram of krill FP sinking velocities (m $d^{-1}$) measured at stations ICE1 and ICE2 during JR291 and JR304 ..... 95

Figure 4-6: Frequency distribution of krill density (ind. $m^{-2}$) records from KRILLBASE in a 300 km x 300 km box centred on the study sites. One record with an extreme density of 1128 ind. $m^{-2}$ is not plotted. ..... 95

Figure 4-7: Krill FP fluxes estimated in the South Orkneys at A) ICE1 JR291, B) ICE2 JR291, and C) ICE2 JR304. Krill FP fluxes estimated in MSC at MLD+10 and MLD+110 are shown by light grey bars (error bars show maximum and minimum fluxes based on the range of measured FP POC contents). Predicted FPP at a swarm depth of 20 m is shown by dark grey bars, with error bars showing maximum and minimum fluxes based on the range of krill densities from KRILLBASE (mean ±1SE). ..... 97

Figure 4-8: Attenuation of krill FP flux in the upper mesopelagic at the ICE stations. Estimated FPP is shown by the black triangle with upper and lower bounds based on upper and lower KRILLBASE krill density estimates. Krill FP fluxes estimated by MSC are shown by red squares with error bars based on the range of measured FP POC contents. Calculated krill FP attenuation from FPP and krill FP fluxes at MLD+110 ($b_{FPP}$) is shown by the solid black line (grey dashed lines show maximum and minimum attenuation based on upper and lower FPP estimates). The very high FP flux at ICE2 JR291 (light red square with dashed outline) was not included in the derivation of $b_{FPP}$. For comparison, attenuation in krill FP flux based on a *b* value of 0.86 (Martin et al. 1987) is also illustrated (black dashed line), as well as *b* values of 0.10-0.62 (grey shaded area) from the literature range in krill FP attenuation (see section 4.5.4) ..... 99

Figure 5-1: Locations of data used to derive algorithms for export production from Henson (grey circles), Dunne (black crosses) and Laws (white triangle) with reference to the maximum ice extent (black dashed line, 15% sea ice concentration during period Oct $1^{st}$-$13^{th}$ 1994-2014). ..... 112

Figure 5-2: Estimated krill faecal pellet production (FPP) in the marginal ice zone, Antarctica. The marginal ice zone, from fortnightly sea ice concentration data (15-80% ice cover), is divided into 5 ° zonal grids, and is coloured by FPP flux (mg C $m^{-2}$ $d^{-1}$) based on mean krill density measurements from KRILLBASE (black dots) and literature krill FP production rates. Regions of the marginal ice zone where no KRILLBASE records occurred are coloured in grey. ..... 114

Figure 5-3: Seasonal FP export fluxes (Tg C) in the MIZ. a) The maximum MIZ extent in 1994-2014 (15% sea ice concentration for period Oct 1st-13th, 1994-2014) used as the upper boundary of longitudinal estimates of POC export derived from empirical algorithms. b) FP export fluxes for the climatological MIZ of 1994-2014 (red line) and 1980-1990 (orange line), as well as the mean annual POC export from satellite-derived algorithms (blue line) and standard deviation of these estimates (shaded light blue). .....115

Figure 5-4: Comparison of estimates of krill FP fluxes at 100 m for different climatologies of sea ice data. Error bars for current estimates (1994-2014) relate to maximum and minimum estimates using maximum and minimum FPP rates respectively (sensitivity runs B and C). Historical estimates relate to sensitivity run H (Table 5-2). .....119

Figure 6-1: Schematic highlighting A) the processes thought to drive the loss of POC prior to this thesis, and B) the additional processes investigated as part of this thesis. Rates of particle-associated microbial respiration were found to be low and almost constant with depth at the PAP site in the North Atlantic, and could not account for missing carbon sinks in the upper mesopelagic. It is hypothesised here that zooplankton fragmentation of fast-sinking POC into slow and non-sinking POC may account for some of this missing carbon sink. .....129

Figure 6-2: Schematic illustrating the zooplankton mediated transfer of fast-sinking particles into slow and non-sinking particles which can be respired slowly over the season. This loss of fast-sinking particulate organic carbon (POC) to slow and non-sinking POC may help account for imbalances between sources and sinks of fast-sinking POC in the mesopelagic. .....130

Figure A-1: Light microscope imagery of phytoplankton cells collected in tray (fast-sinking fraction) of Marine Snow Catchers. Diatom species *Thalassiosira* and *Fragilariopsis* are labelled and scale bars of 0.25mm are shown for reference. .....135

Figure B-1: Schematic of flow chamber set up for measurement of particle-associated microbial respiration in particles using microelectrodes. .....136

Figure B-2: Schematic illustrating measurement of oxygen gradients within aggregates using microelectrodes. Adapted from Ploug et al. (1997). .....136

Figure C-1: Estimated krill faecal pellet production (FPP) in the marginal ice zone (MIZ), Antarctica for the period 1980-1990. The MIZ, from fortnightly sea ice concentration data (15-80% ice cover), is divided into 5 ° zonal grids, and is coloured by FPP flux (mg C $m^{-2}$ $d^{-1}$) based on mean krill density measurements from pre 1990 KRILLBASE data (black dots) and literature krill FP production rates. Regions of the marginal ice zone where no KRILLBASE records occurred are coloured in grey..... 137

# DECLARATION OF AUTHORSHIP

I, Anna Belcher declare that this thesis entitled “Controls on the attenuation of sinking particulate organic carbon in the mesopelagic” and the work presented in it are my own and has been generated by me as the result of my own original research.

I confirm that:

1. This work was done wholly or mainly while in candidature for a research degree at this University;
2. Where any part of this thesis has previously been submitted for a degree or any other qualification at this University or any other institution, this has been clearly stated;
3. Where I have consulted the published work of others, this is always clearly attributed;
4. Where I have quoted from the work of others, the source is always given. With the exception of such quotations, this thesis is entirely my own work;
5. I have acknowledged all main sources of help;
6. Where the thesis is based on work done by myself jointly with others, I have made clear exactly what was done by others and what I have contributed myself;
7. Parts of this work have been published as:

Belcher, A. Iversen, M. Giering, S. Riou, V. Henson, S.A. Berline, L. Guilloux, L. Sanders, R. 2016. Depth-resolved particle-associated respiration in the northeast Atlantic*, Biogeosciences,* 13, 4927-4943, doi:10.5194/bg-13-4927-2016.

Belcher, A. Iversen, M. Manno, C. Henson, S. Tarling, G. Sanders, R. 2016. The role of particle associated microbes in remineralization of fecal pellets in the upper mesopelagic of the Scotia Sea, Antarctica. *Limnology and Oceanography,* 61 (3), 1049-1064, DOI: 10.1002/lno.10269.

Signed: .....

Date: .....

# Acknowledgements

A big thank you to my many supervisors who have supported me over the past three years; Clara, Manno for your amazing enthusiasm about science, research and life in general and for encouraging my desire to want to make the most of every opportunity! Geraint Tarling, for taking on another Belcher, always offering advice and encouraging me to aim high. Richard Sanders for those great conversations about holidays and climbing mountains - with a side of science, and Steph Henson for keeping me on track, holding everything together and keeping the Belcher worries at bay when things got overwhelming! Thanks also to Richard Lampitt for showing me the ways of the Snow Catcher on my first PAP cruise and for accompanying me to the Southern Ocean as my 'helper'. Additional thanks to Duncan Purdie for overseeing everything as my panel chair, and for helping me figure out that I do in fact fit in the biological oceanographer box.

I have had the pleasure of working with many great people over the past three years and would particularly like to thank Morten Iversen for essentially being a surrogate supervisor and teaching me to break pocket eggs rather than microsensors. Sally Thorpe, who didn't mind me as an extra office mate for the summer at BAS, but who was always a smiling supporting face and my 'go to' for physical oceanography problems. A huge thanks to Pete Ward for spending the last weeks of his long career at BAS picking through zooplankton samples to support my Southern Ocean work.

My PhD wouldn't have been half as fun without the daily banter with my many office mates, thanks for all the fun chats, advice and attempts to make me drink tea! Sorry for replacing you part time with the crazies of Basingstoke library, but thanks for the many times you kicked my computer back into action when I was working remotely. Thanks to Emma Cavan for shared snow catcher joys and woes - you're right, it is never the last snow catcher! The list of friends who have put me up on their sofas or spare beds in Southampton to save me the commute in is endless, but major thanks to Helen Burns and Jesse Cusack for the many climbing and curry nights followed by a good nights kip at my 'Southampton home'. When I was able to face the commute, thanks to Jan Steele at Highfield for giving me and my trusty steed Merlin the Brave a lift and for the great conversations where we set the world to rights on many an occasion! And of course thanks to the gaggle at BAS for all the fun summer adventures that made lab days more bearable.

Having spent much of my PhD at sea, special thanks go to Elena "shut up its funny" Ceballos Romero and Clare "think about it" Fothergill for making that first Southern Ocean cruise so special. Manon Duret, my particle buddy, for working so hard to help me with snow catcher samples even when she was swamped with her own work. And of course a huge thanks to the wonderful captains and crew of the *RRS James Clark Ross, James Cook* and *Discovery*, it was a pleasure sailing with all of you. Thanks to long time mentor and friend Rick Keil for sparking my enthusiasm for research cruises and life at sea with all those fantastic cruises before my PhD.

The final thank you goes to my family and Steve for putting up with all the highs and the lows, my rambles about science and academia, and for helping to stop that Belcher overthinking tendency from going too mad! Steve, thanks for providing a refreshing break from my thesis and for the many adventures in VANessa and now Pippa. There's not much a trip to a mountain or the seaside with your partner and best friend for life can't solve.

"That is all".

# Definitions and Abbreviations

A: Area

APF: Antarctic Polar Font

b: martin's b-value (attenuation coefficient)

BATS: Bermuda Atlantic Time Series

BCP: Biological carbon pump

BGE: Bacterial growth efficiency

$CO_2$: Carbon dioxide

$C_{resp}$: Carbon respiration

$C_{spec}$: Carbon specific respiration

CTD: Conductivity-temperature-depth

DBL: Diffusive boundary layer

DIC: Dissolved inorganic carbon

DOC: Dissolved organic carbon

DW: Dry weight

E: FP egestion rate

ESD: Equivalent spherical diameter

F: Flux of POC

FP: Faecal pellet

$FP_{100}$: FP flux at 100m

$FP_{100,MIZ}$: $FP_{100}$ averaged over total MIZ area

$FP_{100,SEA}$: Total $FP_{100}$ over MIZ area during productive season

$FP_{100,TOT}$: Total $FP_{100}$ in MIZ area

FPP: Faecal pellet production

$FPP_{MIZ}$: FPP averaged over total MIZ area

$FPP_{TOT}$: Total FPP in MIZ area

h: Height

HBLE: High biomass, low export

m: Mass

MIZ: Marginal ice zone

MLD: Mixed layer depth

MSC: Marine Snow Catcher

NBST: Neutrally buoyant sediment trap

$\overline{N}_k$: Mean krill density

NSIDC: National Snow Ice Data Centre

PA: Phytodetrital aggregate

PAP: Porcupine Abyssal Plain

PGE: Prokaryotic growth efficiency

POC: Particulate organic carbon

RQ: Respiratory quotient

SACCF: Southern Antarctic Circumpolar Front

SB-ACC: Southern Boundary - Antarctic Circumpolar Current

T: Temperature

w: Sinking velocity

WAP: Western Antarctic Peninsula

z: Depth

# Chapter 1. Introduction

## 1.1 The ocean's role in the global carbon cycle

As the largest non-geological reservoir of carbon on the planet and containing over 38,000 Pg C (Ciais et al. 2013) (over 50 times the atmospheric reservoir), the oceans are a key component of the global carbon cycle (Figure 1-1). The ocean carbon reservoir is mostly in the form of dissolved inorganic carbon (DIC), with smaller amounts stored as dissolved organic carbon (DOC) and in marine biota. Net primary production (i.e. gross primary production minus respiration) in the

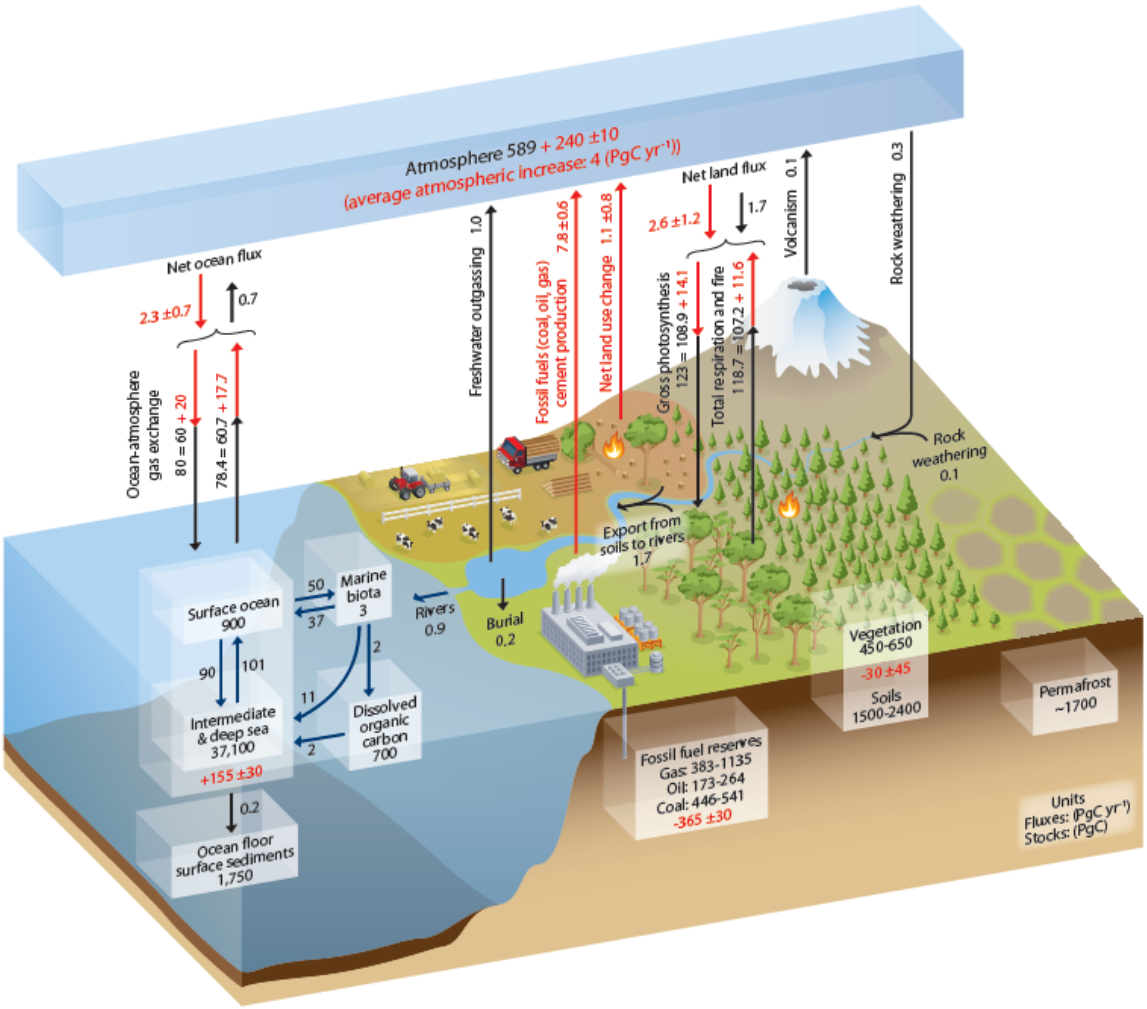


**Figure 1-1: The global carbon cycle illustrating the mass of carbon in each reservoir (Pg C) and the annual carbon exchange fluxes (Pg C $yr^{-1}$). Black numbers and arrows show reservoir sizes and fluxes for the pre-Industrial Period (pre 1750). Red numbers in the reservoirs indicate the change in anthropogenic carbon in the Industrial Period (1750-2011), and red arrows and numbers denote annual 'anthropogenic' fluxes averaged over the 2000-2009 period. Figure from Ciais et al. (2013).**

ocean has been estimated to be 48.5 Pg C (Field et al. 1998), and although only a small fraction ( ~0.2 Pg C $yr^{-1}$) of this production is exported by biological processes and reaches the sea floor, it can be stored in these sediments for millennia or longer (Ciais et al. 2013) making ocean biology key to the long-term global cycling and storage of carbon. Additionally, during the Industrial Era, the burning of fossil fuels has resulted in perturbation of the natural carbon cycle, with an input of 555±85 Pg C between 1750 and 2011 (Ciais et al. 2013). The oceans have taken up about 28% of this (155±30 Pg C), highlighting their key role in mitigating the effects of anthropogenic carbon dioxide emissions on the climate system (Ciais et al. 2013).

## 1.2 The biological carbon pump

Ocean biological processes play a key role in storing carbon dioxide ($CO_2$) in the ocean interior: without them atmospheric $CO_2$ would be about 200 ppm higher than current levels (Parekh et al. 2006). This storage occurs in part via the surface production, sinking and interior remineralisation of particulate organic carbon (POC), a process which maintains a vertical gradient of DIC in the ocean corresponding to a carbon pool 3.5 times larger than the atmospheric $CO_2$ pool (Gruber and Sarmiento 2002). Even small perturbations to oceanic ecosystems, such as changes in mineralisation depth, can result in large feedbacks on the climate system (Kwon et al. 2009).

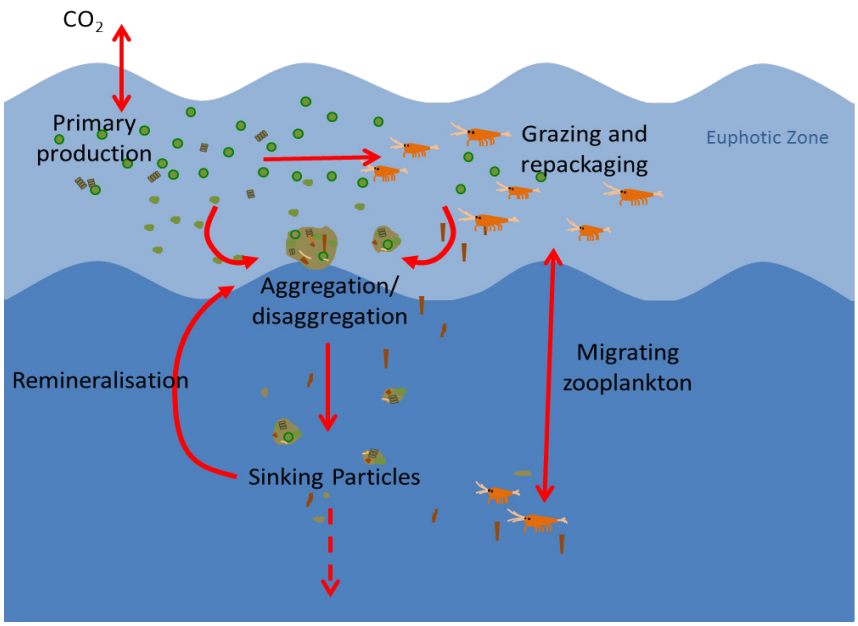


**Figure 1-2: Simplified schematic of the biological carbon pump.**

Phytoplankton in the surface ocean fix inorganic carbon into organic carbon increasing phytoplankton biomass. Some of this primary production is remineralised (respired by grazers or exuded as DOC and respired by bacteria (Azam et al. 1983)), but a fraction (generally ranging between 2-20%) sinks out of the euphotic zone in particles with an organic component (Boyd and

Trull 2007) (Figure 1-2). This biological carbon pump (BCP) (Volk and Hoffert 1985) is estimated to flux 5-20 GtC $yr^{-1}$ to the ocean interior (Henson et al. 2011). However, the magnitude of both new primary production (NPP) and the flux of sinking particles (POC flux) to the upper and deep oceans can vary spatially by orders of magnitude (Figure 1-3). Measuring the magnitude of POC flux is important for quantifying the ocean uptake and sequestration of carbon.

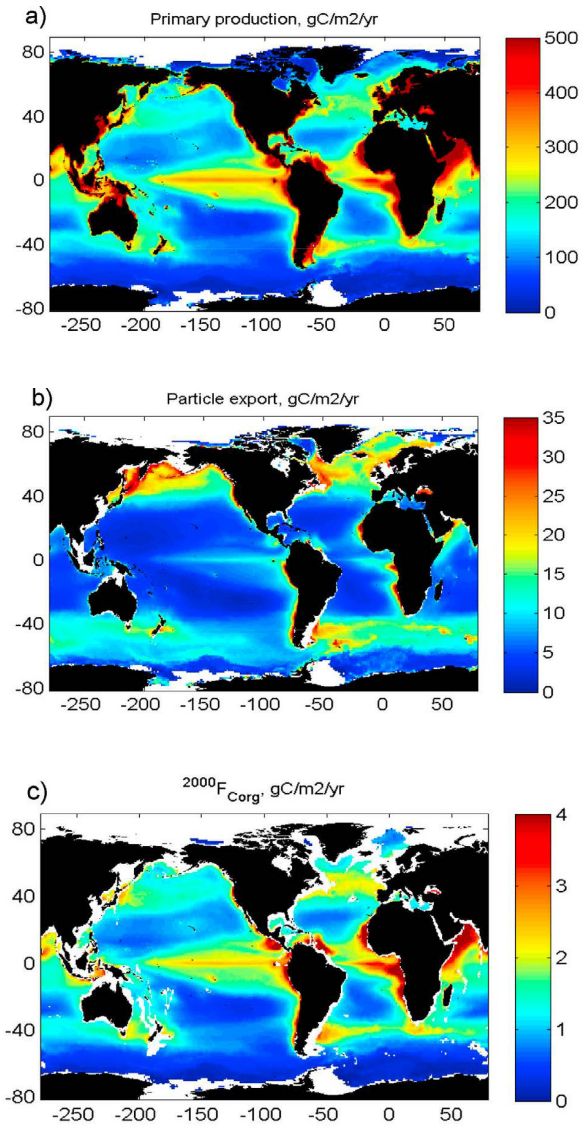


**Figure 1-3: Global maps of satellite-derived estimates of a) primary production, b) POC export at 100 m, and c) POC flux at 2000 m. Taken directly from Henson et al. (2012a).**

### 1.2.1 Particle type

There is a large diversity of particles sinking through the ocean, representing the range of organisms producing and repackaging particles. When making measurements of POC flux in the ocean it is important to be able to resolve the type of sinking particles to allow identification of the processes driving particle export. Typically the flux of POC is due to faecal pellets,

phytodetrital aggregates and the direct sinking of phytoplankton blooms (e.g. diatom mats, Kemp et al. (2000)), although other material such as sinking carcasses may also be prevalent (De La Rocha and Passow 2007; Turner 2015). The relative importance of different particles to POC flux can be highly variable, both spatially and temporally, for example faecal pellets can have been measured to be <1 - >100% of total POC flux (Turner 2015). Wilson et al. (2013) suggested based on a literature compilation, that deep ocean fluxes of POC were negatively correlated to deep FP POC fluxes, with periods of high POC flux dominated by non-faecal pellet sources such as phytodetritus or marine snow.

#### 1.2.1.1 Phytodetrital aggregates

Marine aggregates originate from aggregated phytoplankton (Figure 1-4) and can have many other particles associated with them such as faecal pellets, living zooplankton, microbes, zooplankton carcasses, abandoned larvacean houses and inorganic mineral particles (Simon et al. 2002). Macroscopic aggregates (marine snow) are >500 µm in diameter (Alldredge and Silver 1988) and can be highly abundant in the water column (Simon et al. 2002). Marine snow and microscopic aggregates (1-500 µm) are important not only for the transfer of POC through the water column, but also host microbial abundances 2-5 orders of magnitude higher than those found free-living in the surrounding water column (Silver and Alldredge 1981; Thiele et al. 2015). Marine aggregates are therefore important microenvironments for the degradation of organic compounds and the release of organic matter to the surrounding water column.

#### 1.2.1.2 Faecal pellets

Zooplankton graze on phytoplankton cells, marine aggregates and other phytodetritus, producing faecal pellets (FP) (Figure 1-4) which make up a variable, but often substantial, component of deep sea POC fluxes (Wilson et al. 2013; Manno et al. 2015; Turner 2015) in part due to their high sinking rates in comparison to individual phytoplankton cells (5-2700 m $d^{-1}$ compared to <1 m $d^{-1}$ (Smayda 1970; Turner 2002)). The sinking rates of FP are controlled by their size and density, which in turn reflect the overlying zooplankton community. Identifying the producers of FP found in particle collecting devices such as sediment traps is complicated by factors such as diet and food absorption (Atkinson et al. 2012), ballast (Ploug et al. 2008a) and temperature (Giesecke et al. 2009), as well as through interception by other zooplankton (Lampitt et al. 1990). A number of FP morphologies have been linked to particular zooplankton producers, for example, large tabular faecal pellets can be attributed to salps, appendicularians and other tunicates (Gleiber et al. 2012; Turner 2015), cylindrical pellets to large copepods and euphausiids (Bathmann et al. 1991;

González 1992; Atkinson et al. 2012) and spherical pellets to small copepods, crustacean nauplii and amphipods (González 1992; Yoon et al. 2001). Oval pellets can originate from a number of different groups including, chaetognaths, small copepods and pteropods (González 1992; Yoon et al. 2001; Manno et al. 2010). FP can sink rapidly through the water column, with sinking rates as high as 2700 m $d^{-1}$ measured for salp FP, but more typical rates of 5-220 m $d^{-1}$ for copepod FP (Turner 2002).

This transfer of slowly sinking material into fast-sinking FP means that FP have the potential to act as a 'highway' for the transfer of POC to the deep ocean. However, the contribution of FP to sinking particle fluxes is highly variable (<1% to >100% (Turner 2015)) as FP can also be rapidly remineralised, particularly in the upper mesopelagic (González 1992; Urban-Rich et al. 1999; Wexels Riser et al. 2007), providing an important source of food for mesopelagic populations.

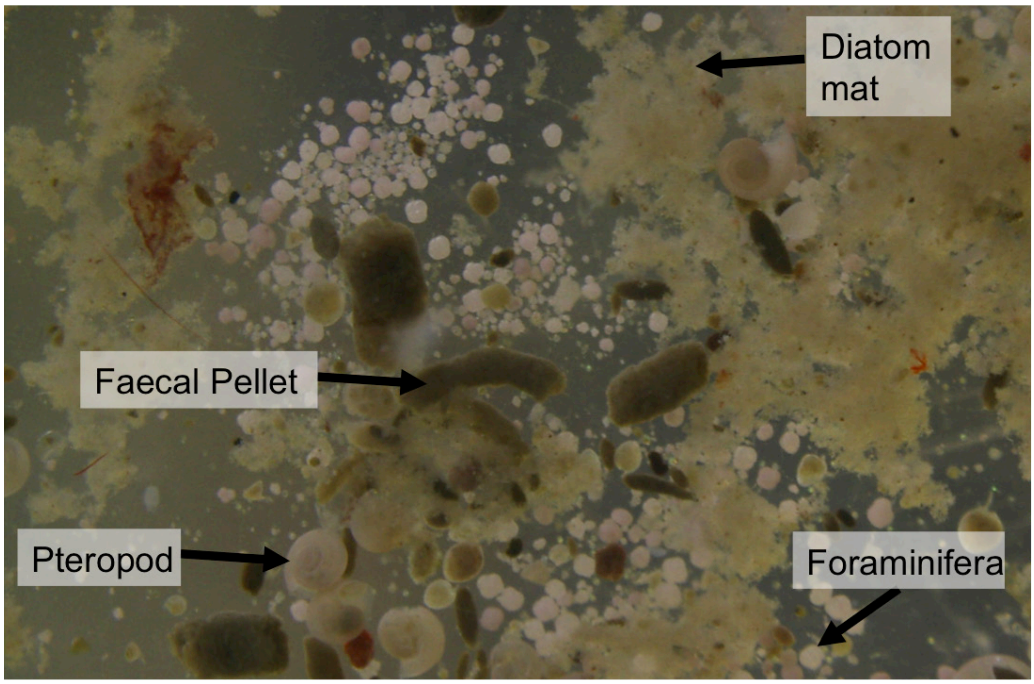


**Figure 1-4: Example of sinking particles collected from the bathypelagic ocean.**

## 1.3 Flux attenuation

Only a minor fraction of the material sinking out of the euphotic zone reaches the deep ocean, and it is this deep carbon flux and the depth of remineralisation which are important when assessing ocean carbon storage on climatically relevant timescales. Quantifying the rate at which POC is attenuated with depth is therefore important.

The decline in POC with depth, most of which occurs between 100 and 500 m (e.g. Martin et al. 1987), is driven by heterotrophic consumption through a number of complex interactions. Both

zooplankton and microbes utilise sinking POC (consumed directly, or first solubilised to DOC) to meet their metabolic requirements, the contributions of which are not well characterised (De La Rocha and Passow 2007; Steinberg et al. 2008). The roles of zooplankton and microbes on the removal of POC from the mesopelagic are discussed further in sections 1.5.1 and 1.5.2. Despite the complexity of processes governing the loss of POC with depth, a number of attempts have been made to mathematically define the decline of POC with depth, with perhaps the most notable being the Martin curve defined by Martin et al. (1987),

$$\boldsymbol{F_z = F_{z0} * (z/z_0)^{-b}} \qquad \textbf{(Equation 1-1)}$$

where $F_{z0}$ = surface layer export at the reference depth $z_0$, $F_z$ = flux at depth $z$, and $b$, flux attenuation. The higher the value of $b$, the stronger the flux attenuation. The rate at which POC is lost with depth can also be quantified via the remineralisation length scale which is defined as the depth interval over which the flux decreases by a factor of 1/e (e.g. Lutz et al. 2002). Further, the efficiency of the BCP at both exporting POC from the euphotic zone and transferring it through the mesopelagic zone can be assessed via the export efficiency (the fraction of total primary productivity that is exported out of the euphotic zone) and the transfer efficiency (the proportion of POC exported out of the euphotic zone which is transferred deeper in the ocean) (Figure 1-5). The transfer efficiency can be calculated as the ratio of the export flux to the POC flux reaching 2000 m (Francois et al. 2002; Henson et al. 2012a), but can also be calculated based on the POC flux reaching 100 m below the euphotic zone ($T_{100}$) (Figure 1-5). Despite these numerous methods to quantify the rate of POC remineralisation and BCP efficiency, the controlling mechanisms are still poorly understood.

## 1.4 Transfer efficiency

Many measurements of export efficiency have been made (Turner 2015), yet the attenuation of POC below the euphotic zone is poorly understood. This is the region where the most rapid changes in POC occur (Suess 1980; Martin et al. 1987) and yet is relatively under sampled, and hence the transfer efficiency through the upper mesopelagic is the focus of this thesis. Both satellite-derived and data-based estimates of POC flux show highest POC export fluxes in the high latitude Northern Hemisphere, in shelf areas, the Arabian Sea and in upwelling regions (Figure 1-3B) (Henson et al. 2012a). However, as primary production is highest in equatorial regions (Figure 1-3A), particle export efficiency is greatest in the high latitudes (~15-20% of POC produced by PP is exported below the euphotic zone) and decreases towards the equator (Figure 1-6A) (Henson et al. 2012a). The efficiency by which POC is transported from the euphotic zone to the

deep ocean however shows opposing geographical distributions to the export efficiency (Figure 1-6A).

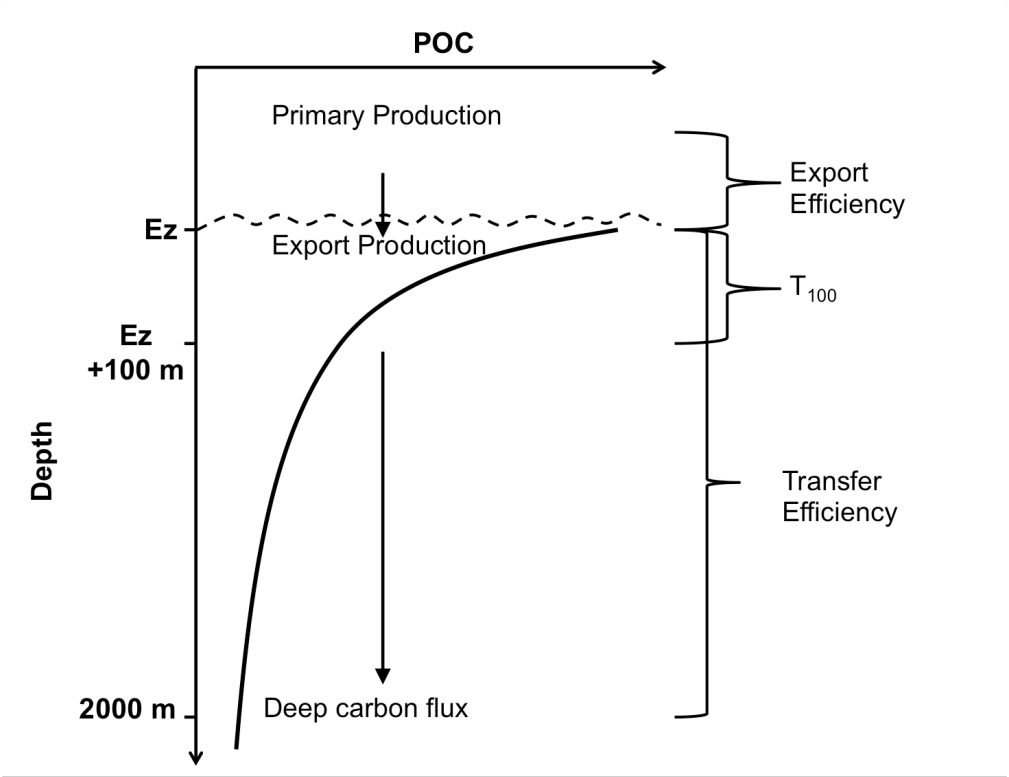


**Figure 1-5: Schematic defining the export efficiency out of the euphotic zone, the transfer efficiency ($T_{100}$) to 100 m below the euphotic depth (Ez), and the deep transfer efficiency to 2000 m used by Francois et al. (2002) and Henson et al. (2012a). A "Martin type" attenuation curve of particulate organic carbon (POC) is also shown (thick black line).**

The efficiency by which the BCP transports carbon to the deep ocean is ultimately dependent on the rate at which the particles sink and the rate at which they are remineralised. The remineralisation of sinking particles is driven by a number of processes, including: zooplankton grazing, coprophagy (ingestion of FP), coprorhexy (fragmentation of FP), microbial remineralisation, as well as physical aggregation and disaggregation (Lampitt et al. 1990; Wilson et al. 2008; Poulsen and Iversen 2008; Turner 2015). The rate of these processes varies both spatially and temporally with changing community structure and particle type, and as such it is not easy to accurately predict the efficiency of the BCP and hence flux of POC to the deep sea.

Martin et al. (1987) measured a composite value of attenuation factor *b* of 0.858 from six stations in the North Pacific which has been widely applied in many biogeochemical models (e.g. Najjar et al. 1992; Sarmiento et al. 1993). However, considering the aforementioned processes controlling the rate at which sinking particles are remineralised, it seems unlikely that POC attenuation

should be constant either spatially or temporally. In fact, subsequent studies, both observational and modelling, suggest that POC attenuation is much more variable than the canonical Martin's *b* value (Figure 1-7) (Buesseler et al. 2007b; Lam and Bishop 2007; Henson et al. 2012a; Guidi et al. 2015; Marsay et al. 2015). More recent models allow regional variability, for example by incorporating the protection of sinking POC by minerals following Armstrong et al. (2002) (e.g. Yool et al. 2011, Dunne et al. 2013), or by a relationship with temperature (e.g. Aumont and Bopp 2006).

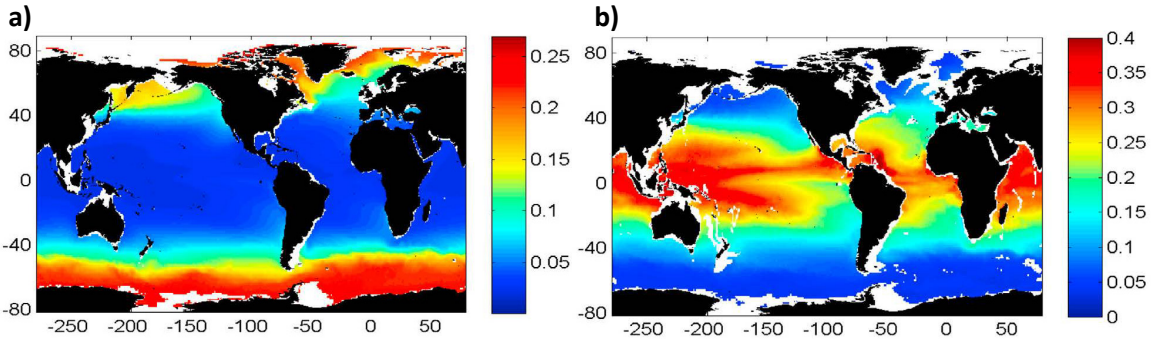


**Figure 1-6: Global maps of satellite-derived a) particle export efficiency and b) transfer efficiency to 2000 m. Taken directly from Henson et al. (2012a).**

Mineral composition of deep POC fluxes has been suggested to explain global patterns of transfer efficiency with a positive correlation between deep fluxes of calcium carbonate ($CaCO_3$) and transfer efficiency to 2000 m (Francois et al. 2002). More recently it has been suggested that the upper ocean export of $CaCO_3$ has only small influence on transfer efficiency whereas opal export shows strong negative correlation with transfer efficiency (Henson et al. 2012a). These global patterns can be explained by ecosystem structure, with regions of high relative diatom abundance supporting high export efficiencies in part due because diatoms are relatively large and dense so can sink rapidly and avoid significant remineralisation in the surface ocean (Martin et al. 2011). However, as opal (the main chemical component of diatom frustules) dissolution can begin at 100 m (Treguer et al. 1995; Boyd et al. 2004), any protection or ballasting of POC by opal will be removed at relatively shallow depths and hence result in a relatively low transfer efficiency of diatom derived material in the mesopelagic (Henson et al. 2012a). Conversely, the phytoplankton dominating low latitudes are generally small and sink slowly resulting in high remineralisation in surface waters and low export efficiency out of the euphotic zone (Henson et al. 2012a). Low export efficiencies suggest extensive recycling in the euphotic zone, meaning that the material that is finally exported will likely be refractory leading to high transfer efficiencies in the mesopelagic (Henson et al. 2012a).

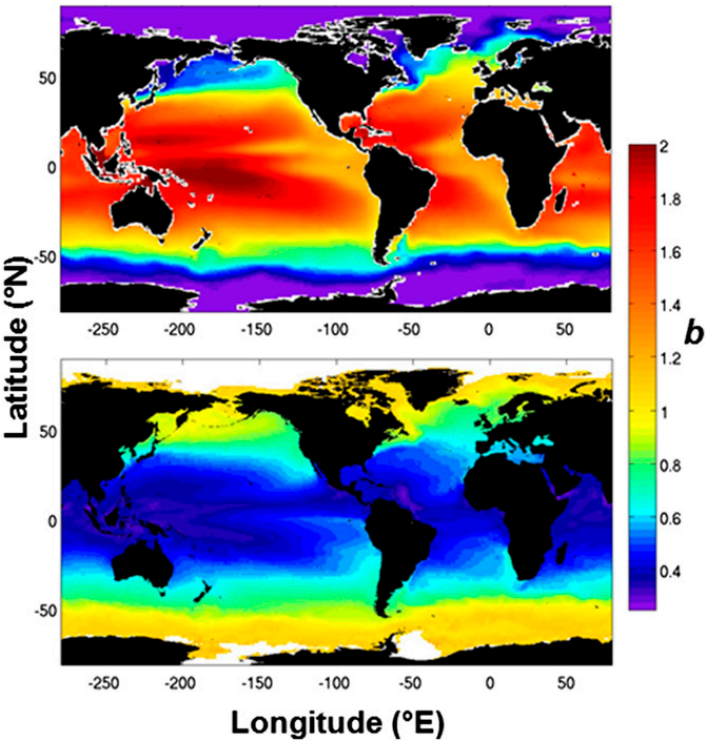


**Figure 1-7: Comparison of estimates of Martin's *b* value. Figure taken from Marsay et al. (2015) which compares their estimated values of *b* over the upper 500 m with *b* from Henson et al (2012) calculated over the upper 2000 m.**

Marsay et al. (2015) hypothesise that spatial variability in Martin's *b* value can be explained by mean upper ocean temperatures (upper 500 m). Although metabolic rates are strongly tied to temperature (e.g. Ikeda 1985; Le Fèvre et al. 1998; Grossart and Ploug 2001), there are many other factors affecting both the composition and remineralisation rate of sinking particles, such as mineral ballasting (Klaas and Archer 2002; Francois et al. 2002), community structure (Boyd and Newton 1999; Guidi et al. 2009) and oxygen (Devol and Hartnett 2001). In fact Henson et al. (2012) estimate very different spatial variability in Martin's *b* value based on satellite-derived export estimates and deep sea POC fluxes (Figure 1-7). The fact that analysing POC flux attenuation over different depth ranges gives such contrasting results highlights the complexity of the biological carbon pump. Untangling these different processes is not an easy task, particularly as temperature can correlate with many other processes making it difficult to distinguish controlling mechanisms. The confounding effects of temperature can be reduced by studying regions where there are gradients in key processes such as community structure or ballasting, but temperatures are relatively constant.

### 1.4.1 Remineralisation depth

The depth at which material is remineralised in the ocean is tightly coupled to atmospheric levels of $CO_2$ (Figure 1-8). An accurate assessment of the strength of the BCP is therefore key if we are to

understand and predict how the BCP might change with climate, and the subsequent effects on atmospheric levels of $CO_2$. However, the practical difficulties of making measurements of POC flux in the upper mesopelagic where most remineralisation occurs means that there is limited data with which to validate global biogeochemical models. Measurements of deep ocean POC fluxes are subject to fewer problems (Buesseler et al. 2007a), however spatial and temporal coverage is still poor (Honjo et al. 2008). It is therefore unsurprising that the range of estimates of global export is so large (5-20 GtC $yr^{-1}$) (Henson et al. 2011). The biological processes governing particle formation and attenuation undergo seasonal cycles, resulting in orders of magnitude seasonal variations of POC flux (Accornero et al. 2003; Buesseler et al. 2007a; Wilson et al. 2013; Manno et al. 2015). It seems likely that a spatially and temporally variant attenuation factor would improve the accuracy of our global biogeochemical models, however this requires both more observational data and a better mechanistic understanding of the processes controlling particle flux and remineralisation. In particular, identifying these processes requires resolving not only the magnitude but also identifying the type of particles comprising the flux.

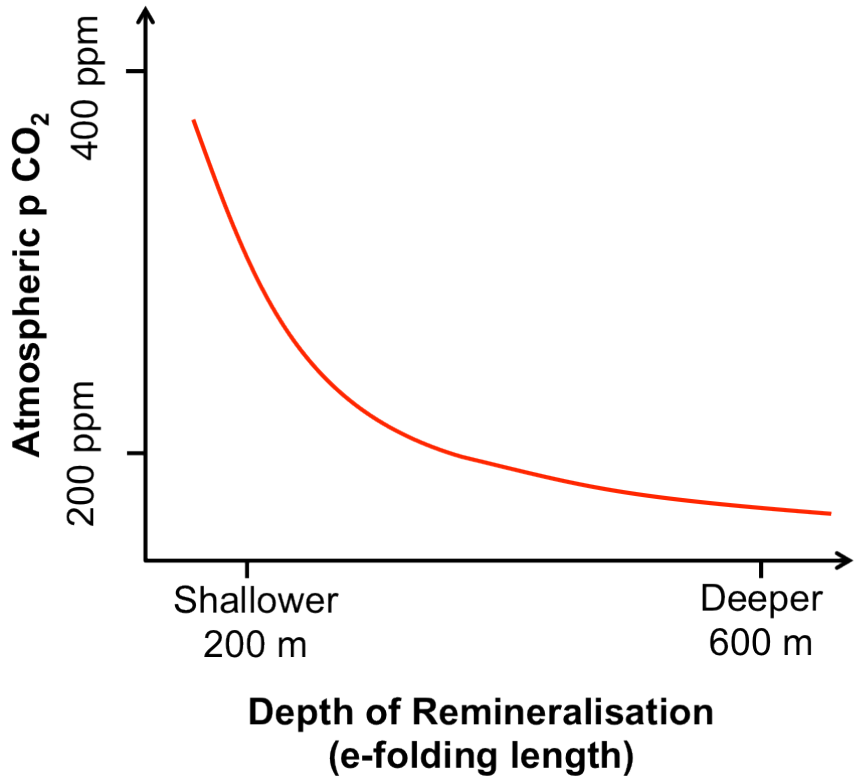


**Figure 1-8: Modelled relationship between remineralisation depth of POC and atmospheric $CO_2$. Redrawn from Kwon et al. (2009).**

## 1.5 Mesopelagic carbon budget

Accurate quantification and prediction of particle flux attenuation with depth requires in-depth understanding of the major sources and sinks of carbon in the ocean. As the region where many particles are formed and where the most rapid loss of POC occurs, constraining the balance between processes supplying carbon and removing carbon in the mesopelagic is important. Despite the complexities of carbon loss from sinking marine particles (Figure 1-9), the ultimate loss of carbon from the organic pool is via respiration, and hence the loss of POC in the mesopelagic should be explained by community respiration (Buesseler and Boyd 2009). A number of studies have compared the loss of POC with zooplankton and bacterial respiration, yet few have found a balance and there is a lack of consensus as to the relative roles of zooplankton and bacteria (Boyd et al. 1999b; Steinberg et al. 2008; Burd et al. 2010; Giering et al. 2014).

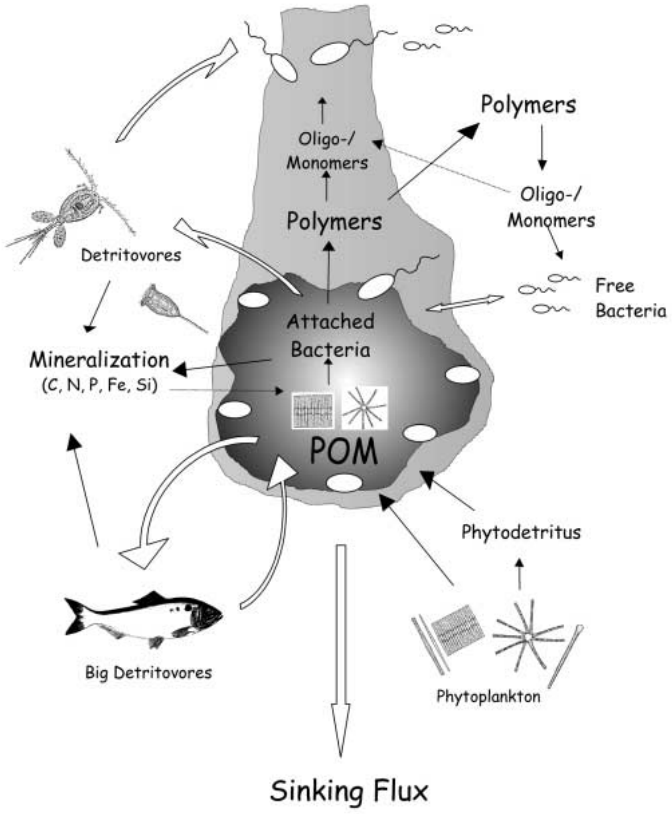


**Figure 1-9: Schematic to illustrate the loss of carbon from sinking aggregates. POM= Particulate organic matter. Taken directly from Simon et al. (2002).**

The seminal work of Steinberg et al. (2008) found that the mesopelagic (150-1000 m) bacterial carbon demand was 3-10 times higher than the loss of sinking POC flux (Figure 1-10). Recently Giering et al. (2014) managed to reconcile these imbalances for a site in the northeast Atlantic by making a number of improvements to the way in which we define the source and sink terms of the budget. However, when examining their balanced budget in more detail, Giering et al. (2014)

found large and compensating imbalances between source and sink terms in depth discrete layers with an excess of POC supply to the upper mesopelagic (50-150 m depth), and an excess of respiration in the lower mesopelagic (150-1000 m). These imbalances suggest that either there are inaccuracies in the measurement of terms included in the budget, or that there are additional terms that have not yet been accounted for, such as particle-associated microbial respiration.

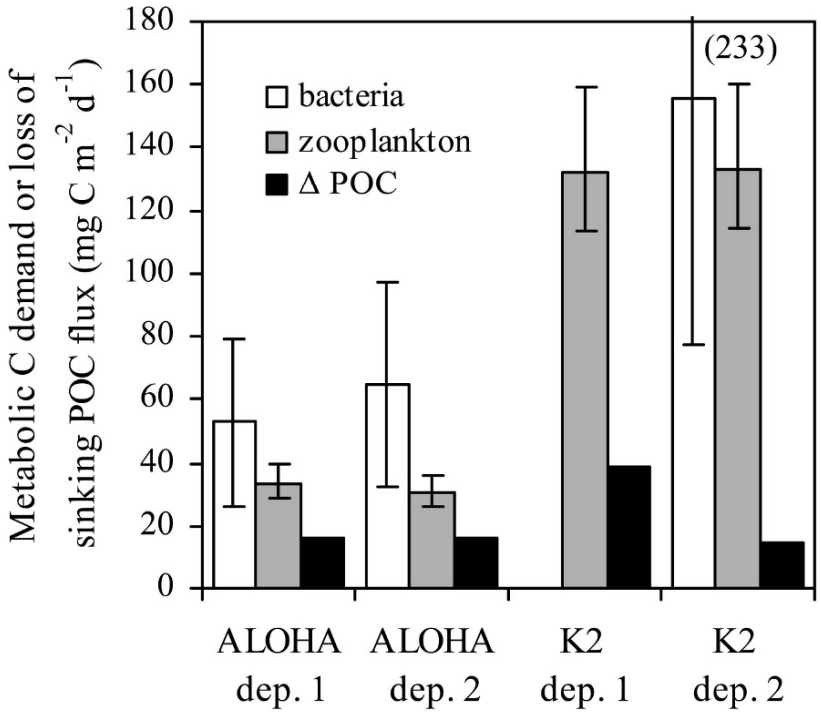


**Figure 1-10: Example of measured imbalances in the mesopelagic carbon budget, taken from Steinberg et al. (2008). The carbon demand of bacteria (white bars) and zooplankton (grey bars), far exceeds the POC supply (black bars) over the mesopelagic (150 – 1000 m)**

### 1.5.1 The role of zooplankton

Zooplankton are an important part of ocean ecosystems, providing a link between primary producers and higher trophic levels. In addition, they play a key role in the export of POC through a number of processes including, grazing and repackaging, particle fragmentation, and vertical migrations. The repackaging of slow-sinking individual phytoplankton cells into fast-sinking FP can promote efficient export of POC out of the euphotic zone (Hamm et al. 2001). The contribution of FP to deep sediment trap fluxes can be large (>90%) (Carroll et al. 1998; Wilson et al. 2013; Manno et al. 2015), providing direct evidence of the importance of zooplankton FP to the transport of carbon to the deep ocean.

In addition, both diel and seasonal migrations of zooplankton can directly transport carbon out of the euphotic zone to the mesopelagic, bypassing the region of rapid remineralisation (Steinberg

et al. 2000; Kobari et al. 2008; Jónasdóttir et al. 2015). Diel vertical migration (DVM) of zooplankton and excretion at different depths will influence the POC flux (e.g. Emerson and Roff 1987) and has the potential to support increased deep POC fluxes. A number of zooplankton species have been observed to migrate daily, rising to the surface during the night to source food, but migrating deeper in the water column during the day to avoid predation (Longhurst and Harrison 1988). These migrating zooplankton actively transport relatively fresh detrital material deeper in the ocean if gut passage times are sufficiently long. If egestion times are short then faecal pellets will be produced in the region in which the zooplankton are feeding and zooplankton migration will not act to increase the transfer efficiency of faecal pellets. Variations in the migration depths of zooplankton populations (both seasonally and between species) will therefore contribute to variability in the transfer efficiency and POC flux to depth. Excretion of DOC and respiration at depth by migrating zooplankton also increases the transfer of organic carbon below the euphotic zone (Steinberg et al. 2000). In addition, seasonal carbon sequestration occurs through the vertical transport and respiration of lipids by hibernating zooplankton (Jónasdóttir et al. 2015).

However, zooplankton can also act as a retention filter through coprophagous feeding on, and fragmentation of, sinking FP, reducing the flux of POC to the deep ocean (González and Smetacek 1994; Svensen et al. 2012). It has been previously suggested that microcopepod species such as *Oithona* spp. can account for significant reworking of sinking FP, most likely through coprorhexy (Poulsen and Kiørboe 2005; Iversen and Poulsen 2007), leading to retention and remineralisation in the upper ocean (Suzuki et al. 2003; Svensen and Nejstgaard 2003). Indeed, when comparing measurements of FP production to FP export, a number of studies have found significant retention of FP (Riser et al. 2001; Wexels Riser et al. 2007), but the mechanisms of this retention are not well understood. Both free-living bacteria and bacteria internally within FP have also been found to contribute significantly to their degradation (Jing et al. 2012; Cnudde et al. 2013). Protozooplankton (dinoflagellates and ciliates) have been suggested as a main driver of FP remineralisation (Poulsen and Iversen 2008), however Svensen et al. (2012) found that FP degradation by dinoflagellates and ciliates was too slow to account for the FP retention they observed. More recently, it has been proposed that interactive effects must be considered, with the mechanical break up of large FP by copepods supporting further degradation by dinoflagellates and prokaryotes (Svensen et al. 2012, 2014; Giering et al. 2014).

Differences in the abundance, behaviour and community composition of zooplankton in the mesopelagic can have differential effects on the transfer of POC through the mesopelagic (Wilson et al. 2008). Despite this importance, most global biogeochemical models do not consider many, if any, different zooplankton functional types (e.g. Sarmiento et al. 1993; Ridgwell et al. 2007; Yool

et al. 2013) and, as such, model estimates may not accurately characterise biogeochemical cycling in all regions of the ocean (Le Quéré et al. 2016; Cavan et al. 2017). Studies measuring POC flux and particle type concurrently with ecosystem structure are key to support a better mechanistic understanding of the biological carbon pump and more accurate estimates of its strength. In addition, we need to focus our efforts on groups of the community that are as yet poorly understood, but may play a disproportionate role on carbon cycling (Robinson et al. 2010).

### 1.5.2 The role of microbes

Microbes are ubiquitous in the marine environment, and are either free-living or associated with particles. Particles are microbial hotspots in terms of microbial abundance (Silver and Alldredge 1981; Thiele et al. 2015) and heterotrophic activity (Grossart et al. 2007). Hence particle-associated microbes could account for significant POC remineralisation. To date, most of our knowledge of microbial remineralisation in the ocean is that driven by prokaryotes, although the importance of protists in this process has more recently been studied (Poulsen and Iversen 2008; Poulsen et al. 2011). There is a close coupling between particle-associated and free-living prokaryotes as:

1. Some motile prokaryotes can attach and detach from particles (Kiørboe 2003).
2. Particle-associated prokaryotes produce hydrolytic enzymes (Smith et al. 1992) that are responsible for the release of dissolved organic matter in the vicinity of the particle, the 'particle plume', which is consumed by free-living prokaryotes (Figure 1-9) (Kiørboe and Jackson 2001).

Even though the distinction between free-living and particle-associated microbial communities is dynamic, recent studies suggest that these two communities are fundamentally different from one another (e.g.Simon et al. 2002; Nagata et al. 2010).

Compared to other marine organisms such as zooplankton, prokaryotes occur in very high abundances in the mesopelagic ocean and have low growth efficiencies (i.e. a small proportion of the organic carbon they consume is turned into biomass) (del Giorgio and Cole 2000; Reinthaler et al. 2006; Baltar et al. 2009, 2010a). There is therefore the potential for prokaryotes to drive significant remineralisation of organic carbon to inorganic carbon through respiration. Indeed, Giering et al. (2014) found that free-living mesopelagic (50-1000 m) prokaryotes accounted for 70-92% of the community carbon respiration, and a model by Anderson and Tang (2010) suggested that bacteria alone accounted for 84.7% of respiration in the mesopelagic. However, as large particles represent a large component of the POC flux (Fowler and Knauer 1986), for free-living prokaryotic respiration to be the dominant control on observed POC flux attenuation, this first

requires mechanical breakdown into slow- and non-sinking POC and DOC to make it accessible to prokaryotes (Giering et al. 2014). Indeed, small sinking particles have recently been shown to be an important part of total POC flux in some regions (Dall'Olmo and Mork 2014; Durkin et al. 2015; Giering et al. 2016). A number of studies have suggested that zooplankton and protozoa are responsible for this breakdown through 'sloppy feeding' which fuels prokaryotic respiration (Lampitt et al. 1990; Iversen and Poulsen 2007; Poulsen and Iversen 2008; Poulsen et al. 2011).

The proportion of carbon that is respired by prokaryotes to DIC (i.e. production of $CO_2$) versus the production of POC, which is passed onto higher trophic levels, is dependent on the prokaryotic growth efficiency (PGE), which can range over orders of magnitude (e.g. 0.01-0.64 measured by del Giorgio and Cole (2000)). Production by free-living bacteria can be estimated by measuring leucine uptake rates, and then converted to respiration which relies on leucine conversion factors and bacterial growth efficiencies. However, leucine conversion factors can also vary by an order of magnitude and should be measured empirically (Alonso-Sáez et al. 2007; Baltar et al. 2010a). Prokaryotic respiration can also be measured directly, for example by measuring changes in dissolved oxygen or the reduction of the tetrazolium salt 2-(p-iodophenyl)23-(p-nitrophenyl)25-phenyltetrazolium chloride (INT) (e.g. Aristegui et al. 2005; Reinthaler et al. 2006; Martinez-Garcia 2017), avoiding the uncertainties associated with PGE.

Uncertainties surrounding estimates of free-living bacterial respiration can be large and can lead to inconsistency in attempts to balance mesopelagic carbon budgets (Steinberg et al. 2008; Burd et al. 2010; Giering et al. 2014). Anderson et al. (2007) found that there was a balance between the bacterial carbon demand and the supply of POC to the mesopelagic using a PGE of 0.27. However, using a lower growth efficiency value would have resulted in an imbalanced budget. Conversely, Steinberg et al (2008) found that bacterial carbon demand in the mesopelagic (150-1000 m) was up to 10 times greater than the loss of sinking POC flux. This highlights the impact of PGE measurement uncertainties on budget calculations and the need for accurate measurements. Additionally, (Baltar et al. 2010b) suggested that mismatches between heterotrophic carbon demand and POC supply may be at least partially explained by non-sinking POC also fuelling prokaryotic respiration.

Most carbon budget studies to date have only considered free-living bacteria due to the lack of measurements of particle-associated bacterial respiration (e.g. Steinberg et al. 2008; Giering et al. 2014), therefore missing their role in the regulation of the mesopelagic carbon budget. In addition, other organisms in the microbial community, such as protists are also likely to be important for remineralisation (Poulsen and Iversen 2008; Poulsen et al. 2011). A recent study has shown that particle-associated microbial respiration can contribute 32-93% of the total

respiration measured *in situ* (McDonnell et al. 2015), thus highlighting the role of these microbes in the carbon budget and the need for more respiration rate measurements on sinking particles. Sinking particles are the main vehicle for the transfer of carbon to depth by the biological carbon pump (Fowler and Knauer 1986) and hence understanding the processes governing their degradation, such as the remineralisation activities of particle-associated microbes, is key.

Most sinking particles in the ocean are in the form of aggregates, particularly marine snow aggregates which are ubiquitous in the ocean (Fowler and Knauer 1986; Alldredge and Silver 1988). The fragile nature of marine snow aggregates makes sampling and respiration measurements difficult, with many studies resorting to artificially made aggregates formed in roller tanks (Grossart and Ploug 2001; Iversen et al. 2010; Iversen and Ploug 2010, 2013). Few previous studies have managed to collect *in situ* aggregates and measure heterotrophic production of associated bacteria (Alldredge and Youngbluth 1985; Smith et al. 1992). However, in these studies aggregates were incubated on a solid surface, which has been shown to cause diffusion limitation and result in biased measurements (Ploug and Jorgensen 1999).

For these reasons, the roles of particle-associated microbes on POC remineralisation have been poorly studied and more measurements are required to allow incorporation into future carbon budget studies.

## 1.6 Measuring particle flux

Numerous methods have been employed over the past few decades to measure the flux of large passively sinking particles in the ocean, from early sediment traps (Berger, 1971), thorium tracers (Buesseler et al. 1992), and Marine Snow Catchers (Lampitt et al. 1993), to newly developed neutrally buoyant sediment traps (Buesseler et al. 2008; Lampitt et al. 2008) (Figure 1-11). Measuring particle flux is not straight forward, particularly in the upper mesopelagic where ocean currents can be strong, and each of these methods has its own uncertainties and biases which determine its suitability for a particular study. Understanding these biases and the timescales over which each technique makes its measurements is necessary before attempting to interpret the data they collect.

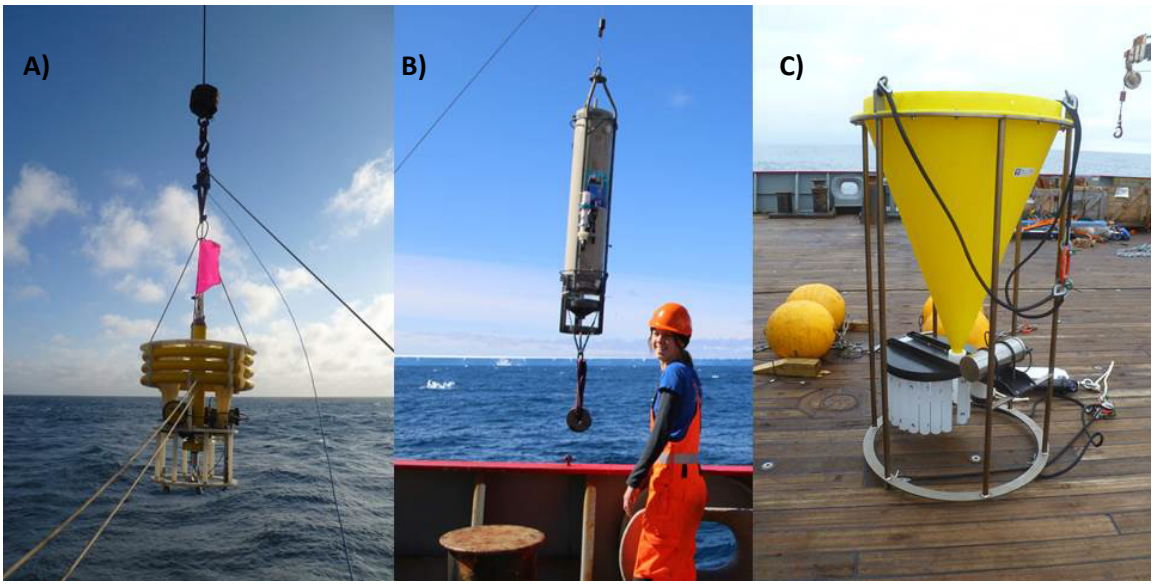


**Figure 1-11: Methods employed to measure particle flux. A) PELAGRA neutrally buoyant sediment trap, B) Marine Snow Catcher, C) McClane sediment trap**

### 1.6.1 Sediment traps

Modern sediment traps have been in use since the early 1970's (e.g. Berger 1971), relying on a cone, tube or other device (of known area) to directly intercept sinking particles (Figure 1-11C). Traps can be deployed for hours to years, with multiple collector cups allowing user defined temporal resolution over the sampling period. The ability to deploy multiple sediment traps at multiple depths and to leave these traps *in situ* collecting data over long periods of time, makes them a very powerful tool for understanding seasonal changes in particle flux and attenuation with depth. Mooring platforms allow sediment traps to be deployed together with numerous other instruments to measure parameters such as chlorophyll, dissolved oxygen, $CO_2$ and nutrients (e.g. Hartman et al. 2012). Long-term moored sediment traps are also needed to investigate seasonality in the polar regions where winter measurements can be difficult to obtain from oceanographic vessels (e.g. Manno et al. 2015).

However, the material collected in each sediment trap sample is amalgamated, and although it is possible to isolate some individual particles such as faecal pellets, more fragile material such as phytodetrital aggregates will be combined together preventing determination of, for example, individual particle sizes. Many studies additionally use polyacrimide gels within sediment traps to allow the original characteristics of individual particles to be maintained (e.g. Ebersbach and Trull 2008), however the use of gels limits the ability to measure the chemical composition of particles.

The main problem with sediment traps is the hydrodynamic bias due to flow over the trap mouth resulting in under- or over-trapping, particularly in the upper ocean where currents are typically

stronger (Buesseler et al. 2007a). In addition, planktonic organisms (whose abundances are highest in the upper ocean) are attracted to traps and contaminate samples with their carcass as well as modifying the sample through, for example, feeding and defaecation before they die (Buesseler et al. 2007a). However, the upper ocean is the region where most particles are formed and where the most rapid changes in particle flux occur; being able to accurately characterise particle flux in this region is important. Some of these problems can be reduced through the use of neutrally buoyant sediment traps (NBST) (Buesseler et al. 2000; Lampitt et al. 2008) which move with the water flow and thus reduce the water flow relative to the trap.

### 1.6.2 Thorium tracers

Although long-term sediment trap deployments can help build up a seasonal picture of particle flux, many sediment trap deployments are on much shorter timescales. In these instances, particle flux measurements represent more of a snapshot of particle export, which may or may not accurately reflect 'typical' conditions at a particular study site. Steady state is often assumed when comparing traps at multiple depths to quantify the attenuation of particle flux, however this can result in inaccuracies, particularly in regions where seasonal changes are large (Giering et al. 2017). The use of radioactive tracers, such as thorium, allow for a time-integrated estimate of export, avoiding some of the problems with snapshot measurements.

Among the different radioactive tracers, the most commonly used is the pair throrium-234 and uranium-238 ($^{234}$Th-$^{238}$U). $^{234}$Th is particle reactive whereas its parent $^{238}$U is non-reactive and shows conservative behaviour in an oxic system. The daughter isotope ($^{234}$Th) is scavenged onto particles and effectively removed from the surface ocean, which generates a measurable deficit of $^{234}$Th relative to $^{238}$U. This leads to a disequilibrium between parent and daughter isotopes which can be used to quantify particle flux (Buesseler et al. 1992; Waples et al. 2006). The larger the disequilibrium in total activities the higher the particle flux, assuming no significant loss of thorium by lateral advection. The half-life of $^{234}$Th (24.1 days) makes it an ideal tracer for studying processes that occur on time-scales of days to weeks. Thorium derived flux measurements can also be used in combination with sediment traps to help detect over- or under-trapping. Accurate determination of sinking fluxes of POC does however rely on knowledge of the ratio of POC to $^{234}$Th on sinking particles, which has been shown to vary with both depth and particle size (Buesseler et al. 2006).

### 1.6.3 Marine Snow Catchers

A Marine Snow Catcher (MSC) is a 95 L PVC closing water bottle designed to minimise turbulence and capture intact sinking particles (Figure 1-12) (Riley et al. 2012; Cavan et al. 2015). The MSC is deployed open to the depth of interest, and the bottle closed at this depth using a mechanical release mechanism. The MSC is then recovered on board and left for two hours to allow particles to settle. The sinking velocities of particles in the MSC cover a continuous spectrum of velocities, which are partitioned into three classes; fast-, slow- and suspended sinking particles, based on the distance sunk in the settling time. Particles that have settled in the collector tray at the bottom of the MSC are defined as fast-sinking, and particles in the base defined as slow-sinking (operationally defined as 0-18 m $d^{-1}$). The remaining material in the top section of the snow catcher is defined as suspended (Figure 1-12).

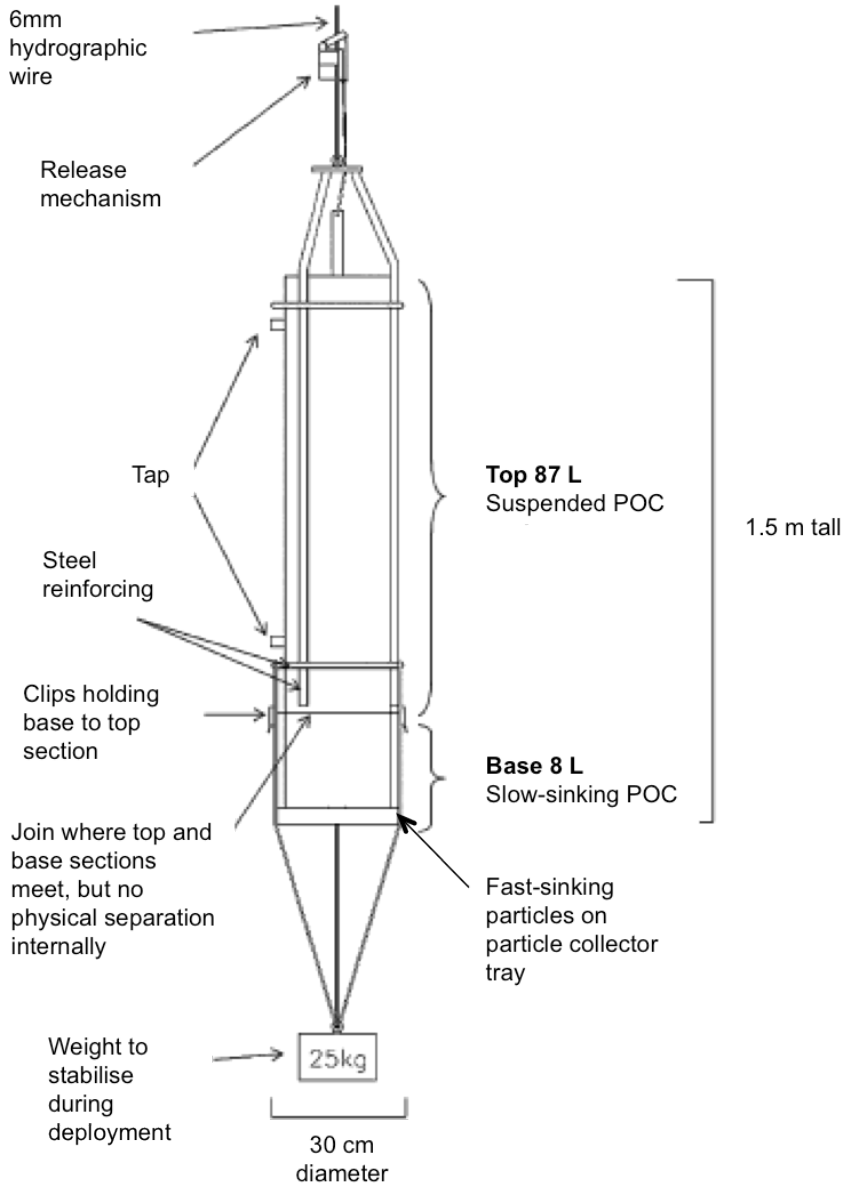


**Figure 1-12: Diagram of Marine Snow Catcher. Adapted from Riley et al. (2012)**

Typically, MSCs are deployed in pairs in quick succession (Cavan et al. 2015) at the base of the euphotic zone and 100 m below this, allowing the attenuation of POC flux with depth to be calculated. The distinct advantage of the MSC is the ability to obtain intact sinking particles which can be used for chemical analysis and further experiments such as particle respiration studies and sinking velocity measurements. Fluxes measured using the MSC are snapshot measurements, which, although enabling high resolution assessments of short-term variability, can lead to uncertainties if only single measurements are made in non-steady state conditions.

### 1.6.4 Other methods

More recently optical methods such as the Underwater Vision Profiler (UVP), and the particle camera (ParCa) have been used to measure particle size distributions at high spatial and temporal resolutions (e.g. Guidi et al. 2008; Picheral et al. 2010; Iversen et al. 2010). The size of particle that can be measured by these optical techniques depends on the optical resolution (lower size limit) and the volume imaged (upper size limit), most typically allowing the imaging of particles > 100 µm. Optical methods, although powerful for providing high resolution profiles of particle size distributions, do not provide direct estimates of particle flux. Studies have relied on empirical relationships (through comparison with, for example, sediment trap particle fluxes) to convert from particle size to particle flux (Guidi et al. 2008; Iversen et al. 2010; Roullier et al. 2014). Particle flux can also be calculated based on spikes in chlorophyll and backscatter data (Briggs et al. 2011), a promising technique allowing high resolution estimates of particle flux during aggregate flux events using for example underwater gliders.

## 1.7 Study sites

### 1.7.1 The Southern Ocean

The Southern Ocean is a site of ocean ventilation and exhibits high surface concentrations of carbon and nutrients due to the upwelling of nutrient rich waters (Toggweiler 1994). Despite these high nutrient inputs, much of the Southern Ocean is considered to have relatively low productivity (high nutrient, low chlorophyll (HNLC) regions), which has been attributed in part to low iron (de Baar et al. 1995; Boyd and Trull 2007). The biological carbon pump in the Southern Ocean is therefore not operating at full efficiency resulting in biologically unutilised nutrients (‘preformed’ nutrients (Ito and Follows 2005)) being transported into the ocean interior, supplying much of the global ocean with preformed nutrients and hence fuelling global biological production (Sarmiento et al. 2004). Changes in global circulation and the efficiency of the

Southern Ocean biological carbon pump are therefore strongly tied to atmospheric $CO_2$ (Marinov et al. 2006, 2008; Kwon et al. 2009).

There are many regions in the Southern Ocean that are not HNLC regions, including the area downstream of South Georgia, that are iron fertilised through inputs from, for example, shelf sediments (Holeton et al. 2005; Bakker et al. 2007; Jouandet et al. 2008; Korb et al. 2008; Nielsdóttir et al. 2012) and that support large phytoplankton blooms. Higher productivity and blooms of large diatoms are predicted to support high export of biogenic carbon (Korb et al. 2012; Lasbleiz et al. 2016). Distinct variability in phytoplankton and zooplankton abundance and community composition around South Georgia (Korb et al. 2010) is likely reflected in high variability in export (Korb et al. 2012).

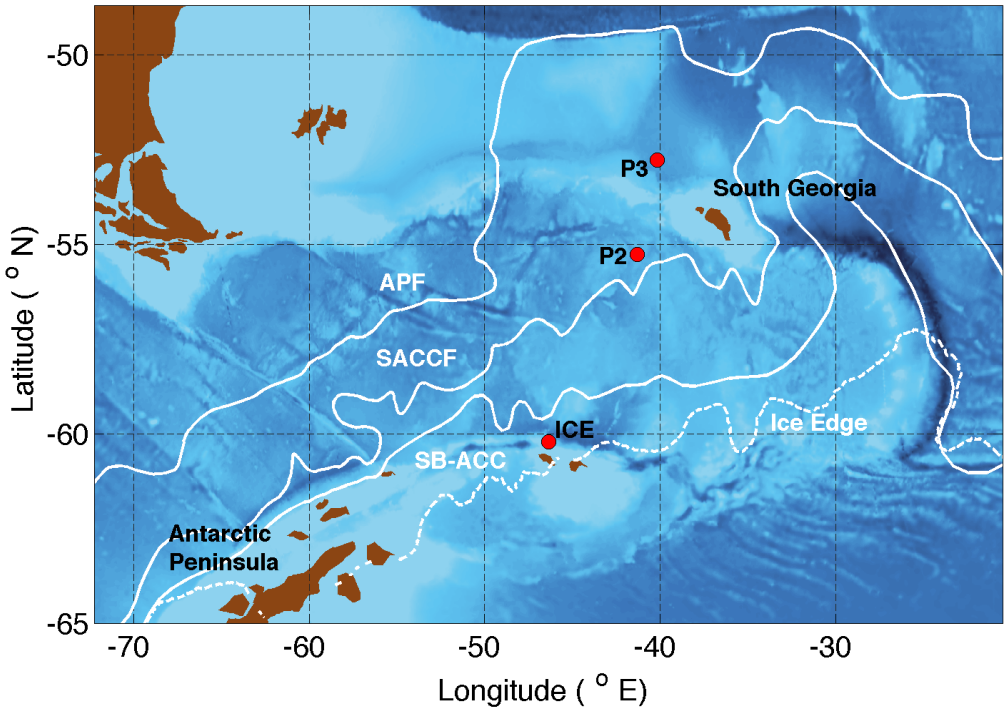


**Figure 1-13: The Scotia Sea region in the Southern Ocean. Red dots show positions of stations sampled in this study. White lines indicate mean frontal positions. APF=Antarctic Polar Font (Orsi et al. 1995), SACCF = Southern Antarctic Circumpolar Current Front (Thorpe et al. 2002), SB-ACC-=Southern Boundary - Antarctic Circumpolar Current (Orsi et al. 1995). White dotted lines indicates the position of the ice edge on 3rd Dec 2013 (OSTIA Sea Ice satellite data).**

The region around South Georgia (the Scotia Sea, Figure 1-13) contains a number of diverse oceanographic regimes within a narrow temperature range, providing a unique region to assess the role of community composition on export without the added influence of temperature variability. The community composition, as well as the timing of trophic interactions, play an

important role in prescribing both the flux of carbon from the euphotic zone and transfer efficiency through the mesopelagic. As part of this study, stations upstream (P2) and downstream (P3) of South Georgia were sampled. These stations support marked differences in community structure, with large rapidly sinking diatoms likely to be more prevalent in the iron fertilised downstream region (Smetacek et al. 2004; Korb et al. 2012). Additionally, a site in the southern Scotia Sea near the South Orkneys was sampled, which unlike the northern Scotia Sea, is seasonally ice covered. The biological communities of the northern and southern Scotia Sea differ, separated by the Southern Antarctic Circumpolar Current Front (Figure 1-13) (Ward et al. 2012b). The phytoplankton community of both regions of the Scotia Sea is dominated by diatoms, with heavily silicified species such as *Fragilariopsis spp*. and *Corethron pennatum* prevalent in the southern Scotia Sea, whereas lightly silicified diatoms such as *Pseudonitzchia lineola* and *Thalassionema nitzschoides* make up a large proportion of the community in the northern Scotia Sea (Korb et al. 2012). In addition, zooplankton communities differ with higher abundances in the northern Scotia Sea (Ward et al. 2012b).

The epipelagic biomass of the Southern Ocean is dominated by Antarctic krill (*Euphausiia superba*), which forms the link between primary production and higher trophic levels (Murphy et al. 2007). Krill form large swarms (up to 100 $km^2$, Tarling and Fielding (2016)) and produce large FP which can sink quickly through the water column (Atkinson et al. 2012). These swarms can rapidly exploit phytoplankton, and the subsequent bulk egestion of FP can result in large fluxes of carbon to the ocean interior (Atkinson et al. 2012). However, the low number of flux measurements in the Southern Ocean (particularly in the marginal ice zone) and patchy nature of krill means these potentially large fluxes are poorly captured by observational studies, and hence poorly represented in empirically derived model algorithms.

### 1.7.2 The Porcupine Abyssal Plain observatory

The Porcupine Abyssal Plain (PAP) observatory is a long-term monitoring site in the northeast Atlantic (Figure 1-14). Measurements have been made from the surface to the seabed from research vessels visiting the site for the past 30 years, with a fixed-point mooring put in place in 2002 (Hartman et al. 2012). The site was chosen based on its location away from the continental slope and the Mid-Atlantic Ridge in the hope of avoiding the complexities associated with these systems. Productivity at the PAP site undergoes a strong seasonal cycle characteristic of mid to high latitude systems, with increased chlorophyll associated with spring and summer phytoplankton blooms (Hartman et al. 2010). Similarly the PAP site is characterised by a seasonal cycle in POC flux, peaking in late summer and exhibiting high inter-annual variability (Lampitt et al. 2010).

Recently the PAP observatory was the focus of a study attempting to reconcile imbalances in the mesopelagic carbon budget (Giering et al. 2014) that have been previously found elsewhere (e.g. Steinberg et al. 2008; Baltar et al. 2009; Reinthaler et al. 2006). Despite managing to balance the budget between 50-1000 m, large and counteracting imbalances were found when looking at the upper (50-150 m) and lower (150-1000 m) mesopelagic separately. The PAP site therefore represents a region where we have the most complete knowledge of the mesopelagic carbon budget, making it an ideal site to investigate terms that may be missing from the budget and that may help reconcile depth resolved imbalances.

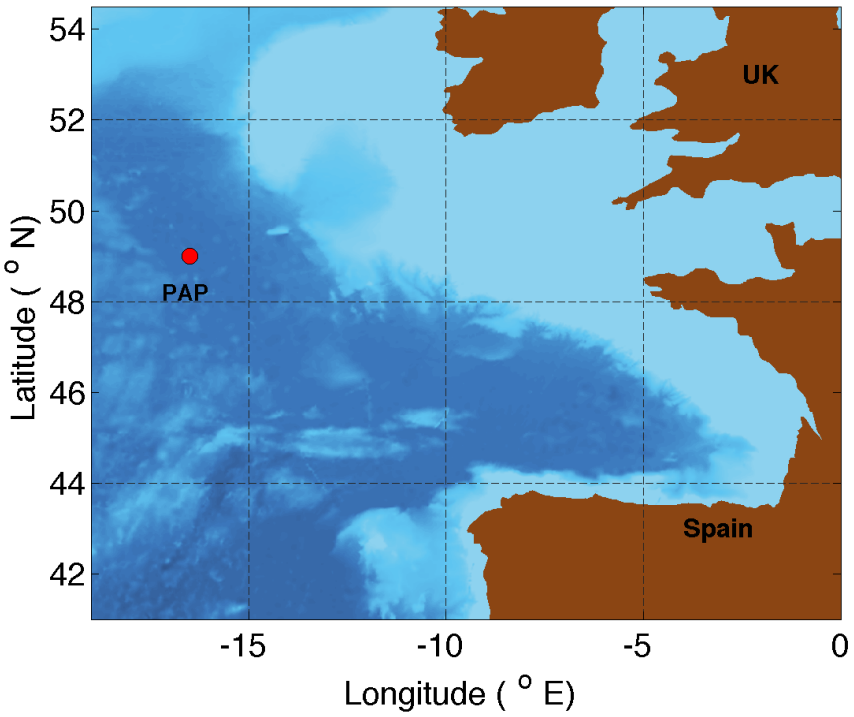


**Figure 1-14: Location of PAP observatory site in northeast Atlantic.**

## 1.8 Research aims

The main objectives and associated hypotheses (H1-H4) of this PhD thesis are outlined below:

1. To measure POC flux and particle type at a number of sites and determine if knowledge of the type of sinking particles can help explain the processes driving the flux.
   **H1: Particle type is a major determinant of the magnitude of the POC flux out of the euphotic zone and its subsequent attenuation.**
   Regions dominated by FP will show lower flux attenuation than those dominated by sinking phytoplankton cells and phytodetrital aggregates.

2. To assess the role of zooplankton community composition on the transfer efficiency of sinking particles through the mesopelagic of the ocean in isolation of large changes in temperature.
   **H2: Zooplankton community structure is a major driver of the magnitude and efficiency of the BCP: when large microzooplankton are dominant, the transfer of POC through the mesopelagic is more efficient than when microzooplankton dominate.**
   Large macrozooplankton repackage slowly sinking individual phytoplankton into large fast-sinking faecal pellets, which will drive efficient transfer of POC through the mesopelagic. Conversely, regions dominated by microzooplankton will exhibit high rates of attenuation driven by coprophagy and coprorhexy. A change in community structure can therefore result in differences in transfer efficiency even when ocean temperatures are similar.

3. To investigate the role of particle-associated microbes on governing the rate of attenuation of POC in the mesopelagic, and how this varies with depth.
   **H3: Particle-associated microbial respiration accounts for large losses of POC with depth, especially in regions where abundances of sinking particles are high and sinking velocities are relatively low.**

4. To address the potential for respiration by particle-associated microbes to resolve imbalances in the upper mesopelagic carbon budget.
   **H4: Accounting for the loss of POC by particle-associated microbes decreases the gap between POC sources and POC sinks in the upper mesopelagic.**

The structure of this thesis is as follows:

Chapter 2: An assessment of the role of particle-associated microbial respiration on the attenuation of POC in the Southern Ocean. Direct measurements of respiration on *in situ* collected FP, combined with zooplankton net tow surveys allow the relative roles of microbes and zooplankton on mesopelagic POC flux attenuation to be determined. Measurements of POC flux are made at three different sites of similar temperature (-1 to 5 °C) but contrasting ecosystem structure. This chapter addresses research aims 1-3 and has been published in Limnology and Oceanography.

Chapter 3: An investigation into whether particle-associated microbial respiration can resolve depth-related imbalances in the mesopelagic carbon budget at the PAP observatory site. Vertical profiles of particle-associated microbial respiration in phytodetrital aggregates allow an

assessment of this poorly quantified part of the mesopelagic carbon budget. This chapter addresses research aims 1,3 and 4 and has been published in Biogeosciences.

Chapter 4: An investigation into the importance of Antarctic krill for the efficient transfer of POC through the upper mesopelagic of the Southern Ocean. This chapter combines *in situ* observations of FP flux attenuation with historical krill density data to calculate FP attenuation rates, to assess whether krill FP can drive more efficient transfer of POC than typically assumed for bulk POC by many global biogeochemical models. This chapter addresses research aims 1 and 2, and is in review at Polar Biology.

Chapter 5: An extension of the work of chapter 4, making first order estimates as to whether the aforementioned flux of krill FP accounts for a substantial, and as yet poorly accounted for, part of total Southern Ocean export fluxes when scaled up to the whole marginal ice zone. In doing so, the aim is to establish whether there is a need for further measurements in other marginal ice zones to validate the importance of krill FP, and allow incorporation into biogeochemical models. This chapter addresses research aims 1 and 2.

Chapter 6: This chapter aims to assimilate the results of the previous chapters, enabling overarching conclusions based on the entirety of the work in this thesis. In addition, the areas for future work highlighted by this PhD thesis are discussed.

# Chapter 2. The role of particle-associated microbes in remineralisation of faecal pellets in the upper mesopelagic of the Scotia Sea, Antarctica

This chapter had been published in Limnology and Oceanography as:

Belcher, A. Iversen, M. Manno, C. Henson, S.A. Tarling, G. Sanders, R. 2016. The role of particle associated microbes in remineralization of fecal pellets in the upper mesopelagic of the Scotia Sea, Antarctica*, Limnology and Oceanography*, 61 (3), 1049-1064, DOI: 10.1002/lno.10269.

Additional material has been added to the methods section as well as new zooplankton data. A. Belcher collected the field data, carried out the data analysis and wrote and edited the manuscript. M. Iversen supported the development of techniques to measure respiration rates on individual particles and provided technical advice on analysis of these data. C. Manno provided advice on faecal pellet identification. S. Henson and R. Sanders were involved in early hypothesis development and G. Tarling provided supporting data and advice on zooplankton populations. In addition new zooplankton data added following publication were provided by P. Ward from the British Antarctic Survey.

## 2.1 Abstract

Faecal pellets (FP) are a key component of the biological carbon pump, as they can, under some circumstances, efficiently transfer carbon to depth. Like other forms of particulate organic carbon (POC), they can be remineralised in the ocean interior (particularly in the upper 200 m), or alternatively they can be preserved in the sediments. The controls on the attenuation of FP flux with depth are not fully understood, in particular, the relative contributions of zooplankton fragmentation and microbial/zooplankton respiration to FP loss. Collection of sinking particles using Marine Snow Catchers at three ecologically contrasting sites in the Scotia Sea, Antarctica, revealed large differences in the type of sinking POC (5-96% FP) and the POC flux attenuation despite similar temperatures. To determine the importance of microbial respiration on FP loss in the upper mesopelagic, small scale oxygen gradients were measured through the boundary layer at the interface of krill FP collected from the Scotia Sea. Estimated rates of carbon-specific microbial respiration within FP (0.010 - 0.065 $d^{-1}$) were too low to account for the observed large decreases in FP flux over the upper 200 m. Therefore, the observed rapid declines in downward FP flux in the upper mesopelagic are more likely to be caused by zooplankton, through

coprophagy, coprorhexy, and coprochaly. Microbial respiration is likely to be more important in regions of higher temperatures, and at times of the year (such as before the spring bloom), or in depths of the ocean, where zooplankton abundances are low and therefore grazing and fragmentation processes are reduced.

## 2.2 Introduction

The biological carbon pump drives the transfer of carbon from the atmosphere, through the ocean interior and ultimately to the deep ocean and sediments (Volk and Hoffert 1985), reducing levels of carbon dioxide ($CO_2$) in the atmosphere. However, of the 5-20 GtC $yr^{-1}$ that is estimated to be exported out of the euphotic zone globally (Henson et al. 2011), only a minor fraction reaches the sea bed. The reduction in particulate organic carbon (POC) flux with depth (attenuation) is particularly rapid in the upper mesopelagic, driven by microbial remineralisation, zooplankton grazing and, coprophagy (ingestion of faecal pellets (FP)), coprorhexy (fragmentation of FP), coprochaly (removal of FP membrane), as well as physical aggregation and disaggregation (Lampitt et al. 1990; Wilson et al. 2008; Poulsen and Iversen 2008; Turner 2015). However, the practical difficulties of making measurements in this dynamic region of the ocean mean that, despite the importance of remineralisation depth to atmospheric $CO_2$ levels (Kwon et al. 2009), the balance of processes determining POC flux attenuation are poorly understood (Giering et al. 2014).

The repackaging of phytoplankton, and loosely packed slow-sinking aggregates, into fast-sinking FP by zooplankton may increase greatly transfer efficiencies through the mesopelagic. FP can be a substantial component of deep sea sediment trap fluxes, but this contribution is highly variable, both spatially and temporally (Wilson et al. 2013; Manno et al. 2015; Turner 2015). Zooplankton may attenuate the flux of POC producing smaller, slower sinking particles that are more readily accessible to marine microbes (Lampitt et al. 1990; Iversen and Poulsen 2007; Mayor et al. 2014). Temperature has also been identified as a main control on POC flux attenuation, with higher temperatures driving increased rates of heterotrophic respiration and high attenuation (Iversen and Ploug 2013; Marsay et al. 2015). However, it is not clear whether processes such as particle type and lability, and zooplankton fragmentation and grazing, play a minimal role on flux attenuation, or whether temperature acts as a proxy for these variations. In order to establish whether the temperature trend suggested by Marsay et al. (2015) is applicable globally, these biological processes need to be investigated in regions where temperature is invariant.

Studies aiming to identify the main mechanisms controlling the retention of FP in the upper mesopelagic have drawn differing conclusions. Jing et al. (2012) found that FP are rapidly

colonised by free-living bacteria which may contribute significantly to their degradation, whereas Cnudde et al. (2013) suggest that degradation by bacteria packed inside the FP is equally important. Conversely, FP incubations carried out by Poulsen and Iversen (2008) demonstrated that protozooplankton were the main driver of FP remineralisation. More recently, it has been suggested that interactive effects must be considered, with the mechanical break up of large FP by copepods supporting further degradation by dinoflagellates (Giering et al. 2014; Svensen et al. 2014).

Considering the important (and at times dominant) role that FP play in the transfer of carbon out of the upper ocean and to the deep sea, an improved understanding of the balance between zooplankton and microbial decomposition of FP within the mesopelagic is needed (Steinberg et al. 2008; Iversen et al. 2010; Giering et al. 2014). This requires not only knowledge of mesopelagic POC flux, but also the type of sinking material, rates of microbial respiration on sinking particles, as well as concurrent information on ecosystem structure.

In this study, particle flux and type were measured at a number of sites in the Scotia Sea, Antarctica. The Scotia Sea contains several diverse oceanographic regimes within a narrow range of temperatures, providing an ideal setting to assess the balance of microbial and zooplankton degradation processes without the added complication of temperature variability. It is hypothesised that contrasting community structures will lead to differences in particle flux and flux attenuation, despite similar temperatures. The first direct measurements of microbial respiration rates of *Euphausia superba* FP are presented and these rates are used to assess the balance between zooplankton- and microbe-driven flux attenuation processes in the upper mesopelagic.

## 2.3 Materials and methods

Total particle flux and oxygen concentration gradients of particles were measured on *RRS James Clark Ross* cruise JR304 to the Scotia Sea, Antarctica in austral spring 2014 (Figure 2-1). Samples were collected from three main sites, P2 and P3, upstream and downstream of South Georgia (at 55.248 °S, 41.265 °W and 52.812 °S, 39.972 °W respectively), and ICE (59.962 °S, 46.160 °W). The ICE station was characteristic of the marginal ice zone with intermittent ice cover in the weeks prior to sampling. Additional FP were obtained from the Western Core Box site (Figure 2-1). Vertical profiles of the water column at each site were made using a Conductivity-Temperature-Depth (CTD) unit (Seabird 9Plus with SBE32 carousel); these profiles were used to define the base of the mixed layer for further instrument deployments.

### 2.3.1 Chlorophyll-a

Water samples (300 ml) for chlorophyll-a were taken from the ship's uncontaminated underway supply (6 m) and the CTD rosette, filtered onto 0.8 $\mu$m MPF300 glass fibre filters, and frozen at -20 °C. Samples were extracted in 90% acetone for 22-24 hours at 4 °C and fluorescence measured on a Trilogy Turner Designs 7200 lab fluorometer calibrated with a pure chlorophyll-a standard (Sigma, UK).

Aqua MODIS 9 km, 8-day satellite chlorophyll-a data (downloaded from the NASA Ocean Biology website; http://oceancolor.gsfc.nasa.gov/cms/) were averaged over a 110x110 km box (~1 ° latitude) centred on each station, to provide seasonal context and allow bloom timing to be inferred.

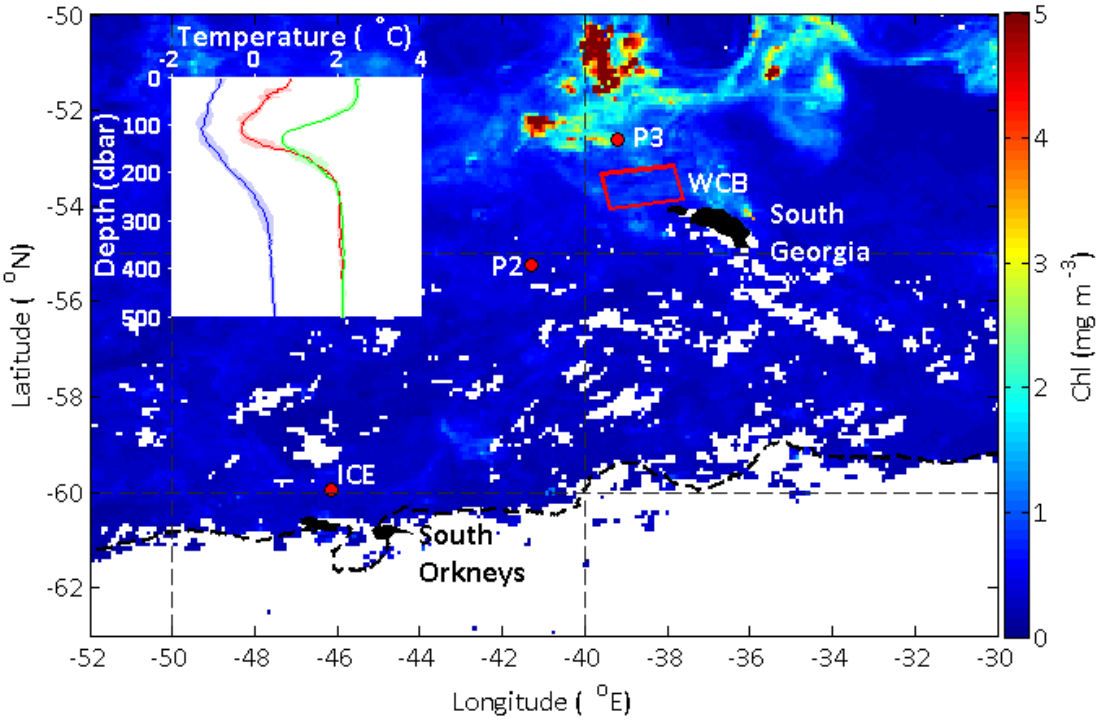


**Figure 2-1: Station locations (indicated by red circles and red square) overlain on MODIS Aqua satellite chlorophyll for December 2014. Position of ice edge on December 14th 2014 shown by black dotted line (OSTIA sea ice data). Inset displays vertical temperature profiles at ICE (blue), P2 (red) and P3 (green), lighter shades indicate standard deviations based on multiple deployments at each site.**

### 2.3.2 Particle flux and type

Sinking marine particles were collected using Marine Snow Catchers (MSC), large (95 L) PVC closing water bottles designed to minimise turbulence (Lampitt et al. 1993). MSCs were deployed

in rapid succession at 10 and 110 m below the base of the mixed layer depth (MLD), identified from the most recent CTD profile, herein referred to as MLD+10 and MLD+110. As MLD were defined visually from CTD profiles, we conservatively sample at 10 m below the MLD to avoid sampling within the mixed layer. This resulted in sampling between 39 and 183 m. The strategy of sampling at fixed depths relative to a variable mixed layer depth, rather than at absolute depths, allows comparison of export flux between sites (Buesseler and Boyd 2009). MSCs were deployed at 4-5 time points within a 36 hour period at each station.

**Table 2-1: MSC deployments during cruise JR304 to the Scotia Sea, Antarctica**

| Site | Latitude | Longitude | Date | Time (GMT) | Time of Day | Depth of MSC (m) |
|---|---|---|---|---|---|---|
| ICE | -59.9623 | -46.1598 | 25/11/2014 | 10:16 | Day | 60 |
| ICE | -59.9623 | -46.1598 | 25/11/2014 | 10:38 | Day | 160 |
| ICE | -59.9623 | -46.1597 | 25/11/2014 | 18:18 | Day | 71 |
| ICE | -59.9623 | -46.1597 | 25/11/2014 | 18:39 | Day | 172 |
| ICE | -59.9623 | -46.1597 | 26/11/2014 | 00:55 | Night | 72 |
| ICE | -59.9623 | -46.1597 | 26/11/2014 | 01:19 | Night | 172 |
| ICE | -59.9629 | -46.1603 | 26/11/2014 | 16:44 | Day | 61 |
| ICE | -59.9629 | -46.1603 | 26/11/2014 | 17:12 | Day | 163 |
| P2 | -55.2527 | -41.3022 | 28/11/2014 | 11:33 | Day | 55 |
| P2 | -55.2527 | -41.3022 | 28/11/2014 | 11:51 | Day | 157 |
| P2 | -55.2484 | -41.2640 | 28/11/2014 | 20:14 | Day | 57 |
| P2 | -55.2484 | -41.2640 | 28/11/2014 | 20:30 | Day | 159 |
| P2 | -55.2477 | -41.2649 | 29/11/2014 | 03:16 | Night | 37 |
| P2 | -55.2477 | -41.2661 | 29/11/2014 | 03:53 | Night | 140 |
| P2 | -55.2477 | -41.2649 | 29/11/2014 | 09:54 | Day | 39 |
| P2 | -55.2477 | -41.2649 | 29/11/2014 | 10:07 | Day | 138 |
| P2 | -55.2475 | -41.2651 | 29/11/2014 | 17:34 | Day | 47 |
| P3 | -52.8116 | -39.9727 | 12/12/2014 | 22:14 | Sunset | 73 |
| P3 | -52.8116 | -39.9727 | 12/12/2014 | 22:40 | Sunset | 176 |
| P3 | -52.8120 | -39.9725 | 13/12/2014 | 07:53 | Day | 74 |
| P3 | -52.8120 | -39.9725 | 13/12/2014 | 08:24 | Day | 176 |
| P3 | -52.7623 | -40.3038 | 13/12/2014 | 14:11 | Day | 72 |
| P3 | -52.8118 | -39.9727 | 13/12/2014 | 22:25 | Sunset | 81 |
| P3 | -52.8118 | -39.9726 | 13/12/2014 | 22:47 | Sunset | 183 |

Following a two hour settling period (Riley et al. 2012), the particle collector tray (divided into four quadrants to allow sample splitting) was carefully removed from the base of the MSC and stored at 4 °C for further analysis. The particles that sank fast enough to reach the particle collector tray in the two hour settling period (here termed 'fast-sinking particles'), were picked from three quadrants using a wide-bore pipette, filtered onto pre-combusted (450 °C, 24 h) glass fibre filters (25 mm diameter GF/F, Whatman), and oven dried at 50 °C for replicate analysis of POC. Filters were subsequently fumed with 37% HCl in a vacuum desiccator for 24 hours, and

dried for 24 hours at 50 °C. Filters and filter blanks were placed in pre-combusted (450 °C, 24 h) tin capsules as in Hilton et al. (1986), and POC measured by a CE-440 elemental analyser (Exeter Analytical.285 Inc).

Particles in the remaining quadrant were used to estimate sinking velocity and to make respiration rate measurements. POC fluxes (*F*) were calculated as follows:

$$\boldsymbol{F\left(mg\ m^{-2}\ d^{-1}\right)} = \frac{\boldsymbol{Mass}}{\boldsymbol{Area}} \times \frac{\boldsymbol{w}}{\boldsymbol{l}}, \qquad \textbf{(Equation 2-1)}$$

where *mass* refers to the total mass (mg) of sinking POC collected from the MSC, *area* the area of the MSC opening based on inner MSC diameter, *w* the measured sinking velocity (m $d^{-1}$), and *l* the length of the snow catcher (1.53 m). Particle sinking velocities of particles visible by eye (Equivalent Spherical Diameter (ESD) > 0.15 mm) at each site were measured using a flow chamber (as for FP, see later section), and the mean value for each site used for flux calculations. Flux attenuation was assessed via a measure of transfer efficiency, $T_{100}$, the ratio of POC flux at MLD+110 to the POC flux at MLD+10 (Buesseler and Boyd 2009). An exponential fit has been applied to the POC flux data and the remineralisation length scale ($z^*$) (Boyd and Trull 2007) calculated:

$$\boldsymbol{F_z = F_{z0} \times exp\frac{(z-z_0)}{z^*}} \qquad \textbf{(Equation 2-2)}$$

where $z$ is the depth of the flux, $F_{z0}$ is flux at the reference depth (in this case MLD+10), and $F_z$ the flux MLD+110. Attenuation coefficients (*b* values) were also calculated following the commonly used method of Martin et al. (1987):

$$\boldsymbol{F_z = F_{z0} \times (z/z_0)^{-b}} \qquad \textbf{(Equation 2-3)}$$

High values of *b* are indicative of shallow remineralisation and low values of deep remineralisation. These methods of assessment of POC flux attenuation do not consider any *in situ* particle production between POC measurement depths and hence represent lower bound estimates of flux attenuation. In addition they do not take into account addition or removal processes via lateral advection.

Additionally, at each site, particle type was assessed through microscopic analysis of the collected sinking material. Particles were photographed using an Olympus SZX16 microscope with Canon EOS 60D camera and Olympus BX-SZX Micro Cam, and classified into: faecal pellets, faecal pellet fluff, phytodetrital aggregates, phytoplankton cells, zooplankton, lithogenic material and unidentified phytodetritus. Phytodetrital aggregates were identified as aggregations >0.1 mm ESD containing phytoplankton cells and other phytodetrital material. Individual particle dimensions were measured using ImagePro and volumes calculated using formulae for a sphere, ellipsoid or

cylinder depending on particle shape. Conversions from phytoplankton cell volume to carbon were based on the equation of Menden-Deuer and Lessard (2000) for diatoms >3000 µm$^3$ : *log (pgCcell$^{-1}$) = -0.933 + 0.881 · log(Volume (µm$^3$)*, and conversions from phytodetrital aggregate volume to carbon based on the equation of Alldredge (1998): *µC agg$^{-1}$= 0.99 · (Volume (mm$^3$)$^{0.52}$)*. The carbon content of faecal pellets (FP) was estimated based on POC to volume ratios calculated from FP collected during the research cruise (see following section). These size based estimates of POC content are associated with potentially large, but generally unquantifiable, uncertainties and carbon flux estimates are probably accurate to an order of magnitude. However, direct measurements are not easily obtained in the field for all particles and usage of these parameterisations is consistent with previous studies (Alldredge 1998; Ebersbach et al. 2011; Laurenceau-Cornec et al. 2015a) supporting the use of this method to make inter-site comparisons.

### 2.3.3 Faecal pellet collection

Several methods were employed to collect additional FP from the Scotia Sea for use in microbial respiration experiments. At the ICE station, paired motion-compensating Bongo nets (61 cm mouth diameter, 2.8 m long, 100 and 200 µm mesh) were deployed to 100-200 m and hauled vertically to the surface at about 0.22 m s$^{-1}$. This depth range encompasses the region where zooplankton populations are likely to be feeding and hence producing FP (Fielding et al. 2012; Ward et al. 2012a). FP believed to be from *Euphausia superba* (Figure 2-2G, assessed visually by a zooplankton taxonomist via comparison with FP from egestion experiments (see below)) were picked using a wide bore pipette, rinsed three times with filtered sea water and stored at 4 °C until analysis (Figure 2-2A). There is a chance that this rinsing may have removed some of the attached microbes from the particles which would result in an underestimation of respiration rates. Some FP were also collected using the MSC at P2 (e.g. Figure 2-2D, Figure 2-2F) at a depth of 45 m (just below the base of the mixed layer), where particle concentrations were expected to be higher (Prairie et al. 2013).

Additional FP for microbial respiration studies were obtained via targeted and non-targeted trawls for krill at the Western Core Box site (Figure 2-1) using an RMT 8 (Rectangular Midwater Trawl, Roe and Shale 1979). This consists of two opening and closing nets (4 mm mesh) activated by a telemetering net monitor that provided real time information on water depth as well as environmental parameters such as temperature and salinity. Samples were obtained from two trawls carried out in the upper 50 m of the water column, where krill populations are likely to reside at night (Fielding et al. 2012). Undamaged individuals of *Euphausia superba* were carefully picked from the cod-ends and transferred into buckets containing surface seawater from the

ship's underway system. The buckets were stored in a temperature controlled room (4 °C) for 3-5 hours to allow *E. superba* to egest their gut contents. FP were then carefully picked (Figure 2-2G), rinsed three times with filtered sea water (0.22 µm) and stored at 4 °C until analysis. *Euphausia superba* are a major component in the Scotia Sea ecosystem (Murphy et al. 2007) and the occurrence of large swarms (Fielding et al. 2012) have the potential to support POC transfer to the deep ocean through the production of large FP which can sink quickly through the mesopelagic (Atkinson et al. 2012; Manno et al. 2015).

### 2.3.4 Oxygen fluxes and respiration rates

Respiration rates of the microbial communities associated with FP (collected as described above) were calculated from direct measurements of oxygen gradients using microsensors and a temperature controlled flow chamber system (Appendix Figure A1, A2) (Ploug and Jorgensen 1999). The flow chamber contained filtered sea water (0.22 µm), taken from the MSC deployed at each site or the ship's underway system in the case of the Western Core Box. Within 24 hours of collection, FP were placed carefully in the flow chamber, their x, y, and z dimensions measured using a horizontal dissection microscope with a calibrated ocular. ESD was calculated based on cylindrical or spherical volumes. Flow was then supplied from below the net, adjusted using a needle valve, resulting in a uniform flow field across the upper chamber. The flow was adjusted so that the FP was suspended one particle diameter above the net. At this point the sinking velocity is balanced by the upward flow velocity (Ploug et al. 2010). Three sinking velocity measurements were made for each FP.

The oxygen gradients (in steps of 10-50 $\mu$m) were measured through the diffusive boundary layer (DBL) downstream of the FP, between the FP surface and surrounding water using a Clark-type oxygen microelectrode with a guard cathode (Revsbech 1989) mounted in a micromanipulator. Sensors were calibrated at 0% and 100% oxygen. The microsensor had a tip diameter of 10 µm, with a 90% response time of <1 s and stirring sensitivity of <0.3%. Net oxygen fluxes of sinking aggregates measured on the upstream and downstream side were previously shown not to be significantly different (Ploug and Jorgensen 1999). The surface of the FP was penetrated with the microsensor but complete profiles through the centre of the FP were often not possible due to FP stickiness and the potential to damage the microsensor and break the FP.

Despite the relatively small size of FP, thin DBLs and the dynamic nature of shipboard laboratory work, a total of 22 FP were measured, and 2-3 replicate profiles were taken for each FP where possible. Oxygen fluxes were calculated using a diffusion-reaction model based on Fick's first law of diffusion, using temperature and salinity corrected oxygen diffusion coefficients of 1.171-1.253

x $10^{-5}$ $cm^2$ $s^{-1}$ based on experimental temperatures of 3-5 °C (Broecker and Peng 1974). An Excel solver routine was utilised to find the optimum solution minimising the sum of the squares between measured and modelled oxygen concentrations (Ploug et al. 1997). At steady state, the area integrated flux of oxygen through the DBL is equal to the total oxygen being consumed by the microbial community associated with the FP due to the net exchange of oxygen via molecular diffusion. The volumetric oxygen respiration rate can therefore be determined from measured oxygen concentration gradients and calculations of the thickness of the DBL. Total oxygen consumption within the FP was determined using geometric equations for the surface area of a cylinder, sphere or ellipsoid and carbon respiration calculated assuming a respiratory quotient of 1 mol $O_2$ to 1 mol $CO_2$ (Ploug et al. 1997; Ploug and Grossart 2000), which sits conservatively in the range of literature values typically applied (0.7-1.2) for respiration of carbohydrates and lipids (Berggren et al. 2012). Without more detailed knowledge of the exact composition of FP, or of the exact form of carbon utilised for microbial respiration, this represents the best available estimate.

### 2.3.5 Faecal pellet POC content

Where it was possible to collect large numbers of FP, CHN analysis of FP POC content was conducted. Carbon to volume ratios were calculated from FP egested from krill captured in RMT 8 nets at the Western Core Box site, and collected from Bongo nets at the ICE station. FP (10-15 per replicate filter) were rinsed three times in filtered sea water, photographed under a microscope to obtain size measurements, filtered onto pre-combusted glass fibre filters (25 mm diameter GF/F, Whatman) and oven dried at 50 °C for analysis of POC. Filters were subsequently fumed with 37% HCl in a vacuum desiccator for 24 hours, and dried for 24 hours at 50 °C. Filters and filter blanks were placed in pre-combusted (450 °C, 24 h) tin capsules as in Hilton et al. (1986), and POC measured in a CE-440 elemental analyser (Exeter Analytical.285 Inc). These experimentally derived values (0.022 – 0.058 mg C $mm^{-3}$) compare to literature values for euphausiid FP, which range from 0.016 mg C $mm^{-3}$ for FP collected in sediment traps in the upper 100 m in Norway (González 1992), to 0.0306 mg C $mm^{-3}$ for FP produced from egestion experiments from *Euphausia superba* collected from the Antarctic marginal ice zone (Suzuki et al. 2001).

### 2.3.6 Statistical analysis

To examine attenuation of POC with depth regression lines were fitted to the data using the statistical package R. The significance of calculated remineralisation length scales and Martin's *b* values were assessed via calculated $r^2$ and *p* values. Results for exponential and Martin (power-law) fits were similar, (e.g. at P2; exponential, $r^2 = 0.84$, $p<0.001$ and power, $r^2 = 0.84$, $p = 0.001$, and at P3; exponential, $r^2 = 0.71$, $p = 0.018$ and power, $r^2 = 0.70$, $p = 0.020$), so exponential fits are

used here as they are less sensitive to the choice of reference depth (Buesseler and Boyd 2009). Inter-site differences between sinking velocities of particles, and in particular of FP, were assessed via Student's T-tests and Mann-Whitney U-tests, after first testing data for normality and variance homogeneity. Trends between FP size (length, width, volume or ESD) and carbon-specific respiration rate were assessed via a linear model fit in R, and differences in carbon-specific respiration rates between sites evaluated via a Student's T-test. Results were considered significant only at the 95% level (i.e. when $p < 0.05$).

### 2.3.7 Ancillary zooplankton data

During the cruise, mesozooplankton samples were taken at each site using a paired motion-compensating Bongo net (61 cm mouth diameter, 2.8 m long, 100 µm mesh). The net was equipped with solid cod ends, deployed to 200 m and hauled vertically to the surface at about 0.22 m $s^{-1}$. Samples were preserved in 4% formalin (weight/volume) in seawater before being analysed using a binocular microscope. Zooplankton were identified to species/taxa and staged where appropriate. At least 500 individuals were counted per sample. Counts were converted into ind. $m^{-2}$ (0-200 m) based on the area of the Bongo net mouth and the depth of deployment. A total of 11 zooplankton net tows were carried out during the day and night, 5 at the ICE station, 3 at P3 and 3 at P2. Mean abundances were calculated for each species at each site.

## 2.4 Results

### 2.4.1 Hydrography and surface chlorophyll-a

Near surface chlorophyll-a from the underway system ranged from 0.34 to 6.68 mg $m^{-3}$ with the highest values occurring near P3. Near surface (5 m) samples from vertical CTD profiles display the same trend with highest concentrations (3.31-5.21 mg $m^{-3}$) at P3 and lower concentrations at P2 and ICE (0.61-0.76 mg $m^{-3}$ and 0.81-1.01 mg $m^{-3}$ respectively). Despite the limitations of cloud cover, satellite data suggest that P3 was sampled during the start of the spring bloom with surface chlorophyll-a concentrations doubling by mid-January. Conversely the ICE station was sampled before the seasonal peak at the end of December, and limited data at P2 suggest that samples were taken following a decline in surface chlorophyll-a.

Surface temperatures (mean over the upper 5 m) ranged from -0.81 °C at ICE, 0.89 °C at P2, and 2.47 °C at P3 (Figure 2-1–inset). Temperatures in the Western Core Box ranged from 1.1 – 3.8, averaging 1.9 °C.

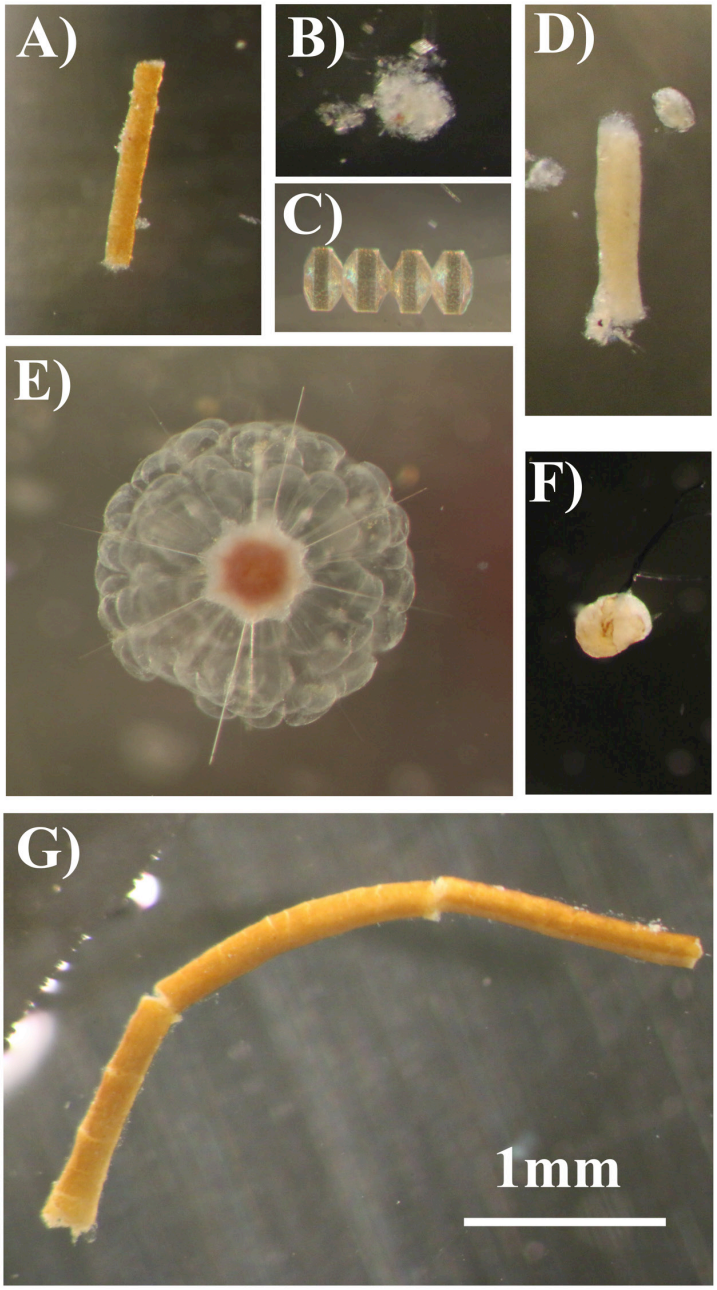


**Figure 2-2: Microscope photos of sinking material collected in Marine Snow Catchers, A) faecal pellet from ICE station, B) marine snow aggregate from P2, C) diatom chain from P2, D) cylindrical faecal pellet from P2, E) radiolarian from P2, F) round faecal pellet from P2, G) *Euphausia superba* faecal pellet from Western Core Box site. Scale bar refers to all photos.**

### 2.4.2 Sinking material

A total of 24 MSC deployments were made during the cruise (Table 2-1), with full microscopic analysis of particle type being carried out on 8 samples. In terms of carbon content, FP dominated POC flux (66.7-96.3%) at all depths and stations, with the exception of MLD+10 at P2, where

phytoplankton cells accounted for 86.1% of the flux (Figure 2-3). Phytodetrital aggregates (Figure 2-2B) were a minor component of the POC flux, accounting for <10% at all stations.

### 2.4.3 POC flux

Particle sinking velocities ranged from 2-570 m $d^{-1}$ with mean velocities of 151, 144, and 88 m $d^{-1}$ at ICE, P2, and P3 respectively. However, intra site variability was large (2-507, 9-570 and 13-371 m $d^{-1}$ at ICE, P2 and P3 respectively) reflecting the range of particle types, shapes and densities. Sinking velocity distributions were non-normal and only P3 and ICE were found to be statistically different (Mann-Whitney U-test, $p = 0.006$). Sinking velocity measurements were limited to those particles visible by eye (ESD > 0.15 mm) and hence averages are an upper estimate. Measured velocities do however agree well with previous measurements in the Southern Ocean ranging from 50-430 m $d^{-1}$ (Fischer and Karakas 2009; Cavan et al. 2015).

POC fluxes at the base of the mixed layer (MLD+10) ranged from 172 mg C $m^{-2}$ $d^{-1}$ at ICE, to 1454 mg C $m^{-2}$ $d^{-1}$ at P2 (Figure 2-4). One significantly higher value (5668 mg C $m^{-2}$ $d^{-1}$) was observed at P2 due to the occurrence of siphonophore remains in the sample, highlighting the high temporal variability and episodic nature of flux events. Exponential curves have been fitted to flux data (Figure 2-4), providing a statistically significant fit at P2 ($p < 0.001$) and P3 ($p = 0.018$), but not at ICE ($p = 0.419$) where flux attenuation was low and even negative in one case. The extreme POC flux observed at P2 was excluded from this fit.

Flux attenuation between MLD+10 and MLD+110 was quite variable, both spatially and temporally. Rapid POC flux attenuation was measured at P2, with $T_{100}$ from 2.6% to 38.8% (mean 18%, and *b* value 1.60), and slower remineralisation at P3 ($T_{100}$ from 36.7% to 80.9%, mean 55%, and *b* value 0.78). The highest $T_{100}$ values and hence highest transfer efficiencies occurred at the ICE station (maximum $T_{100}$ of 84.9% and *b* of 0.19) and, at one time point, the flux actually increased with depth. Calculation of $T_{100}$ values based on mean POC fluxes at MLD+10 and MLD+110 at each station revealed the same trend, with higher attenuation at P2 ($T_{100} = 20.6\%$, $b = 1.43$) and lower attenuation at P3 and ICE ($T_{100} = 55.1\%$, $b = 0.69$, and $T_{100} = 80.7\%$, $b = 0.23$ respectively). The range in measured sinking velocities was large and without full knowledge of the particle spectrum adds uncertainty to POC flux calculations. Therefore, a sensitivity analysis has been carried out to assess the influence of changing sinking rates on POC flux. Recalculating POC fluxes based on mean sinking rates ± one standard error, result in POC fluxes changing by just ± 12-15% providing confidence in the calculated attenuation rates.

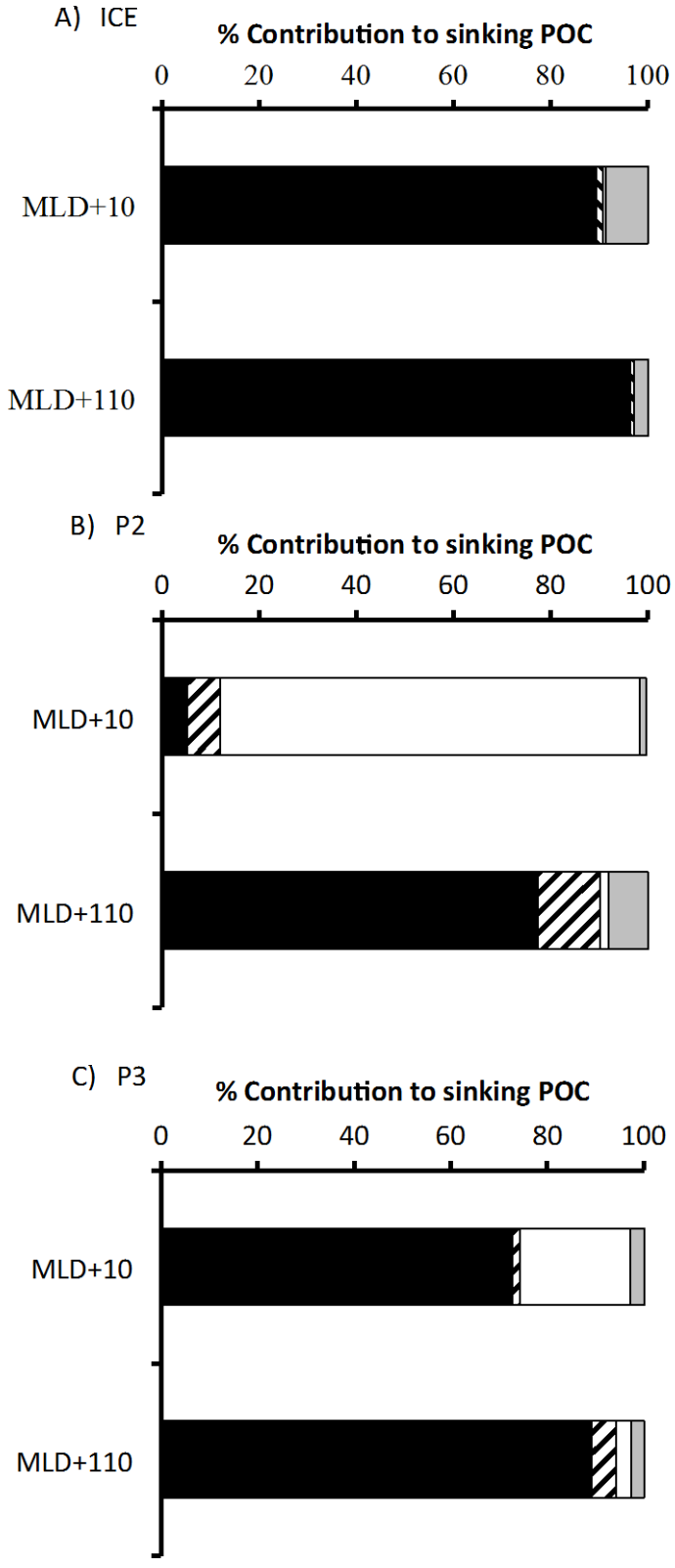


**Figure 2-3: Composition (particle type) of fast-sinking POC at A) ICE, B) P2, and C) P3 stations based on microscope analysis and calculated carbon content. Black = faecal pellets, hashed = phytodetrital aggregates, white = phytoplankton cells and grey = other. MLD+10 and MLD+110 represent measurements at 10 and 110 m below the base of the mixed layer depth (MLD) respectively.**

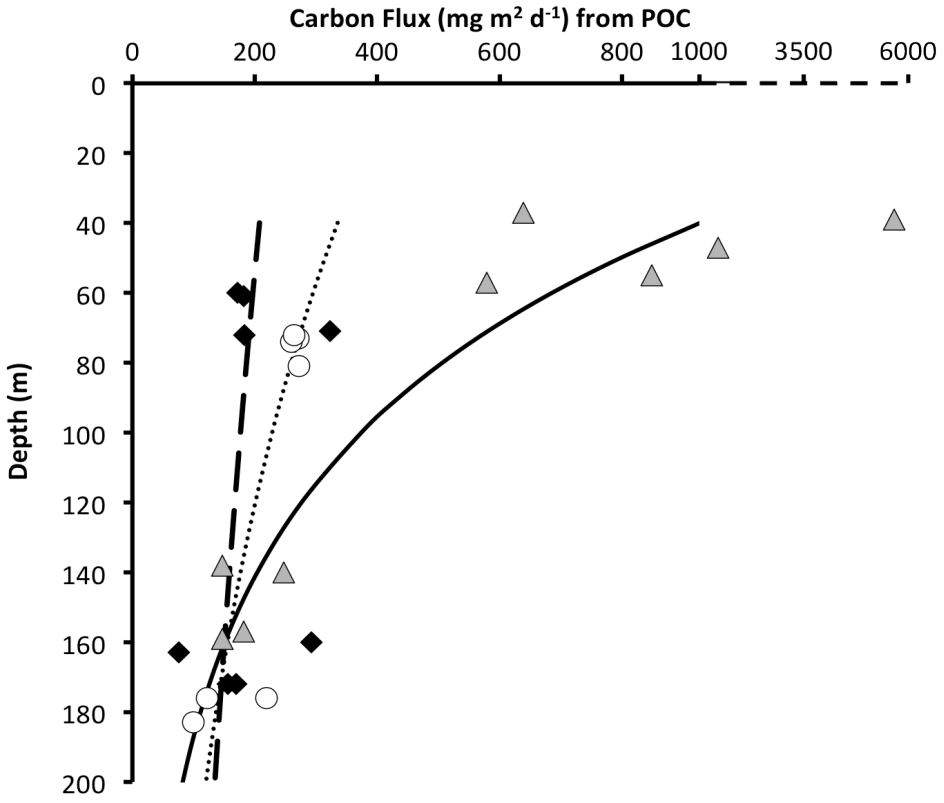


**Figure 2-4: Flux of particulate organic carbon (POC mg C $m^{-2}$ $d^{-1}$) measured at a number of time points over the diel cycle at ICE (black diamonds), P2 (grey triangle) and P3 (open circle) in the Scotia Sea Antarctica. Exponential curves have been plotted for ICE (thick black dashed), P2 (solid black) and P3 (dotted) to illustrate flux attenuation, $p < 0.001$, 0.018 and 0.419 at P2, P3 and ICE respectively. Note the break in the x axis scale for extreme value at P2 which has been excluded from the exponential fit.**

### 2.4.4 Faecal pellet flux

Microscope analysis of particles collected in Marine Snow Catchers revealed two clear morphological types of FP, cylindrical and round, with cylindrical FP dominating at ICE and P3 stations (80-100%) and round FP being more important at P2 (63-78%). A couple of ellipsoidal FP were also observed at P2 and ICE. FP ranged in colour: dark orange, brown, yellow and white/translucent, but there were no clear trends with depth or station. Mean FP size was lower at P2 and P3 (ESD = 0.25 mm and 0.24 mm respectively), compared to ICE (ESD = 0.31 mm), due to the dominance of cylindrical FP at ICE. Cylindrical FP were significantly larger (ESD = 0.29 mm) than round FP (ESD = 0.21 mm) across all sites (Student's t-test $p < 0.05$).

Sinking velocities of FP at P3 (mean 88 m $d^{-1}$) were statistically lower than those at P2 and ICE (195 m $d^{-1}$ and 168 m $d^{-1}$ respectively, Mann-Whitney U-test $p < 0.005$), however data were limited to 10 measurements at P2. FP POC fluxes showed similar patterns of decline as observed for the POC

fluxes, with higher attenuation at P2 and P3 ($T_{100}$of 59% and 42% respectively) compared to ICE where only a slight decrease in FP POC flux was measured ($T_{100}$ = 93%). Despite a decrease in abundance of FP with depth at each station, the percentage contribution of FP increased, due primarily to the rapid decrease in the number of sinking phytoplankton cells, suggesting a higher transfer efficiency of FP, an additional deeper source of FP or diel vertical migration.

### 2.4.5 Microbial respiration rates

FP used for respiration experiments were predominantly cylindrical, with the exception of one round FP (0.37 mm diameter) collected at P2 from the Marine Snow Catcher. At ICE and P3 cylindrical FP accounted for >80% of FP and data are thus broadly representative of the mean conditions at those stations. The data presented here may be less applicable to P2 where round FP were dominant and as such respiration measurements on other FP morphologies are an important area of further research. Cylindrical FP used in respiration experiments ranged in length from 0.95 to 5.37 mm, (mean 2.01 mm), and in width from 0.21 to 0.42 mm (mean 0.28 mm). Sinking velocities of FP used for respiration measurements were between 177 m $d^{-1}$ and 663 m $d^{-1}$ (mean 351 m $d^{-1}$) (Figure 2-5A, Table 2-2). Sinking velocities of FP collected at the Western Core Box site were higher (mean 413 m $d^{-1}$) than those from ICE and P2 stations (mean 263 m $d^{-1}$) (Student's t-test $p < 0.005$).

**Table 2-2: Size and respiration rates of FP measured in the Scotia Sea, Antarctica**

| | FP volume (x $10^7$ $\mu m^3$) | FP sinking velocity (m $d^{-1}$) | POC:volume ratio (mg C $mm^{-3}$) | Total $O_2$ consumption (nmol $O_2$ $FP^{-1}$ $hr^{-1}$) | Volumetric $O_2$ consumption (fmol $O_2$ $\mu m^{-3}$ $d^{-1}$) | Carbon respiration rate (ng C $FP^{-1}$ $h^{-1}$) | Carbon-specific respiration rate ($d^{-1}$) |
|---|---|---|---|---|---|---|---|
| Mean | 11.9 | 351 | 0.036 | 0.433 | 0.085 | 5.19 | 0.028 |
| Maximum | 32.5 | 663 | 0.058 | 1.630 | 0.172 | 19.56 | 0.065 |
| Minimum | 1.9 | 177 | 0.022 | 0.082 | 0.028 | 0.98 | 0.010 |

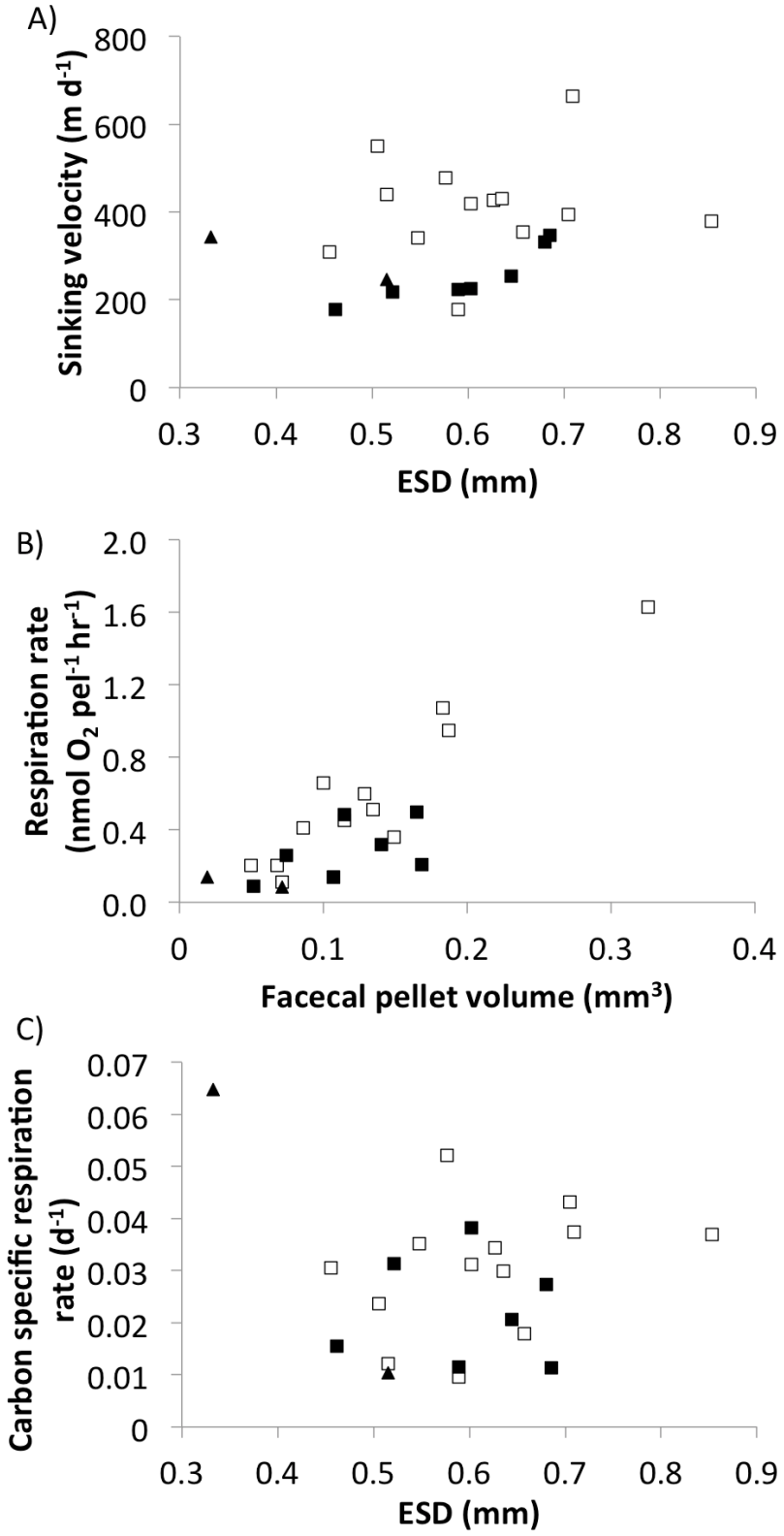


**Figure 2-5: Sinking velocities and respiration rates of FP collected at the Western Core Box (open squares), ICE (filled squares) and P2 (filled triangles) stations. A) FP sinking velocity versus equivalent spherical diameter (ESD), B) FP respiration rate versus FP volume with linear fit (Y = 4.8208X -0.1497, $R^2$ = 0.56 (Pearson's correlation), $p$ < 0.001), C) Carbon-specific respiration rates versus FP ESD (no significant relationship, $p$ > 0.05).**

The carbon content of FP ranged from 0.022-0.058 mg C $mm^{-3}$ which, based on the range of observed FP colours from light yellow to yellow-brown, may reflect variability in the type and abundance of food available for *Euphausia superba*, as well as the feeding state of the individual producing the FP (Urban-Rich et al. 1998). Lighter, translucent FP may be indicative of feeding on detritus, whereas brown colours may indicate feeding on phytoplankton, and lighter brown colours on a mixture of diatoms, protists and marine snow (Wilson et al. 2008).

In agreement with the one other published study of this kind (Ploug et al. 2008b), measured diffusive boundary layers (DBL) of FP were thin, ranging from 23-98 $\mu$m. Oxygen concentrations decreased towards the water-pellet interface and, on the occasions where the FP remained intact when penetrated, oxygen concentrations continued to decrease within the FP, but were still well above anoxic conditions. Oxygen fluxes to the FP ranged from 0.082-1.630 nmol $O_2$ $FP^{-1}$ $hr^{-1}$ (mean 0.433), increasing with FP ESD ($R^2$ = 0.56 (Pearson's correlation), $p < 0.001$) (Figure 2-5B). This corresponds to volumetric fluxes (oxygen flux per unit volume of FP) of 0.028-0.172 fmol $O_2$ $\mu m^{-3}$ $d^{-1}$ (mean 0.085 fmol $O_2$ $\mu m^{-3}$ $d^{-1}$), and respiration rates of 0.98-19.56 ng C $FP^{-1}$ $h^{-1}$ (mean 5.19 ng C $FP^{-1}$ $h^{-1}$) (Table 2-2). Respiration rates increased linearly with FP POC, although this is in part due to the constant FP carbon to volume ratio used for each site (see below) and hence reflects the trends shown in Figure 2-5B.

### 2.4.6 Zooplankton abundance

Zooplankton abundances in the upper 200 m were 10 and 19 times higher at P2 and P3 respectively when compared to those at the ICE station (Figure 2-6A). Copepods were the most abundant at all three stations, however it is important to note that the method of sampling utilised here does not allow for accurate quantification of *Euphausia superba* (Antarctic krill) due to the patchy distribution of swarms. Small microcopepod species (*Oithona* spp., *Oncaea* sp. *Microcalanus* sp. and *Ctenocalanus* sp.) were numerically dominant at all stations (Figure 2-6B), when compared to the main large calanoid copepod species (*Rhincalanus gigas, Calanoides acutus, Calanus similimus, Calanus propinquus, Euchaeta* spp. and *Metridia* spp).

## 2.5 Discussion

### 2.5.1 Role of bloom timing in export flux

Highest POC fluxes at the base of the mixed layer (MLD+10) were recorded at P2 despite low surface chlorophyll-a, and were likely associated with the declining phase of the bloom (suggested by satellite data). The observed high fluxes out of the euphotic zone at P2, which were composed

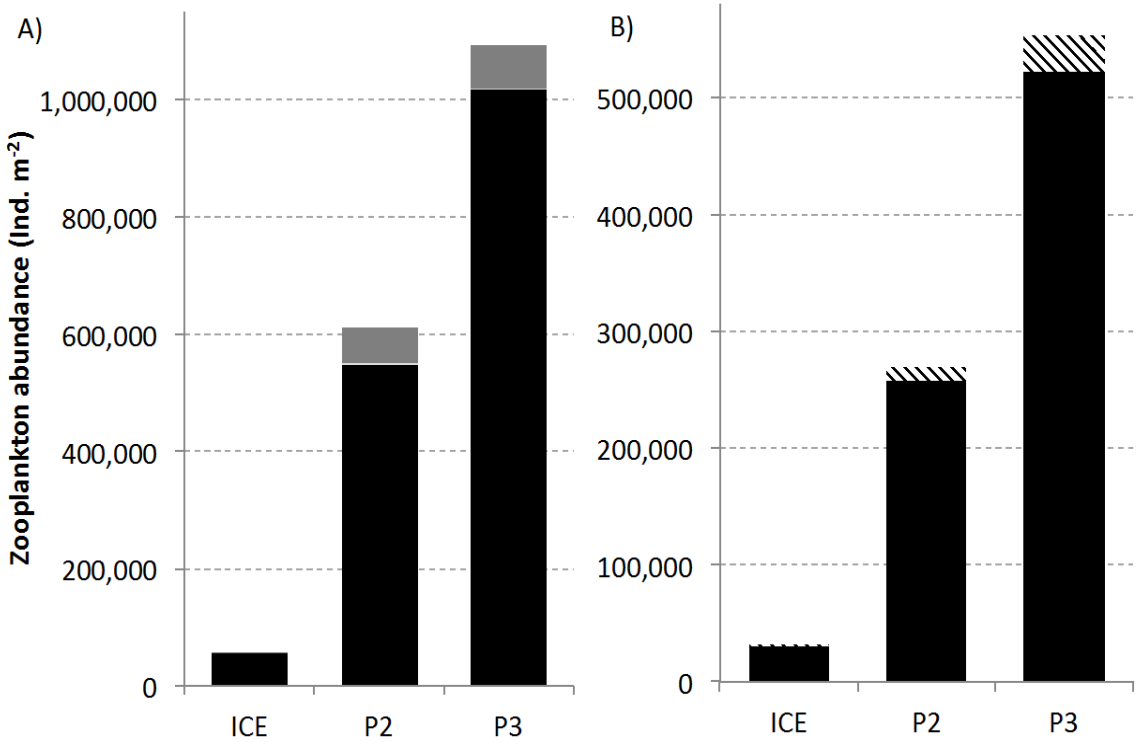


**Figure 2-6: Zooplankton abundances (ind. $m^{-2}$ (0-200m)) measured in the Scotia Sea in December 2014 using a 100 µm mesh. A) Copepods (black), euphausiids (light grey), other (dark grey). B) Copepod abundances (excluding nauplii) divided into two groups; small microcopepods (black), and large calanoids (hashed) (see text for full details on groups).**

mainly of individual and chained phytoplankton cells (86%), may have resulted from increased cell death and bloom decline due to nutrient limitation (e.g. Thornton 2002).

The region downstream of the islands of South Georgia (encompassing the P3 site) is characterised by large spring phytoplankton blooms (Borrione and Schlitzer 2013) supported by increased iron supply from the shelf sediments of South Georgia (Nielsdóttir et al. 2012). These large blooms result in high fluxes of material to the deep ocean (Manno et al. 2015), yet low POC fluxes were observed at the base of the mixed layer at P3 (2-10 times smaller than at P2) despite high and increasing surface chlorophyll-a. Lower contributions of phytoplankton cells to sinking POC flux at P3 (25%) support the idea of an actively growing phytoplankton population, and fewer dead and senescent cells sinking out of the euphotic zone. At this early stage of the bloom, decoupling between primary producers and their consumers likely results in a lag between primary production and export, in agreement with model studies predicting a lag of 20-30 days in the Southern Ocean (Henson et al. 2015).

As expected at this time of year (Ward et al. 2012b), low chlorophyll-a levels were measured at the ICE station, and this early phase of production may explain the observed low fluxes of POC out of the euphotic zone (mean 215 mg C $m^{-2}$ $d^{-1}$).

### 2.5.2 Particle type and mesopelagic flux attenuation

The fitted exponential curves (Figure 2-4) demonstrate that POC flux attenuation was variable between sites. Rapid attenuation (mean $T_{100}$ value of 20.6%) at P2 resulted in low POC fluxes at MLD+110 despite high fluxes out of the euphotic zone. Material sinking out of the euphotic zone was comprised mostly of individual and small chained phytoplankton cells of (diatom species, *Fragilariopsis spp.* and *Thalassiosira spp.* based on qualitative visual observations (Appendix A)), which have low sinking velocities (Smayda 1970) and are likely to be more labile and easily degraded than FP (Turner 2002; Laurenceau-Cornec et al. 2015a).

POC flux attenuation was less rapid at P3, which may in part be explained by higher FP contributions (71% and 89% at MLD+10 and MLD+110 respectively, Figure 2-3), most of which were cylindrical suggesting the importance of larger copepods and euphausiids (Wilson et al. 2013). Despite lower POC fluxes out of the euphotic zone at ICE, fluxes at MLD+110 were comparable to, and at times higher than, those measured at the more productive P2 and P3 sites. Higher $T_{100}$ values (maximum of 84.9%) suggest efficient transfer through the upper mesopelagic at ICE which again could be explained by a dominance (89-96%) of FP (mostly cylindrical). The opposite trend, lower FP contributions at MLD+110 and higher attenuation, was observed at P2, supporting the theory that the repackaging of slowing sinking phytoplankton cells and phytodetrital aggregates into fast-sinking FP by zooplankton may drive higher transfer efficiencies. Manno et al. (2015) measured higher contributions of FP to POC flux in deep (1500-2000 m) sediment traps in spring at P3 (48%) compared to P2 (20%), supporting this hypothesis.

Higher transfer efficiencies with higher contributions of FP could in part be explained by increased FP sinking velocities in comparison to phytoplankton cells (Turner 2002). Mean particle sinking velocities were in fact similar at ICE and P2 despite differences in particle flux composition (particle type), and were actually lower at P3 than P2 (not statistically significant). However, sinking velocity data are limited and are skewed towards the large end of the particle spectrum as it was only possible to determine sinking velocities of individual phytoplankton cells with ESD > 0.15 mm (mean 85 m $d^{-1}$). Considering the dominance of phytoplankton cells in sinking material at P2, it is likely that mean sinking velocities would be lower if the full particle spectrum had been measured. POC flux calculations are therefore also an upper estimate based on the operational limitations of sinking velocity measurements.

### 2.5.3 Role of zooplankton in mesopelagic flux attenuation

Inter-site differences in flux attenuation may also reflect differences in zooplankton abundance due to both spatial variability and/or contrasting bloom stage. Zooplankton abundances in the upper 200 m were almost twice as high at P3 when compared to P2 which may explain higher FP contributions to the POC flux. Previous surveys in the Scotia Sea in spring 2006 showed lower mesozooplankton biomass at P3 compared to P2 (13.41 g DW $m^{-3}$ and 57.50 g DW $m^{-3}$, respectively), as well as lower biomass at more southerly stations (encompassing the ICE station) (Ward et al. 2012a). However, zooplankton community composition, diet, migration patterns, as well as bloom timing and coupling with primary production are all important factors to consider rather than just zooplankton abundance.

Previous studies have shown negative relationships between POC export and the presence of microcopepod species such as *Oithona* spp. (Suzuki et al. 2003; Svensen and Nejstgaard 2003). These microcopepod species have a lifestyle based around coprophagy and coprorhexy which limits the export of FP to depth. Abundances of the dominant small microcopepod species were much higher at P3 compared to P2, however the ratio of small microcopepods to large calanoids was greater at P2 (20.9:1, compared to 16.7:1). This may result in a strong retention filter, reducing the efficiency of FP transfer through the upper mesopelagic at P2, which is in line with the greater levels of attenuation observed at P2. In support of this, qualitative visual assessment of FP collected in the MSC suggests that FP were more fragmented in the deeper (MLD+110) MSC samples and that cylindrical pellets in particular showed more signs of fragmentation (broken ends or considerable loss of cylindrical structure) at P2 than P3. The way in which krill FP strings are produced makes it difficult to ascertain whether FP ends were broken on production, and limits the ability to make quantitative assessment of fragmentation here. It was also not possible to distinguish between biotic and abiotic mechanical breakup. However, qualitative assessments are consistent with sediment trap data indicating a higher degree of fragmentation of cylindrical, round and ellipsoidal FP at P2 compared with P3 (Manno et al. 2015). Fragmentation of larger FP may not only aid ingestion (both intentional and unintentional) by smaller zooplankton, but may also increase exposure to microbial degradation (Ploug et al. 2008b; Svensen et al. 2012) which may in itself be a feeding strategy ('microbial gardening' (Mayor et al. 2014)), resulting in increased attenuation of POC. Data here therefore support the increasing evidence for high attenuation of POC flux and the key role of the recycling mesozooplankton community across large areas of the Southern Ocean (Cavan et al. 2015; Laurenceau-Cornec et al. 2015a; Rembauville et al. 2015b). Nevertheless, Poulsen and Kiørboe (2005), Reigstad et al. (2005) and Iversen and Poulsen (2007) provide alternative views on the role of small zooplankton in FP

degradation suggesting direct ingestion by some species is unlikely and coprorhexy is more important.

Zooplankton abundances were over an order of magnitude lower at the ICE station compared to P2 and P3, yet this is where the highest FP contribution to the POC flux was observed. This may be explained by the presence of *Euphausia superba,* whose patchy swarm distributions prevent an accurate quantification of abundance from being made here. FP collected at the ICE station are believed to be derived from *E. superba,* which are known to be common in this marginal ice zone (Hewitt et al. 2004), as well as some contribution from copepod species. The tendency of *E. superba* to form swarms (Hamner et al. 1989) has the potential to support high POC fluxes to the mesopelagic through a 'rain' of rapidly sinking FP, some of which would overload and bypass any detrital feeders. In addition to this, diel vertical migration of zooplankton and excretion at depth (Emerson and Roff 1987) may contribute to the dominance of FP in sinking POC at ICE (Figure 2-3).

### 2.5.4 Microbial respiration

This study presents the first direct measurements of respiration rates in euphausiid FP in an attempt to understand the key processes driving flux attenuation in the mesopelagic. A few studies have measured microbial respiration of copepod FP (Hansen et al. 1996; Ploug et al. 2008b; Shek and Liu 2010; Köster et al. 2014; Svensen et al. 2014), only one of which utilises the direct methods employed here (Ploug et al. 2008b).

To calculate the carbon-specific respiration rate, which is essentially a measure of FP remineralisation by particle-associated microbes, the carbon respiration rate was divided by the FP POC content. For ICE and Western Core Box stations it was possible to use values derived from additional FP collected at the same site (see Methods), however at P2, where insufficient FP were available for direct measurement, the FP POC content measured at ICE (0.032 mg C $mm^{-3}$) was used. The lack of direct measurement of FP POC at P2 increases the uncertainty in the estimate of carbon-specific respiration rate of FP at P2, but as it was only possible to measure respiration rates on two FP at this site it is not likely that this uncertainty significantly affects conclusions drawn here which utilise mean respiration rates across all sites.

Carbon-specific respiration rates were low, ranging from 0.010-0.065 $d^{-1}$ (mean 0.028 $d^{-1}$) (Figure 2-5C). There was no significant trend with FP size (length, width, volume or ESD), and no significant differences were found in carbon-specific respiration rates between sites (Student's t-test $p > 0.05$). Sensitivity tests using alternative FP POC conversions (0.016 mg C $mm^{-3}$ based on sediment traps at 50 and 100 m González 1992; and 0.0306 mg C $mm^{-3}$ based on freshly egested

FP Suzuki et al. 2001) give mean carbon-specific respiration rates of 0.063 $d^{-1}$ and 0.033 $d^{-1}$ respectively (Figure 2-7).

Low carbon-specific respiration rates suggest that particle-associated microbial respiration plays a minimal role in the attenuation of FP POC flux in the upper mesopelagic of the Scotia Sea, agreeing well with low respiration rates of 0.01 ± 0.02 $d^{-1}$ (which were deemed undetectable based on their detection limits), measured along the western Antarctic Peninsula (McDonnell et al. 2015). Ploug et al. (2008) conducted experiments on small copepod FP (over 500 times smaller volume than analysed here) at 15 °C, and measured much higher rates of carbon-specific respiration (0.08-0.20 $d^{-1}$). FP size may in part explain differences between studies (Svensen et al. 2014), however no relationship was observed between FP ESD and carbon-specific respiration rate over the small size range of FP measured here (0.33-0.85 mm ESD). A clear trend of increasing respiration rate (in terms of oxygen flux per FP) with increasing FP ESD and FP volume (Figure 2-5B) was however observed; larger FP are able to support larger populations of microbes and hence oxygen fluxes to the FP are expected to be higher. However, the range in carbon-specific respiration rates was relatively small, suggesting that microbial respiration increased with increasing carbon content, and hence reactions are not diffusion limited (Ploug 2001), but rather are limited by substrate, temperature, or surface area.

In order to assess the importance of microbial respiration for the attenuation of FP POC flux in the mesopelagic, the mean measured carbon-specific respiration rate (0.028 $d^{-1}$) was used to predict the FP flux at MLD+110 that would result if the only loss was via particle-associated microbial respiration (Figure 2-7). Calculations were based on the relationship between the remineralisation length scale ($L$ ($m^{-1}$)) (Iversen et al. 2010), carbon-specific respiration rate ($C_{spec}$ ($d^{-1}$)) and sinking velocity ($w$ (m $d^{-1}$)).

$$\boldsymbol{L = \frac{C_{spec}}{W} = \left(-ln\left(\frac{F_z}{F_0}\right)/(z - z_0)\right)} \qquad \textbf{(Equation 2-4)}$$

Comparisons to observed FP fluxes at MLD+110, revealed that degradation by particle-associated microbes caused very little of the observed alteration of the flux over this depth range and that it is a poor predictor of FP flux at P2 and P3 (Figure 2-7). This implies that other mechanisms, such as coprorhexy and coprophagy by zooplankton, were more important in reducing FP flux. Conversely, predicted FP flux at MLD+110 was similar to the measured FP flux at the ICE station suggesting that low flux attenuation here was predominantly due to microbial respiration of the FP, and that other processes were less important at the time of sampling (Figure 2-7). FP were the dominant component of POC fluxes (Figure 2-3) in particular at ICE and P3 stations, and hence processes dominating the attenuation of FP POC are likely to play an important role in the attenuation of total POC. However, if rates of microbial respiration on sinking phytoplankton cells

and detrital aggregates are significantly different to those of FP, this could alter the balance between zooplankton and microbe driven POC attenuation. Similarly respiration rates may be different on slow- or non-sinking particles, however, as the focus here is on the attenuation of fast-sinking particles, higher rates of respiration on slower sinking pools of POC cannot alone explain the rapid attenuation of fast-sinking POC that was observed without additional particle transformation processes.

Based on the measured low rates of particle-associated microbial respiration, it is hypothesised that zooplankton can drive rapid attenuation of the FP POC flux when zooplankton abundances are high (in particular of the recycling mesozooplankton community) and are tightly coupled with primary production. Temporal and spatial variability in zooplankton abundance and community structure may therefore offer one explanation for variability in FP POC flux attenuation, but temperature has also been proposed as a controlling mechanism. Marsay et al. (2015) suggest that an increase in remineralisation rates by a factor of 2-3 with an increase in temperature of 10 °C ($Q_{10}$ coefficient), as reported for other biological rate processes, could explain the differences in POC attenuation they observed in the North Atlantic and North Pacific. Iversen and Ploug (2013) measured a 3.5 fold increase in carbon-specific respiration rates measured in aggregates at 4 °C and 15 °C. Applying this factor to adjust respiration rates at 4 °C measured in this study, gives rates of 0.032-0.228 $d^{-1}$ at 15 °C, which is very similar to the range of estimates of Ploug et al. (2008). Temperature controls on rates of respiration may therefore account for differences between rates measured here and in other studies, although other characteristics such as the lability of sinking material and substrate availability may also be key (Pomeroy and Wiebe 2001; McDonnell et al. 2015), especially considering microbial adaptions to low temperatures (Russell 1990; Pomeroy and Wiebe 2001). It is unlikely that temperature significantly affects rates of zooplankton fragmentation. Although there are short-term responses to changes in temperature, populations of zooplankton acclimate over longer ecological timescales such that the species-specific respiration rate of populations in colder waters are similar to those in warmer waters (Saborowski et al. 2002). Assuming that respiration rates are a good proxy for levels of activity, rates of fragmentation by these organisms are not likely to be a function of temperature across clines where local populations are acclimatised to the ambient temperature. Results presented here therefore support the conclusions of Marsay et al. (2015), but only in cases where microbial respiration is the dominant control on POC flux attenuation, such as when and where production is low and cannot sustain high zooplankton populations, or when primary producers and consumers are decoupled. Simple relationships between temperature and export flux are therefore confounded by community structure, and may in part

explain the poor ability of many simple empirical models based primarily on temperature to replicate in situ observations (Henson et al. 2015; Maiti et al. 2016).

There is some uncertainty in the carbon-specific respiration rates derived here due to the lack of direct measurement of the POC content of individual FP used for respiration experiments. However, calculations based on the range of literature values for euphausiid FP POC cannot produce the observed declines in FP POC (error bars of Figure 2-7). Carbon-specific respiration rates would need to be between 4 and 32 times larger than those calculated to match the observed decline in FP POC flux between MLD+10 and MLD+110. Given the measured oxygen fluxes to FP, this would require FP POC contents to be 6, 43, or 34 times smaller than measured here to match observed FP degradation at ICE, P2, and P3 respectively. This is unlikely considering that minimum reported literature values of POC:volume for FP are 0.016 mg C $mm^{-3}$ (González 1992), and that mean measurements on the fresh FP made here (0.039 mg C $mm^{-3}$) are similar to measurements made on FP collected from sediment traps at 1500-2000 m at P2 and P3 (0.030 mg C $mm^{-3}$) (Manno et al. 2015).

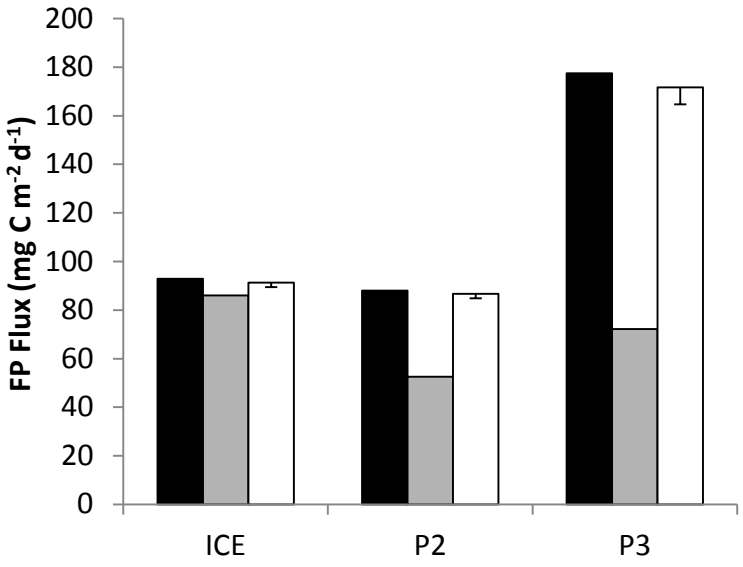


**Figure 2-7: Comparison of FP fluxes measured at MLD+10 (black) and MLD+110 (grey), to those predicted at MLD+110 (white). MLD+10 and MLD+110 represent measurements at 10 and 110 m below the base of the mixed layer depth (MLD) respectively. Predicted fluxes are based on measured FP fluxes at MLD+10 and mean FP respiration rates (0.028 $d^{-1}$) derived during this study. Hence, the predicted fluxes only consider microbial degradation via respiration. Error bars show minimum predicted values using minimum literature values for euphausiid FP POC content (González 1992). FP POC contents measured in this study lie at the upper end of literature estimates and hence there is no upper error bar.**

Respiration rates reported in this study were representative of particle-associated microbes only. Free-living microbes may also play a large role in the attenuation of POC. The role of free-living bacteria versus particle-associated bacteria within FP is not yet clear (Cnudde et al. 2013; Turner 2015), and in fact a study by Poulsen and Iversen (2008) demonstrated that free-living bacteria did not significantly contribute to FP degradation. Instead protozooplankton were the key organisms for the recycling of copepod FP. It is possible that additional colonisation of FP by free-living bacteria in the surface ocean (Thiele et al. 2015) may lead to increased densities of particle-associated microbes and increased degradation rates of FP as they sink through the water column (Jing et al. 2012). Fragmentation via zooplankton could also increase FP colonisation, increasing degradation rates. In addition, several studies have shown significant loss of FP carbon to the dissolved organic carbon (DOC) pool, driven by ecto-enzymatic hydrolysis by bacteria as well as abiotically via diffusion (Urban-Rich 1999; Møller et al. 2003; Thor et al. 2003). Particle-associated bacteria can enhance the release of DOC from FP, which would result in more rapid microbially driven attenuation of FP POC than suggested by respiration rates measured here. DOC leakage has been observed to occur rapidly after egestion (Urban-Rich 1999) and hence, depending on the depth of FP production, a significant proportion of this POC loss may have already occurred by MLD+10 thus contributing less to attenuation below this depth. A 40-70% loss of FP POC is required to account for the observed rapid declines in FP POC between MLD+10 and MLD+110 at P2 and P3, which is not likely to be explained by DOC leakage alone (e.g. Møller et al. 2003, their Figure 2). It is probable that a combination of mechanical break up via zooplankton and enzymatic hydrolysis drive the rapid loss of POC via a transfer to slowly sinking or suspended POC or DOC. Future studies combining direct measurements of particle-associated FP respiration with FP incubations in the presence of free-living microbes are needed to better balance the budget of microbial and zooplankton driven degradation processes.

Microbial respiration may represent a slow background process of degradation of the POC flux, which is always occurring but sometimes overshadowed by intense fragmentation and reworking by zooplankton populations. It is hypothesised that at times of high productivity such as during the spring bloom, and when zooplankton are exerting tight grazing control, high production is efficiently grazed and recycled in the upper mesopelagic, leading to the high biomass, low export (HBLE) situation noted by Lam and Bishop (2007). Conversely, in pre-bloom situations, when both algal and zooplankton biomass are low, POC attenuation occurs primarily via microbial respiration (Figure 2-8). In the post-bloom phase, nutrient limitation may lead to sinking of phytoplankton cells (Smayda 1971; Bienfang 1981), which depending on their sinking rate may be remineralised faster than large fast-sinking FP. The phytoplankton community structure will therefore influence the degree to which they are remineralised as well as the degree of coupling with the zooplankton

community. The high contribution of individual phytoplankton cells to the POC flux at P2 at MLD+10 but minimal contribution to the flux at MLD+110 supports the hypothesis of low sinking rates and rapid remineralisation of phytoplankton cells at the time sampled. Future studies could address these hypotheses by conducting incubation experiments with natural zooplankton communities, or mesocosm studies to assess the degree of FP loss via zooplankton fragmentation at different stages of the bloom.

### 2.5.5 Limitations

This is the first study to conduct direct measurements of oxygen gradients, and hence respiration rates, on individual FP in the Southern Ocean. Respiration rates calculated from direct measurements have been used across the study region even though it was not possible to conduct respiration measurements at each station due to the difficulty and time intensive nature of the experiments, as well as operational limitations on FP collection. Therefore, although microbial communities may differ between stations, a best estimate is presented here based on the available data.

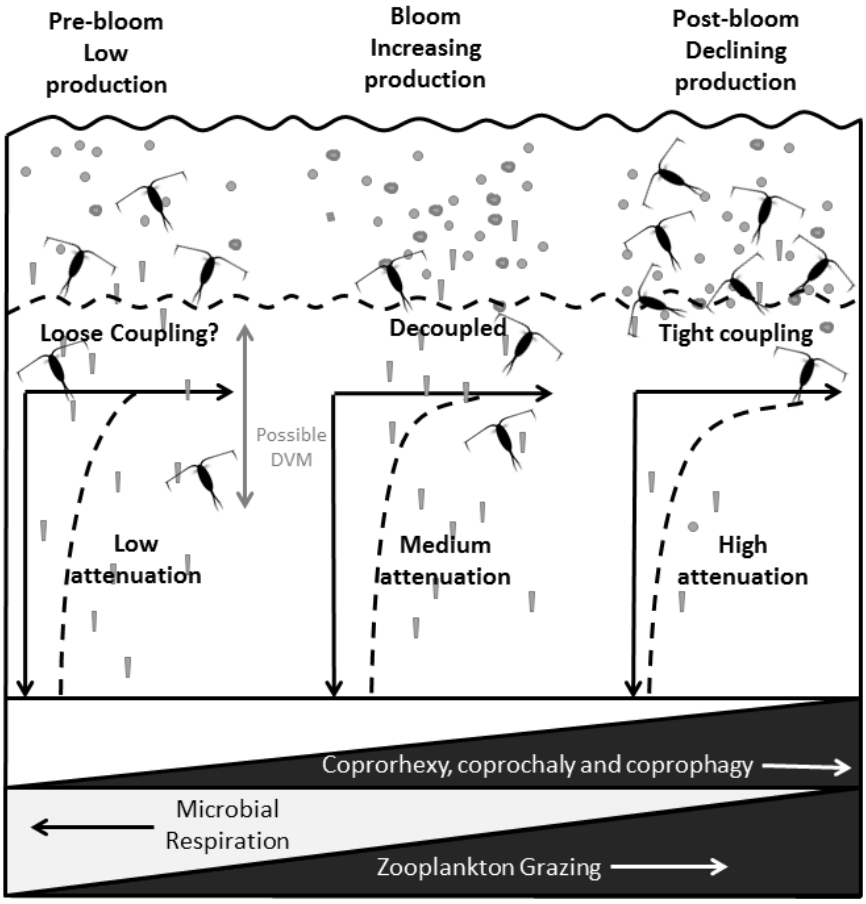

**Figure 2-8: Schematic to illustrate the mechanisms contributing to flux attenuation in the upper mesopelagic in the Scotia Sea, Antarctica, and the influence of bloom phase on these mechanisms.**

It was not possible to collect FP from the different sites at the same stage of the bloom, as the blooms in these regions do not occur concurrently. Variable zooplankton diet, due to different bloom type, may therefore lead to seasonal variability in FP degradation rate, which is not possible to separate from spatial variability in this study. Despite the inevitable uncertainties involved in this, this basin wide compilation provides a good estimate of particle-associated microbial respiration in the Scotia Sea. The data presented here therefore represent a spatial and temporal average and there is need for caution before applying these rates to specific regions and at specific stages of the bloom.

## 2.6 Conclusions

Rates of flux attenuation in the mesopelagic vary widely throughout the global oceans and a number of mechanisms have been proposed to explain these variations. High flux attenuation in the upper mesopelagic of the Scotia Sea region is likely driven by zooplankton, through fragmentation and possible ingestion processes. In these cold regions, microbial respiration is likely to be slow but may still be important for flux attenuation when zooplankton abundances are low, such as during the pre-bloom conditions in the marginal ice zone of the South Orkneys. Temperature may be able to explain global differences in POC flux attenuation, as proposed by Marsay et al. (2015), but only in regions, and at times of the year, where zooplankton abundances are low, and grazing and fragmentation processes are reduced. The stage of the bloom, zooplankton community structure and food web interactions are therefore key to determining the rate of POC flux attenuation, and more combined studies measuring POC flux and composition (at least in terms of particle type) concurrently with ecosystem structure are required for accurate estimates of the strength of the global biological carbon pump.

# Chapter 3. Depth-resolved particle-associated microbial respiration in the northeast Atlantic

This chapter has been published in Biogeosciences as:

Belcher, A. Iversen, M. Giering, S. Riou, V. Henson, S.A. Berline, L. Guilloux, L. Sanders, R. 2016. Depth-resolved particle-associated respiration in the northeast Atlantic*, Biogeosciences,* 13, 4927-4943, doi:10.5194/bg-13-4927-2016.

A. Belcher collected the field data, carried out the data analysis and wrote and edited the manuscript. M. Iversen supported the development of techniques to measure respiration rates on individual particles and provided technical advice on analysis of these data. L. Berline and L. Guilloux provided zooplankton net tow data. M. Iversen, S. Giering, and V. Riou provided advice on data analysis through insightful discussions. S. Henson and R. Sanders were involved in early hypothesis development and provided funding.

## 3.1 Abstract

Atmospheric levels of carbon dioxide are tightly linked to the depth at which sinking particulate organic carbon (POC) is remineralised in the ocean. Rapid attenuation of downward POC flux typically occurs in the upper mesopelagic (top few hundred meters of the water column), with much slower loss rates deeper in the ocean. Currently we lack understanding of the processes that drive POC attenuation, resulting in large uncertainties in the mesopelagic carbon budget. Attempts to balance the POC supply to the mesopelagic with respiration by zooplankton and microbes rarely succeed. Where a balance has been found, depth resolved estimates reveal large compensating imbalances in the upper and lower mesopelagic. In particular, it has been suggested that respiration by free-living microbes and zooplankton in the upper mesopelagic are too low to explain the observed flux attenuation of POC within this layer. In this study, the hypothesis that particle-attached microbes contribute significantly to community respiration in the mesopelagic is tested. Particle-associated microbial respiration of POC was measured in the northeast Atlantic through shipboard measurements on individual marine snow aggregates collected at depth (36-500 m). Very low rates of both absolute and carbon-specific particle-associated microbial respiration (<3% $d^{-1}$) were found, suggesting that this term cannot solve imbalances in the upper mesopelagic POC budget. The relative importance of particle-associated microbial respiration increases with depth, accounting for up to 33% of POC loss in the mid mesopelagic (128-500 m). It is suggested here that POC attenuation in the upper mesopelagic (36-

128 m) is driven by the transformation of large, fast-sinking particles to smaller, slow-sinking and suspended particles via processes such as zooplankton fragmentation and solubilisation, and that this shift to non-sinking POC may help to explain imbalances in the mesopelagic carbon budget.

## 3.2 Introduction

The biological carbon pump plays a key role in regulating the partitioning of carbon dioxide ($CO_2$) between the ocean and atmosphere, and without it atmospheric $CO_2$ would likely be 200 ppm higher than it is today (Parekh et al. 2006). Key to determining its effectiveness is the efficiency with which organic carbon sinks through the ocean interior (quantified as the transfer efficiency), and thus the depth at which material is remineralised (Francois et al. 2002; Kwon et al. 2009). However, despite its importance, the processes governing the loss of organic carbon within the mesopelagic are poorly understood (Burd et al. 2010).

Particulate organic carbon (POC) sinking out of the euphotic zone can be transformed within the mesopelagic in many ways, including zooplankton feeding, fragmentation via sloppy feeding, microbial solubilisation to dissolved organic carbon (DOC), and physically driven aggregation and disaggregation processes (e.g. Azam and Malfatti, 2007; Burd and Jackson, 2009; Steinberg et al. 2008). Ultimately carbon is lost from the organic carbon pool as dissolved inorganic carbon via respiration, and hence, in theory at steady state, community respiration should be balanced by the supply of POC (Burd et al. 2010). However, settling organic matter is often found to be insufficient to meet the energy demands of microbes in the dark ocean, thus leading to an imbalanced mesopelagic carbon budget (Steinberg et al. 2008; Baltar et al. 2009; Herndl and Reinthaler 2013).

A recent study managed to close the mesopelagic carbon budget between 50 and 1000 m in the North Atlantic (Giering et al. 2014) by making key changes to the terms included in the budget. However, Giering et al. (2014) found large and compensating imbalances between sources and sinks in upper and lower mesopelagic layers, with an excess of POC supply to the upper mesopelagic (50-150 m depth), and an excess of respiration in the lower mesopelagic (150-1000 m depth). This oversupply in the upper mesopelagic has not previously been identified, likely because previous budget studies have not taken a depth resolved approach. In addition, most previous studies use a fixed upper mesopelagic boundary of 100-200 m, rather than a dynamic upper boundary (such as the base of the mixed layer, (Buesseler and Boyd, 2009)) and therefore may have missed the region of most rapid POC attenuation. Our understanding of the mesopelagic carbon budget is therefore still incomplete. Giering et al. (2014) found prokaryotes to be responsible for most of the respiration (70-92%) across both depth ranges however,

respiratory loss due to particle-associated prokaryotes has typically not been included in mesopelagic carbon budget studies (Steinberg et al. 2008; Giering et al. 2014). Data from the subtropical North Atlantic and west Antarctic Peninsula show that particle-associated microbial respiration can contribute 32-93% of the total respiration measured *in situ* (McDonnell et al. 2015), suggesting that particle-associated microbes could play an important role in the loss of POC in the mesopelagic. It is hypothesised here that POC losses via particle-associated respiration (a term not directly measured by Giering et al. 2014 or Steinberg et al. 2008) may help to address imbalances in the upper mesopelagic carbon budget.

Marine snow particles (aggregates of detritus, living organisms and inorganic matter >0.5 mm in diameter, (Alldredge and Silver, 1988)) can make up a large fraction of the sinking POC in the ocean and host microbial abundances 2-5 orders of magnitude higher than those found free-living in the surrounding water column (Silver and Alldredge 1981; Thiele et al. 2015). The fragile nature of marine snow particles makes sampling and measurement difficult; many previous measures of particle-associated respiration have been carried out on roller tank formed marine snow aggregates, either from laboratory cultures of phytoplankton or natural sea water samples (Grossart and Ploug 2001; Iversen et al. 2010; Iversen and Ploug 2010, 2013). A few experiments have utilised divers or submersibles to collect *in situ* aggregates and estimate heterotrophic bacterial production by measuring leucine uptake (Alldredge and Youngbluth 1985; Smith et al. 1992) with few measuring respiration directly on individual aggregates (e.g. Ploug et al. 1999). Only two studies have combined direct measures of respiration on aggregates collected at depth with measurements of POC flux (Collins et al. 2015; McDonnell et al. 2015), both of which lack sufficient vertical resolution in the upper mesopelagic to capture the region of most rapid change. Collins et al. (2015) collected particles *in situ* and carried out incubations on board, measuring rates of substrate-specific microbial respiration of 0.007±0.003 $d^{-1}$ to 0.173±0.105 $d^{-1}$ in the North Atlantic. McDonnell et al. (2015) used sediment trap incubators (RESPIRE) to measure *in situ* rates of 0.01±0.02 $d^{-1}$ and 0.4±0.1 $d^{-1}$ at the western Antarctic Peninsula and Bermuda Atlantic Time Series station respectively. Previous studies are therefore inconclusive as to the importance of particle-associated microbes on the attenuation of POC, with some studies suggesting they play a minor role (Ducklow et al. 1982; Alldredge and Youngbluth 1985; Karl et al. 1988; Iversen et al. 2010; Collins et al. 2015) and others suggesting a larger contribution (Ploug et al. 1999; Turley and Stutt 2000; Iversen and Ploug 2013).

To build upon these previous studies, this chapter assesses the role of particle-associated microbial respiration in POC flux attenuation, presenting a vertical profile of particle-associated respiration rates measured on individual marine snow particles collected at depth. In an attempt to assess whether this term can improve our ability to balance the fast-sinking POC budget in the

upper mesopelagic, measurements were made in the northeast Atlantic at the site of Giering et al. (2014) where we have the most complete knowledge of the mesopelagic carbon budget. Sampling was focussed on the upper ocean (mixed layer depth-500 m) where the most rapid attenuation occurs, a region that is not well understood and poorly represented in model studies (Henderson and Marchal 2015).

## 3.3 Methods

### 3.3.1 Study site

Measurements were made during research cruise DY032 (20$^{th}$ June – 8$^{th}$ July 2015) to the Porcupine Abyssal Plain (PAP) observatory site (49 °N, 16.5 °W) in the northeast Atlantic aboard RRS *Discovery* (Figure 3-1). Vertical profiles of the water column at each site were made using a Conductivity-temperature-depth (CTD) unit (Seabird 9Plus with SBE32 carousel). The mixed layer depth (MLD) was determined as the depth where temperature was 0.5 °C lower than the surface temperature (Monterey and Levitus 1997).

### 3.3.2 Chlorophyll-a

Depth profiles of chlorophyll-a were measured during the cruise using water samples (200 mL) collected with the CTD rosette. Samples were filtered onto 0.8 µm MPF300 glass fibre filters, and frozen at -20 °C. Pigments were extracted in 90% acetone for 22-24 hours at 4 °C and fluorescence measured on a Trilogy Turner Designs 7200 lab fluorometer calibrated with a pure chlorophyll-a standard (Sigma, UK).

Aqua MODIS 9 km, 8-day satellite chlorophyll-a data (downloaded from the NASA Ocean Biology website; http://oceancolor.gsfc.nasa.gov/cms/) were used to assess mesoscale variability (e.g. passage of eddies) during the sampling period. Changes in surface chlorophyll are examined prior to and post sampling by averaging chlorophyll data over the study region (48.5-49.5 °N, 16.0-17.0 °W).

### 3.3.3 Particle flux and particle type

Particle flux and composition (particle type) were measured using Marine Snow Catchers (MSC), large (95 L) PVC closing water bottles designed to minimise turbulence (Riley et al. 2012; Cavan et al. 2015). MSCs were deployed between 36 and 500 m, closed at depth, retrieved on deck and left for particles to settle to the base of the MSC. Deployment depths were chosen based on the MLD, determined as the depth with steepest gradient in temperature from the most

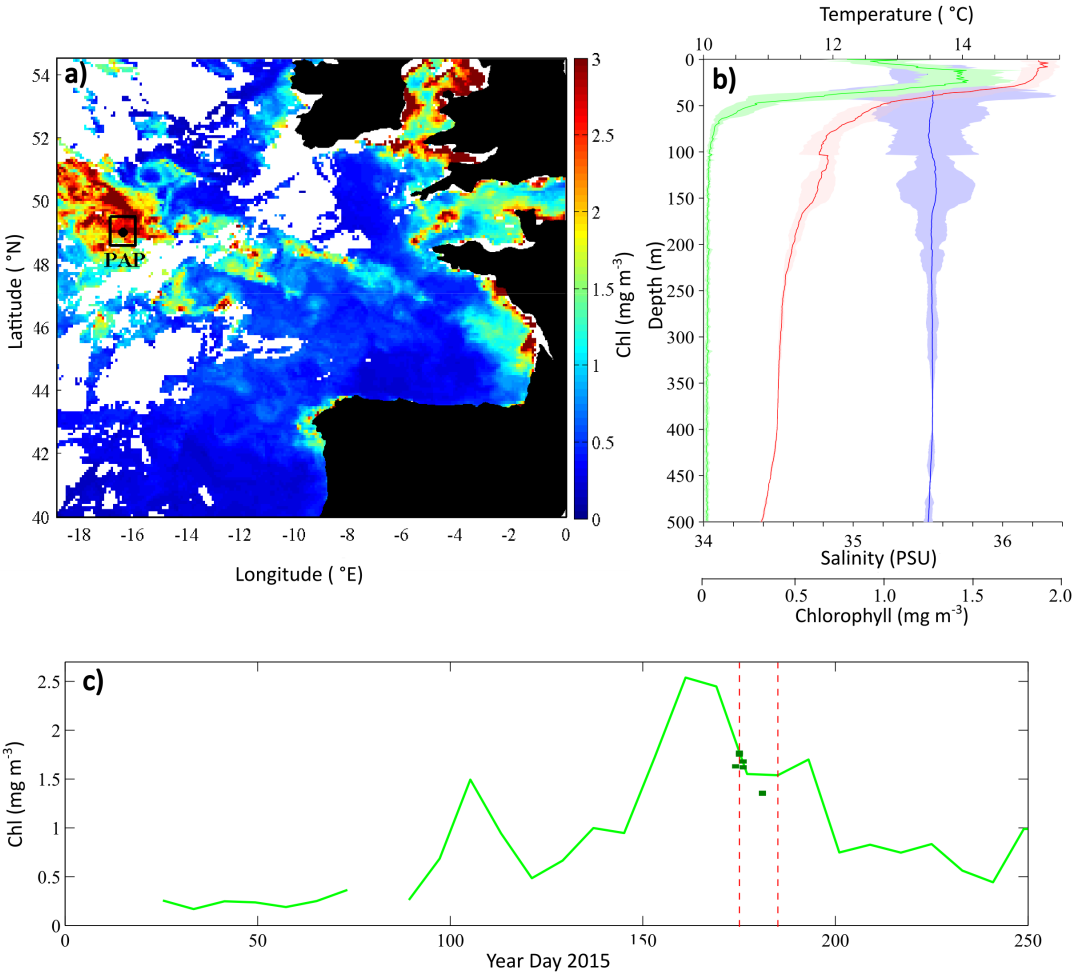


**Figure 3-1: Surface chlorophyll concentration (mg $m^{-3}$) at the PAP site, (a) PAP study region (black box) overlain on 9 km Aqua MODIS satellite chlorophyll for 18/06/2015-25/06/2015. (b) Mean vertical temperature, salinity and chlorophyll profiles measured at the PAP site (red, blue and green lines respectively) and the standard deviation (light shading) of CTD deployments coinciding with MSC deployments. (c) Temporal change in surface chlorophyll (mg $m^{-3}$) over the PAP study region based on 8-day, 9 km Aqua MODIS satellite data. Gaps in data are due to cloud cover. Vertical red lines indicate start and end of sampling period, and dark green squares are discrete measurements made from the CTD at depths of 5-10 m.**

recent CTD profile. MSC deployments were carried out during the day with the exception of the two samples at 36 m and 128 m, which were deployed at night due to logistical limitations. Particles were allowed to settle onto a particle collector tray at the base of the MSC for two hours (defined as 'fast-sinking' as in Riley et al. 2012), after which those visible by eye (>0.15 mm diameter) were picked from three quadrants using a wide bore pipette, filtered onto pre-combusted (450 °C, 24 h) glass fibre filters (25 mm diameter GF/F, Whatman), and oven dried at 50 °C for replicate analysis of POC. Filters were subsequently fumed with 37% HCl in a vacuum

desiccator for 24 hours, and dried for 24 hours at 50 °C. Filters and filter blanks were placed in pre-combusted (450 °C, 24 h) tin capsules as in Hilton et al. (1986), and POC was measured by a CE-440 elemental analyser (Exeter Analytical.285 Inc). Particles in the remaining quadrant were transferred to a temperature controlled laboratory (10 °C) and used for measurements of sinking and respiration rates (section 3.3.4).

The flux of POC (*F* in mg C $m^{-2}$ $d^{-1}$) associated with fast-sinking particles was calculated as follows:

$$\boldsymbol{F} = \frac{\boldsymbol{m}}{\boldsymbol{A}} \times \frac{\boldsymbol{w}}{\boldsymbol{h}}, \qquad \textbf{(Equation 3-1)}$$

where *m* refers to the total mass (mg) of fast-sinking POC collected from the MSC, *A* the area (0.059 $m^2$) of the MSC based on inner MSC diameter, *w* the measured sinking velocity (m $d^{-1}$) from laboratory measurements, and *h* the height of the snow catcher (1.53 m). Sinking velocities of marine aggregates were measured in a flow chamber (section 3.3.4), and the median value for each depth horizon used to avoid bias by rare aggregates. The rate of particle flux attenuation was assessed by fitting a power-law function (Martin et al. 1987) to the flux data,

$$\boldsymbol{F_z = F_{z0} \times (z/z_0)^{-b}}, \qquad \textbf{(Equation 3-2)}$$

where *z* is the depth of the flux, and $F_{z0}$ is the flux at the reference depth (in this case 26 m, i.e. the mixed layer depth). A high value of *b* corresponds to high attenuation (shallow remineralisation) and vice versa. As *in situ* particle production at depth is not considered, this represents a lower bound estimate of flux attenuation.

The type of fast-sinking particles at each depth was assessed under a microscope and photographs taken using a Leica DM-IRB inverted microscope and Canon EOS 1100D camera. Particles were classified into phytodetrital aggregates (PA; aggregates >0.15 mm equivalent spherical diameter (ESD) containing phytoplankton cells and other phytodetrital material, Figure 3-2), faecal pellets (FP), and unidentified phytodetritus. Individual particle dimensions were measured using ImageJ (version 1.49p) and volumes calculated using formulae for a sphere, prolate ellipsoid or cylinder depending on particle type and shape. Conversions from PA volume to PA POC were based on measurements of POC content of marine aggregates collected at depth (section 3.3.4), and a carbon to volume ratio of 0.08 mg C $mm^{-3}$ used for FP based on literature estimates (range 0.01-0.15 mg C $mm^{-3}$, (Wilson et al. 2008)). FP carbon content can vary greatly even within species depending on factors such as food type and concentration (Urban-Rich 2001), which introduces uncertainty into estimates made here of their contribution to the total POC flux.

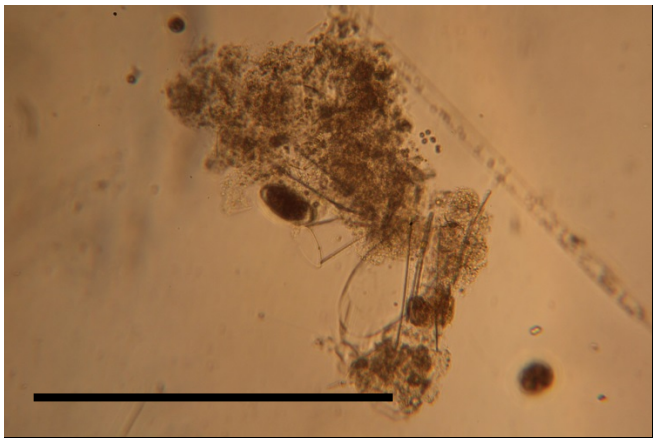

**Figure 3-2: Example light microscope image of a phytodetrital aggregate collected from depth. Scale bar=0.5 mm**

### 3.3.4 Oxygen gradients in marine snow aggregates

The rates at which sinking particles were degraded due to the respiration of particle-associated microbes were calculated from direct measurements of oxygen gradients within PA. PA were transferred into a temperature controlled flow chamber system (Appendix Figure A1, A2) (Ploug and Jorgensen 1999) containing filtered sea water (0.22 µm), taken from the MSC deployed at 36 m and maintained at 10 °C (at the low end of temperatures measured during the study, Figure 3-1). Only one incubation temperature was possible due to laboratory and space limitations. The salinity in the flow chamber was 35.5 PSU which, considering the low variation in salinity profiles (standard deviation of 0.008 PSU at 36 m depth) should represent conditions at all depths sampled. Within 24 hours of collection, PA were placed carefully in the flow chamber using a wide bore pipette. The wide bore pipette lifts the particles with the surrounding water so that the particles remain suspended in water during the handling and minimal physical stress is exerted on the particles. The microbial communities associated with the aggregates are not removed by this method (Kiørboe et al. 2002). The x, y, and z dimensions of PA were measured using a horizontal dissection microscope with a calibrated ocular, and three measurements of the sinking velocity made for each PA by suspending the PA with an upward flow. The formula of an ellipsoid was used to calculate PA volumes from their x, y, z dimensions, and ESDs were computed.

A profile of oxygen was measured from the ambient water, through the diffusive boundary layer (DBL) and into the PA using a Clark-type oxygen microelectrode and guard cathode (Revsbech 1989) mounted in a micromanipulator. Measurements were made in increments of 50-200 $\mu$m on the downstream side of the particle and oxygen fluxes calculated using a diffusion-reaction model based on Fick's first law of diffusion (diffusion coefficients of 1.4691 x$10^{-5}$ $cm^2$ $s^{-1}$ for 10 °C and

salinity 35 PSU, Broecker and Peng, 1974). Two to three replicate profiles were taken for each PA where possible. A solver routine was used to find the optimum solution minimising the sum of the squares between measured and modelled oxygen concentrations (see Ploug et al. (1997) for full details). Total oxygen consumption within the PA was calculated using the equation for the surface area of an ellipsoid assuming that net oxygen fluxes do not vary significantly on the upstream and downstream sides (Ploug and Jorgensen 1999). As oxygen consumption in the DBL is a measure of the respiration rate of the microbial community associated with the PA due to net exchange of oxygen via molecular diffusion, the carbon respiration ($C_{resp}$ in mg C $mm^{-3}$ $d^{-1}$) can be calculated based on a respiratory quotient (RQ) (here,1 mol $O_2$ to 1 mol $CO_2$, Ploug and Grossart, 2000; Ploug et al. 1997). This RQ was chosen as a conservative value in the range of literature values typically applied (0.7-1.2 mol:mol) for respiration of carbohydrates and lipids (Berggren et al. 2012), but adds uncertainty to the estimates made here that cannot be better constrained without knowledge of the form of carbon within the PA utilised for microbial respiration.

Following respiration measurements, PA were stored in 1.5 mL Eppendorf tubes before pooling PA into size classes based on ESD and placing onto pre-combusted (450 °C, 24 h) glass fibre filters (25 mm diameter GF/F, Whatman) for measurement of POC as described in section 3.3.3. This enabled the carbon content per unit volume (mg C $mm^{-3}$) for each size class at each depth range to be calculated and hence the POC content of individual PA to be estimated. POC to volume ratios of two size classes (typically <0.6 mm ESD, >0.6 mm ESD) were measured at each depth horizon (with the exception of samples at 128, 200 and 500m where all measured particles were <0.6 mm ESD so only one size class was used) to take into account the geometry of aggregates and non-linear volume to POC ratio (Alldredge 1998). These PA POC contents ([POC] in mg C $mm^{-3}$) were then used to calculate carbon-specific respiration rates ($C_{spec}$ in $d^{-1}$) as follows:

$$\boldsymbol{C_{spec} = C_{resp}/[POC].} \qquad \textbf{(Equation 3-3)}$$

### 3.3.5 Statistics and error analysis

Attenuation of fast-sinking POC flux with depth was best described by a power-law relationship fit (of form, $F_z = F_{z0} (z/z_0)^{-b}$, $R^2$=0.42, $p$=0.06, n=9) (Martin et al. 1987) compared to an exponential fit ($R^2$=0.30, $p$=0.128, n=9) (of form, $F_z = F_{z0} \exp(z\text{-}z_0/z^*)$, where z* is the characteristic remineralisation length scale for the flux decrease below z0 as in Buesseler and Boyd, (2009). Tests were conducted for any statistical relationship between carbon-specific respiration rates and depth. All statistics were carried out in RStudio (version 0.98.1091; R development core team, 2014). A relation between particle ESD and sinking velocity was calculated by applying a power-law fit to the data using the NLS function in RStudio. The choice of a power-law relationship, based on the findings of previous studies (e.g. Iversen and Ploug, 2010), was motivated by the

observed divergence of marine snow aggregates from Stokes Law due to their irregular shapes (Logan and Wilkinson 1990).

Time and methodological constraints of measuring very small particles, prohibited the measurement of the respiration rate of every particle collected in the MSC. Hence, before using these measurements to assess the contribution of particle-associated microbial respiration to the mesopelagic carbon budget, upper and lower bounds to estimates were first defined based on the uncertainties. A Monte Carlo analysis (with 10,000 iterations) of the individual parameters used in the calculations of carbon-specific respiration and remineralisation length scale was conducted. Measured volumetric oxygen respiration rates were randomly sampled (with replacement) at each depth. For each of these randomly selected particles the corresponding sinking velocity and ESD in subsequent calculations of carbon-specific respiration and remineralisation length scale was used. For the RQ, a uniform distribution of possible values over the range of RQ values typically applied in the literature (0.7-1.2, Berggren et al. 2012) was defined. PA were pooled into size classes and could only be measured once for POC content. For each depth, a normal distribution of possible POC:volume ratios for each size class was created, with the measured value as the mean, and standard deviation calculated from the standard deviation of the individual aggregate volumes within a size class. Based on the 10,000 iterations for each of the aforementioned parameters a range of estimates for the remineralisation length scale (via particle-associated microbial respiration) was obtained at each depth. The mean of these distributions ±standard deviation was then used to put error bounds on the estimates of the POC loss via particle-associated microbial respiration.

### 3.3.6 Zooplankton respiration

Zooplankton were sampled in vertical net hauls (0-200 m) at 1 m $s^{-1}$ speed using a 200 µm mesh size WP2 net with a 57 cm frame diameter, fitted with filtering cod-ends. Collected organisms were fixed directly after collection with formaldehyde at 10% final concentration for further analyses. In the laboratory, fixed samples were digitized with the ZooScan digital imaging system (Gorsky et al. 2010) to determine the size structure of the community. Each sample was divided into two fractions (<1000 and >1000 µm) for accurate estimation of rare large organisms in the scanned subsample (Vandromme et al. 2012). Fractions were split using a Motoda splitting box until containing approximately 1000 objects. The resulting aliquots were poured onto the scanning cell and individual zooplankton were manually separated with a wooden spine in order to avoid overlapping organisms. Each scanned image was later processed using ZooProcess (Gorsky et al. 2010). Each object in the image was automatically classified into five zooplankton categories (copepods, chaetognatha, appendicularia, other crustaceans and other zooplankton)

and three non-living categories (detritus, fibers and out of focus) using Plankton Identifier (http://www.obs-vlfr.fr/~gaspari/Plankton_Identifier/index.php) and manually validated. Finally, dry weight (DW) of each zooplankton object was estimated from its area using Lehette and Hernández-León's (2009) allometric relationships corresponding to the five zooplankton categories. Respiration per individual (µg C individual$^{-1}$ h$^{-1}$) was computed from DW using the relationship from Ikeda et al. (2001) for copepods and (Ikeda 1985) for other groups:

$$\boldsymbol{Zooplankton\ respiration} = \boldsymbol{exp}(\boldsymbol{a_1} + \boldsymbol{a_2}\ln(\boldsymbol{DW}) + \boldsymbol{a_3 T}) \times \boldsymbol{RQ} \times \mathbf{12/22.4} \quad \textbf{(Equation 3-4)}$$

Here DW is dry weight (mg C individual$^{-1}$), RQ is the respiratory quotient (0.8 mol C/mol $O_2$), T is the mean temperature over the top 200 m (12.5 °C), 12/22.4 is the molar conversion factor and parameters $a_1$, $a_2$, and $a_3$ were dependent on the type of zooplankton. Total zooplankton respiration (0-200 m) was calculated by summing the respiration values for each individual. Day and night respirations were calculated for 16 and 8 hours respectively based on day length at the study site.

## 3.4 Results

### 3.4.1 Hydrography and surface chlorophyll-a

The consistency of vertical temperature profiles suggests little variation in water mass structure during the cruise (Figure 3-1b). Temperatures ranged from 15.2 °C at the surface to 10.9 °C at 500 m, with salinity remaining relatively constant with depth (mean 35.34-35.56, Figure 3-1b). The mixed layer shallowed from 32 m to 26 m (Figure 3-1b), with peak chlorophyll just above the MLD at 15-25 m, and decreasing from 1.9 to 1.4 mg m$^{-3}$ during the course of the cruise based on discrete measurements (Figure 3-1c). The MLD was typically within ±5 m of the 1% photosynthetically active radiation (PAR) level. Satellite chlorophyll data are consistent with *in situ* data, declining from 1.8 to 1.2 mg m$^{-3}$ in the PAP region, suggesting sampling was carried out in the 'post peak' phase (Figure 3-1c).

### 3.4.2 Particle type

A total of 10 MSC deployments were made over an 11-day period with particle type and respiration measurements carried out for seven deployments (Table 3-1).

The dominant component of fast-sinking particles were PA (Figure 3-2) at all depths sampled (one MSC sample per depth), accounting for 96% of sinking POC at 36 m and decreasing to 66% at 500 m associated with an increasing abundance of FP with depth (Figure 3-3). The lack of FP observed

**Table 3-1: Deployment table for cruise DY032 to the PAP site and details of particle flux composition (particle type) and sinking rates.**

| Depth (m) | Date | Time (GMT) | POC Flux (mg C $m^{-2}$ $d^{-1}$) | # PA (in 95 L sample)** | # FP (in 95 L sample)** | Mean PA ESD (mm) | Median PA sinking rate (m $d^{-1}$) |
|---|---|---|---|---|---|---|---|
| 36 | 24/06/2015 | 02:10 | 281.4 | 785 | 23 | 0.60 | 33.2 |
| 128 | 24/06/2015 | 02:35 | 76.2 | 259 | 61 | 0.44 | 30.6 |
| 73 | 26/06/2015 | 14:45 | 122.8 | 252 | 15 | 0.65 | 34.0 |
| 113 | 28/06/2015 | 11:50 | 66.0 | 198 | 0 | 0.49 | 30.1 |
| 500 | 28/06/2015 | 17:50 | 99.4 | 282 | 92 | 0.44 | 34.4 |
| 46 | 30/06/2015 | 18:45 | 63.7 | 702 | 61 | 0.53 | 11.7 |
| 204 | 02/07/2015 | 10:00 | 51.8 | 275 | 76 | 0.41 | 18.3 |
| 30 | 04/07/2015 | 13:00 | 266.8 | | | | |
| 60 | 04/07/2015 | 13:20 | 38.7 | | | | |
| 100 | 04/07/2015 | 13:30 | 85.5 | | | | |

PA: Phytodetrital aggregate; FP: Faecal Pellet; ESD: Equivalent spherical diameter.
**Refers to counts of fast-sinking material collected from deployment of 95 L snow catcher bottle. Counts have been scaled up from smaller sample split (1/4).

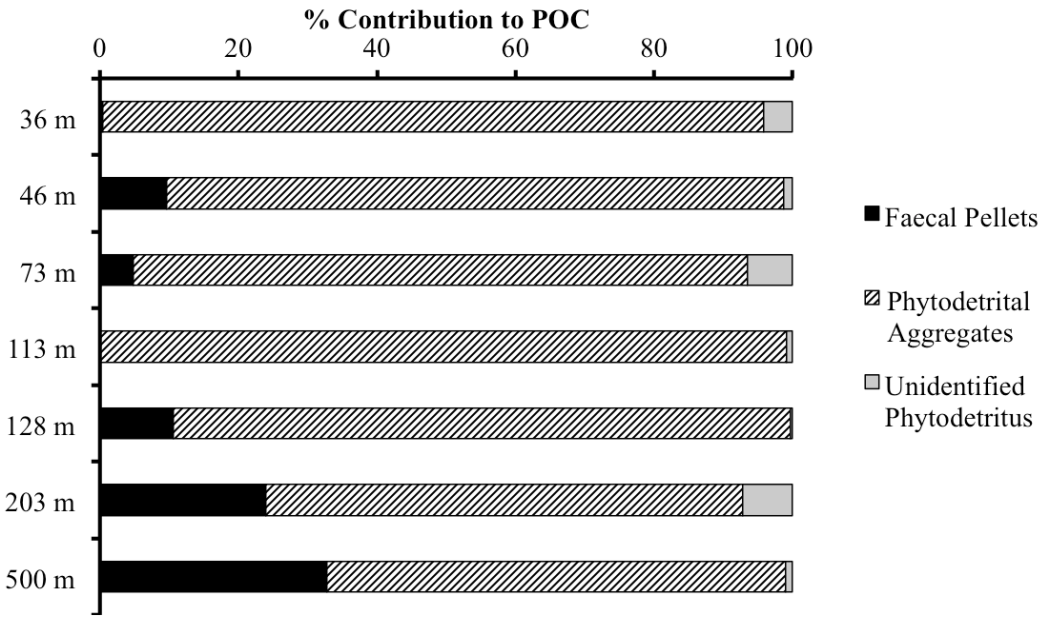


**Figure 3-3: Composition (particle type) of fast-sinking POC at each measured depth horizon. The percent (%) contribution of faecal pellets (black), phytodetrital aggregates (hatched), and unidentified phytodetritus (grey) to the total mass of fast-sinking POC collected in Marine Snow Catchers at each depth horizon. See Table 3-1 for numbers of particles in each category.**

in the sample at 113 m may be due to the heterogeneous distribution of FP at a particular depth associated with patchy zooplankton distributions. The increase in FP numbers below 100 m may relate to an increase in zooplankton populations with depth, zooplankton diel

vertical migration and/or increased FP loss in the upper mesopelagic due to processes such as fragmentation and coprophagy. Qualitative assessment of FP morphology shows that FP were longer, thinner and darker deeper in the water column, implying a change in zooplankton community composition with depth.

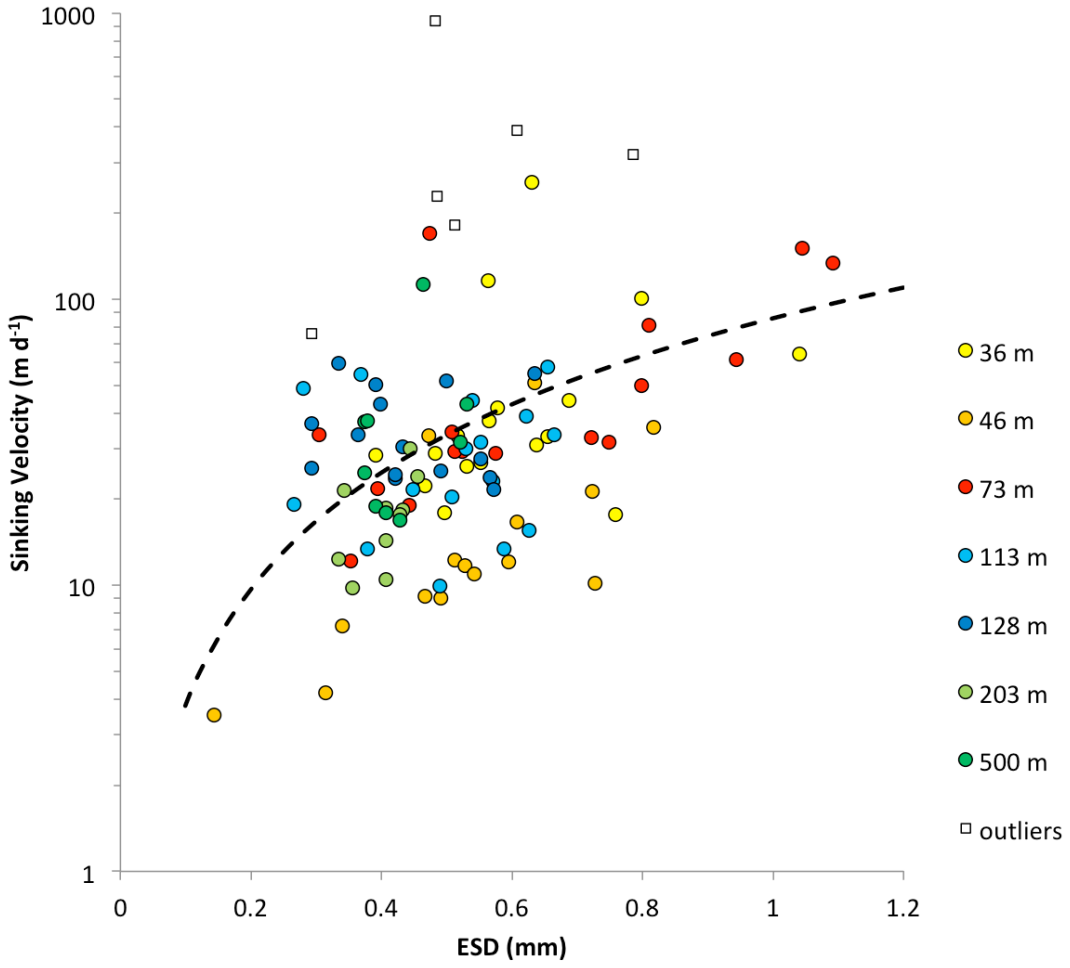


**Figure 3-4: Relationship between sinking velocity (m $d^{-1}$) and equivalent spherical diameter (ESD, mm) of phytodetrital aggregates. The depth from which aggregates were sampled is shown by the colour of circles (36 m=yellow, 46 m=orange, 73 m=red, 113 m, light blue, 128 m=dark blue, 203 m=light green, 500 m=dark green). Note the log scale on the Y axis. A power-law fit between sinking velocity and aggregate ESD (dotted line $Y = 85.8X^{1.4}$) is applied. Six outliers (black open squares), defined as being outside 2 standard deviations from the mean, were excluded from the power-law fit.**

### 3.4.3 Particle sinking velocities

Sinking velocities of PA collected at depth ranged from 4-255 m $d^{-1}$ (Figure 3-4), reflecting both the range in size of PA measured (0.14-1.09 mm ESD) and the heterogeneous composition of PA

(Figure 3-2). Median sinking velocities showed less variability ranging from 11-34 m $d^{-1}$ (10-32 m $d^{-1}$ and 21-62 m $d^{-1}$ for aggregates <0.6 mm (n=74) and >0.6 mm (n=24) ESD respectively). There was no significant relationship between PA sinking velocity and depth for either size class ($R^2$=0.004, $p$>0.1, n=98). PA sinking velocity was significantly ($R^2$=0.17, $p$<0.0001, n=98) related to ESD (six outliers, defined as being outside 2 standard deviations from the mean, were excluded in this relationship). The low $R^2$ suggests that the influence of particle size on the sinking velocity is limited and that particle composition may exert a higher influence.

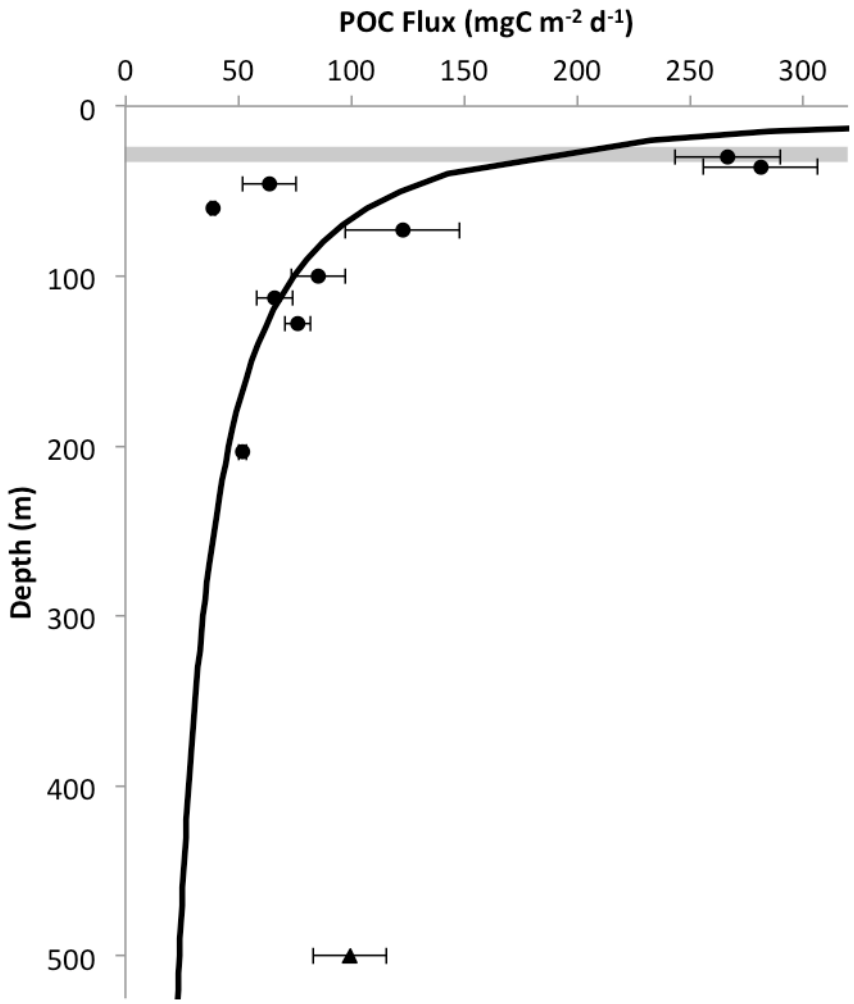


**Figure 3-5: Flux of POC (mg C $m^{-2}$ $d^{-1}$) with depth at the PAP site. POC fluxes of fast-sinking particles measured in June 2015 at the PAP site via deployment of Marine Snow Catchers. Error bars relate to replicate filters per sample. A power-law curve was fitted to the data (black line), $Y=194.9 \cdot (X/MLD)^{-0.71}$ ($R^2$= 0.42, $p$=0.060, n=9), excluding the point at 500 m (triangle) which is likely due to non-steady state conditions. The grey shaded area indicates the mixed layer depth over the study period.**

### 3.4.4 Particle flux

Consistent with other studies, a sharp decline in fast-sinking POC concentration (not shown) and fast-sinking POC flux with depth was observed (Figure 3-5)(e.g. Martin et al. 1987; Riley et al. 2012; Giering et al. 2014). Based the sampling depths of this study, the upper mesopelagic (36-128 m) is defined as the region where the most rapid POC flux attenuation occurs, and the mid mesopelagic as the region below (128-500 m) where a slower decrease and possibly even an increase in POC flux below 128 m, is observed. This change in the rate of flux attenuation with depth suggests that different processes may be controlling POC attenuation in the upper and mid mesopelagic, or that the rates of processes vary with depth. Interestingly, there was an increase in flux between 203 and 500 m, which may reflect higher surface production in the days prior to sampling (Figure 3-1c) and the time taken for material to reach this depth from the surface (i.e. non-steady state, Giering et al. 2017). Based on a median sinking rate of 34 m $d^{-1}$ measured at 500 m, material at this depth would have originated at the surface on Julian day 164, 15 days prior to sampling, which corresponds to the peak in surface chlorophyll concentrations (Figure 3-1c). This increase in flux is associated with twice as much FP POC at 500 m compared to 203 m, and a 29% increase in PA POC. Considering the decrease in resident zooplankton populations with depth (Giering et al. 2014), it seems unlikely that FP production was higher at this depth unless there is a large contribution by diel vertical migrators, and may instead reflect reduced FP loss. However, this scenario could also be due to zooplankton patchiness. Excluding this potentially non-steady state value at 500 m, the calculated Martin's *b* value is 0.71 which is in line with previous studies at this study site (Riley et al. 2012; Giering et al. 2014), but note that this fit is just outside the 5% significance level ($R^2$=0.42, p=0.06, n=9). To assess the uncertainty surrounding the *b* value calculated here, a bootstrap analysis with 100,000 simulations has been applied, giving a mean *b* of 0.67 ± 0.34 (standard deviation).

### 3.4.5 Microbial respiration in phytodetrital aggregates

Using the microelectrode approach, oxygen concentrations were found to decrease from the ambient water towards the PA surface, reaching a minimum at the centre of the PA (but remaining well above anoxic conditions in all PA measured) (Figure 3-6). Mean oxygen fluxes to PA did not vary significantly with the depth at which particles were collected, ranging from 11.7-19.1 nmol $O_2$ $mm^{-3}$ $d^{-1}$ (Figure 3-7), but variability between PA collected at each depth was large (3.1-43.8 nmol $O_2$ $mm^{-3}$ $d^{-1}$ over the depth range measured, Table 3-2).

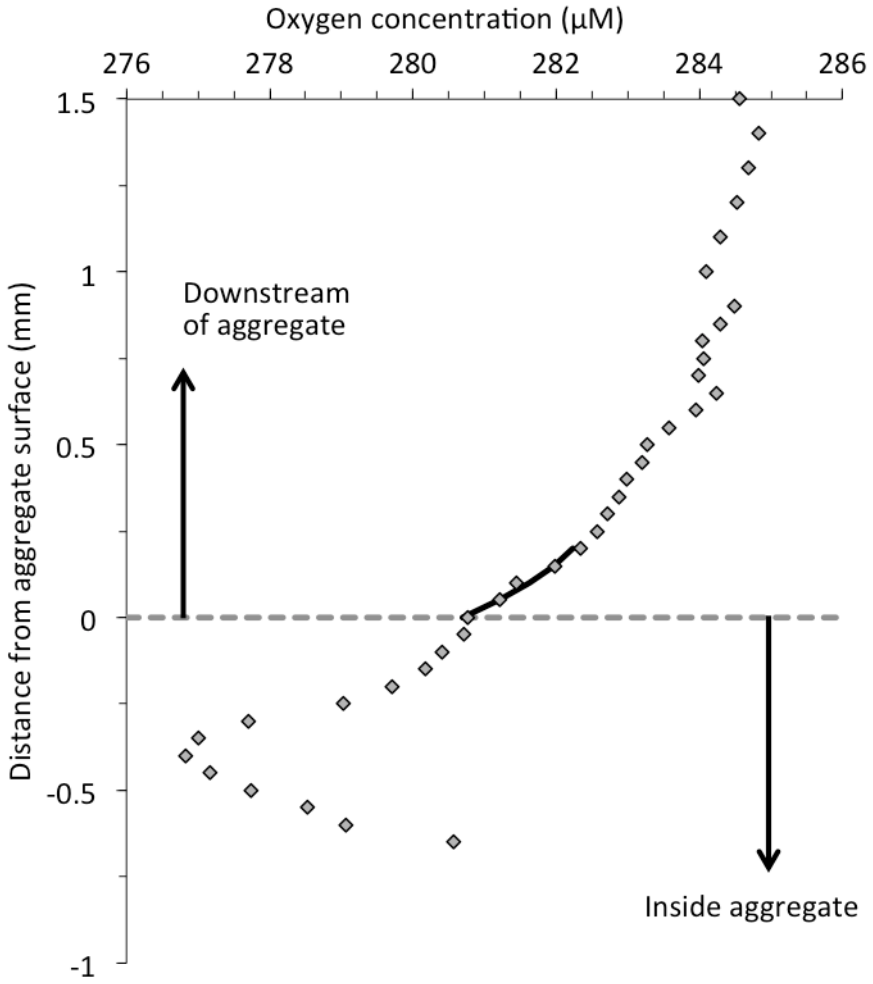


**Figure 3-6: Example oxygen profile (µM) through a phytodetrital aggregate collected at 46 m depth. Measurements were made with microsensors in steps of 50-100 µm, with negative values reflecting the distance into the aggregate from the surface. The solid black line shows the model fit used to calculate the oxygen flux in the diffusive boundary layer.**

For each depth horizon the POC contents of the PA used in respiration experiments were measured (see section 3.3.4, Table 3-3). POC contents of PA ranged from 11.7-30.6 µg C $mm^{-3}$ (mean 15.4 µg C $mm^{-3}$) for PA <0.6 mm ESD, and 6.7-11 µg C $mm^{-3}$ (mean 9.0 µg C $mm^{-3}$) for PA >0.6 mm ESD. The POC content of both size classes peaked at 46 m depth, showing a general decline below this (Table 3-3). POC measurements are based on filters containing a relatively low number of aggregates; 9-13 aggregates and 4-6 aggregates for aggregates <0.6mm ESD and >0.6mm ESD, respectively. However, despite the low concentrations of carbon measured, sample POC was significantly higher than POC filter blanks (Welch's t-test, $p$<0.001).

**Table 3-2: Rates of particle-associated microbial respiration rates in phytodetrital aggregates. Means are given for each depth with full range in brackets. Results are for experiments carried out at 10 °C.**

| Depth (m) | Total $O_2$ consumption (nmol $O_2$ $agg^{-1}$ $d^{-1}$) | Volumetric $O_2$ consumption (nmol $O_2$ $mm^{-3}$ $d^{-1}$) | $C_{resp}$ (µg C $mm^{-3}$ $d^{-1}$)* | $C_{spec}$ ($d^{-1}$) ** | # aggregates measured |
|---|---|---|---|---|---|
| 36 | 1.25 (0.56-2.81) | 13.18 (8.03-17.77) | 0.158 (0.096-0.213) | 0.014 (0.006-0.030) | 6 |
| 46 | 2.04 (0.65-3.89) | 19.12 (9.49-43.76) | 0.230 (0.114-0.525) | 0.012 (0.004-0.021) | 10 |
| 73 | 2.46 (0.22-6.92) | 13.47 (4.69-37.67) | 0.162 (0.056-0.452) | 0.012 (0.004-0.030) | 15 |
| 113 | 0.98 (0.07-2.80) | 11.66 (3.10-32.39) | 0.140 (0.037-0.390) | 0.011 (0.002-0.024) | 10 |
| 128 | 0.93 (0.20-1.88) | 13.40 (3.22-19.73) | 0.161 (0.039-0.237) | 0.014 (0.003-0.020) | 8 |
| 204 | 0.46 (0.14-0.87) | 15.25 (4.05-36.77) | 0.183 (0.049-0.441) | 0.013 (0.003-0.031) | 7 |
| 500 | 0.74 (0.17-1.24) | 13.95 (4.86-24.71) | 0.167 (0.058-0.297) | 0.012 (0.004-0.021) | 5 |

* Volume specific respiration rate ($C_{resp}$)
**Carbon-specific respiration rate ($C_{spec}$)

**Table 3-3: Particulate organic carbon (POC) content of marine snow aggregates (PA). PA were grouped into size classes for bulk carbon measurement (see methods). ND=No Data**

| | ***Aggregate POC (*µg C $mm^{-3}$**) | |
|---|---|---|
| *Size range (ESD, mm)* | *<0.6* | *>0.6* |
| ***Sample Depth (m)*** | | |
| 36 | 17.0 | 6.7 |
| 46 | 30.6 | 11.0 |
| 73 | 15.0 | 8.9 |
| 113 | 16.5 | 9.4 |
| 128 | 11.7 | ND |
| 204 | 14.2 | ND |
| 500 | ND | ND |

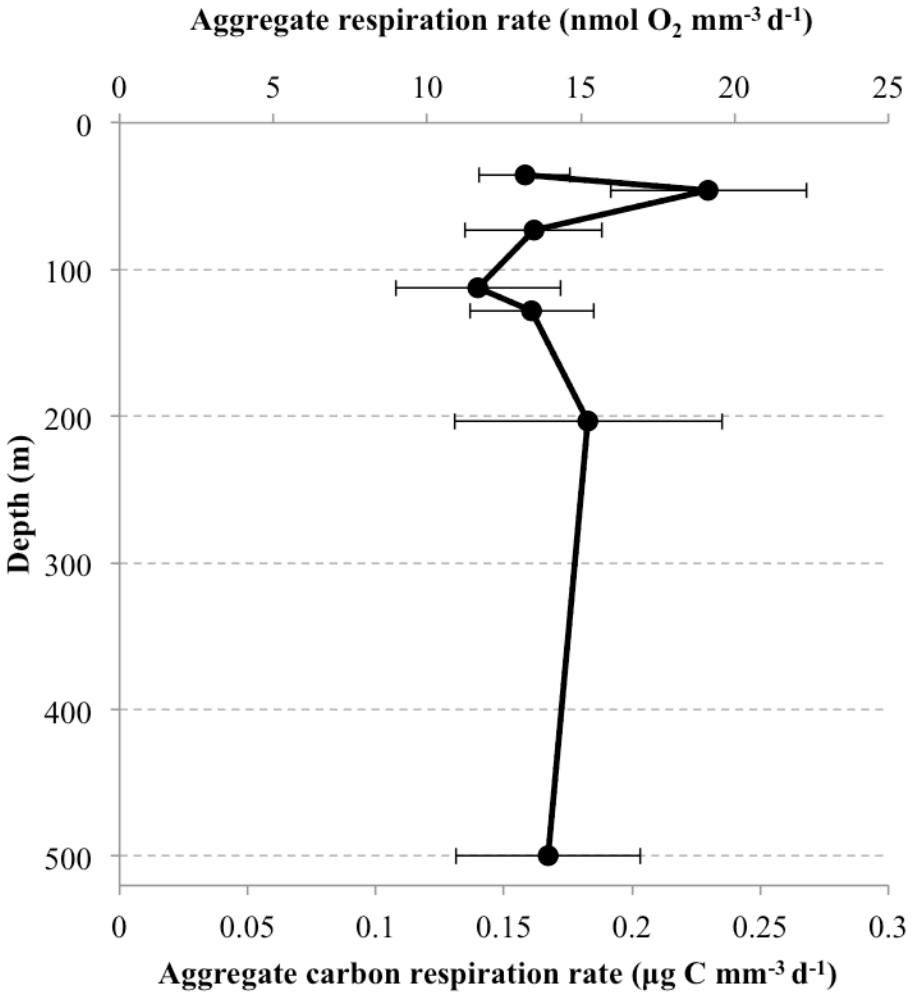


**Figure 3-7: Respiration rates of phytodetrital aggregates with depth. Oxygen fluxes to aggregates (nmol $O_2$ $mm^{-3}$ $d^{-1}$). For reference aggregate respiration rates are also shown in terms of carbon per aggregate volume (µg C $mm^{-3}$ $d^{-1}$). Data are for experiments carried out at 10 °C. Error bars represent ± one standard error of the mean.**

### 3.4.6 Zooplankton respiration

A total of four zooplankton net tows were carried out during the cruise alongside MSC deployments, one during the day and three at night. Daytime zooplankton DW over the upper 200 m was 313.4 mg DW $m^{-2}$, with night values ranging from 419.1 to 942.7 mg DW $m^{-2}$. Calculated zooplankton respiration rates ranged from 5.1 to 10.1 mg C $m^{-2}$ $d^{-1}$.

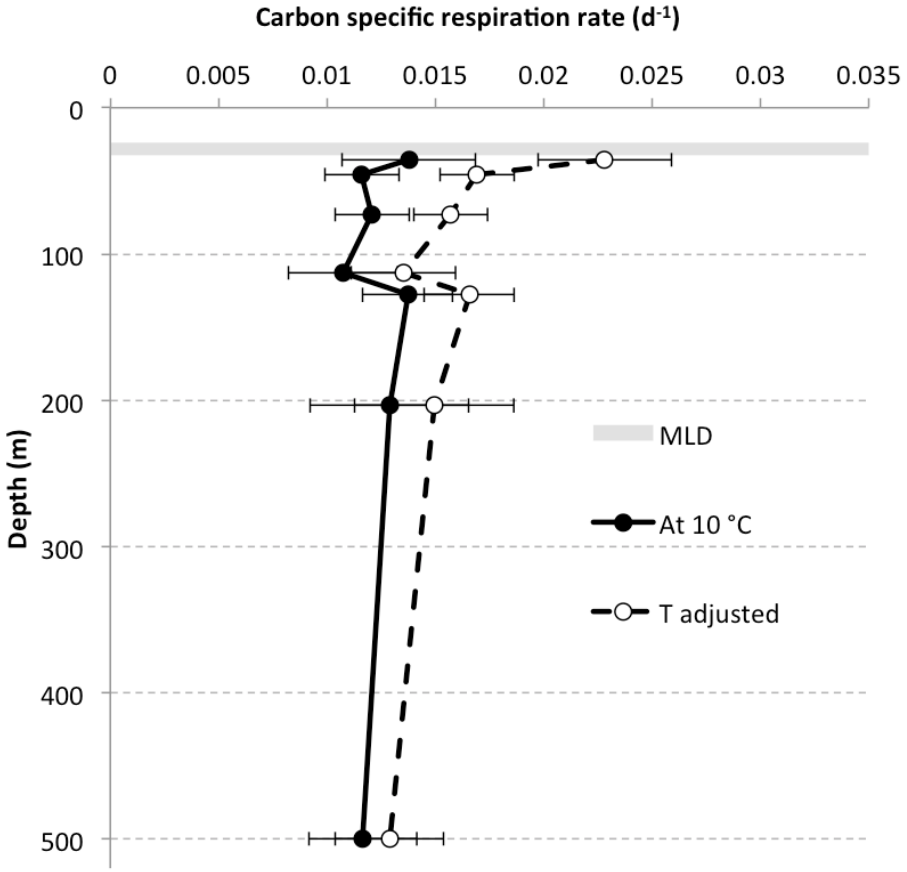


**Figure 3-8: Carbon-specific respiration rates ($d^{-1}$) for aggregates collected at depth. Rates adjusted to the *in situ* temperature (T) are shown by the dashed black line (open circles). Grey shading shows the range in mixed layer depth over the study period, and error bars represent ± one standard error of the mean.**

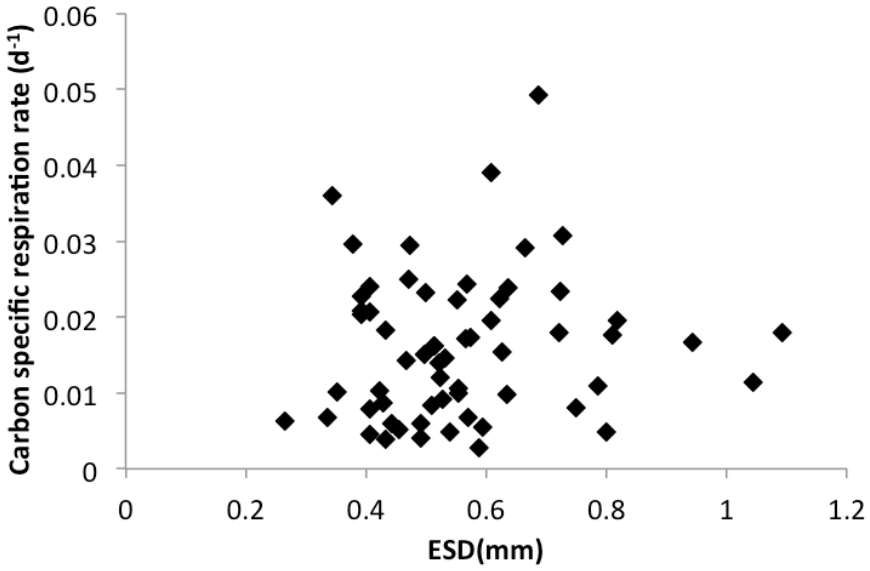

**Figure 3-9: Carbon-specific respiration rates ($d^{-1}$) of phytodetrital aggregates collected at depth. Data have been adjusted for *in situ* temperatures.**

## 3.5 Discussion

### 3.5.1 Rate of particle-associated microbial respiration

Although rates of respiration per PA volume were found to be relatively uniform with depth, there was variability within each depth range. This may reflect the heterogeneity in the availability of labile carbon and/or variation in microbial abundance, composition or activity within the PA. It may also simply be a result of the range in aggregate sizes at each depth, with higher respiration per volume in smaller aggregates that have higher POC:volume ratios (due to large aggregates having more complex shapes and structures, Logan and Wilkinson, 1990). The aggregate (0.14-1.09 mm ESD) POC contents measured here are 1.2-10.1 times higher than defined by the size relationship of Alldredge (1998) based on *in situ* collected 1-5 mm ESD marine snow of mixed composition, and are at the high end of the range of values measured on roller tank formed phytoplankton culture aggregates (0.9-4.6 mm ESD) by Iversen and Ploug (2010). The POC contents of >0.6 mm ESD PA (6.7-11 µg C $mm^{-3}$) do however compare well with the study of Laurenceau-Cornec et al. (2015) on aggregates formed in roller tanks from *in situ* collected phytoplankton assemblages; their regression between aggregate volume and POC content ($POC=0.58 \cdot Volume^{0.35}$) gives POC of 7.4 µg C $mm^{-3}$ for aggregates of 0.6 mm ESD.

In order to assess whether size related changes in carbon content of PA is the main cause of variability in volume specific respiration rates, the carbon-specific respiration rate ($C_{spec}$) has been calculated (Figure 3-8) based on the POC content of individual aggregates. There is a relatively small range in mean $C_{spec}$ (0.011-0.014 $d^{-1}$) for PA for each depth horizon. Iversen and Ploug (2010) measured higher rates of $C_{spec}$ (0.13 $d^{-1}$) in roller tank formed phytoplankton culture aggregates with lower POC contents, suggesting that POC content was not the limiting factor for respiration at the PAP site at the time of sampling. There was large variability in $C_{spec}$ for individual aggregates within each depth horizon (full data set range: 0.002-0.031 $d^{-1}$,Figure 3-8), but mean values of $C_{spec}$ showed only small variations with depth. This suggests that the factors driving the variability in $C_{spec}$ are either also quite constant with depth or counteracting. This study does not however account for any changes in respiration that may occur as a result of pressure changes with depth (see section 3.5.4). If microbes largely attach to particles in the surface ocean (Thiele et al. 2015), the starting abundance of microbes will be in part limited by the residence time of the particle in the surface ocean as dictated by sinking rate. The highest volume-specific abundances of microbes have been measured on the smallest aggregates (Grossart et al. 2003) which would be

expected to have lower sinking velocities. Variable microbial densities, driven by differences in sinking velocity and colonisation time, may therefore account for some of the variability in the rate of respiration per aggregate volume or POC content. Assuming no other factors are limiting respiration, increased microbial densities within an aggregate would lead to greater consumption of organic carbon and higher carbon-specific respiration rates. If colonisation times are controlled by the surface area of the aggregate, then smaller particles would have higher microbial densities due to higher surface area to volume ratios. However, large aggregates could also have high microbial densities following the aggregation of smaller aggregates, which may explain why there is no relationship between $C_{spec}$. and aggregate size. The abundance of microbes in an aggregate is determined by colonisation, detachment, growth and grazing mortality which in turn will be influenced by properties of the aggregate such as sinking speed, surface area to volume ratio, and carbon content and lability (Kiørboe 2003). Of these factors, grazing has been modelled to have a higher impact on bacterial abundances in aggregates than sinking rate (Kiørboe 2003). The microbial community on PA can be highly variable between PA (Grossart pers. comm.) and hence may also drive variability in respiration rate in PA.

Considering that all respiration measurements in this study were carried out at 10 °C (which is just below the temperature measured at 500 m depth), they therefore may not reveal the true vertical structure of particle-associated microbial respiration due to the influence of temperature on metabolic rates. To account for this a Q10 temperature coefficient of 3.5 was applied based on a study on PA (Iversen and Ploug 2013) and each $C_{spec}$ adjusted to the *in situ* temperature (dashed line Figure 3-8). In this way the rate expected to be occurring at *in situ* temperature is calculated. This gives higher rates in the upper ocean where temperature changes are higher, but the range with depth is still relatively narrow (mean 0.013-0.023 $d^{-1}$, full range 0.002-0.037 $d^{-1}$) and there is no relationship between PA size and $C_{spec}$ (Figure 3-9). In comparison, Ploug and Grossart (2000) measured $C_{spec}$ of 0.083 ± 0.034 $d^{-1}$ on aggregates formed from phytoplankton cultures at 16 °C. Iversen and Ploug (2010) measured an mean $C_{spec}$ of 0.13 $d^{-1}$ at 15 °C, but a range of 0.005-0.422 $d^{-1}$, for lab formed aggregates of three different phytoplankton cultures. Similarly, rates of 0.13 $d^{-1}$ (range 0.02-0.36 $d^{-1}$) were measured at 18 °C in aggregates formed in roller tanks from peak fluorescence waters off Cape Blanc, Africa (Iversen et al. 2010). These studies find a lack of size dependency in $C_{spec}$, consistent with the observations of this study. Measurements made here are towards the low end of these literature measurements which cannot be explained by differences in temperature alone based on a Q10 factor of 3.5 (Iversen and Ploug 2013). Recalculating the mean $C_{spec}$ at each depth based on the upper bound of respiratory quotients that are typically applied in the literature (1.2, Berggren et al. 2012), increases values of $C_{spec}$ to 0.019-0.033 $d^{-1}$, which are still lower than the aforementioned studies.

There have been limited measurements made on natural aggregates formed *in situ*. McDonnell et al. (2015) utilised *in situ* incubators to measure $C_{spec}$ of 0.4 $d^{-1}$ at the Bermuda Atlantic Time Series (BATS) station and 0.01 $d^{-1}$ off the western Antarctic Peninsula (WAP). Collins et al. (2015) carried out incubations with and without sinking particles collected in the North Atlantic, revealing $C_{spec}$ of 0.007-0.084 $d^{-1}$ with one higher value at 0.173 $d^{-1}$. These rates are more in line with those measured here, yet there are still considerable differences between studies.

### 3.5.2 Role of particle-associated microbes in mesopelagic POC flux attenuation

Despite the uncertainties in the mechanisms governing rates of particle-associated microbial respiration, it is still possible to assess the importance of particle-associated microbial respiration on the attenuation of fast-sinking POC in the mesopelagic and compare results to the small number of other recent studies (Collins et al. 2015; McDonnell et al. 2015). The flux of fast-sinking POC ($F_z$) at each depth ($z$) that would result if the only loss was via particle-associated microbial respiration was calculated. Calculations were based on the relationship between the remineralisation length scale ($L$ in $m^{-1}$) (see Iversen and Ploug, 2013; Iversen et al. 2010), carbon-specific respiration rate ($C_{spec}$ in $d^{-1}$) and sinking velocity ($w$ in m $d^{-1}$).

$$\boldsymbol{L = \frac{C_{spec}}{w} = (-ln(F_z/F_{z0})/(z - z_0))} \qquad \textbf{(Equation 3-5)}$$

Upper and lower bounds on the remineralisation length scale were calculated based on uncertainties in measurements of $C_{spec}$ and $w$ made in this study, as described in section 3.3.5. Comparisons are made between the observed fast-sinking POC flux attenuation and predicted losses via particle-associated microbes over two discrete depth horizons; a region of rapid attenuation of 36-128 m (upper mesopelagic) and slow attenuation zone of 128-500 m (mid mesopelagic). Note that the non-steady state value of POC flux at 500 m is excluded and instead the value predicted from the power-law fit is used (Figure 3-5) with bounds based on the standard deviation of the $b$ value estimated via bootstrap analysis (see section 3.3.5). The data of this study suggest that particle-associated microbial respiration plays only a minor role in POC attenuation in the upper mesopelagic (8%; range: 1-14%), but becomes more important below this (33%; range: 12-50%) as the rate of POC attenuation decreases (Figure 3-10a). Measurements are based on a subsample of the total assemblage of particles found in the water column, in particular only PA. If rates of microbial respiration are vastly different on other particle types, such as FP or appendicularian houses, then this would affect calculations of POC removal by particle-associated microbes. However, considering the dominance of PA in samples (Figure 3-3) it is believed that measurements reflect the bulk of the sinking material at the time of sampling. It was not possible to measure respiration rates on FP due to their low numbers and small size which adds

uncertainty to the estimate of the contribution of particle-associated microbial respiration to POC loss. However, rates measured on FP in the Scotia Sea, Antarctica are low (0.01-0.065 $d^{-1}$, Chapter 2) and even if FP were respired completely, they account for less than 10% of the flux between 36 and 128 m and thus could not resolve the large imbalances between POC supply and respiration observed here in the upper mesopelagic.

Low rates of respiration result in only a very small loss of POC with depth below the euphotic zone. Thus the data presented here agree with a recent study (Collins et al. 2015), suggesting that only a small fraction of fast-sinking POC is removed by particle-associated bacteria. Despite being hotspots for microbial activity compared to the water column (Thiele et al. 2015), particle-associated microbial respiration on fast-sinking particles may still be a minor contributor to the reduction in POC flux when compared to rapid loss via processes such as zooplankton grazing and fragmentation (Dilling and Alldredge 2000; Stemmann et al. 2000; Svensen et al. 2014). This hypothesis is supported by measurements made in the mesopelagic of the Scotia Sea on FP (Chapter 2) and on PA off Cape Blanc, Africa (Iversen et al. 2010), as well as model studies (Stemmann et al. 2004; Gehlen et al. 2006).

### 3.5.3 Mesopelagic carbon budget

A number of previous studies have revealed large imbalances in the mesopelagic carbon budget with heterotrophic organic carbon demand (typically assessed from 100 to 1000 m) exceeding POC supply by 2-3 orders of magnitude (Reinthaler et al. 2006; Steinberg et al. 2008; Baltar et al. 2009; Burd et al. 2010). Recently, advances in our understanding enabled the mesopelagic carbon budget at the PAP site to be balanced over 50-1000 m (Giering et al. 2014). However, a more in depth analysis revealed an imbalance between POC supply and bacterial carbon demand when the upper (50-150 m) and lower mesopelagic (150-1000 m) were examined separately, with an oversupply of POC in the upper mesopelagic and an undersupply in the lower mesopelagic (Giering et al. 2014). The same imbalance in the upper mesopelagic is found here, and as particle-associated respiration was not directly measured in the aforementioned study, measurements made here allow assessment of whether this term could help to explain observed imbalances. In this way it is possible to test whether the low respiration rates (0.001-0.173 $d^{-1}$) measured by Collins et al. (2015) are also applicable to the PAP site or whether the higher rates, such as observed in the western subtropical North Atlantic gyre (0.4 $d^{-1}$) by McDonnell et al. (2015) are more appropriate. As the zooplankton net tows were integrated to 200 m, sources and sinks of POC are compared over the depth range of 36-200 m.

Although low rates of both absolute and carbon-specific PA microbial respiration (<3% $d^{-1}$) were measured, suggesting that this term cannot resolve imbalances in the upper mesopelagic carbon budget, the importance of particle-associated microbes may have been underestimated if solubilisation of POC to DOC by ecto-enzymatic hydrolysis was significant (Smith et al. 1992; Grossart and Simon 1998; Alldredge 2000). This solubilisation to DOC is likely to fuel the respiration of free-living microbes, and hence remineralisation to DIC. Smith et al. (1992) estimated that 97% of the hydrolysates produced by bacteria in marine snow were released, with the remaining 3% being utilised by bacteria in the aggregate. However, this value was based on nitrogen-rich amino acids in fresh aggregates (from the upper 25 m) and hydrolysis for carbon is likely lower as it is lost more slowly than nitrogen from sinking particles. Additionally, solubilisation losses are probably lower in older detritus (Anderson and Tang 2010); Grossart and Ploug (2001) estimated that 26% of the POC was taken up by particle-associated bacteria on old aggregates. To calculate potential hydrolysis of carbon from particles, following Anderson and Tang (2010) a value of 50% is conservatively assumed (i.e. assuming the measured loss via respiration is 50% of the total POC loss via particle-associated microbes). This value sits between Smith et al.'s (1992) value and carbon solubilisation losses of <30% measured in copepod faecal pellets which are much less porous (Møller et al. 2003). Conservative upper and lower bounds of 30 and 80% solubilisation are set based on the aforementioned studies. With additional loss of fast-sinking POC via solubilisation particle-associated microbes can explain 25% (9-72% based on Monte Carlo analysis on respiration rates and the above range in solubilisation) of POC losses over the upper 36-200 m (Figure 3-10b). In spite of the limitations in estimations of solubilisation it is clear that a large discrepancy still remains in terms of an excess POC supply of 172 mg C $m^2$ $d^{-1}$ (65-210 mg C $m^{-2}$ $d^{-1}$) over the upper 36-200 m.

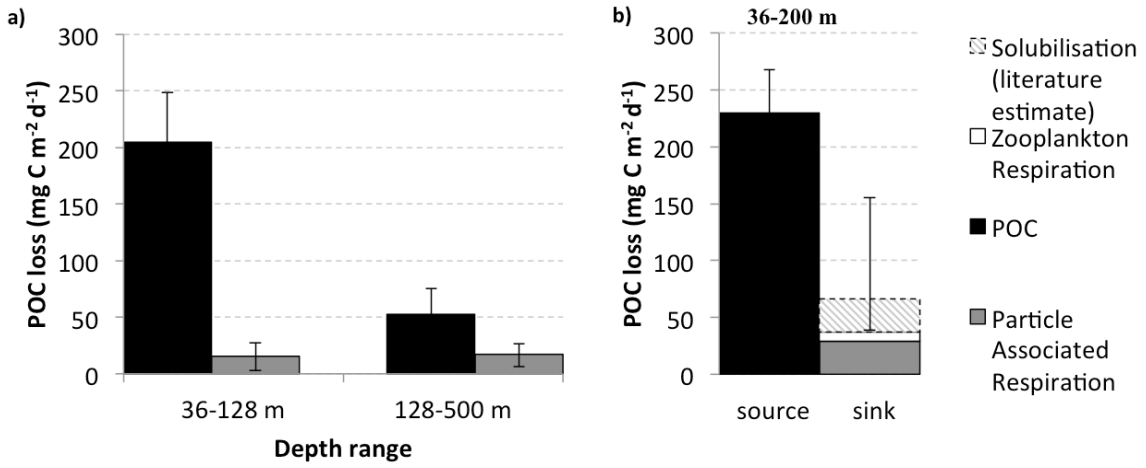


**Figure 3-10: Balance of processes controlling fast-sinking POC flux attenuation. (a) Comparison of observed POC loss (black bars) and estimated POC loss based on particle-associated microbial respiration (grey bars) over two depth horizons (36-128 m,**

**and 128-500 m). (b) POC sources and sinks in the upper 200m. Additional losses ('sinks') via solubilisation of POC to DOC by particle-associated microbes (estimate based on respiration, see section 3.5.3), and zooplankton respiration (estimate based on zooplankton biomass and allometric equations). Error bars show uncertainties from sensitivity analysis.**

The other direct loss of POC in the mesopelagic is via zooplankton respiration and 'sloppy feeding' (cell breakage during feeding and subsequent release of DOC) (Jumars et al. 1989). Zooplankton respiration rates measured here are likely an overestimate of their contribution to POC losses between 36 and 200 m as they include both migratory and non-migratory individuals, as well as individuals above the mixed layer depth. Even with these overestimations, zooplankton respiration (5.1-10.1 mg C $m^{-2}$ $d^{-1}$) accounts for only a small POC sink in this upper region of the mesopelagic (Figure 3-10b). Losses of POC to DOC or suspended POC via sloppy feeding cannot be accounted for here.

The direct hydrolysis by attached microbes likely supplies free-living communities with DOC (Cho and Azam 1988; Karl et al. 1988; Kiørboe and Jackson 2001). However, by definition free-living microbes are not associated with particles and hence do not contribute directly to the loss of large fast-sinking POC measured here, and as such this loss process is not considered. The definition of dissolved and particulate is operationally based on the pore size of a GF/F filter, and therefore microbes defined as 'free-living' may in fact be able to utilise colloids (Arístegui et al. 2009). However as only the loss of large, fast-sinking POC is measured, free-living prokaryotes are excluded from analysis of fast-sinking POC loss processes. Free-living prokaryotic respiration may account for the ultimate loss of organic carbon from the organic carbon pool but it is suggested here that this is reliant on mechanical breakdown of large, fast-sinking POC by zooplankton and protozoa (Lampitt et al. 1990; Iversen and Poulsen 2007; Poulsen and Iversen 2008; Poulsen et al. 2011) and enzymatic hydrolysis (Smith et al. 1992). Previous measurements at the PAP site suggest that prokaryotic respiration results in loss rates of 42 mg C $m^2$ $d^{-1}$ between 36 and 203 m which greatly exceed estimated DOC input to the upper 1000 m (15 mg C $m^2$ $d^{-1}$) (Giering et al. 2014), supporting this hypothesis.

POC loss via zooplankton respiration, particle-associated microbial respiration and solubilisation, as typically invoked in model studies (e.g. Anderson and Tang, 2010) can therefore not account for observed losses of fast-sinking POC in the upper mesopelagic, suggesting our knowledge of the mesopelagic carbon budget is still poorly constrained and/or incomplete.

### 3.5.4 The missing piece of the mesopelagic carbon budget?

Before beginning to examine whether there is indeed missing a piece of the upper mesopelagic carbon budget puzzle, the limitations of estimates made thus far must be examined, which may in themselves rectify imbalances. Large uncertainties surround estimates of solubilisation by particle-associated microbes. A solubilisation of 87% is required to balance the budget presented here (36-200 m) which is believed to be high considering estimates of 97% for nitrogen in fresh aggregates (Smith et al. 1992) which is remineralised first proportionally. In addition, as particle-associated microbial respiration is able to account for a greater proportion of the fast-sinking POC loss in the mid mesopelagic (200-500 m), solubilisation losses would need to be lower over this depth region (66%) to maintain a balance. Increased solubilisation would present itself in the form of increased DOC and/or increased rates of microbial respiration, however, these terms are included in the estimate by Giering et al. (2014) and a large imbalance in the upper mesopelagic is still apparent in their budget. In this study, it is not possible to rule out increased solubilisation in the upper mesopelagic as an additional sink term, but it is considered unlikely to solve the imbalance.

Although the method of measuring particle-associated microbial respiration utilised here attempts to avoid bottle effects and accurately simulate the environment of a sinking particle, it was not possible to simulate pressure changes. Colonisation of particles by pressure adapted microbial communities at depth may lead to an underestimation of *in situ* microbial activity using decompressed samples (Tamburini et al. 2013). Recent work suggests that the attached microbial community on sinking particles is 'inherited' from the fluorescence maximum (Thiele et al. 2015); these organisms are not adapted to changes in pressure (Tamburini et al. 2006, 2009) and temperature, and therefore exhibit lower prokaryotic growth efficiencies (PGE) and overall metabolic rates. Similarly, the experiments of this study were carried out at constant temperatures whereas particles sinking through the water column will experience the range of water column temperatures, likely impacting all metabolic processes. A further limitation of this study is the lack of replicate MSC deployments at each depth. Although numerous aggregate respiration rates were measured from each sample, high patchiness in the type and source location of sinking particles could result in greater variability in respiration rates.

Additionally it was not possible to measure mechanical disaggregation via processes such as fluid shear which could provide additional losses of large sinking POC. The forces required to break apart large marine snow aggregates have been shown to be higher than typical estimates of energy dissipation in the ocean, suggesting that this would not be a major loss process (Alldredge et al. 1990). Physical disaggregation could be more important in surface waters where dissipation

rates can exceed the forces required to break marine snow aggregates (Alldredge et al. 1990; Burd and Jackson 2009). However, it is suspected that only a small fraction of sinking POC would be fragmented by abiotic processes to particles <0.15mm and hence would not explain the large loss of fast-sinking POC measured in this study.

In order to address imbalances in the sources and sinks of fast-sinking POC to the upper mesopelagic an additional loss process of POC is required. One key term missing from the budget is that of free-living protozoans which would not be collected in zooplankton nets and can make up a substantial part of marine planktonic ecosystems (Biard et al. 2016). Laboratory experiments on copepod FP reveals that dinoflagellates degraded FP over three times faster than bacteria (0.18 $d^{-1}$ compared to 0.04 $d^{-1}$), and the combined effects of bacteria, dinoflagellates and copepods led to FP degradation rates of 1.12 $d^{-1}$ (Svensen et al. 2014). Dinoflagellates and ciliates have been shown to feed on FP (Poulsen and Iversen 2008; Poulsen et al. 2011) and PA (Tiselius and Kiørboe 1998). Therefore POC loss via protozoan respiration may account for at least some of the additional POC loss required to resolve imbalances in upper mesopelagic carbon budgets, although respiration by any attached protozoans would be included in the microsensor measurements presented here.

Loss of sinking POC via fragmentation of large sinking particles into small (<0.15 mm ESD) and non-sinking particles by both abiotic and biotic means may also explain some of the observed imbalance in the upper mesopelagic as the POC fluxes measured here are for 'fast-sinking' particles only (see section 3.3.3). These slow-sinking particles may be an important part of the part of total POC flux in some regions (Alonso-González et al. 2010; Riley et al. 2012; Dall'Olmo and Mork 2014; Durkin et al. 2015; Giering et al. 2016). Slow-sinking particles have been found to have the same degradation state as, or be fresher than, fast-sinking particles (Abramson et al. 2010; Alonso-González et al. 2010) and may be an important carbon source for mesopelagic biota (Giering et al. 2016). However, loss processes such as respiration rates on slow-sinking particles were not measured in this study, and hence it is not possible to extend the budget presented here to this carbon pool. Determining rates of respiration on slow-sinking particles is a key area for future research and may help reconcile imbalances in the carbon budget when looking at the total organic carbon pool. It is hypothesised here, in line with a growing number of other studies (Iversen et al. 2010; Cavan et al. 2015; Collins et al. 2015), that zooplankton living in the upper mesopelagic may stimulate the loss of large, fast-sinking POC via fragmentation from sloppy feeding, swimming activities and/or microbial gardening (Iversen and Poulsen 2007; Mayor et al. 2014). Fast-sinking particles can reach the deep ocean with minimal degradation due to the short time in which they are available for degradation (Iversen and Ploug 2010). Conversely, once fragmented, the increased residence times (in terms of their sinking velocity) of slow and non-

sinking POC allows removal to occur at low rates, on longer timescales by microbial respiration. Assuming that all of the measured excess POC (i.e. not explained by particle-associated microbial respiration, zooplankton respiration or solubilisation) in the upper 36-200 m is turned into slow-sinking POC with an mean sinking velocity of 9 m $d^{-1}$ (Alonso-González et al. 2010; Riley et al. 2012), it is possible to calculate the respiration rate required to completely remove this excess POC based on equation 3.5. This slow-sinking material would need to be respired at a rate of 0.08 $d^{-1}$ (0.04-0.13 $d^{-1}$), which is not too dissimilar from the rates measured here on fast-sinking particles, thus providing support to the hypothesis of fragmentation.

In theory, a seasonal balance in POC driven by fragmentation of fast-sinking particles should present itself in the form of an increase in slow and non-sinking POC following the seasonal peak in fast-sinking POC and a more gradual decline over the season. This less rapid seasonal decline in slowly sinking material is apparent in the results of a biogeochemical model study for subpolar regions (Henson et al. 2015). Seasonal cycles in particulate carbon in the upper 75 m (seasonal range of 2.3 µM via GF/F filtering) have been detected following analysis of long-term time series data at station ALOHA in the Pacific (Hebel and Karl 2001). They suggest that the buildup and removal of standing stocks of POC do not require a large degree of decoupling between production and loss processes and can exist due to small but sustained differences. Considering the highly dynamic nature of the typical bloom-bust scenario of the North Atlantic it seems unlikely that a balance in source and sink processes would be found by snapshot measurements such as those made here.

Additional inputs/losses of organic carbon could be driven via physical processes such as advection or changes in mixed layer depth (e.g. Dall'Olmo and Mork, 2014). Although the mixed layer was relatively stable during the period of study, the winter deepening in MLD to 250 m (Hartman et al. 2015) could provide a seasonal balance to the budget if concentrations of slow and non-sinking particles are sufficiently high (Bochdansky et al. 2016). Similarly, advective processes are unaccounted for as a source/sink of carbon in this study and could result in closer agreement between sources and sinks.

## 3.6 Conclusions

This chapter presents a unique vertical profile of particle-associated microbial respiration measured directly on sinking marine aggregates collected at depth. Rates of carbon-specific respiration were relatively constant with depth, and particle-associated microbial respiration amounts to a small loss term in the mesopelagic carbon balance. It is suggested here that it may be possible to explain the loss of fast-sinking particles (>0.15 mm ESD) in the upper mesopelagic

through a combination of particle-associated microbial respiration, solubilisation, and the conversion into small (<0.15 mm ESD) and non-sinking POC via zooplankton and protozoan mediated processes. Material lost through fragmentation would be retained in the upper mesopelagic allowing it to be slowly respired over time and enabling a balance of the mesopelagic carbon budget over seasonal timescales. However, detailed information about fragmentation processes are lacking and are needed to better constrain the upper mesopelagic carbon flows. Moreover, there is a need for seasonally resolved studies (of fast and slow-sinking pools of carbon) to get a better appreciation of how changing primary production in a non-steady state system can influence seasonal fluxes of POC in the mesopelagic.

# Chapter 4. Antarctic krill facilitate efficient carbon export at the marginal ice zone in spring

This chapter in in review at the journal Polar Biology as:

Belcher, A. Tarling, G.A. Manno, C. Ward, P. Atkinson. A. Henson, S.A. Sanders, R. *in review* Antarctic krill facilitate efficient carbon export at the marginal ice zone in spring*, Polar Biology*

Data collection, analysis and manuscript writing was led by Anna Belcher. G. Tarling, C. Manno and P. Ward were involved in early hypothesis development, and G. Tarling also advised data analysis. A. Atkinson provided supporting KRILLBASE data, and R. Sanders and S. Henson provided funds to support the PhD studentship and fieldwork of Anna Belcher as well as advice on the manuscript.

## 4.1 Abstract

Antarctic krill (*Euphausia superba*) play a central role in the food web of the Southern Ocean, forming the link between primary production and large predators. Krill produce large, rapidly sinking faecal pellets (FP) which can be a large component of mesopelagic particulate organic carbon (POC) fluxes. However, the patchy distribution of krill swarms means that limited moored sediment trap coverage in the Southern Ocean may not fully capture these episodic, but potentially large, carbon fluxes. Particle flux and composition (particle type) were measured using Marine Snow Catchers in the marginal ice zone near the South Orkneys, Antarctica. Krill FP were the dominant component of the POC flux in the upper 200 m (typically 60-85%). These direct estimates of krill FP POC flux (33-154 mg C $m^{-2}$ $d^{-1}$) are compared to estimates of krill FP production based on a database of krill density and literature FP egestion rates, and krill FP attenuation rates in the upper mesopelagic were calculated. Concurrence between these two approaches indicates that krill FP are transferred very efficiently through the upper mesopelagic. In this chapter, it is proposed that POC fluxes in the Southern Ocean may be underestimated in regions where krill densities are high, particularly in marginal ice zones such as those in the Atlantic sector where abundances of smaller recycling metazoan species are low. Taking account of krill distributions and reduced attenuation of their FP instead of assuming globally averaged attenuation rates of POC, would mean that the biological pump in the Southern Ocean is stronger than currently estimated by global biogeochemical models.

## 4.2 Introduction

The Southern Ocean is a region where key processes within the global carbon cycle occur, with the region south of 40 °S (~21% of the ocean area) estimated to account for 26 ± 6% of global export production (defined as the material exported out of the surface ocean) (Primeau et al. 2013). Empirical models suggest that the export of material out of the euphotic zone in the Southern Ocean is efficient but that the transfer of this material through the mesopelagic to the deep ocean is inefficient (Henson et al. 2012a). The efficiency with which carbon sinks through the mesopelagic by the biological carbon pump (BCP) is intrinsically linked to levels of atmospheric $CO_2$ (Kwon et al. 2009). Further, the BCP in much of the Southern Ocean does not operate at maximum efficiency as primary production is limited by factors including light and iron (Boyd et al. 1999), leading to upwelled nutrients being subducted unused into the ocean interior.

However, this picture conceals the existence of high biomass, low export (HBLE) conditions in some regions of the Southern Ocean (Lam and Bishop 2007, Ebersbach et al. 2011, Rembauville et al. 2015). These can support intense export events associated with sinking diatoms (e.g. Smetacek 1985, Beaulieu 2002, Roca-Marti et al. 2015), diatom resting spores (Rembauville et al. 2015a), enhanced iron supply (e.g. Bidigare et al. 1999, Savoye et al. 2008, Pollard et al. 2009, Smetacek et al. 2012, Jouandet et al. 2014), and the influence of marginal ice zones (Smith and Nelson 1985; Fischer et al. 1988; Buesseler et al. 2001; Cavan et al. 2015). Short term, high export events can make up a substantial fraction of the annual POC flux. In the Bransfield Strait, 97% of the annual POC flux occurred in the two most productive months, associated with *Euphausia superba* (herein referred to as krill) faecal pellets, (Bodungen et al. 1987; Wefer et al. 1988), yet limited observations in these marginal ice zones mean that krill and their large faecal pellet fluxes are not well represented in global biogeochemical models.

In certain periods of the year, faecal pellets (FP) can make up a large component of the POC flux collected by sediment traps in the Southern Ocean and are often linked to the presence of krill (Wefer et al. 1988; Dubischar and Bathmann 2002; Accornero et al. 2003; Gleiber et al. 2012). Krill are present in high densities in some regions of the Southern Ocean (Atkinson et al. 2008) often occurring in large swarms (Hamner et al. 1989). The production of large numbers of FP by krill swarms can result in large fluxes of FP out of the euphotic zone (Bodungen 1986; Accornero et al. 2003). However, the patchy distribution of krill swarms and the highly variable composition and sinking speed of the FP (Cadée et al. 1992; Atkinson et al. 2012) means that their contribution to flux can be episodic and therefore difficult to sample.

Cadée (1992) deployed floating sediment traps for <1 day at 50-75 and 150 m in the Weddell-Scotia Sea, observing that krill FP dominated the trap material. One station in particular (out of 5)

exhibited exceptionally high POC fluxes (0.7 g C $m^{-2}$ $d^{-1}$ at 75 m, and 1.5 g C $m^{-2}$ $d^{-1}$ at 150 m) dominated by krill FP. Cadée (1992) postulated that this large export event was related to a krill swarm, observed following trap deployment. High export of krill FP has also been observed during short term sediment trap deployments in the Bransfield Strait and Weddell Sea (Dunbar 1984; Bodungen et al. 1987; Bathmann et al. 1991). Similarly, a long term sediment trap study in Terra Nova Bay in the Ross Sea noted atypically high POC fluxes (11.13 mg $m^{-2}$ $d^{-1}$ at 95 m) in late April-mid June (Accornero et al. 2003), dominated by cylindrical faecal pellets (74-80% of FP) suggesting that large swarms of euphausiids could also be important contributors to flux in the winter. High organic carbon fluxes (139.9 mg C $m^{-2}$ $d^{-1}$) were observed at depths of 1588 m in the Bransfield Strait by Wefer et al. (1988) associated with krill FP. Observational evidence therefore suggests that krill FP can both provide a vehicle for high export of POC, and may also transfer carbon efficiently through the mesopelagic.

Pellets may however be broken up by zooplankton as they sink, decreasing the efficiency of export to the deep sea (Iversen and Poulsen 2007), as has been suggested to explain high retention of krill FP in the study of González (1992). González (1992) suggests that where krill FP production is high relative to abundances of the zooplankton recycling community, a large percentage of krill FP can pass undisturbed through the mesopelagic zone and reach deep sediment traps. Even if krill FP are grazed upon by deeper dwelling zooplankton populations this could still result in fresh pellets reaching the deep sea via a cascade effect (Urrere and Knauer 1981; Bodungen et al. 1987; Miquel et al. 2015).

The classic 'Martin curve' was defined on the basis of sediment trap deployments in the Pacific, which revealed that the loss of POC with depth can be described by a power-law curve with attenuation rate (*b* value) of 0.86 (Martin et al. 1987). Previous global biogeochemical (GBC) models, such as that of Sarmiento et al. (1993) and those in the Ocean Carbon Model Intercomparison Project 2 (OCMIP-2, Najjar and Orr 1998) used a uniform and temporally invariant value to quantify the loss of POC with depth. However, this is overly simplistic and more recent studies show regional variability in POC attenuation (Lutz et al. 2007; Honjo et al. 2008; Henson et al. 2012a; Marsay et al. 2015). Some newer models allow regional variability, for example by incorporating the protection of sinking POC by minerals following Armstrong et al. (2002) (e.g. Yool et al. 2011, Dunne et al. 2013), or by a relationship with temperature (e.g. Aumont and Bopp 2006). However, there are no GBC models that incorporate the episodic but potentially large export fluxes driven by krill FP or which attenuate these fluxes accurately. Inclusion of these episodic fluxes into GBC models requires knowledge of the amplitude and attenuation rate of these fluxes, as well as knowledge of the krill distributions and the regions where these fluxes are significant.

Krill occur mostly in swarms which may produce enough FP to overload the capacity of the zooplankton community (mainly microzooplankton species such as *Oncaea* spp. and *Oithona* spp.) to fragment and/or remineralise their FP before they sink to the ocean interior. However the patchy distribution of krill swarms and the relatively sparse number of FP flux measurements in the Southern Ocean, means that this potentially large export flux of POC to the mesopelagic is poorly quantified and it is not yet clear from previous studies whether krill FP are transferred efficiently through the upper mesopelagic (e.g. Cadée et al. 1992, González 1992, Le Fèvre et al. 1998, Gleiber et al. 2012). The ratio of krill grazers to smaller recycling metazoan species may have an important influence on the proportion of krill FP that reach the mesopelagic layers and variations in this ratio (related to the patchy nature of krill swarms) may in part explain contrasting observations on the contribution of krill FP to POC flux.

To ascertain the potential contribution of krill FP to POC flux, sampling was conducted in the marginal ice zone (MIZ) near the South Orkney Islands, a region where krill abundances are known to be high but mesozooplankton abundances low (Atkinson et al. 2008; Ward et al. 2012a; b). In this chapter, I attempt to quantify directly the transfer of krill FP through the upper mesopelagic by comparison of krill FP production rates in the epipelagic and observations of krill FP flux in the mesopelagic made in Austral spring.

## 4.3 Methods

### 4.3.1 Study site

Faecal pellet (FP) fluxes were estimated aboard RRS *James Clark Ross* during cruises JR291 and JR304 to the Scotia Sea, Antarctica in austral spring 2013 and 2014 respectively (Figure 4-1A). Samples were obtained in the marginal ice zone at stations ICE1 (60.21 °S, 46.34 °W) and ICE2 (59.96 °S, 46.16 °W) during JR291 (01/12/2013), and ICE2 only during JR304 (26/11/2014). There was no ice cover at the time of sampling, but satellite data reveal intermittent ice cover in the weeks prior to sampling (Figure 4-2).

### 4.3.2 Particle collection

Sinking particles were collected using Marine Snow Catchers (MSCs). These are large (95 L) PVC closing water bottles designed to minimise turbulence (Riley et al. 2012). Vertical profiles of temperature, salinity and fluorescence were taken prior to MSC deployments using a Conductivity-Temperature-Depth (CTD) unit (Seabird 9Plus with SBE32 carousel) to define the base of the mixed layer and thus MSC deployment depths. To assess the attenuation of FP in the

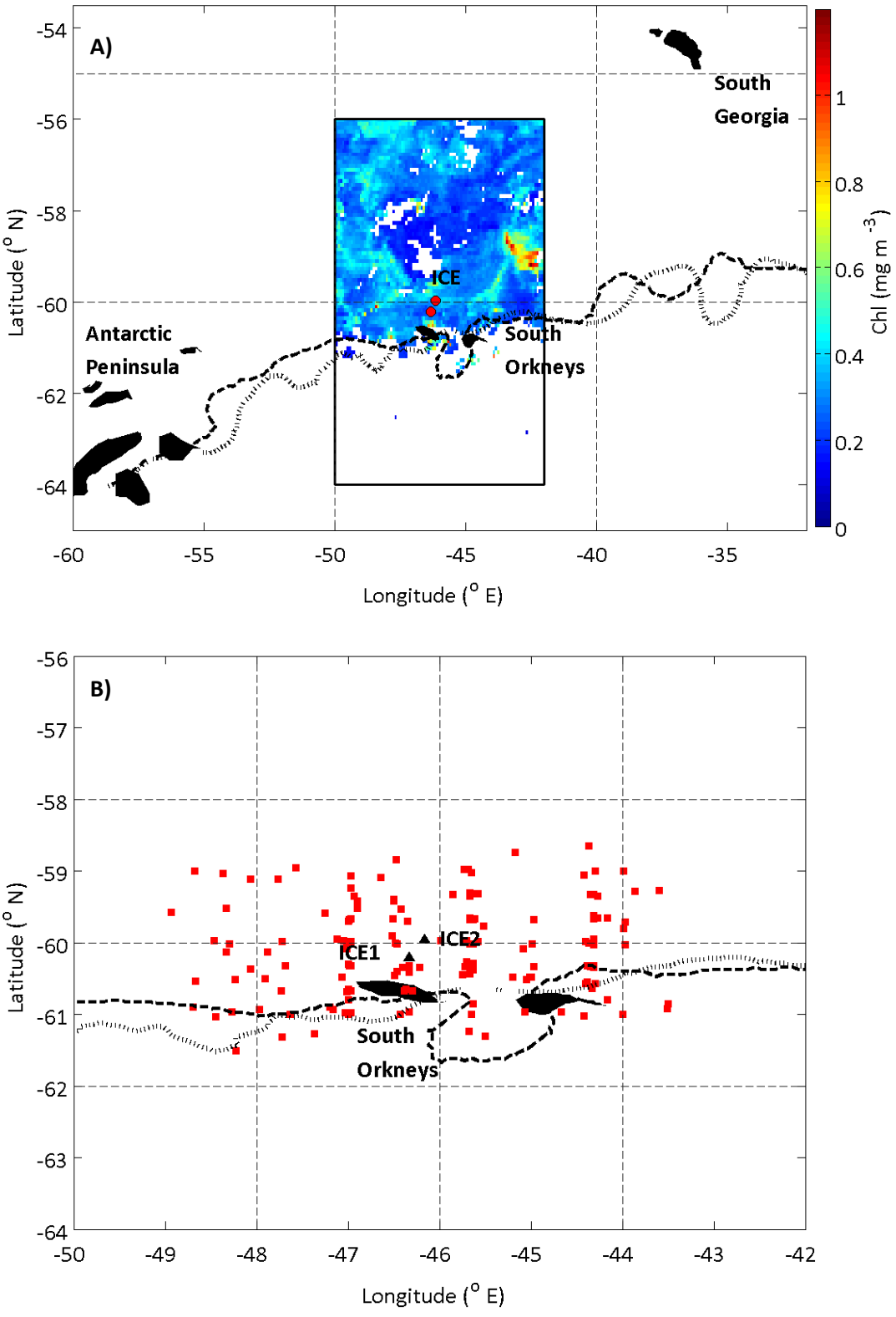


**Figure 4-1: A) ICE station locations (indicated by red circles) overlain on MODIS Aqua satellite chlorophyll (mg $m^{-3}$) for December 2014. Position of ice edge on December 14th 2014 (thick black dashed line) and December 3rd 2013 (black dotted line) (OSTIA sea ice data). Black box shows region covered by Figure 3-1B. B) Location of krill density samples taken from KRILLBASE for ICE1 and ICE2 (red squares). ICE1 and ICE2 stations are shown by large black triangles.**

upper mesopelagic, two MSCs were deployed in quick succession at 10 m and 110 m below the base of the mixed layer depth (MLD), herein referred to as MLD+10 and MLD+110 respectively. MSCs were deployed during the day at ICE2 during both cruises and, due to logistical constraints, 1-1.5 hours after sunset at ICE1.

Following deployment and recovery of the MSCs (which typically took 0.25-0.5 hours), they were left on deck for a two hour settling period, before draining the bottle and carefully removing the particle collector tray (divided into four quadrants for sample splitting) from the base which was stored at 2-4°C for further analysis. Fast-sinking particles are operationally defined here as particles sinking fast enough to reach the base of the MSC during this time (Riley et al. 2012), which, given the height of the snow catcher of 1.53 m requires a minimum sinking rate of 18.4 m $d^{-1}$ for particles to reach the base of the MSC. This settling period is more than sufficient to allow FP to reach the tray based on previous direct measurements of FP sinking velocity in the Southern Ocean which range from 27 m $d^{-1}$ to 1218 m $d^{-1}$ (Atkinson et al. 2012; Cavan et al. 2015; Chapter 2).

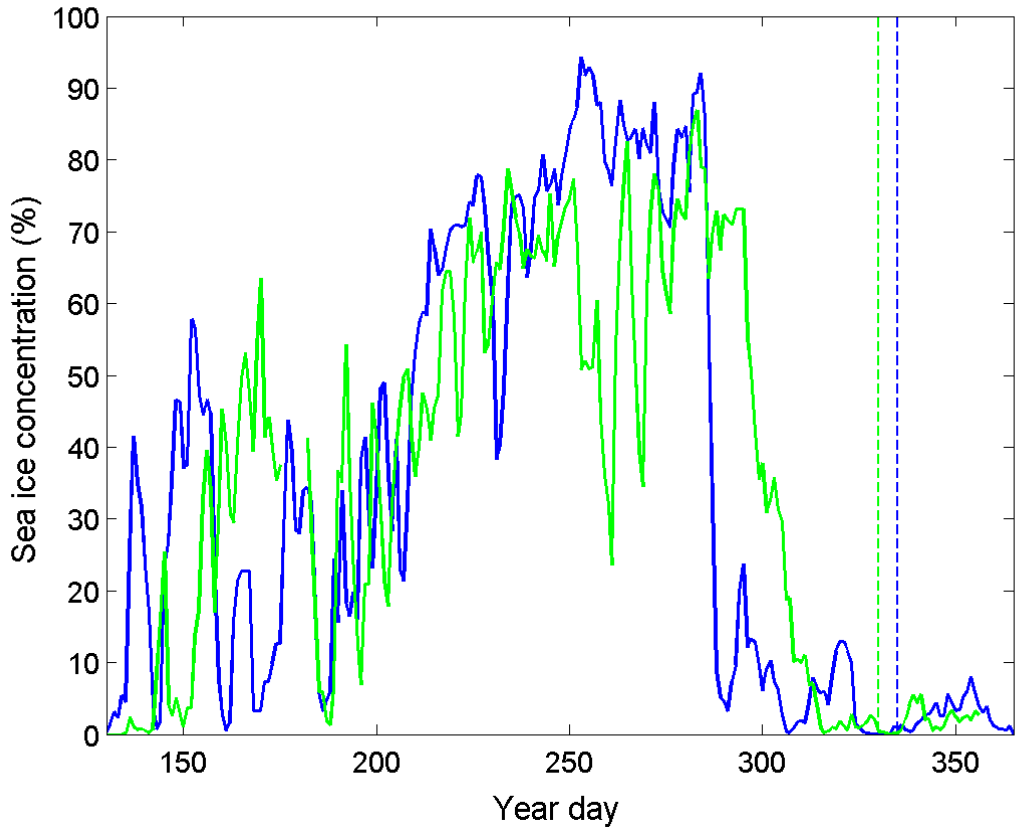


**Figure 4-2: Sea ice concentrations (%) (OSTIA sea ice data, averaged over 1 ° box centred on ICE1) during 2013 (blue solid line) and 2014 (green solid line). Sampling dates for JR291 (blue) and JR304 (green) are shown by vertical dotted lines.**

### 4.3.3 Particle type

During both JR304 and JR291, 1-3 sample splits were photographed using an Olympus SZX16 microscope with Canon EOS 60D camera and Olympus BX-SZX Micro Cam and particles classified into: krill FP, other FP, phytodetrital aggregates, phytoplankton cells, and other phytodetritus. Phytodetrital aggregates were identified as aggregations >0.1 mm equivalent spherical diameter (ESD) containing phytoplankton cells and other phytodetrital material. Individual particle dimensions were measured using ImageJ and volumes calculated using formulae for a sphere, ellipsoid or cylinder depending on particle shape. *Euphausia superba* FP were identified via comparison with freshly egested FP (Chapter 2). FP carbon contents were calculated from measured volumes based on direct measurements at the study site (see below). Conversions from volume to carbon for phytoplankton cells were based on the equation of Menden-Deuer and Lessard (2000) for diatoms >3000 µm$^3$: $log\ (pgCcell^{-1}) = -0.933 + 0.881 \cdot log(Volume\ (\mu m^3))$ (only diatoms were observed in MSC samples of sinking particles), and conversions from phytodetrital aggregate and other phytodetrital material volume to carbon based on the equation of Alldredge (1998): $\mu C\ agg^{-1} = 0.99 \cdot (Volume\ (mm^3)^{0.52})$. The use of literature conversions introduces uncertainties, but use of these conversions is consistent with previous studies (e.g. Alldredge 1998; Laurenceau-Cornec et al. 2015). Further, the interest here is in determining the relative reduction, rather than the absolute amount, of flux between depths, so reducing the effect of these uncertainties.

All FP were counted and their length and widths measured manually using ImageJ. Equivalent spherical diameters (ESD) were also calculated. Volumes were calculated from these measurements using the formula for a cylinder, and FP carbon content calculated according to a FP carbon to volume ratio of 0.032 mg C mm$^{-3}$ (range 0.022-0.042 mg C mm$^{-3}$) based on measurements made on FP (10-15 per replicate filter) collected from Bongo nets at ICE2 during JR304 (see Chapter 2 for details of Bongo deployments). FP were rinsed three times in filtered sea water, photographed under a microscope to obtain size measurements, filtered onto pre-combusted glass fibre filters (25 mm diameter GF/F, Whatman) and oven dried at 50 °C for analysis of POC. Filters were then fumed with 37% HCl in a vacuum desiccator for 24 hours, and dried for 24 hours at 50 °C, before placing both filters and filter blanks in pre-combusted (450 °C, 24 h) tin capsules as in Hilton et al. (1986), and measuring POC in a CE-440 Elemental analyser (Exeter Analytical.285 Inc).

### 4.3.4 Faecal pellet flux

Following calculation of the total mass (*m*) of sinking FP carbon in the MSC, FP flux (*F*) was calculated as follows:

$$\boldsymbol{F\left(mg\ C\ m^{-2}d^{-1}\right) = \frac{m}{A} \times \frac{w}{h},} \qquad \textbf{(Equation 4-1)}$$

where *A* refers to the area of the MSC opening based on inner MSC diameter, *w* the measured sinking velocity (m $d^{-1}$) from laboratory measurements, and *h* the height of the snow catcher (1.53 m). Krill FP flux was calculated based on krill FP sinking velocities only.

During JR291, FP sinking velocities were measured in a temperature controlled laboratory (at 2°C) using a 1 L graduated glass cylinder (7 cm diameter). Laboratory temperatures were at most ~3 °C warmer than *in situ* water temperatures which could result in overestimations of sinking speed of up to 15% based on theoretical calculations of the effects of viscosity (Taucher et al. 2014). However, observational studies have not observed differences in sinking velocity at different temperatures (Trull et al. 2008; Iversen and Ploug 2013) so this small difference in temperature is unlikely to bias measurements made in this study. FP were carefully removed from the particle collector tray using a plastic pipette and transferred into a graduated cylinder which was filled with seawater collected from the MSC at the ICE station. The sinking velocity of each FP was calculated from the mean of the time taken to sink past two marked distances (10 cm apart), with the starting point more than 10 cm from the water surface. Results were discarded where the walls of the cylinder were observed to interfere with the sinking FP. During JR304, sinking velocities were measured in a temperature controlled (at 4°C) flow chamber system (Ploug and Jorgensen 1999) containing filtered sea water (0.22 µm filter) taken from the MSC deployed at ICE stations. FP were placed carefully in the chamber and three measurements of the sinking velocity made for each FP by suspending the FP with an upward flow (Ploug and Jorgensen 1999). Sinking velocity measurements were limited to those particles visible by eye (ESD>0.15 mm). Sinking velocities measured during JR291 and JR304 by these two different methods were not significantly different (Student's t-test, $p$=0.2), suggesting that the use of two different methods to measure sinking velocity did not bias results.

### 4.3.5 Krill density

Krill density (ind. $m^{-2}$) estimates were obtained from KRILLBASE, a database of 9922 individual net hauls taken in the Southern Ocean since 1926 (Atkinson et al. 2008, and their supplementary material). This is the most comprehensive database of krill density to date and provides good spatial coverage in our study region. To estimate krill density at each site, KRILLBASE records

(standardised to a common sampling method 0-200 m, see supplementary material of Atkinson et al. 2008) within a 300 km x 300 km box centred over the ICE stations were extracted from the database. The proximity of the two stations resulted in large overlap in the KRILLBASE records and so the records were combined. The mean of the resultant 158 records (± 1 standard error (SE)) collected between November and April, was then used for FP production calculations (Figure 4-1B).

### 4.3.6 Faecal pellet production

Estimates of FP production (FPP) were obtained from the work of Clarke et al. (1988) who carried out FP egestion experiments on *Euphausia superba* collected from Arthur Harbour, on Anvers Island, Antarctica, as well as the Bransfield Strait, Antarctica. They measured a range in egestion rates (0.25-2.35 mg FP dry weight $ind^{-1}$ $h^{-1}$), giving an egestion of 0.7-6.3 mg C $ind^{-1}$ $d^{-1}$ assuming an organic C content of 11.15% dry weight (average of open ocean sites (8.1-13.7%) from Clarke et al. (1988)). Taking their 'representative' egestion rate of 1.2 mg FP dry weight $ind^{-1}$ $h^{-1}$, gives a FPP rate of 3.2 mg C $ind^{-1}$ $d^{-1}$ for a krill of wet weight 600 mg (Clarke et al. 1988). There will be some variability in FP size (and hence FPP in terms of carbon) due to size differences of individual krill, however a wet weight of 600 mg (which the Clarke et al. 1988 measurements were standardised to) matches the most frequently occurring krill length of 41 mm in the Scotia Sea in Spring, based on acoustic surveys and relationships between krill wet weight and length (Hofmann and Lascara 2000; Fielding et al. 2012). This estimate of FPP from Clarke et al. (1988) is similar to the estimate of 4.3 mg C $ind^{-1}$ $d^{-1}$ by Tarling and Johnson (2001) based on the fraction of krill body weight ingested and egested, providing confidence in estimates of FPP, however see section 4.5.3 for full sensitivity analysis.

### 4.3.7 Faecal pellet flux attenuation

The rate of mesopelagic FP flux attenuation was assessed by fitting a power-law function (Martin et al. 1987) to the FP flux data. We use a power-law function here to allow comparison to past studies of global POC attenuation (e.g. Henson et al. 2012a; Marsay et al. 2015).

$$\boldsymbol{F_z = F_{z0} \times (z/z_0)^{-b}}, \qquad \textbf{(Equation 4-2)}$$

where $z$ is the depth of the flux (m), and $F_{z0}$ is flux (mg C $m^{-2}$ $d^{-1}$) at the reference depth. A high absolute value of $b$ corresponds to high attenuation (shallow remineralisation) and vice versa. Attenuation rates through the mesopelagic (between MLD+10 and MLD+110) were calculated based on our MSC estimates of FP flux which are defined here as $b_{MSC}$. Additionally, the attenuation rate between predicted FPP at a swarm depth of 20 m (based on mean swarm depths

of 18.9 m measured in the southern Scotia Sea in spring (Fielding et al. 2012)) and estimated FP fluxes at MLD+110m are calculated ($b_{FPP}$). In reality krill FPP will not occur solely at a depth of 20 m due to variations in the depth of individual krill as well as DVM. However, an acoustic assessment of krill in the region of the ICE stations revealed that most krill swarms were shallower than 60 m in summer (Fielding et al. 2012). DVM of krill in South Orkney Islands area have also been shown to be small (Taki et al. 2005).

## 4.4 Results

### 4.4.1 Oceanographic setting

Surface temperatures were consistent between sites and between years ranging from -0.83°C to -0.59 °C (Figure 4-3). At ICE1 JR291 and ICE2 JR304, chlorophyll peaked at 0.5 mg $m^{-3}$ at 30 m. Chlorophyll was elevated at ICE2 JR291, peaking at 1 mg $m^{-3}$ at 38 m (Figure 4-3).

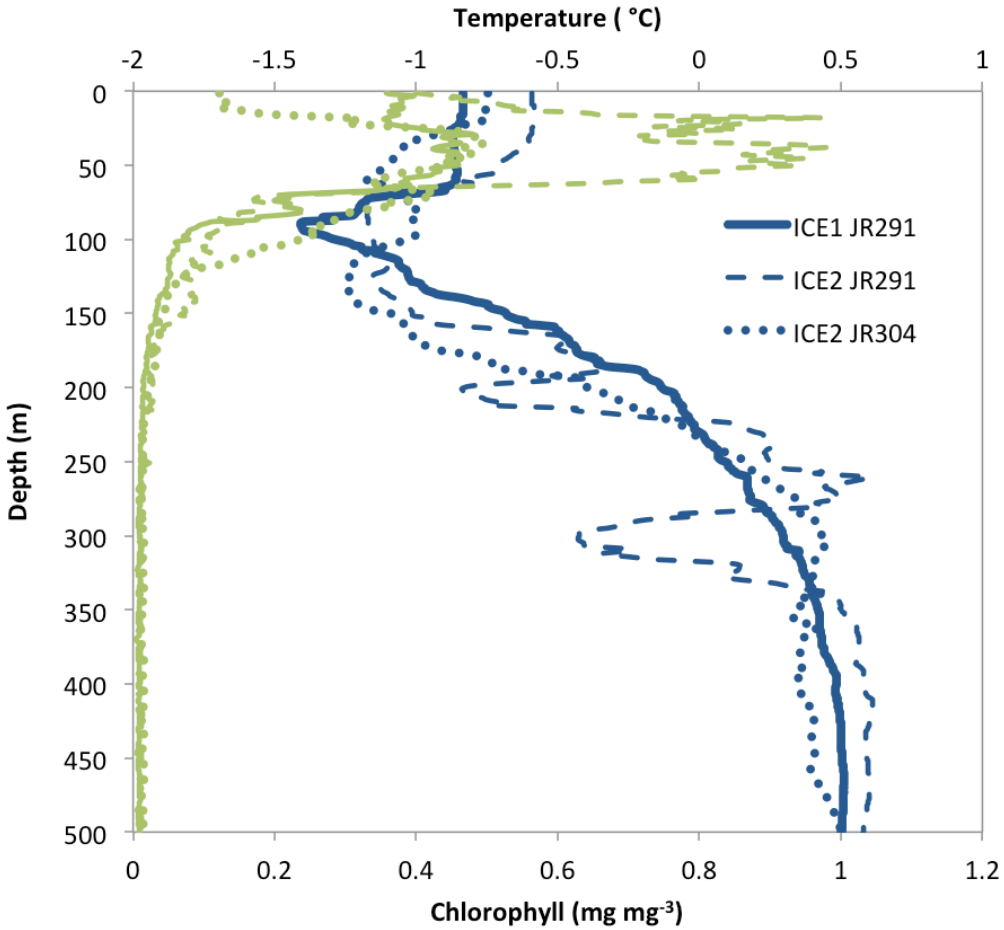


**Figure 4-3: Vertical profiles of temperature (blue lines) and chlorophyll (green lines) from CTD deployments at ICE1 (solid line), and ICE2 (dashed line) during JR291, and ICE2 during JR304 (dotted line).**

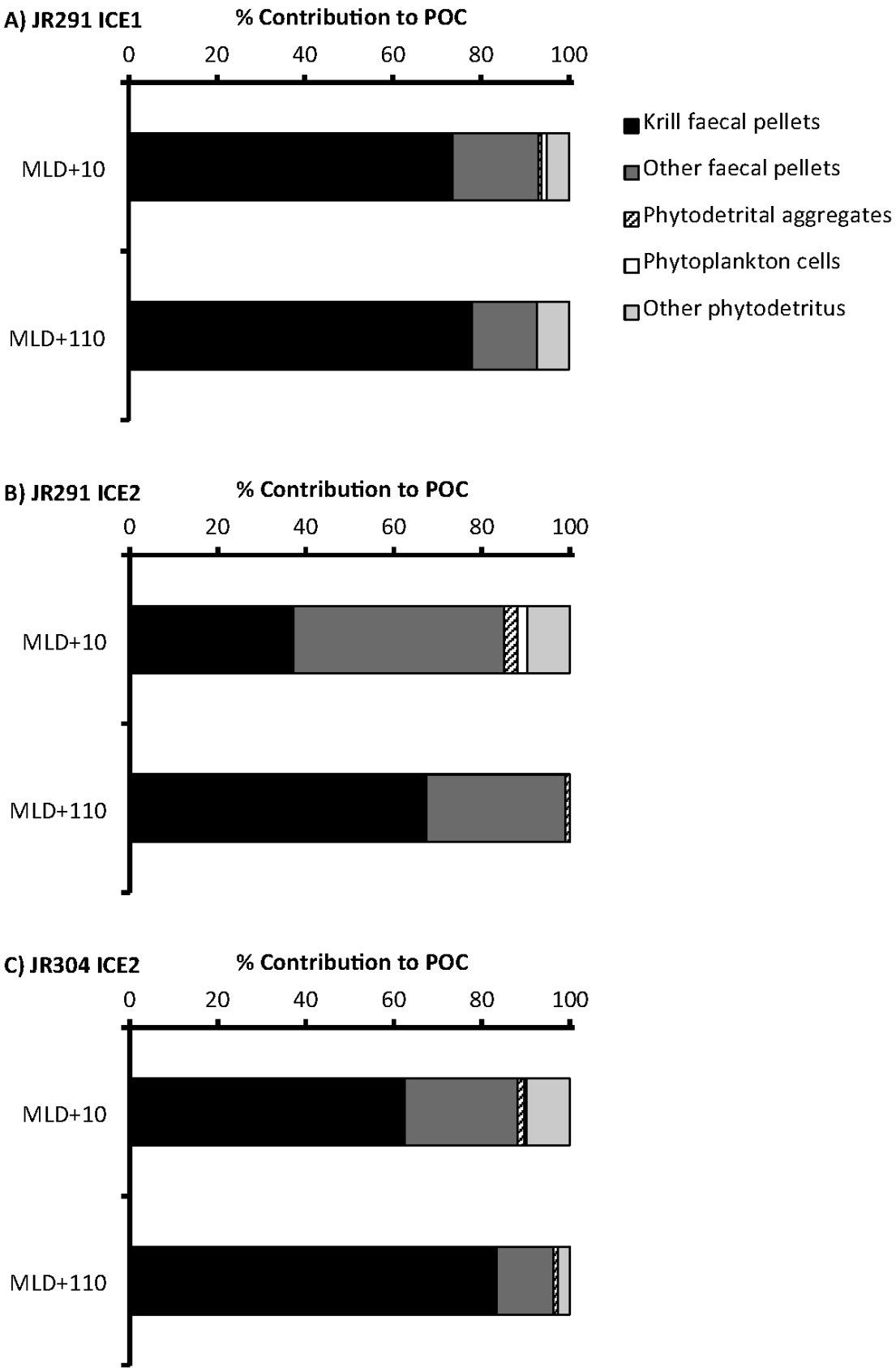


**Figure 4-4: Composition (particle type) of fast-sinking POC at A) ICE1 JR291, B) ICE2 JR291, and C) ICE2 JR304 stations based on microscope analysis and calculated carbon content. Black=krill faecal pellets, dark grey=other faecal pellets, hashed=phytodetrital aggregates, white=phytoplankton cells and light grey=other phytodetritus.**

### 4.4.2 Particle flux and type

FP were the dominant component of the flux at all stations (Figure 4-4), accounting for 85.0-93.1% of the sinking POC at MLD+10, and 92.7-98.9% at MLD+110. As it was only possible to directly measure the POC content for FP, there is some uncertainty in these percentages, however, even in terms of numerical abundance (based on counts made before conversion to POC), FP accounted for 52-58% of total sinking particle abundance at MLD+10 and 56-95% at MLD+110. Most of these FP belonged to Antarctic krill, with the exception of the MLD+10 sample at ICE2 JR291 where krill FP accounted for 43.6% of the FP POC. The remaining FP were smaller cylindrical pellets that may originate from copepods or smaller euphausiid species. Krill FP were on mean 0.15, 0.13, and 0.14 mm in width at MLD+10, and 0.15, 0.17 and 0.16 mm at MLD+110 at ICE1 JR291, ICE2 JR291 and ICE2 JR304 respectively. Krill FP lengths were on mean 1.03, 0.70, and 1.28 mm at MLD+10, and 0.69, 0.91 and 0.90 mm at MLD+110 at ICE1 JR291, ICE2 JR291 and ICE2 JR304 respectively. However, as krill FP are produced in strings which can be easily broken, we calculate FP fluxes in terms of carbon rather than by absolute abundances.

**Table 4-1: Marine Snow Catcher deployment data for cruises JR291, and JR304 to the South Orkneys, Antarctica, also showing total faecal pellet (FP), and krill FP POC fluxes.**

| Site | Date | Time (GMT) | Depth (m) | FP flux (mg C $m^{-2}$ $d^{-1}$) | Krill FP Flux (mg C $m^{-2}$ $d^{-1}$) |
|---|---|---|---|---|---|
| ICE1 JR291 | 01/12/2013 | 01:45 | 64 | 88.5 | 66.7 |
| | | 02:21 | 165 | 94.3 | 75.5 |
| ICE2 JR291 | 01/12/2013 | 12:58 | 76 | 74.2 | 33.0 |
| | | 13:37 | 178 | 221.4 | 154.1 |
| ICE2 JR304 | 26/11/2014 | 16:44 | 61 | 92.9 | 68.0 |
| | | 17:12 | 163 | 86.1 | 77.3 |

Median krill FP sinking velocities were 172, 267 and 161 m $d^{-1}$ at ICE1 JR291, ICE2 JR291 and ICE2 JR304 respectively, ranging from 15-507 m $d^{-1}$ (n=54,Figure 4-5). A Student's t-test on sinking velocities at each site revealed no statistically significant differences between the means of each site ($p > 0.05$). Krill FP fluxes were very similar at ICE1 JR291 and ICE2 JR304 at both MLD+10 (66.7 and 68.0 mg C $m^{-2}$ $d^{-1}$) and MLD+110 (75.5 and 77.3 mg C $m^{-2}$ $d^{-1}$), showing a slight increase in flux with depth (Table 4-1). Conversely, at ICE2 JR291, a large increase in krill FP flux was observed between MLD+10 and MLD+110 (33.0 to 154.1 mg C $m^{-2}$ $d^{-1}$).

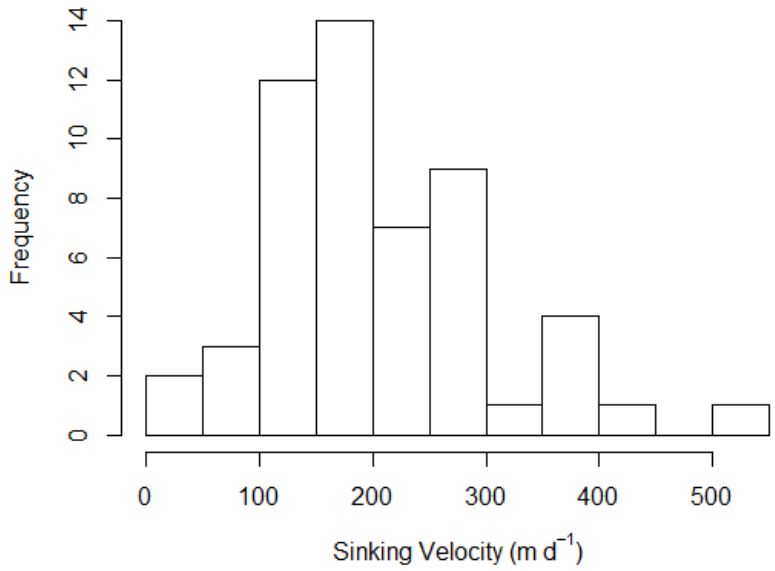


**Figure 4-5: Histogram of krill FP sinking velocities (m d$^{-1}$) measured at stations ICE1 and ICE2 during JR291 and JR304.**

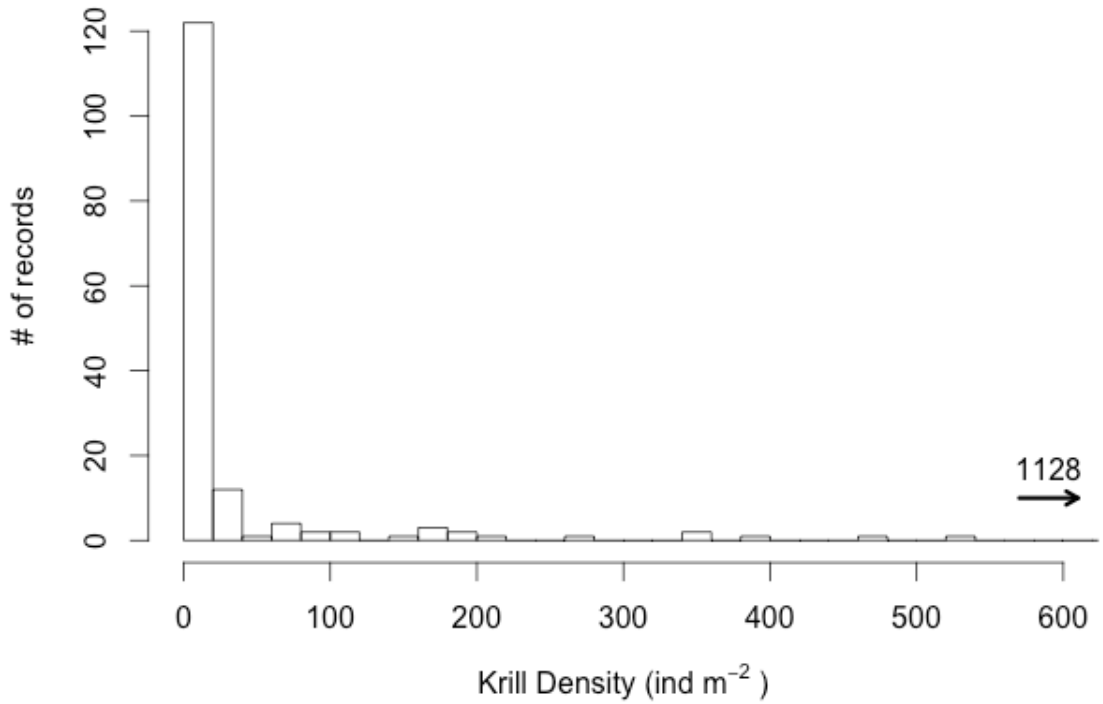


**Figure 4-6: Frequency distribution of krill density (ind. m$^{-2}$) records from KRILLBASE in a 300 km x 300 km box centred on the study sites. One record with an extreme density of 1128 ind. m$^{-2}$ is not plotted.**

### 4.4.3 Krill density and faecal pellet production

The KRILLBASE database reveals mean krill densities ($\overline{N}_k \pm SE$) of 38± 10 ind. $m^{-2}$ in the region of the ICE stations. This is equivalent to 0.19 ±0.05 ind. $m^{-3}$ over the sampling depth of 0-200 m. The range of krill densities measured in the region of the ICE stations is large (0-1128 ind. $m^{-2}$, Figure 4-6) reflecting the patchy distributions of krill swarms, but the bulk of records (85%) exhibit densities below 40 ind. $m^{-2}$. Although KRILLBASE data were collected over a long time period (1926-2004), 83% of the data records in the region of the ICE stations were collected from 1980 onwards. Recent assessments of acoustically derived krill data suggest that although there is a 4-5 year periodicity in krill density there was no significant trend between 1997-2013 (Fielding et al. 2014), giving confidence in use of the KRILLBASE dataset. Additionally, although there will be some seasonal variability in krill distributions, the net tows compiled in KRILLBASE were collected between October and June, 87% of which were collected in the spring-summer period (Oct-Mar). Applying a FPP rate of 3.2 mg C $ind.^{-1}$ $d^{-1}$ from Clarke et al. (1988) to $\overline{N}_k$ gives FPP of 122.0 ± 32.1 mg C $m^{-2}$ $d^{-1}$ at the ICE stations (Figure 4-7).

### 4.4.4 Faecal pellet flux attenuation

At all sites there was an increase in krill FP between MLD+10 and MLD+110 in MSC samples resulting in negative attenuation coefficients ($b_{MSC}$) of -0.13, -1.81, and -0.13 at ICE1 JR291, ICE2 JR291 and ICE2 JR304 respectively. Comparing estimates of FPP derived from KRILLBASE krill densities at a swarm depth of 20 m, with the estimates of krill FP fluxes at MLD+110 at ICE1 JR291 and ICE2 JR304 made here results in an attenuation coefficient ($b_{FPP}$) of 0.23 (black solid line Figure 4-8). The proximity and oceanographic similarity of the ICE stations gives confidence in combining flux data for this calculation. However, the one very high value of ICE2 JR291 is excluded (see section 4.5.2), making the estimate of $b_{FPP}$ conservative. A shallower swarm depth would result in lower estimated attenuation coefficients, and vice versa for a deeper swarm depth.

## 4.5 Discussion

### 4.5.1 Faecal pellet flux

FP were the dominant component of the sinking flux at ICE1 and ICE2 stations (Figure 4-4) highlighting their importance for the transfer of POC through the upper mesopelagic layer in this MIZ region. MSC estimated krill FP fluxes at ICE1 and ICE2 (75.5-154.1 mg C $m^{-2}$ $d^{-1}$) are high compared to fluxes of cylindrical FP (presumed from krill) measured in sediment traps deployed

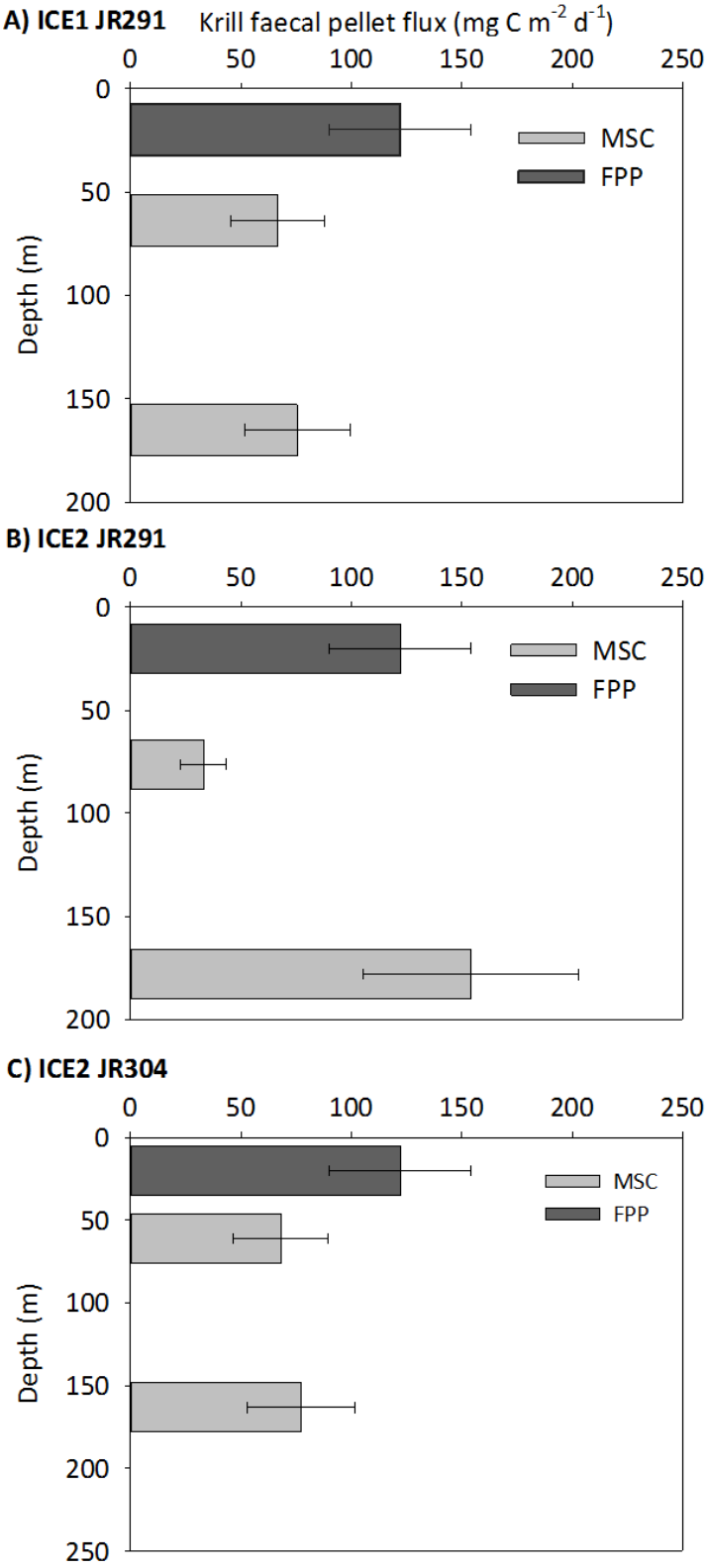


**Figure 4-7: Krill FP fluxes estimated in the South Orkneys at A) ICE1 JR291, B) ICE2 JR291, and C) ICE2 JR304. Krill FP fluxes estimated in MSC at MLD+10 and MLD+110 are shown by light grey bars (error bars show maximum and minimum fluxes based on the range of measured FP POC contents). Predicted FPP at a swarm depth of 20 m is shown by dark grey bars, with error bars showing maximum and minimum fluxes based on the range of krill densities from KRILLBASE (mean ±1SE).**

on the Western Antarctic Peninsula at 170 m in summer (11.36 mg C $m^{-2}$ $d^{-1}$) (Gleiber et al. 2012). However, Gleiber et al. (2012) also recorded peaks in cylindrical krill FP flux of up to 125.5 mg C $m^{-2}$ $d^{-1}$. Measurements made at 50 m in the MIZ of the Scotia Sea (FP fluxes of ~60 mg C $m^{-2}$ $d^{-1}$, dominated by krill by Cavan et al. (2015) are slightly lower than krill FP fluxes measured at the ICE stations. Antarctic krill FP may therefore make a major contribution to POC fluxes to the upper mesopelagic in MIZ (85-100%, Cavan et al. 2015; Chapter 2).

### 4.5.2 Faecal pellet attenuation

There was an increase in krill FP flux between MLD+10 and MLD+110 (negative attenuation) at all sites suggesting non steady state FP production, minimal attenuation with depth, FP production between the measurement depths and/or inputs via lateral advection. Satellite derived surface current data (OSCAR, 1/3 degree grid, 5 day resolution) suggest that surface velocities were <0.15 m $s^{-1}$ at the ICE stations during the period of this study and thus lateral advection is likely to be small.

At ICE1 JR291 and ICE2 JR304, only a slight increase in krill FP with depth was observed ($b_{MSC}$ = -0.13), which may be a result of low attenuation and an additional input via satiation sinking (i.e. sinking as a result of being full), as supported by previous studies in the region (Lancraft et al. 1991; Tarling and Johnson 2001). Tarling and Johnson (2001) estimate that krill spend 40% of the night-time period below the surface mixed layer due to satiation sinking, and egest 1.7 mg C ind. $^{-1}$ $d^{-1}$ during this time. This would equate to 81.6 mg C $m^{-2}$ $d^{-1}$ for our mean krill density of 38 ind. $m^{-2}$. Tarling and Johnson (2001) estimate that krill can descend 9-46 m during satiation sinking, and with most krill swarms in the region occurring within the upper 50 m in spring (Fielding et al. 2012), this could account for the increase in FP flux between sampling depths observed at ICE2 JR291.

FP production at depth due to satiation sinking cannot however explain the observed fourfold increase in krill FP between MLD+10 and MLD+110 at ICE2 JR291, even in the unlikely situation that no remineralisation of the FP produced during satiation sinking occurred. An acoustic study of krill swarms (Fielding et al. 2012) found that swarms mostly occur in the upper 50 m in spring in the southern Scotia Sea, although they were observed as deep as 400 m, suggesting that FP production between MLD+10 and MLD+110 could account for increases in FP abundance with depth at ICE2 JR291. The occurrence of krill at depth may be due to diel vertical migration (DVM) or short-term intermittent vertical migrations (Godlewska and Klusek 1987). ICE2 JR291 was sampled during the day (10:58-11:37 local time) and, if gut passage times were sufficient, then DVM may explain the high FP fluxes at this site. However, ICE2 JR304 was also sampled during the

day (14:44-15:12 local time) and similarly large increases in FP fluxes with depth were not observed.

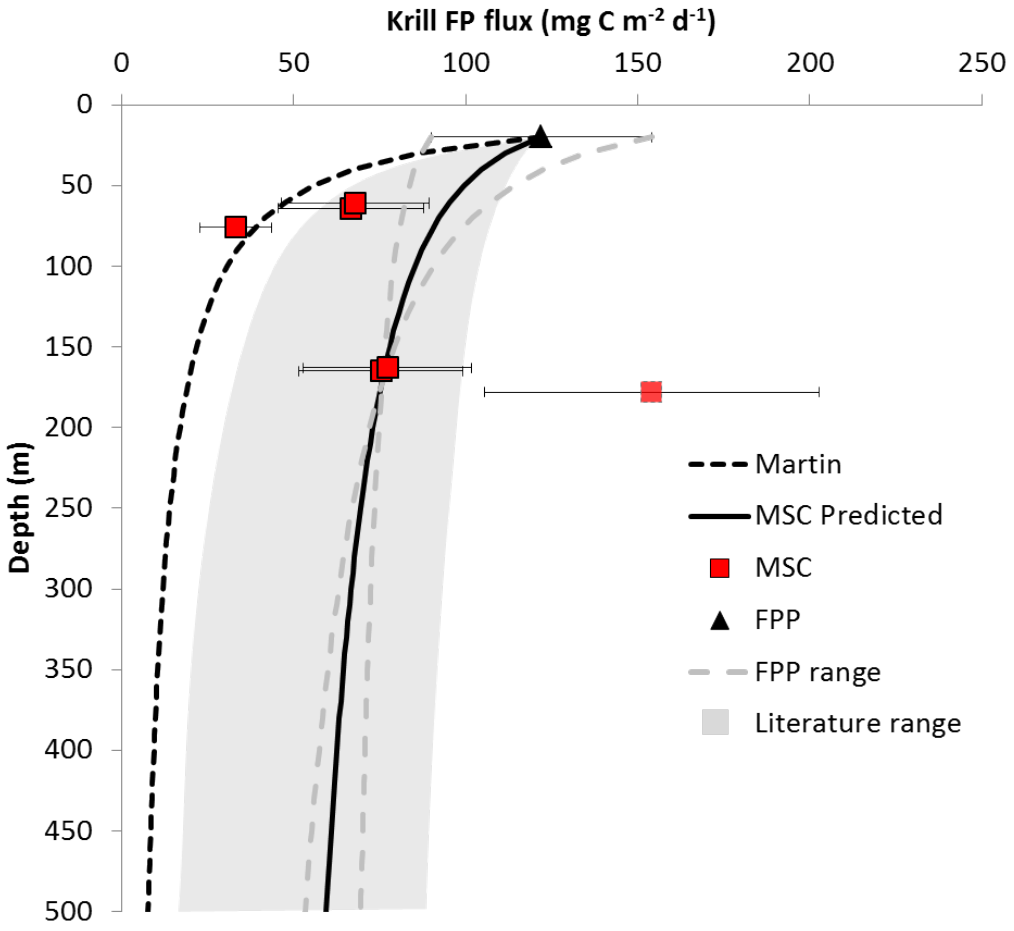


**Figure 4-8: Attenuation of krill FP flux in the upper mesopelagic at the ICE stations. Estimated FPP is shown by the black triangle with upper and lower bounds based on upper and lower KRILLBASE krill density estimates. Krill FP fluxes estimated by MSC are shown by red squares with error bars based on the range of measured FP POC contents. Calculated krill FP attenuation from FPP and krill FP fluxes at MLD+110 ($b_{FPP}$) is shown by the solid black line (grey dashed lines show maximum and minimum attenuation based on upper and lower FPP estimates). The very high FP flux at ICE2 JR291 (light red square with dashed outline) was not included in the derivation of $b_{FPP}$. For comparison, attenuation in krill FP flux based on a *b* value of 0.86 (Martin et al. 1987) is also illustrated (black dashed line), as well as *b* values of 0.10-0.62 (grey shaded area) from the literature range in krill FP attenuation (see section 4.5.4)**

Acoustic data collected by Fielding et al. (2012) revealed that most krill swarms were shallower than 60 m in summer, particularly in their open ocean site nearest to the ICE stations. Additionally, Japanese fishery data suggest that diel vertical migrations of krill are small in the

South Orkney Islands area (Taki et al. 2005). Therefore it is unlikely that DVM could result in the large increase in FP at depth observed at ICE2 JR291. Considering the lower percentage contribution of krill FP at MLD+10 at this site compared to ICE1 and ICE2 JR304 (43.6% compared to >85%, Figure 4-4), this apparent increase with depth may reflect non steady state FP production, with increased production (perhaps associated with the increased chlorophyll concentration (Figure 4-3), or with the passing of a krill swarm) prior to sampling resulting in higher FP fluxes at MLD+110 as the FP sank through the ocean. At a median sinking rate of 267 m $d^{-1}$ (measured at ICE2 JR291) krill FP would take 9 hours to sink between our measurement depths of MLD+10 and MLD+110. A krill swarm feeding in the region just 9 hours prior to sampling could therefore have caused the observed FP flux at ICE2 JR291, highlighting the patchy nature of krill swarms and hence FP fluxes. Regardless of the mechanism involved, the measurements made here of krill FP in the upper mesopelagic of the MIZ suggest efficient transfer of krill FP POC through this layer.

Additionally, conservative estimates of krill FP attenuation are calculated here based on predicted FPP at a swarm depth of 20 m and estimated FP fluxes at MLD+110. These calculations give a krill FP attenuation coefficient ($b_{FPP}$) of 0.23 derived from measurements at MLD+110 at ICE1 JR291 and ICE2 JR304 (solid black line, Figure 4-8). Krill FP can occur in high abundances (up to ~1.35 g C $m^{-2}$ $d^{-1}$, (Cadée 1992)) in sediment traps in the mesopelagic (e.g. Bodungen et al. 1987, Cadée 1992, Accornero et al. 2003) and have high average sinking rates (Turner 2002), and hence low attenuation rates measured here are not surprising. The data presented here agree with a recent modelling study on copepod FP (Stamieszkin et al. 2015), suggesting that size is an important driver of FP transfer efficiency, with large copepod FP transferred more efficiently through the mesopelagic than smaller copepod FP. In addition, lower micrometazoan abundance (small copepods such as *Oncaea* spp. and *Oithona* spp. often associated with flux feeding and increased recycling) at the ICE stations, compared to more northerly sites in the Scotia Sea (Ward et al. 2012a), may support lower attenuation rates (Chapter 2). Therefore, evidence suggests that a combination of high krill density in the MIZ and low micrometazoan abundance drives high transfer efficiency of krill FP at the ICE stations.

### 4.5.3 Sensitivity analysis

Sensitivity analyses were performed to examine the influence of certain assumptions made in the calculations of krill FP flux. Taking the range of krill densities from the subset of KRILLBASE records ($\overline{N}_k$ ± 1 SE) results in $b_{FPP}$ of 0.08-0.33, which is lower than both Martin's *b* value, and the global range in b values from empirical models of Henson et al. (2012) and Marsay et al. (2015). This supports the case for reduced attenuation of krill FP compared to the bulk of sinking POC.

Applying Martin's value of *b* to observed krill FP fluxes at MLD+110 to estimate FPP at a swarm depth of 20 m, and back calculating the required krill density, results in krill densities of ~145 ind. $m^{-2}$ (0.73 ind. $m^{-3}$). Higher densities can occur in krill swarms, with Fielding et al. (2012) measuring krill packing concentrations in swarms of 14-420 ind. $m^{-3}$ ($25^{th}$ to $75^{th}$ percentile) during acoustic surveys carried out in the South Orkneys region in Spring. When such high krill densities occur this likely drives much higher FP fluxes to the mesopelagic, a scenario which may have been captured by sampling at ICE2 JR291 (Figure 4-7B). The apparent negative attenuation rate (i.e. an increase in FP flux with depth) calculated at this station may therefore be a result of the average krill densities used in calculations under representing densities typical of swarm conditions, and so

**Table 4-2: Sensitivity analysis of attenuation rates ($b_{FPP}$) at ICE1 JR291, and ICE2 JR304. Attenuation rates were calculated based on the range of krill abundances (ind. $m^{-2}$) from KRILLBASE (mean ±1SE), the range of FPP rates (mg C $ind^{-1}$ $d^{-1}$) from Clarke et al. (1988), and krill FP carbon contents from Clarke et al. (1988) and Atkinson et al. (2012).**

| Site | Krill Abundance (ind. $m^{-2}$) | Krill FPP rate (mg C $ind.^{-1}$ $d^{-1}$) | Krill FP C content (% of DW) | Attenuation ($b_{FPP}$) |
|---|---|---|---|---|
| ICE1 JR291 | 28 | 0.67 | 11.15+ | -0.66 |
| | 48 | 0.67 | 11.15+ | -0.40 |
| | 28 | 6.29 | 11.15+ | 0.40 |
| | 48 | 6.29 | 11.15+ | 0.66 |
| | 28 | 0.23^ | 3.8 | -1.18 |
| | 48 | 0.23^ | 3.8 | -0.93 |
| | 28 | 9.64* | 17.1 | 0.60 |
| | 48 | 9.64* | 17.1 | 0.85 |
| ICE2 JR304 | 28 | 0.67 | 11.15+ | -0.68 |
| | 48 | 0.67 | 11.15+ | -0.42 |
| | 28 | 6.29 | 11.15+ | 0.39 |
| | 48 | 6.29 | 11.15+ | 0.65 |
| | 28 | 0.23^ | 3.8 | -1.17 |
| | 48 | 0.23^ | 3.8 | -0.91 |
| | 28 | 9.64* | 17.1 | 0.60 |
| | 48 | 9.64* | 17.1 | 0.86 |

+ Average of open ocean sites (8.1-13.7%) from Clarke et al. (1988)
^ Based on minimum egestion rates (Clarke et al. 1988) and minimum FP carbon contents measured by Atkinson et al. (2012) in the Scotia Sea in spring
* Based on maximum egestion rates (Clarke et al. 1988) and maximum FP carbon contents measured by Atkinson et al. (2012) in the Scotia Sea in spring

may be explained by the episodic passing of a krill swarm prior to the time of sampling. At an attenuation rate of 0.23, a krill density of 79 ind. $m^{-2}$ is required to result in the observed krill FP flux of 154.1 mg C $m^{-2}$ $d^{-1}$ at MLD+110 at ICE2 JR291.

Krill FP egestion rates were not directly measured here which increases the uncertainty in calculated attenuation rates. Atkinson et al. (2012) measured lower rates (up to 0.745 mg C $ind^{-1}$ $d^{-1}$) than used here. However, they suggest that their estimates are likely to be conservative because krill were not feeding during the incubations, and the initial high phase of gut evacuation may have been missed. Nordhausen and Huntley (1990) carried out shipboard incubations of Antarctic krill, collected from the Antarctic Peninsula in spring, measuring egestion rates for 5 days. Initial egestion rates were high (up to 2.5 mg C $ind^{-1}$ $d^{-1}$ based on their mean krill dry weight (DW) of 45.3 mg) and decreased exponentially during the incubation. They estimate *in situ* egestion rates to be 0.82 mg C $ind^{-1}$ $d^{-1}$. Pakhomov et al. (1997) incubated krill collected from South Georgia in summer for periods of up to 24 hours, measuring egestion rates of 0.977 mg C $ind^{-1}$ $d^{-1}$ (mean krill DW of 137 mg). Antezana et al. (1982) conducted laboratory egestion rate experiments on krill collected from Anvers Island, Antarctica. They observed average egestion rates of 0.07 mg C $ind^{-1}$ $d^{-1}$ with 'active egesters' producing FP at a rate of 0.55 mg C $ind^{-1}$ $d^{-1}$.

The range of FP egestion rates measured by Clarke et al. (1988) (0.7-6.3 mg C $ind^{-1}$ $d^{-1}$), which encompasses all of the aforementioned literature rates with the exception of the outlying low mean value from the laboratory study of Antezana et al. (1982), has been used to conduct a sensitivity analysis (Table 4-2). This range of egestion rates (Clarke et al. 1988; Nordhausen and Huntley 1990; Pakhomov et al. 1997; Atkinson et al. 2012) was used for sensitivity calculations, which results in attenuation rates of between -0.68 and -0.40 for minimum FPP rates, and between 0.39 and 0.66 for maximum FPP rates. Despite this range in attenuation rates, related to poorly constrained egestion rates, all suggest lower attenuation than the widely used value of Martin et al. (1987).

Clarke et al. (1988) measured large variation in the rate of total FP egestion, but found that the loss of organic material showed no significant daily variation during laboratory and field experiments in summer, increasing confidence in the value for FP carbon content used here. However, Manno et al. (2015) observed changes in FP carbon content seasonally and Atkinson et al. (2012) found that egestion rates and absorption efficiencies varied with diet and food availability, measuring carbon contents of 3.8-17.1% in the Scotia Sea in spring. Using this range in FP carbon content and the aforementioned range in FP egestion rates results in FP carbon egestion rates ranging from 0.23 to 9.64 mg C $m^{-2}$ $d^{-1}$. Again this produces a wide range in attenuation rates (Table 4-2), but only an unlikely combination of maximum egestion rates,

maximum FP carbon contents and upper krill densities (mean from KRILLBASE subset +1 SE) results in attenuation rates approaching that of Martin et al. (1987).

These sensitivity analyses, combined with the fact that low attenuation of sinking FP were observed in MSC samples (not reliant on literature egestion rates, Figure 4-7), corroborates the conclusion that high krill densities support high POC fluxes to the upper mesopelagic. The fact that the sensitivity analysis carried out here gives both positive and negative attenuation rates highlights the need for more constrained measurements of krill density and krill FP production alongside krill FP flux measurements at depth to determine just how low these attenuation rates are.

### 4.5.4 Krill as an agent for carbon transfer in the Southern Ocean

Previous studies have suggested that the density of individuals in krill swarms likely results in a 'rain' of FP which may overload detrital feeders and pass mostly undisturbed through the upper mesopelagic (Atkinson et al. 2012; Chapter 2). This has been hypothesised as an explanation for high numbers of krill pellets in sediment traps. However, FPP estimates have not previously been combined with *in situ* FP flux estimates in order to validate these hypothesised high export efficiencies and calculate attenuation rates which could be applied in GBC models. Although high fluxes of krill FP have been noted before, these have often only been measured at one depth so prohibiting quantification of attenuation rate (Dunbar 1984; Bathmann et al. 1991; Gleiber et al. 2012), or visual observations of krill FP have been made rather than measuring FP carbon fluxes directly (Bodungen et al. 1987; Wefer et al. 1988), or attenuation rates have not been calculated (Cadée et al. 1992; Accornero et al. 2003).

Despite the aforementioned limitations of the data presented here, attenuation coefficients measured here are much lower than both Martin's canonical attenuation coefficient of 0.86 (Martin et al. 1987) and that derived more recently from global dissolved inorganic carbon, alkalinity and phosphate data ($b$=0.97, Kwon and Primeau 2008). Regionally resolved estimates of $b$ of 0.5-1.0 in the region of the ICE stations by Henson et al. (2012) and Marsay et al. (2015) are also higher than the estimate of krill FP flux attenuation made here (0.23). If the attenuation rate calculated in this chapter is characteristic of the MIZ with high krill densities, then POC fluxes are likely to be underestimated in these global empirically-derived estimates. However, these estimates are annually averaged; seasonal measurements of krill densities and krill FP fluxes in MIZ regions are needed to determine how representative the calculated krill FP attenuation rate is of the annual average. There are not sufficient data in the KRILLBASE database to resolve seasonal variations in krill abundance at the study site, however estimates are made in Chapter 5

as to the possible annual contribution of krill FP to the total POC flux, in this region and the MIZ of the Southern Ocean.

The large seasonal and latitudinal variability in particle flux in the Southern Ocean (e.g. Honjo et al. 2000, 2008; Dubischar and Bathmann 2002 and refs within) makes it difficult to compare studies and combine all data to create a Martin type curve for sinking krill FP in the Southern Ocean. Where possible, I calculate FP attenuation rates from the literature to compare to the krill FP attenuation rate. Declines in the number of krill FP strings in the upper 150 m of the Scotia-Weddell Seas (Cadée et al. 1992) give attenuation rates of 1.19 and 0.10 in open ocean and melting ice regions respectively. Wefer et al. (1988) observed high contributions of krill FP strings in sediment traps at 494 and 1588 m, and suggest that krill grazing and high sinking rates explain the reduced attenuation of organic carbon flux ($b$=0.60) during the productive period in January (compared to $b$ values of 1.13-3.38 during the rest of the season). Sediment trap deployments at 180 and 868 m in the Ross Sea revealed declines in FP organic carbon ('fragments', mostly cylindrical) with depth, and attenuation of 0.62 and 0.32 (from maximum and annual mean fluxes respectively) (Accornero et al. 2003). Similar to my study, increases in FP fluxes (total, of which krill were the main type) were measured using Marine Snow Catchers in the Scotia Sea (Cavan et al. 2015), resulting in an attenuation of -0.32.

Although high numbers of krill FP were measured at the ICE station, which are not depleted with depth, this may not be the case in all situations Converse to the observations presented here, high rates of krill FP attenuation were observed ($b$~0.6-2.5) by González (1992) in the upper 150 m of the Weddell-Scotia Seas, suggesting that zooplankton grazing can lead to retention. The zooplankton abundance and community structure is therefore an important control on flux attenuation. This is modulated further by physiological processes, with higher feeding/egestion rates reflecting higher carbon content but lower sinking speed (Atkinson et al. 2012). González (1992) did however also measure an increase in krill FP in the upper 150 m, and less rapid attenuation ($b$~0.2) below this (150-300 m), on a second visit to one of their transects. They suggest that heavy grazing by krill and subsequently high FP production can overload the capacity of zooplankton, resulting in a larger percentage of FP sinking out of the photic zone. Therefore the range in literature krill FP attenuation rates applicable to the conditions of our study site of 0.10-0.62 (Figure 4-8, shaded region) are consistent with our value of $b_{FPP}$ of 0.23.

### 4.5.5 Incorporation of krill FP into global biogeochemical models

Although ocean biogeochemical models are developing more mechanistic approaches towards POC flux attenuation (e.g. differentiating slow and fast-sinking pools and effects of ballasting

(Armstrong et al. 2002; Yool et al. 2013)), effects of zooplankton behaviour are generally not included, e.g. DVM, fragmentation, or krill specific (rather than generic mesozooplankton) attenuation rates. The need to incorporate sporadic, large FP fluxes such as those measured here depends critically on both their contribution to annual fluxes as well as whether they penetrate below the winter mixed layer depth. In this study the focus is on the upper mesopelagic, highlighting that, at least in regions of high krill density in the MIZ, krill FP are transferred efficiently through the upper 200 m. There is evidence of krill FP reaching depths of 1588 m in the Bransfield Strait (Wefer et al. 1988), with high POC fluxes in December and January (97% of the annual POC flux) dominated by krill. Wefer et al. (1988) hypothesise that these high fluxes were a result of intense krill grazing on a phytoplankton bloom, suggesting that high FP transport may be typical in high productivity conditions. Suzuki et al. (2003) observed krill FP fluxes of 26.8 mg $Cm^{-2}$ $d^{-1}$ at 537 m in the MIZ of the Pacific sector of the Southern Ocean, but decreasing to 0.9 mg $Cm^{-2}$ $d^{-1}$ at 1259 m. Concurrent increases in FP of a different type suggests coprophagous feeding by deeper dwelling zooplankton (Bodungen et al. 1987; González 1992; Suzuki et al. 2003). Even when remineralisation is high, krill FP may still fuel fluxes of fresh FP to the deep sea via coprorhexy and repackaging (Bodungen et al. 1987; Miquel et al. 2015) suggesting a need to incorporate krill and their FP fluxes in GBC models.

The following chapter makes first order estimates of the possible contribution of krill FP to Southern Ocean POC fluxes in the MIZ to assess the need for their incorporation in GBC models. It would also be valuable to run a sensitivity analysis in GBC models, incorporating lower attenuation rates in MIZ of the Southern Ocean where krill densities are expected to be high. However, further seasonal studies in MIZ with high krill densities are required to identify the periods over which these lower attenuation rates are valid (e.g. productive season only), as well as to test whether this pattern is true of all the major MIZ of the Southern Ocean. This, as well as direct measurements of egestion rates and pellet composition, would improve our ability to assess how applicable the krill FP attenuation rates measured here are to the wider Southern Ocean, and whether the biological carbon pump of the Southern Ocean is more efficient than previously estimated based on average attenuation rates of total POC. Because faecal pellets are major vectors of iron and other essential nutrients in addition to carbon (Schmidt et al. 2012, 2016), a better understanding of the balance between retention and export of these particles is needed.

# Chapter 5. Antarctic krill faecal pellets in the marginal ice zone: The hidden 'highway' for particulate organic carbon flux

This chapter is in prep for submission to Nature Geosciences as:

Belcher, A. Tarling, G.A. Henson, S.A. Manno, C. Thorpe, S. Fretwell, P. Atkinson, A. Ward, P. Ireland, L. Sanders, R. *in prep*. Antarctic krill faecal pellets in the marginal ice zone: The hidden 'highway' for particulate organic carbon flux*, Nature Geosciences.*

A. Belcher collected the field data, carried out the data analysis and wrote and edited the manuscript. G. Tarling, C. Manno and P. Ward supported early hypothesis development. S. Thorpe, L. Ireland and P. Fretwell provided expertise for obtaining and manipulating marginal ice zone data. A. Atkinson provided KRILLBASE data. S. Henson provided model outputs, R. Sanders provided funding support and all authors provided feedback on manuscript discussion.

## 5.1 Abstract

The Southern Ocean is a key part of global biogeochemical cycles, contributing significantly to global export production. However, observational data are limited here, particularly seasonal measurements of particulate organic carbon (POC) flux in seasonally ice-covered regions. The marginal ice zone (MIZ) of Antarctica is an important habitat for Antarctic krill, and a number of studies have noted large episodic fluxes of krill faecal pellets (FP) in the mesopelagic. Analysis of FP flux data in the MIZ of the South Orkneys revealed low attenuation rates of krill FP, suggesting that they could make up a significant portion of Southern Ocean POC export fluxes, but they are poorly quantified due to limited observational data. In this study, first order estimates of the possible magnitude of krill FP in the upper mesopelagic of the MIZ of the Southern Ocean are made based on a historical database of krill densities. Over the productive season, the krill FP export flux is estimated to be 0.054 GT C $yr^{-1}$, suggesting that current satellite-derived export estimates may underestimate the total POC export flux by 9-46% in the MIZ. The magnitude of this largely 'hidden' flux highlights the necessity for further observations of krill FP attenuation in marginal ice zones for more accurate quantification of Southern Ocean krill FP fluxes and, to enable assessment of the need for their inclusion in global biogeochemical models.

## 5.2 Introduction

The flux of particulate organic carbon (POC) through the ocean via the biological carbon pump (BCP) is tightly coupled to atmospheric levels of carbon dioxide ($CO_2$) (Parekh et al. 2006; Kwon et al. 2009). However, observations of POC flux are limited, resulting in poorly constrained empirical and numerical models of POC flux, particularly in the Southern Ocean (Schlitzer 2002). Most studies of POC flux attenuation are non-responsive and cannot account for episodic, intense or localised export events. However, such events may be particularly efficient in transferring POC to the ocean's interior because the remineralisation community becomes overwhelmed. This chapter assesses the potential 'hidden' flux of POC originating from Antarctic krill, whose swarming behaviour (Hamner et al. 1989) could result in a major conduit of carbon to depth through their rapid exploitation of phytoplankton blooms and bulk egestion of rapidly sinking faecal pellets (FP).

Unlike in other oceans, epipelagic zooplankton biomass in the Southern Ocean is dominated by a single organism, Antarctic krill (*Euphausiia superba*), which forms swarms up to 100 $km^2$ (Tarling and Fielding 2016). Krill are an important part of Southern Ocean ecosystems, forming the link between primary producers and higher trophic levels (Murphy et al. 2007). Krill produce large faecal pellets (FP) which can sink quickly through the water column (measurements in the Scotia Sea of 27-1218 m $d^{-1}$, mean 309 m $d^{-1}$ (Atkinson et al. 2012)) and hence may be an important component of carbon export. Indeed, krill FP have been found in high numbers in sediment traps in both the upper and deep ocean (Wefer et al. 1988; Accornero et al. 2003; Gleiber et al. 2012). Although some krill FP may be retained in the upper mixed layer through coprorhexy and remineralisation (Cadée et al. 1992; González 1992), the occurrence of krill in large swarms means that atypically large krill FP fluxes can occur in certain regions at certain times of the year (Bodungen et al. 1987; Accornero et al. 2003; Gleiber et al. 2012) due to the production of a 'rain' of FP which can overload the capacity of detrital feeders (Atkinson et al. 2012; Chapter 2). This would lead to low attenuation rates, suggesting attenuation rates typically used in biogeochemical models (most notably Martin's *b* value (Martin et al. 1987)) may not be applicable in regions of high krill density.

Antarctic krill have a life cycle strongly tied to sea ice, a region of refuge and enhanced primary production which provides nursery areas for the larvae (Atkinson et al. 2004) and rich grazing grounds for the adults (Park et al. 1999). The occurrence of high krill densities, high FP fluxes and low attenuation rates of sinking POC in the MIZ, suggests that the MIZ may play a significant role in POC export in the Southern Ocean (Cavan et al. 2015; Chapter 2). Patchy distributions of krill biomass (Marr 1962) and limited particle flux measurements in the MIZ (in part due to the

difficulties of sampling in the ice) means that there is insufficient observational data of these potentially large krill FP fluxes. Studying krill necessitates that regions of swarming are distinctly targeted. This is contrary to the standard biogeochemical approach of sampling randomly within a defined spatial grid. The contribution of swarming organisms such as krill to particulate carbon export has therefore been effectively hidden from the bulk of biogeochemical studies to date. As the development of empirical algorithms to estimate export globally rely on data sets of *in situ* measurements (Laws et al. 2000; Dunne et al. 2007; Henson et al. 2011), these episodic, but recurrent, krill FP fluxes are likely to be unaccounted for and are therefore potentially underestimating Southern Ocean export flux.

In Chapter 4, it was highlighted that Antarctic krill FP were the dominant component of POC flux in the upper 200 m of a site in the MIZ near the South Orkneys, Antarctica, and were transferred through the upper mesopelagic much more efficiently than the canonical Martin's *b* value (Martin et al. 1987), or more recent estimates of *b* (Henson et al. 2012a; Marsay et al. 2015) would imply. It is therefore hypothesised here that where krill densities are high in the MIZ they drive large FP fluxes, and as such the MIZ accounts for a substantial component of the total POC export in the Southern Ocean. Observational measurements of these krill FP fluxes in the MIZ are limited, and the potential contribution of krill FP to Southern Ocean export flux has yet to be fully quantified. In this chapter, first order estimates of this flux are made based on spatially-discrete krill density data over the past decade (KRILLBASE) and *in situ* measurement of krill FP attenuation in the MIZ.

## 5.3 Methods

### 5.3.1 Krill faecal pellet production

Fortnightly climatologies of the extent of the marginal ice zone (MIZ) in Antarctica were calculated from daily long-term passive microwave sea ice concentration data from 1994-2014 from the National Snow Ice Data Centre (NSDIC) (Cavalieri et al. 1996). Median sea ice concentrations were calculated over the productive season (Oct-Mar (Tarling and Johnson 2001)), and the MIZ region defined as 15-80% ice cover (Stroeve et al. 2016). Each fortnightly MIZ region was further divided into 5 **°** zonal grids. For each fortnightly MIZ region, the mean krill densities in each grid were estimated using KRILLBASE; a database compiling 9922 net hauls taken in the Southern Ocean between 1926-2004 (Atkinson et al. 2008). The net tows compiled in KRILLBASE were collected between October and June, 95% of which were collected in the period analysed here (Oct-Mar). KRILLBASE is the most comprehensive data set of krill density to date, however, the database is not sufficient to accurately resolve krill densities on a fortnightly temporal resolution as used here

for MIZ, and as such the temporal patterns in calculated FP fluxes reflect the position of the MIZ with respect to the mean seasonal krill distribution.

Krill faecal pellet production (FPP) in each grid cell (5 **°** zonal grids bounded by the MIZ) was calculated by multiplying mean krill densities (ind. $m^{-2}$) by a krill FPP rate (E) of 3.2 mg C $ind.^{-1}$ $d^{-1}$ from the literature (Clarke et al. 1988) (see Chapter 4 for full sensitivity analysis of FPP rates). The mean FPP in the whole MIZ area ($FPP_{MIZ}$, mg C $m^{-2}$ $d^{-1}$) was calculated for each fortnightly period using the following equation:

$$\boldsymbol{FPP_{MIZ} = (\sum_{MIZ}(\overline{N}_k \times E \times A))/A_{MIZ}.} \quad \textbf{(Equation 5-1)}$$

Here, *A* is the area of the grid cell ($m^{-2}$), $A_{MIZ}$ the total Southern Ocean MIZ area ($m^{-2}$) for that fortnightly period excluding grid cells with no data, and $\overline{N}_k$ the mean krill density in that cell. Similarly the total flux of FP produced in the MIZ in each fortnightly period ($FPP_{TOT}$, mg C) was calculated using the following equation:

$$\boldsymbol{FPP_{TOT} = (\sum_{MIZ}(\overline{N}_k \times E \times A)) \times 14\ days.} \quad \textbf{(Equation 5-2)}$$

### 5.3.2 Faecal pellet fluxes

The flux of FP at 100 m depth ($FP_{100}$, mg C $m^{-2}$ $d^{-1}$) in each grid cell was estimated based on attenuation rates derived from the aforementioned FPP literature estimates and in situ FP flux measurements made in the MIZ of the South Orkneys in spring using Marine Snow Catchers (as presented in Chapter 4). For simplicity we calculate FP flux at 100 m in all regions rather than using a relative depth compared to mixed layer depths (MLD). Considering the large grid cells used in this study and lack of seasonally resolved krill abundance data, MLD from climatologies or literature studies are not likely to be appropriate. The calculated attenuation rate (*b*=0.23) was applied to the FPP data in each grid cell, using the Martin curve (Martin et al. 1987). For comparison with a previous study measuring krill FP fluxes in sediment traps at 170 m (Gleiber et al. 2012), fluxes have also been calculated at 170 m. A previous study (Cavan et al. 2015) also found low attenuation at a number of sites (in fact noting increases in POC fluxes with depth) in the MIZ near the South Orkneys in austral summer, providing support to the extension of this attenuation rate over the productive season.

$$\boldsymbol{FP_{100} = FPP \times (100/z_0)^{-b}} \quad \textbf{(Equation 5-3)}$$

Here $z_0$ is the depth at which krill FP are produced (taken as 20 m, based on mean swarm depths of 18.9 m measured in the southern Scotia Sea in spring (Fielding et al. 2012)). Assuming that attenuation rates measured in the MIZ of the South Orkneys are representative of other MIZ,

similarly to *FPP* estimates, the flux of FP over the MIZ region ($FP_{100,MIZ}$, mg C $m^{-2}$ $d^{-1}$) and the total flux of FP at 100 m in the MIZ for each fortnightly period ($FP_{100,TOT}$, mg C) were calculated,

$$\boldsymbol{FP_{100,MIZ} = (\sum_{MIZ}(FP_{100} \times A))/A_{MIZ},} \quad \textbf{(Equation 5-4)}$$

$$\boldsymbol{FP_{100,TOT} = (\sum_{MIZ}(FP_{100} \times A)) \times 14\ days.} \quad \textbf{(Equation 5-5)}$$

The total seasonal (Oct-Mar) $FP_{100}$ flux ($FP_{100,SEA}$, mg C) was calculated by summing the fluxes from each fortnightly period,

$$\boldsymbol{FP_{100,SEA} = \sum_{Mar}^{Oct}(FP_{100,TOT}).} \quad \textbf{(Equation 5-6)}$$

In order to assess if krill FP fluxes may have changed over time with MIZ areas and krill densities, and to investigate if any long-term trends may have influenced results, these steps were repeated for sea ice concentration data for the period 1980-1990. An analysis of KRILLBASE data highlighted a 38% decrease in krill densities in the southwest Atlantic over the latter half of the last century (Atkinson et al. 2004). However, more recent assessment of acoustic data collected in the region of South Georgia (1997-2013) suggests periodicity in krill abundances, rather than a long term decline (Fielding et al. 2014). As KRILLBASE data extends only to 2004 and our MIZ data to 2014, we take the first 10 years of the satellite sea ice data record (1980-1990) and only KRILLBASE data up to 1990 to obtain a historical estimate for comparison (see Appendix Figure B1).

### 5.3.3 Model comparisons

FP fluxes have been compared to a number of different modelled export fluxes at 100 m based on satellite-derived primary productivity estimates (Behrenfeld and Falkowski 1997; Carr 2002; Marra et al. 2003) and algorithms for export production (Laws et al. 2000; Dunne et al. 2005; Henson et al. 2011) for the region south of the maximum ice extent during the productive period defined here (15% sea ice concentration during period Oct 1$^{st}$-13$^{th}$ 1994-2014) (Table 5-1). These estimates are herein referred to as 'satellite-derived estimates'. These satellite-derived export estimates first rely on calculation of primary productivity (PP) from satellite chlorophyll-a via three main algorithms, referred to here as Carr (Carr 2002), Marra (Marra et al. 2003) and VGPM (Behrenfeld and Falkowski 1997). Satellite based PP estimates have been shown to disagree (Carr et al. 2006) and likely represent underestimates in the Southern Ocean (Schlitzer 2002; Johnson et al. 2013). PP data are then used to calculate export production via three different algorithms, herein referred to as Henson (Henson et al. 2011), Dunne (Dunne et al. 2007), and Laws (Laws et al. 2000). The Laws algorithm utilises nitrate uptake data and f-ratios (the ratio of new production to total production), however the validity of f-ratio derived export estimates was previously questioned (Yool et al. 2007) as they do not account for nitrification and therefore may overestimate export. In addition, only 1 of 11 samples used in the Laws algorithm are in the MIZ

of the Antarctic. The Dunne algorithm uses estimates of export based on thorium, sediment traps, oxygen and nitrate uptake data with 11 samples out of 122 in the MIZ. The Henson algorithm utilises solely thorium derived particle export which are time integrated export estimates over the half life of thorium (24.1 days). Thorium derived export estimates may therefore be able to better capture the passing of krill swarms and the associated high fluxes. However, even if these high fluxes are captured by these time integrated methods, or if in some MIZ regions large FP fluxes from krill swarms occur regularly enough to be captured by more short-term particle flux methods, the limited number of data points in the MIZ used in the aforementioned algorithms (Figure 5-1) means that the low attenuation rates occurring here will not be well represented. Only 5%, 11% and 9% of data in the Henson, Laws and Dunne algorithms respectively are from the MIZ of the Antarctic. This highlights the need for more observations in the MIZ to support regionally derived estimates of particle flux attenuation, and the incorporation of these into global biogeochemical models.

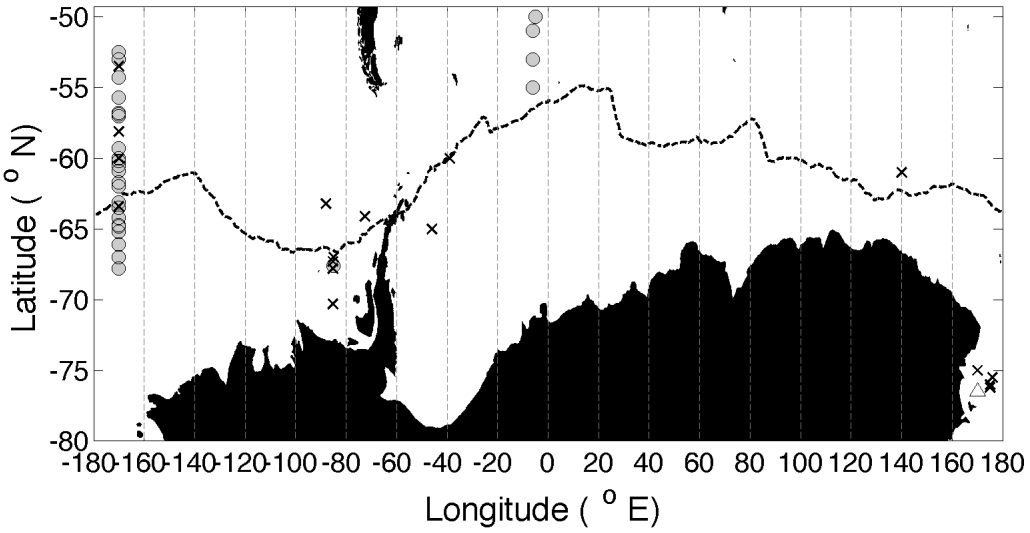


**Figure 5-1: Locations of data used to derive algorithms for export production from Henson (grey circles), Dunne (black crosses) and Laws (white triangle) with reference to the maximum ice extent (black dashed line, 15% sea ice concentration during period Oct 1st-13th 1994-2014).**

In addition, results are compared to three other models estimating carbon export in the Southern Ocean (Table 5-1) (MacCready and Quay 2001; Schlitzer 2002; Primeau et al. 2013). Estimates of Primeau et al. (2013) are based on a data-assimilated (temperature, salinity and radiocarbon distributions) model of ocean phosphate, calculated for their 'Antarctic zone' (~South of 55-60 °S) as defined by latitude of maximum Ekman divergence (Primeau et al. 2013). MacCready et al. (2001) use a diagnostic model to calculate the physical fluxes in the surface nitrate budget, using a

climatology of nitrate concentration (from historical CTD and Niskin bottle data primarily from WOCE and US JGOSFS) to constrain nitrogen export (MacCready and Quay 2001). Schlitzer et al. (2002) estimate carbon export south of 50 °S from an inverse model based on hydrographic, nutrient (accounting for nitrification), oxygen and carbon data (Schlitzer 2002). These regional models are not reliant on snapshot style POC flux measurements and provide better spatial coverage of MIZ.

## 5.4 Results and discussion

### 5.4.1 Krill faecal pellet production

FPP production has been estimated in the MIZ (1994-2014 climatology) at a swarm depth of 20 m from Oct 1$^{st}$-Mar 31$^{st}$ (Figure 5-2). As expected, FPP is highest in the Scotia Sea (mean 459 mg C m$^{-2}$ d$^{-1}$ for Oct-Mar, maximum 1452 mg C m$^{-2}$ d$^{-1}$, 1$^{st}$-15$^{th}$ Oct), downstream of the Antarctic Peninsula; a reflection of krill density estimates (mean 143 ind. m$^{-2}$ for Oct-Mar, maximum 454 ind. m$^{-2}$, 01-15 Oct). The total seasonal FPP over the MIZ region is estimated to be 0.078 GT C.

### 5.4.2 Krill faecal pellet flux

Conservative estimates of the flux of FP at 100 m ($FP_{100}$) were made based on the above estimated FPP and on a Martin type (Martin et al. 1987) attenuation curve with an attenuation coefficient of 0.23 as measured in the MIZ of the South Orkneys (Chapter 4). The total seasonal export of krill FP is highest in the Scotia and Weddell Seas (0.05-8.86 Tg C, Figure 5-3), highlighting both high krill densities and the large extent of the MIZ in this region. Averaged over the entire MIZ area ($FP_{100,MIZ}$), highest FP fluxes of 84.9 mg C m$^{-2}$ d$^{-1}$ occur during the period Oct 15-28$^{th}$ associated with the position of much of the MIZ over the Scotia and Weddell Seas. For comparison maximum fluxes of cylindrical FP of 125.5 mg C m$^{-2}$ d$^{-1}$ were observed in sediment traps at 170 m on the western Antarctic Peninsula (WAP) (Gleiber et al. 2012). This agrees well with the maximum krill FP flux calculated here of 148 mg C m$^{-2}$ d$^{-1}$ at 170 m in the zonal region encompassing the Antarctic Peninsula (-80 to -60 °W).

The location and size of the MIZ can change rapidly (Cavalieri et al. 1996) and therefore using fortnightly MIZ data reduces any over or underestimation of MIZ area and total FP fluxes, that would occur if seasonally averaged MIZ area were used. However, as the krill data used here cannot be resolved at such a high temporal resolution, the total estimate of FP flux over the entire productive season (1$^{st}$ Oct-31$^{st}$ Mar) is assessed, rather than attempting to look at intra-seasonal patterns.

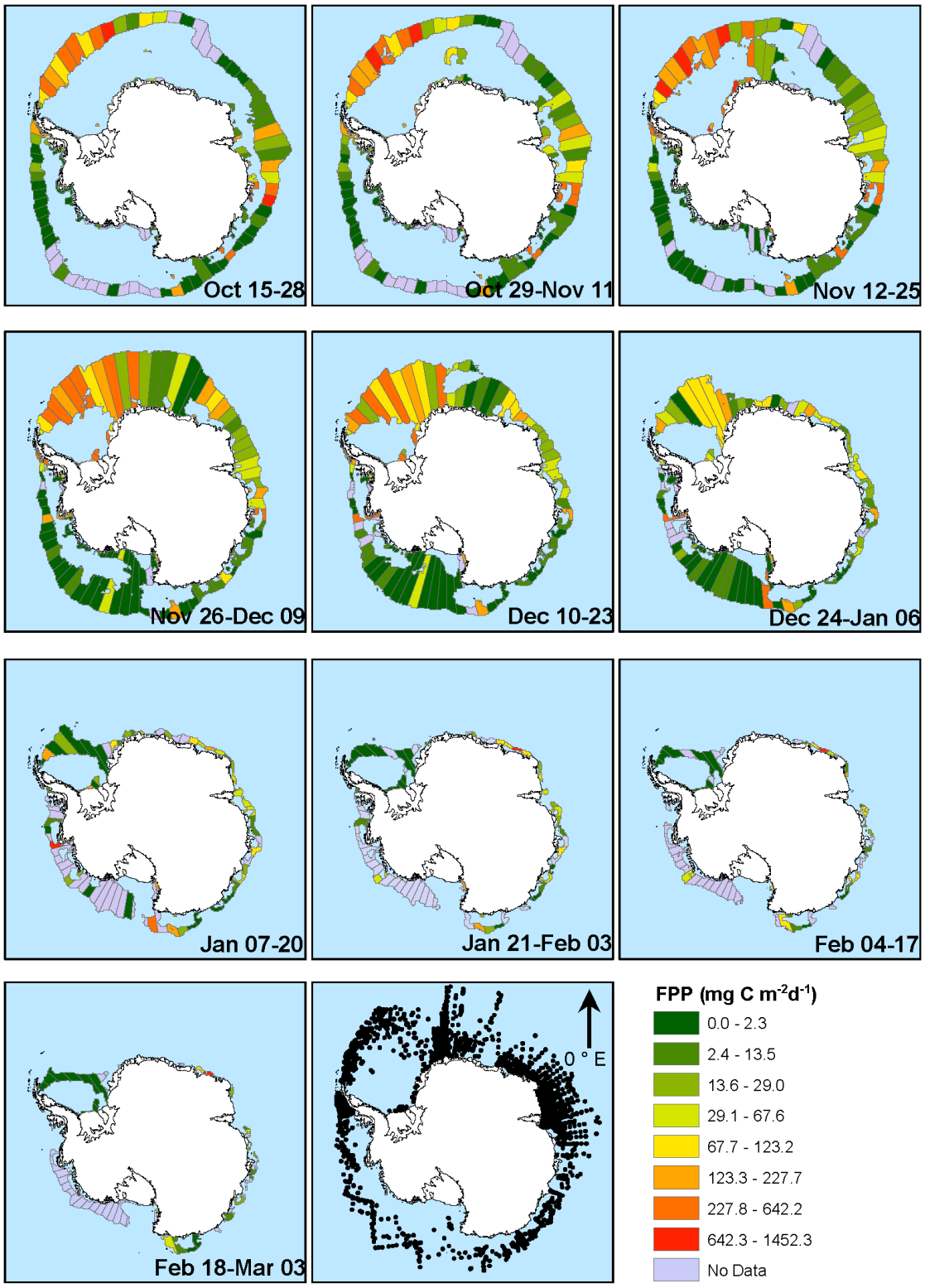


**Figure 5-2: Estimated krill faecal pellet production (FPP) in the marginal ice zone, Antarctica. The marginal ice zone, from fortnightly sea ice concentration data (15-80% ice cover), is divided into 5 ° zonal grids, and is coloured by FPP flux (mg C $m^{-2}$ $d^{-1}$) based on mean krill density measurements from KRILLBASE (black dots) and literature krill FP production rates. Regions of the marginal ice zone where no KRILLBASE records occurred are coloured in grey.**

### 5.4.3 Seasonal krill faecal pellet flux- comparisons with model data

Despite the inability to resolve krill densities at intra-seasonal timescales, by calculating the total seasonal contribution of krill FP to total POC export flux in the Southern Ocean, it is possible to assess the degree to which krill FP enhance the Southern Ocean POC flux. Summed over the productive season, the total flux of krill FP at 100 m in the MIZ ($FP_{100,SEA}$) is estimated to be 0.054 GT C. In order to determine if this flux is significant in terms of Southern Ocean POC fluxes, export estimates from a number of satellite-derived algorithms are compared to the FP fluxes calculated here (Table 5-1). In the region south of the maximum MIZ extent (i.e. poleward of 15% sea ice concentration for period Oct 1st-13th, 1994-2014) krill FP fluxes could make up 24-84% of total POC export based on the different satellite-derived estimates (Table 5-1). Comparing annual zonal means (Figure 5-3), both satellite-derived export estimates and the krill FP estimates suggest

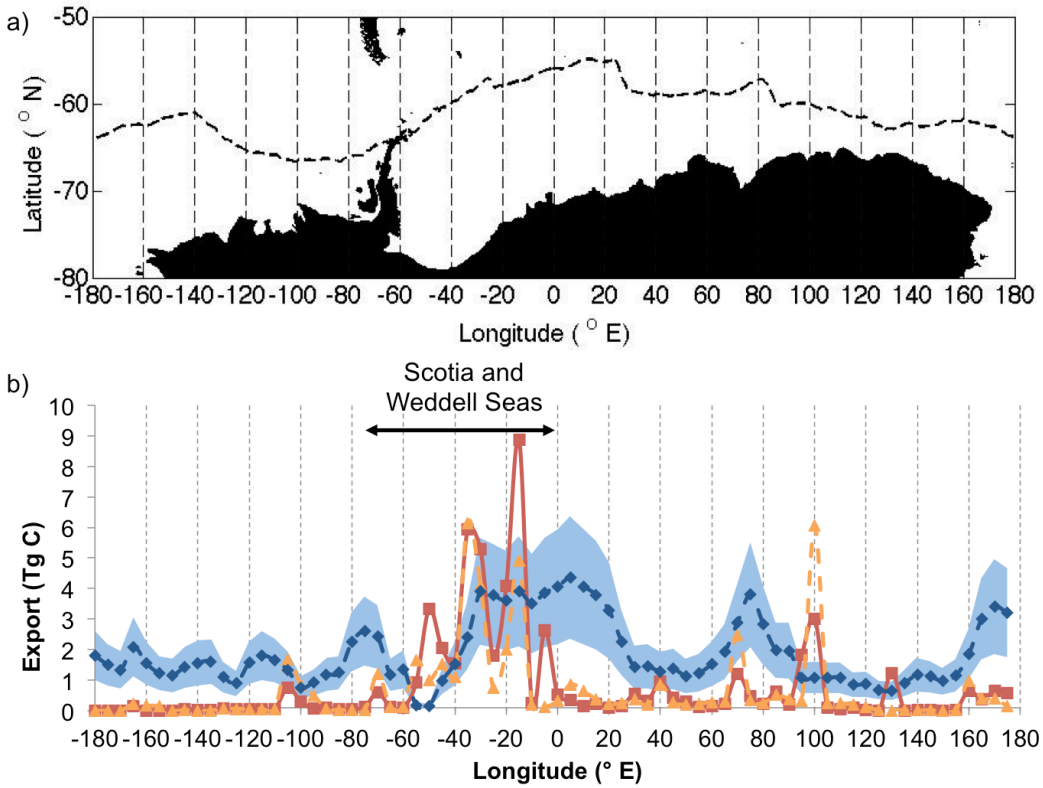


**Figure 5-3: Seasonal FP export fluxes (Tg C) in the MIZ. a) The maximum MIZ extent in 1994-2014 (15% sea ice concentration for period Oct 1st-13th, 1994-2014) used as the upper boundary of longitudinal estimates of POC export derived from empirical algorithms. b) FP export fluxes for the climatological MIZ of 1994-2014 (red line) and 1980-1990 (orange line), as well as the mean annual POC export from satellite-derived algorithms (blue line) and standard deviation of these estimates (shaded light blue).**

highest export in the Scotia and Weddell Seas, and show broadly similar spatial patterns. This likely reflects the association of krill with high productivity areas (Park et al. 1999), which are predicted from the empirical algorithms to be sites of high export. There are a number of regions where the FP export is estimated to exceed the total satellite-derived POC export, providing evidence that satellite-derived algorithms may not fully capture the high krill FP fluxes occurring in the MIZ. Additionally, as these satellite-derived estimates utilise spatially limited export data (Figure 5-1) they are unlikely to capture high krill FP fluxes in the MIZ. Assuming that satellite-derived POC export estimates miss the contribution from krill FP in MIZ, they represent only 54-81% of the total POC export in these regions. Satellite estimates may also underestimate the true export due to their inability to detect sub-surface chlorophyll (the depth of detection is dependent on the turbidity (Gordon and McCluney 1975)).

**Table 5-1: Comparison of krill FP POC export at 100 m with model-derived total POC export for the period Oct- Mar**

| Data Source/Model Algorithm | POC export flux south of MIZ [++] (GT C $yr^{-1}$) | % krill FP | POC export flux south of 60 °S (GT C $yr^{-1}$) | % krill FP |
|---|---|---|---|---|
| This study-krill FP only | 0.05 | | | |
| Carr, Henson ** | 0.08 | 71.1 | 0.10 | 53.2 |
| Carr, Dunne ** | 0.12 | 44.1 | 0.15 | 35.3 |
| Carr, Laws ** | 0.21 | 25.7 | 0.28 | 19.1 |
| Marra, Henson ** | 0.08 | 65.2 | 0.10 | 51.6 |
| Marra, Dunne ** | 0.14 | 39.2 | 0.16 | 33.5 |
| Marra, Laws ** | 0.23 | 23.6 | 0.29 | 18.6 |
| VGPM, Henson ** | 0.06 | 83.7 | 0.09 | 59.8 |
| VGPM, Dunne ** | 0.10 | 52.0 | 0.13 | 39.8 |
| VGPM, Laws ** | 0.18 | 30.3 | 0.25 | 21.4 |
| Primeau et al. 2013 *^ | | | 0.22 | 24.4 |
| Schlitzer et al. 2002 * | | | 1.00 | 5.4 |
| MacCready et al. 2001 * | | | 0.31 | 17.3 |

*Annual export.
** Estimates based on satellite chlorophyll data and the stated algorithms for primary production and export production. See methods for full details.
^Export at base of euphotic zone (73.4 m).
[++] Export for region south of the maximum ice extent during the productive period defined here (i.e. location of 15% sea ice concentration for period Oct $1^{st}$-$13^{th}$, 1994-2014), with the exception of MacCready et al. (2001) and Schlitzer et al. (2002) which are south of 60 °S and 50 °S respectively. The estimate from Primeau et al. (2013) is for their 'Antarctic zone' (~South of 55-60 °S) as defined by latitude of maximum Ekman divergence.

Krill FP export estimates are additionally compared to three models specific to the Southern Ocean (Table 5-1), which utilise nutrient and hydrographic data to constrain model

parameters/budgets (MacCready and Quay 2001; Schlitzer 2002; Primeau et al. 2013) (see Methods). These model estimates do not rely on spatially limited POC flux data and may better capture krill FP fluxes in the MIZ. Estimates of Primeau et al. (2013) and MacCready et al. (2001) are higher than satellite-derived estimates (0.22 and 0.31 GT C $yr^{-1}$ respectively). However, these model values are annual and also encompass larger regions of the Southern Ocean than satellite-derived estimates. Recalculating satellite-derived export annually for the region south of 60 °S increases estimates to 0.09-0.29 GT C $yr^{-1}$ (Table 5-1), closer to but still lower than model values (0.22-1.0 GT C $yr^{-1}$). The seasonal krill FP flux is 5-24% of these model derived POC export fluxes, compared to 19-60% for satellite-derived estimates. The estimate of export south of 50 °S by Schlitzer et al. (2002) is up to an order of magnitude higher than satellite-derived estimates, likely in part due to the inclusion of productive coastal waters off South America and South Georgia, suggesting that krill FP fluxes have lesser importance outside of the MIZ. The estimate of Schlitzer et al. (2002) is therefore not used for further comparison. Based on the models of Primeau et al. (2013) and MacCready et al. (2001), which offer the best coverage of the Southern Ocean region analysed here, krill FP fluxes are 17-24% of the total POC export flux, and hence represent a significant fraction of Southern Ocean POC flux which may not be captured by more global estimates such as the satellite-derived estimates analysed here.

### 5.4.4 Sensitivity analysis

The difficulties of sampling POC fluxes in the upper mesopelagic of the ocean (Buesseler et al. 2007a), in particular in the Southern Ocean, and the patchy nature of krill (Marr 1962), means observational data are limited in this region. It was therefore necessary to make a number of assumptions to estimate the possible flux of krill FP across the MIZ of the Southern Ocean, and these assumptions are explored here (Table 5-2). Total seasonal krill FP fluxes for each sensitivity run are compared to estimates of total POC flux from Primeau et al. (2013) and MacCready et al. (2001) which are believed to be the best estimates for the MIZ region examined here.

The estimates derived for krill FP flux are based on measurements made in the MIZ of the S. Orkneys, a region where krill densities are high (Atkinson et al. 2008; Fielding et al. 2011), and hence may only be valid for such high krill density systems. To assess the sensitivity of the results to this assumption, FP fluxes were recalculated for only grid cells where mean krill densities ($\overline{N}_k$) were > 58 ind. $m^{-2}$ (sensitivity run F). This limit is defined based on krill densities within 150 km of the study site of the South Orkneys (see Chapter 4), taking the mean of all KRILLBASE krill densities in this region + 2 x standard error. This results in a total export of 0.040 GT C over the Oct-Mar period, highlighting that high krill density regions account for 75% of the total krill FP flux

calculated here. The incorporation of low krill density regions does therefore not alter the conclusion that krill FP represent a significant flux of POC in the Southern Ocean.

The estimates of krill FP flux made here rely on literature measurements of FPP rate (Clarke et al. 1988), however FPP rates are poorly constrained. Therefore total krill $FP_{100}$ fluxes were recalculated (sensitivity runs B and C, Table 5-2) based on maximum (6.29 mg C ind.$^{-1}$ d$^{-1}$) and minimum (0.67 mg C ind.$^{-1}$ d$^{-1}$) literature estimates of FPP rate (Clarke et al. 1988, see Chapter 4). This results in a much larger range in $FP_{100,SEA}$ of 0.011-0.106 GT C (Figure 5-4), with krill FP fluxes accounting for 3.6-48.0% of the total export flux based on model estimates of total POC export from Primeau et al. (2013) and MacCready et al. (2001) (Table 5-2).

**Table 5-2: Estimated FP export flux at 100 m for various sensitivity runs for the period Oct-Mar. A is the standard run; the remaining runs are as of run A but with the following adjustments, B: minimum FPP rates, C: maximum FPP rates, D: minimum FP attenuation rates, E: maximum FP attenuation rates, F: only high krill density data, G: only KRILLBASE data collected post 1990, and H: MIZ climatology for 1980-1990 with only KRILLBASE data collected pre 1990.**

| Run | KRILLBASE data | MIZ data period | FPP rate (mg C m$^{-2}$ d$^{-1}$) | Attenuation rate (Martin's *b* value) | Total $FP_{100}$ export flux (GT C) | % of model export^ |
|---|---|---|---|---|---|---|
| A | All | 1994-2014 | 3.2 | 0.23 | 0.054 | 17.3-24.4 |
| B | All | 1994-2014 | 0.67 | 0.23 | 0.011 | 3.6-5.1 |
| C | All | 1994-2014 | 6.29 | 0.23 | 0.106 | 34.0-48.0 |
| D | All | 1994-2014 | 3.2 | 0.10$^{+}$ | 0.066 | 21.3-30.1 |
| E | All | 1994-2014 | 3.2 | 0.62$^{+}$ | 0.029 | 9.2-13.0 |
| F | >58 ind. m$^{-2}$ | 1994-2014 | 3.2 | 0.23 | 0.040 | 13.0-18.3 |
| G | Post 1990 | 1994-2014 | 3.2 | 0.23 | 0.022* | 7.3-10.2** |
| H | Pre 1990 | 1980-1990 | 3.2 | 0.23 | 0.044 | 14.0-19.8 |

*Estimate increases to 0.041 if the fortnightly MIZ areas are scaled up to match those of run A.
**Estimate increases to 13.1-18.5% if the fortnightly MIZ areas are scaled up to match those of run A.
^Total $FP_{100}$ export flux as percentage of total POC export from models of Primeau et al. (2013) and MacCready et al. (2001) (Table 5-1).
+Literature derived FP attenuation rates (Cadée et al. 1992; Accornero et al. 2003).

Additionally, to investigate the influence of a changing MIZ extent and declines in krill density and determine if any longer term trends may be influencing results, calculations were made using sea ice data from 1980-1990, again creating a fortnightly climatology of median sea ice concentration, and using KRILLBASE data up to 1990 (sensitivity run H). During the 1980-1990 period, $FP_{100,SEA}$ was 0.044 GT C, i.e. 19% lower than calculated for 1994-2014. However, when considering the range of literature FPP rates (0.67-3.2 mg C ind.$^{-1}$ d$^{-1}$) and calculating the range in $FP_{100,SEA}$ for the 1994-

2014 estimate, this historical estimate is well within errors of uncertainty (Table 5-2,Figure 5-4). Therefore if any changes have occurred, they are not detectable at the present level of resolution. Historical (1980-1990) estimates of $FP_{100}$ flux were based only on data from KRILLBASE pre 1990, however this was compared to results obtained using the MIZ from 1994-2014 but the full KRILLBASE database (which extends from 1926-2004). Therefore there may be some bias due to the inclusion of historical krill data in the modern estimate. Using only KRILLBASE data post 1990, total $FP_{100}$ between Oct-Mar is estimated to be 0.022 GT C (sensitivity run G). This estimate is artificially low due to the limited geographical coverage of data collected post 1990 and hence the small MIZ area containing data (only MIZ grid cells containing krill density data can be used to estimate total $FP_{100}$ flux). Scaling fortnightly $FP_{100}$ to the same MIZ area as that obtained from the full KRILLBASE database results in an approximate estimate of 0.041 GT C, which is close to the original run A (0.054 GT C) and to the historical estimate (1980-1990, run H) of 0.044 GT C.

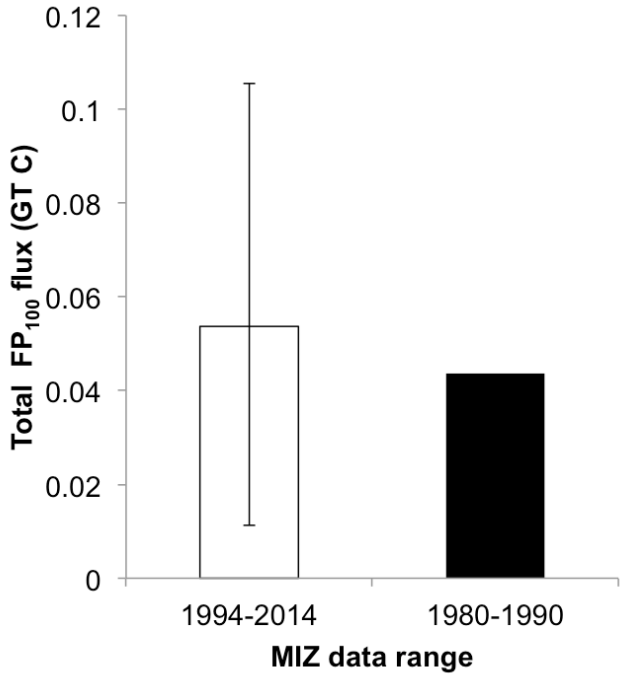


**Figure 5-4: Comparison of estimates of krill FP fluxes at 100 m for different climatologies of sea ice data. Error bars for current estimates (1994-2014) relate to maximum and minimum estimates using maximum and minimum FPP rates respectively (sensitivity runs B and C). Historical estimates relate to sensitivity run H (Table 5-2).**

The major assumption in the method utilised here is that FP attenuation rates from the South Orkneys (*b*=0.23) are representative of the whole MIZ region of the Southern Ocean. There are few previous studies of krill FP fluxes in the MIZ where two depths were sampled to allow the

calculation of krill FP attenuation. The few existing studies applicable to the conditions of our study site (Wefer et al. 1988; Cadée et al. 1992; Accornero et al. 2003; Cavan et al. 2015) have been compared in chapter 4 (see section 4.5.4), resulting in a range in literature FP attenuation rates of 0.10-0.62. Taking upper and lower bounds of this range in attenuation rates results in a $FP_{100,SEA}$ of 0.029 and 0.066 GT C respectively (sensitivity run D and E, Table 5-2). Even at the high end of literature derived attenuation rates, krill FP fluxes could still account for 9.2-13.0% of the total export flux based on model estimates from Primeau et al. (2013) and MacCready et al. (2001). Therefore, although data are limited, the available literature supports the notion that krill FP can contribute significantly to total POC export in MIZ, particularly in regions with high krill abundances.

As shown by sensitivity run H, the estimated FP flux is dominated by high krill density areas. However, this does not consider the effects of differences in zooplankton community structure, particularly in the abundance of microcopepods, many of which have lifestyles based on coprorhexy and coprophagy. The abundance of these microcopepod grazers was low at the time of sampling in the South Orkneys (Chapter 2), but abundances can be much higher elsewhere (Ward et al. 2012b). A number of studies have measured high retention of FP in the euphotic zone, due most likely to copepod retention filters (Riser et al. 2001; Wexels Riser et al. 2007),. Additionally, currents generated by the swimming activities of both krill (Dilling and Alldredge 2000) and copepods (Poulsen and Kiørboe 2005) could cause FP fragmentation, slow sinking rates and make them more available to smaller grazers and microbes. The evidence presented here suggests that it is highly likely that given high enough densities (compared to microzooplankton grazers), Antarctic krill are able to short circuit this retention filter through a ‘rain’ of large, fast-sinking FP (Wefer et al. 1988; Wassmann et al. 2002; Atkinson et al. 2012). Episodic events such as this, as well as for example whale falls and regime shifts, could account for a significant, yet poorly sampled, component of total POC export. The zooplankton community structure is therefore a key consideration when examining the degree to which sinking FP are exported from the euphotic zone (Viitasalo et al. 1999; Wassmann et al. 2000, 2002; Chapter 2).

## 5.5 Conclusions

The calculations carried out here represent a first order estimation of the importance of krill for the export of carbon out of the euphotic zone of the Southern Ocean. Krill FP fluxes in the MIZ are estimated to be large, and could account for 17-24% of modelled estimates of POC export in the Southern Ocean. Satellite-derived export estimates relying on limited empirical flux data in the MIZ of the Southern Ocean are unlikely to capture these fluxes and may underestimate POC export in these regions by 19-46%. This significant potential contribution of krill FP flux highlights

the need for further measurements of FP attenuation in other regions of the Southern Ocean to determine whether krill FP are indeed the POC 'highway' of the Southern Ocean. As a site of deep water formation and also a region where deep nutrient rich waters are exposed to the atmosphere (Toggweiler 1994), the Southern Ocean is a key part of global biogeochemical cycles and contributes significantly to global export production (Schlitzer 2002). It is therefore important to quantify the efficiency of carbon transfer in the Southern Ocean as accurately as possible.

# Chapter 6. Synthesis

## 6.1 Key findings

The work of this thesis has addressed several key unknowns surrounding the controls on the efficiency of the biological carbon pump, drawing a number of important conclusions and highlighting areas for future research. The key findings of the work, in relation to the hypothesis outlined in section 1.8, are:

1. The attenuation of particulate organic carbon (POC) in the upper mesopelagic of the Scotia Sea and northeast Atlantic cannot be explained by particle associated microbial respiration and therefore zooplankton likely play a key role. It is hypothesised that zooplankton drive the transformation of large, fast-sinking particles, into smaller slow-sinking and suspended particles, agreeing with H2 (Chapters 2 and 3).

2. In agreement with H2, variability in the efficiency of the BCP was observed even within a temperature range of -1 to 4 °C in the Scotia Sea. The stage of the phytoplankton bloom, zooplankton community composition, and food web interactions all drive variability in POC attenuation, with transfer efficiency ($T_{100}$) ranging from 2.4-84.9% (Chapters 2, 4, and 5).

3. Assessment of the type of particles contributing to the flux of fast-sinking POC highlighted krill FP to be the main contributor to export in the upper mesopelagic at the ICE stations in the Scotia Sea (confirming H1). The production of faecal pellets by krill in the marginal ice zone of Antarctica has the potential to drive episodic but large fluxes of POC (up to 154.1 mg C $m^{-2}$ $d^{-1}$ at MLD+110 m) out of the euphotic zone, and could be a significant component of Southern Ocean POC export (Chapters 2, 4 and 5).

4. The direct loss of particulate organic carbon by particle-associated microbial respiration on both faecal pellets in the Scotia Sea and phytodetrital aggregates (the fast-sinking fraction) in the northeast Atlantic is low (on average <3 % $d^{-1}$) (Chapters 2 and 3).

5. Respiration of phytodetrital aggregates by particle-associated microbes is approximately constant with depth at the PAP site (contrary to H3) and narrows the gap between POC sources and sinks in the upper mesopelagic (confirming H4), explaining only 8% and 33% of fast-sinking POC loss in the upper and mid mesopelagic respectively (Chapter 3).

## 6.2 Key processes identified as controlling attenuation

### 6.2.1 Particle type

The most rapid loss of POC occurs in the upper mesopelagic of the ocean, a highly dynamic region that presents challenges for accurate measurements of particle flux. To date there have been relatively few studies measuring both the flux and the type of particle making up the POC in the upper mesopelagic, and hence there are large uncertainties surrounding the mechanisms responsible for rapid attenuation in this layer. Data collected as part of this thesis have shown that differences in the type of sinking material can explain both spatial and temporal changes in POC flux attenuation (confirming H1, see section 1.8), with faecal pellets (FP) becoming a more dominant part of the flux with depth at the stations sampled. This suggests that FP can be transferred more efficiently through the mesopelagic than the bulk of sinking POC, and/or that FP are produced deeper in the water column. The high sinking rates of large FP reduces their residence time in the upper ocean, hence increasing the likelihood that they will pass through the upper mesopelagic rather than being disintegrated and remineralised. Increased sinking velocities also reduce the time for colonisation by microbial communities. Although FP can also be remineralised rapidly in the upper ocean (e.g. González 1992), often declines in one type of FP occur concurrently with increases in a different FP type, suggesting coprophagous feeding by deeper dwelling zooplankton (Bodungen et al. 1987; Suzuki et al. 2003). The occurrence of intact FP in deep sediment traps (e.g. Accornero et al. 2003; Manno et al. 2015) may therefore be a result of an indirect, cascade-like transfer through the mesopelagic as they are reprocessed by different zooplankton communities (Urrere and Knauer 1981; Miquel et al. 2015).

Whereas FP were the main component of the flux at sites in the Scotia Sea, PA were dominant at all depths (36-500 m) at the PAP site in the northeast Atlantic. Zooplankton biomass was over an order of magnitude higher at P2 and P3 compared to the PAP site which could drive an increase in FP numbers and decrease in PA through grazing and fragmentation (Dilling and Alldredge 2000; Schnetzer and Steinberg 2002). Zooplankton abundances at the ICE station were more comparable to that at the PAP site, however, FP at the ICE station were primarily from Antarctic krill which were not quantified in the Bongo net tows. Additionally, higher contributions of PA to the particle flux at the PAP site may reflect the time of sampling, i.e. post-bloom and the sinking of phytoplankton with nutrient limitation (Thornton 2002). Of the Southern Ocean stations, P2 had the highest abundance of PA and was also sampled post-bloom. PA abundances may also have differed due to contrasting phytoplankton and bacterial communities resulting in different aggregation potentials (Passow et al. 2001).

Individual phytoplankton cells can also make up an important part of POC fluxes (Rembauville et al. 2015b; Durkin et al. 2016). However, the material captured in sediment trap samples (such as those in the study of Rembauville et al. (2015b)) is amalgamated making it difficult to ascertain whether the observed phytoplankton cells were transferred through the water column as solitary cells or in aggregates. A distinct advantage of using Marine Snow Catchers is the ability to collect and characterise individual particles without aggregation. In this study, the contribution of individual phytoplankton cells (predominantly diatoms based on visual assessment, Appendix A) to the POC flux was high at the MLD at P2 site in the Scotia Sea and was attributed to the demise of the bloom. The PAP site was also sampled in the declining bloom stage yet the contribution of individual phytoplankton cells was low. This may be explained by the findings of previous studies; a dominance of medium to large diatoms (with high export efficiencies (Martin et al. 2011; Henson et al. 2012a)) in the South Georgia region in spring (Korb et al. 2012), compared to a dominance of dinoflagellates at the PAP site in June/July (Henson et al. 2012b), in agreement with qualitative visual assessments made in this study.

Although the abundance of sinking individual phytoplankton cells was high at the base of the mixed layer at the P2 site, their contribution rapidly diminished with depth suggesting rapid remineralisation. However, low contributions at depth may be due to the proximity of sampling to the demise of the bloom and insufficient time having passed for phytoplankton cells to have sunk deeper in the ocean. It is important to remember these non-steady state limitations when making snapshot type measurements such as those made here using Marine Snow Catchers. The low sinking rates of phytoplankton cells (Miklasz and Denny 2010) means they are more likely to be remineralised in the upper water column and aggregation, or the formation of colonial mats, may be required to support high POC fluxes to depth (Kemp et al. 2000; Martin et al. 2011). Phytoplankton cells can also be transported deeper in the ocean without the need for gravitational settling through physical mixing (Dall'Olmo and Mork 2014). Additionally, in low nutrient conditions (such as those typical at the end of a bloom), can lead to cell senescence and affect cell buoyancy leading to changes in sinking rates (Smayda 1971; Bienfang 1981). This may help to explain the presence of individual phytoplankton cells in the deep ocean and on the sea bed, particularly if phytoplankton sink *en masse* in a pulse event (Beaulieu 2002) that is temporally decoupled from, or capable of overloading the capacity of, zooplankton grazers. Indeed significant diatom export events have been observed in spring in sediment traps at 1500 and 2000 m at P3 and P2 respectively (Rembauville et al. 2016). As for krill FP, it is important to be able to capture these episodic fluxes to fully characterise these important transient components of the biological carbon pump.

Results of this thesis highlight the importance of identifying the major component of the POC flux, which can reveal useful information about the mechanisms driving the flux at that location. Incorporating regional and temporal differences in particle type in biogeochemical models is therefore required for accurate prediction of both the magnitude and efficiency of the biological carbon pump. Current models differ in the complexity of particle formation processes (and hence particle type) resulting in uncertainties in the export efficiency, and observational data on particle type is required to better constrain the models (Laufkötter et al. 2016). In addition to measurements of particle type, in depth measurements of their chemical composition and lability would be instructive for biogeochemical models.

### 6.2.2 Zooplankton community composition

Phytoplankton community composition has been suggested to explain some of the global variance in POC attenuation with depth (Boyd and Newton 1999; Guidi et al. 2009), with phytoplankton composition in the euphotic zone estimated to account for 68% in the variance of the downward flux at 400 m (Guidi et al. 2009). Guidi et al. (2009) derived an empirical relationship between the fraction of picophytoplankton and Martin's *b* value, advocating its use in biogeochemical models to attempt to account for regional and temporal variability in POC attenuation rates. However, their relationship only explains 27% of the observed variability in *b*, highlighting the complexity of interacting factors influencing the flux and transformation of sinking particles. The zooplankton community is tied to the phytoplankton community, and certain species can be coupled due to preferential feeding on certain prey (e.g. Knisely and Geller 1986; Kiørboe and Visser 1999). A recent study has highlighted the connection between export flux to the overall community structure, identifying a eukaryotic subnetwork able to predict as much as 69% of the variability in carbon export (Guidi et al. 2016). Their prokaryotic subnetwork was able to predict up to 60% of the variability in carbon export (Guidi et al. 2016). This study highlights the complexity of ecosystems with, for example, microbes and viruses also modulating the zooplankton and phytoplankton community

The activities of zooplankton can both increase and decrease the attenuation of POC with depth, through repackaging, vertical migration as well as coprophagy and fragmentation. The resultant effect of zooplankton on POC flux is therefore complex and the community structure must be considered as well as abundances. The work of this thesis suggests that differences in the abundance and composition of zooplankton in the upper ocean can explain differences in the attenuation rate of POC, confirming H2. Where abundances of small zooplankton, particularly microcopepod species, *Oithona* spp. *Oncaea* spp. *Microcalanus* spp. *and Ctenocalanus* spp. are high, and/or the ratio of small microcopepods to large calanoids is high, increased detrital feeding

as well as fragmentation drive the rapid loss of sinking particles with depth. This POC retention filter has been hypothesised to explain rapid decreases in FP (Riser et al. 2001; Dubischar and Bathmann 2002; Suzuki et al. 2003; Sampei et al. 2004; Huskin 2004; Wexels Riser et al. 2007), however this may, at least for some species, occur via fragmentation rather than intentional ingestion of FP (Poulsen and Kiørboe 2005; Reigstad et al. 2005). The proportion of these microzooplankton species, with life-styles based around coprophagy and coprorhexy, in a community therefore provides an additional control on the rate of POC attenuation. Additionally, high attenuation rates in regions and seasons dominated by small zooplankton species may relate to the small size and low sinking velocity of FP they produce, resulting in their remineralisation at shallow depths (Viitasalo et al. 1999). The size of FP may therefore also explain some differences in the degree to which they are exported to deeper waters (Dagg et al. 2003; Wexels Riser et al. 2007).

Certain zooplankton species may play a disproportionate role in the export and transfer of POC through the ocean. In particular this thesis focuses on the role of Antarctic krill due to the high contribution of krill FP to POC fluxes measured in the upper mesopelagic of the marginal ice zone (MIZ). The swarming behaviour of krill, and large size of their FP, likely supports efficient export of FP from the euphotic zone and transfer through the upper mesopelagic through their rapid exploitation of phytoplankton blooms and bulk egestion of rapidly sinking FP. This 'rain' of FP can overload the remineralising community and so short circuit this retention filter (Wefer et al. 1988; Wassmann et al. 2002; Atkinson et al. 2012). High FP fluxes were observed in the MIZ of the South Orkneys, and if typical of other MIZ regions in the Southern Ocean that support krill populations, the seasonal export of krill FP represents a substantial but largely 'hidden' flux of POC to the ocean interior. This conclusion can be extended to other swarming species, particularly those that produce large FP (e.g. *Salpa thompsoni,* a dominant salp species in the Southern Ocean). Differences in the size of FP alone (and hence the zooplankton community composition) can lead to variability in the flux of FP (Stamieszkin et al. 2015). The zooplankton community structure is therefore a key consideration when examining the degree to which sinking FP are exported from the euphotic zone (Viitasalo et al. 1999; Wassmann et al. 2000, 2002; Chapter 2).

### 6.2.3 Particle-associated microbes

A number of studies have assessed the contribution of free-living microbes (particularly bacteria) to the loss of POC in the mesopelagic (Reinthaler et al. 2006; Steinberg et al. 2008; Baltar et al. 2009; Giering et al. 2014), however direct studies of loss via particle-associated microbes are more limited (Collins et al. 2015; McDonnell et al. 2015) and have not been included in mesopelagic carbon budgets (Figure 6-1A). In this thesis, the focus is on microbes associated with

fast-sinking particles. There is not yet agreement in the literature as to the contribution of particle-associated microbes to POC attenuation, which is in part due to a lack of consistency in the community of microbes which are measured by the various methods, as well as heterogeneity in particle age and composition. For example, Alldredge and Youngbluth (1985) and Turley and Stutt (2000) measured only the respiration of bacteria, whereas more recently respiration of the whole particle-associated microbial community has been measured (Iversen et al. 2010; Iversen and Ploug 2013; Collins et al. 2015). In addition, methods are contrasting as to whether respiration is measured directly, or is calculated using growth efficiencies and measurements of production. A number of studies have noted the importance of protozoa such as ciliates and dinoflagellates for the remineralisation of POC (Tiselius and Kiørboe 1998; Poulsen and Iversen 2008; Svensen et al. 2014). In order to fully characterise the loss of POC occurring within particles, such as required for incorporation into budget studies, the whole particle-associated community needs to be considered.

The work of this thesis shows that, contrary to H3, particle-associated microbial respiration accounts for only small losses (loss rates of <3 % $d^{-1}$) in FP and PA in the Southern Ocean and North Atlantic respectively (Chapter 2 and 3). However, a number of studies have suggested microbes solubilise more POC to DOC via ecto-enzymatic hydrolysis than they require, and hence could be an important source of carbon for free-living microbes (Cho and Azam 1988; Smith et al. 1992). Rates of POC solubilisation are poorly constrained, making it difficult to fully quantify the importance of particle-associated microbes to the loss of POC. Particle-associated microbial respiration needs to be incorporated into budgets, and although including this respiration in an upper mesopelagic budget for fast-sinking POC did not solve imbalances (Chapter 3), the gap was narrowed, confirming H4.

If the low rates of particle-associated microbial respiration measured in this thesis are typical of most regions in the ocean, then this term is likely to be small and make only a small contribution to POC loss in the upper mesopelagic where the most rapid loss of POC is observed (Suess 1980; Martin et al. 1987) (Figure 6-1B). However, measurements of particle-associated microbial respiration made in this thesis were carried out in waters < 10 °C, and, in accordance with metabolic theory, higher rates of respiration may occur in regions of higher temperatures (Regaudie-De-Gioux and Duarte 2012). It is suggested here that zooplankton can (depending on the community structure) drive the rapid loss of large sinking particles in the upper mesopelagic through grazing and fragmentation (Figure 6-1B). This fragmentation to slow sinking POC may account for some of the imbalances in sources and sinks of fast-sinking POC in the upper mesopelagic (Figure 6-2). Deeper in the ocean, where zooplankton abundances are lower,

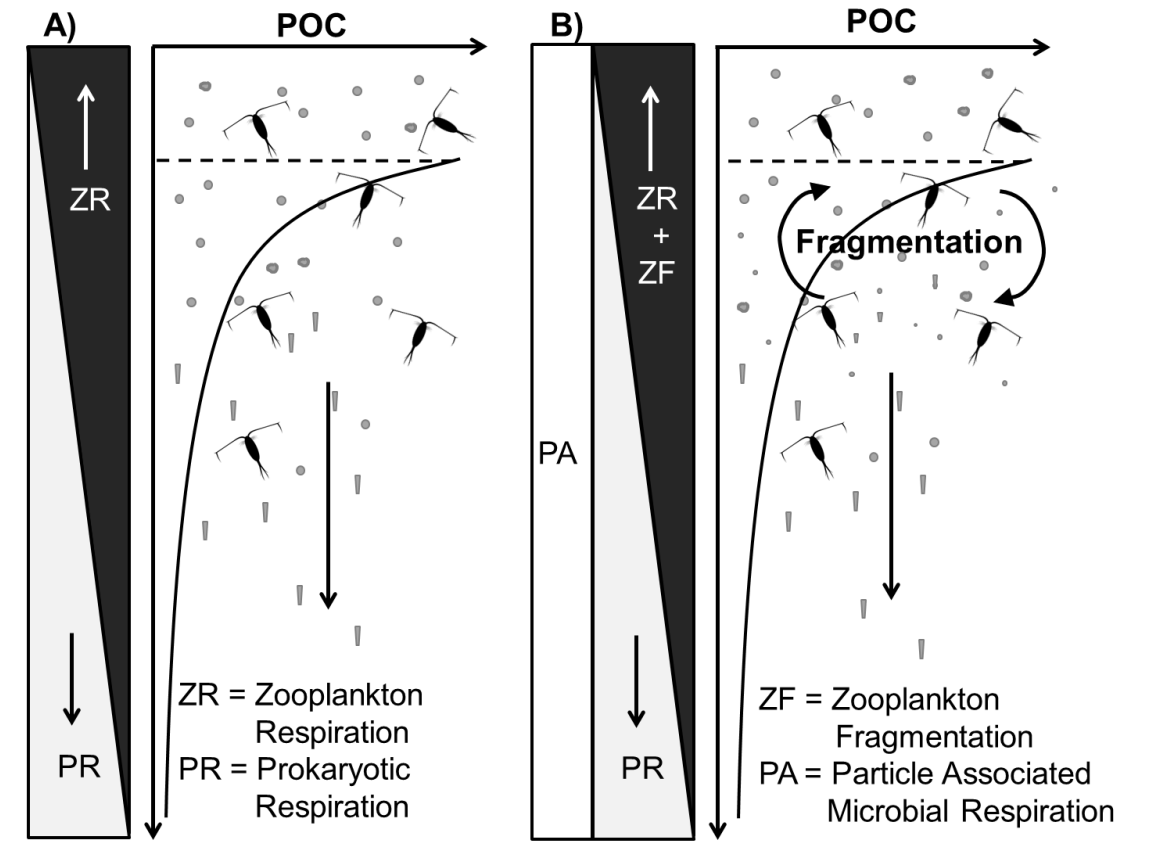


**Figure 6-1: Schematic highlighting A) the processes thought to drive the loss of POC prior to this thesis, and B) the additional processes investigated as part of this thesis. Rates of particle-associated microbial respiration were found to be low and almost constant with depth at the PAP site in the North Atlantic, and could not account for missing carbon sinks in the upper mesopelagic. It is hypothesised here that zooplankton fragmentation of fast-sinking POC into slow and non-sinking POC may account for some of this missing carbon sink.**

particle-associated microbial respiration may explain most of the loss of POC in large sinking particles (Chapter 2). Although many budget studies have found free-living prokaryotic respiration to be the dominant process in POC flux attenuation (Baltar et al. 2009; Anderson and Tang 2010; Giering et al. 2014), to be accessible to these organisms this first requires the transfer of fast-sinking particles of POC into slow- and non-sinking POC and DOC. Direct losses of organic carbon via particle-associated and zooplankton respiration may be small, but fragmentation by zooplankton and solubilisation by particle-associated microbes are important for fuelling the respiration of free-living microbes.

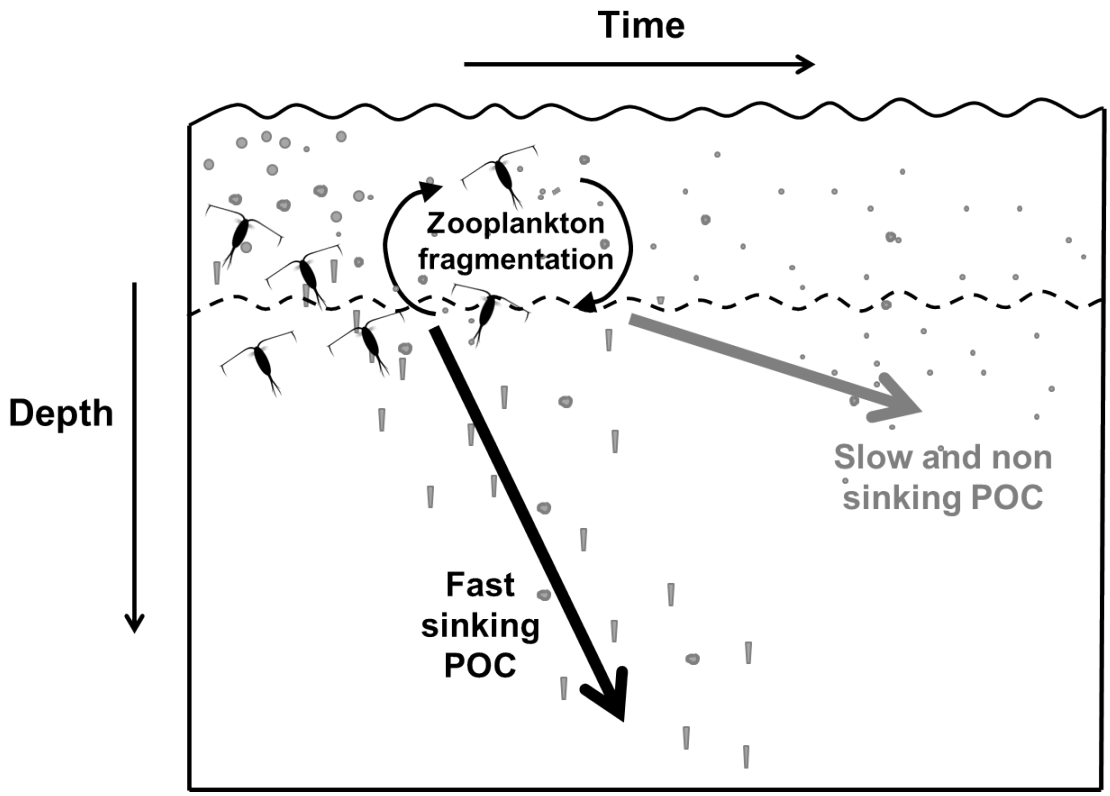


**Figure 6-2: Schematic illustrating the zooplankton mediated transfer of fast-sinking particles into slow and non-sinking particles which can be respired slowly over the season. This loss of fast-sinking particulate organic carbon (POC) to slow and non-sinking POC may help account for imbalances between sources and sinks of fast-sinking POC in the mesopelagic.**

The transfer of fast-sinking particles to slow and non-sinking POC and DOC has the potential to result in increased residence times in the upper ocean (Figure 6-2). These processes essentially introduce a time lag and may therefore help to explain why snapshot type measurements of carbon sources and sinks result in imbalances in the mesopelagic carbon budget (Burd et al. 2010). As suggested by Collins et al. (2015), these slower sinking and suspended pools of carbon may not be respired immediately, with bacterial production lagging primary production and export by days to months (Hansell and Ducklow 2003; Ortega-Retuerta et al. 2014). This hypothesis for a more seasonal balance in the mesopelagic carbon budget (Chapter 3) is supported by observations made in the Arabian sea that prokaryotic abundance in the deep ocean depends on long-term averages of POC flux rather than immediate inputs (Hansell and Ducklow 2003).

Untangling the exact mechanisms driving the remineralisation of POC is therefore not an easy task. However, the vastness of the ocean and huge spatial and temporal variability makes it essential to understand these processes in order to model them mechanistically in global

biogeochemical models and make accurate future predictions of ocean uptake and storage in a changing climate.

## 6.3 Future directions

The ocean is complex and ever changing, presenting many challenges for observational scientific research. Even the most well thought out and planned of experiments can find themselves in a situation of "hurry up and wait" on board a research ship whilst winches and instruments are fixed, weather reports change, and plans are formed, reformed and reformed again. Despite these challenges, which often result in the loss of that key sample, it is these very challenges that make oceanography such a fascinating and ever evolving field to be part of. During the last three years, I have attempted to address some of the key unknowns of the biological carbon pump, making a number of advancements to the field. However, my work has also raised a number of new questions, sparking many ideas for future research which are discussed in this section.

In order to fully assess the role of particle-associated microbial respiration on POC flux attenuation and its potential to resolve imbalances in the upper mesopelagic carbon budget, rates of POC solubilisation need to be measured. Currently, the choice of solubilisation parameter in biogeochemical models is based on very little data and is rather arbitrary (Anderson and Tang 2010). The rate of solubilisation will be highly affected by factors controlling enzyme activity such as temperature, pressure, and the concentration of specific organic molecules (Turley et al. 1995). Hence laboratory studies, for example on roller tank formed aggregates, would enable some of these factors to be controlled and provide a good starting point. Although vast improvements have been made in the ability of laboratory experiments to mimic *in situ* conditions, the validity of any laboratory derived estimates of solubilisation would need to be tested for a number of different particle types in a number of different oceanographic regimes.

Discrepancies between measurements made at atmospheric and *in situ* pressure may help to resolve imbalances in the mesopelagic carbon budget. However, currently the large uncertainties in rates of free-living bacterial respiration make it difficult to ascertain whether an imbalance even exists. Constraining estimates of free-living bacterial respiration is therefore a key priority. Recently, there have been a number of approaches to take the lab to the ocean rather than vice versa, with novel drifting incubation systems such as RESPIRE (Boyd et al. 2015). *In situ* incubations such as this or the novel high pressure incubation system PASS (PArticle Sinking Simulator (Tamburini et al. 2009)), provide the means to determine whether rates of respiration measured at atmospheric pressure (such as those in this study) are a true representation of those

occurring at depth. Where possible, pressure incubations should be carried out for all respiration measurements, particularly those made on samples from the deep sea.

This thesis has highlighted that community structure is an important factor defining the rate at which POC is attenuated with depth. However, to be able to incorporate these effects into models we need to establish whether changes in community structure alter export pathways in predictable ways. Key in determining this is an improved ability to measure POC fluxes, particularly on short timescales, to capture the often short lived and unpredictable biologically driven fluxes such as those associated with diatom resting spores (Rembauville et al. 2015), the "fall dump" (Kemp et al. 2000) and krill swarms (Chapter 4). I believe that improved use of optical techniques (such as the Underwater Vision Profiler (UVP) (Gorsky et al. 2000)) and autonomous vehicles will be key. However, the size range of particle detection of these methods must be sufficient to capture both the large rare particles and small sinking particles. Recent work by Briggs et al. (2011) used spikes in backscatter and fluorescence data from gliders to characterise flux events at high temporal resolution. Applying this technique to future and past glider data will greatly improve our ability to measure episodic fluxes and in turn understand the mechanisms driving them. Additionally the development and implementation of Bio-Argo floats is improving our ability to obtain estimates of carbon export flux from backscatter data, and continued widespread deployment will improve both the temporal and spatial coverage of flux data (Dall'Olmo and Mork 2014). Recently a new sediment trap (the Sedimentation Event Sensor) has been designed and tested that analyses collected material *in situ*, taking macro images of the sample and making fluorescence measurements (Mcgill et al. 2016). The ability to measure the chlorophyll content of settling material (information lost with traditional sediment traps due to the need for preservatives) will enable better assessments of particle freshness. The Sedimentation Event Sensor does not however provide direct estimates of mass flux, and hence would best complement rather than replace traditional sediment traps (Mcgill et al. 2016).

Optical techniques allow the entire particle spectrum to be measured at high spatial and temporal resolutions; however the limitation comes in turning these particle distributions into fluxes which requires knowledge of particle sinking speed. Several studies use a formulation of Stokes Law to relate particle size and sinking velocity, and calculate particle flux from particle concentration size distributions (Guidi et al. 2008; Iversen et al. 2010). However, sinking particles are highly heterogeneous in shape and composition, and as yet, we do not have a universal relationship between particle sinking velocity and particle size (McDonnell and Buesseler 2010). In order to utilise the high resolution data offered by digital imaging systems for high resolution estimates of particle flux, we need to find a relationship between easily measureable parameters and sinking

velocity. Achieving this will require more in depth measurements of particle properties such as composition to assess whether such a relationship can be found.

Additionally long-term, moored observatory systems are required to distinguish climate change from natural variability (Henson et al. 2016), but also to provide full seasonal coverage in regions that are difficult to access year round (e.g. due to ice cover). The flux of carbon through the ocean is an important regulator of the Earth's climate (Kwon et al. 2009), yet measurements of carbon flux are, as yet, hard to derive routinely from autonomous platforms, and the spatial coverage of current observing platforms is limited (Henson 2016). There needs to be a continued push towards the integration of physical and biological measurements through the use of bio-moorings. Incorporating optical methods such as the UVP and Laser In-Situ Scattering and Transmissometry (LISST) onto moorings with sediment traps would help provide high resolution, long-term data to support improved ecosystem models.

As highlighted in chapter 4, the Southern Ocean is a key part of global biogeochemical cycles, but environmental constraints make it difficult to obtain year round data. POC fluxes in the Southern Ocean are poorly constrained, and suffer from a lack of *in situ* data with which to derive empirical models of export flux. Although, "more data" is often suggested as a key step to advancing research, it is not yet feasible to be able to sample the entire Southern Ocean over the whole season. To better quantify particle fluxes in the Southern Ocean, we need to focus our sampling efforts on regions thought to contribute disproportionally to POC flux, such as regions with high krill densities as highlighted in chapter 4. Refined estimates of the flux of FP in the Southern Ocean, which as shown here could make a large and as yet largely 'hidden' contribution to export flux, require both seasonally resolved krill density measurements (which are now much more possible with the improvements in acoustically derived krill biomass estimates using multibeam echosounders, e.g. Fielding et al. 2012), and region and species specific measurements of FP production rates. These data would make it possible to determine the validity of the first order approximations made here. If found to be true, this has important consequences for future changes in export in the Southern Ocean if krill populations continue to decline in the Southern Ocean (Atkinson et al. 2004).

## 6.4 Closing Statement

This thesis has investigated the controls on the attenuation of POC in the mesopelagic ocean, presenting new data which further advance our understanding of the processes affecting the efficiency of the biological carbon pump. Changes in the efficiency of the carbon pump are tightly linked to atmospheric levels of $CO_2$. Continued advancements in this field are therefore needed if

we are to be able to accurately model and predict the response of the biological carbon pump to a changing climate, and in doing so support informed policy decisions for sustainable development.

# Appendix A Images of sinking phytoplankton cells

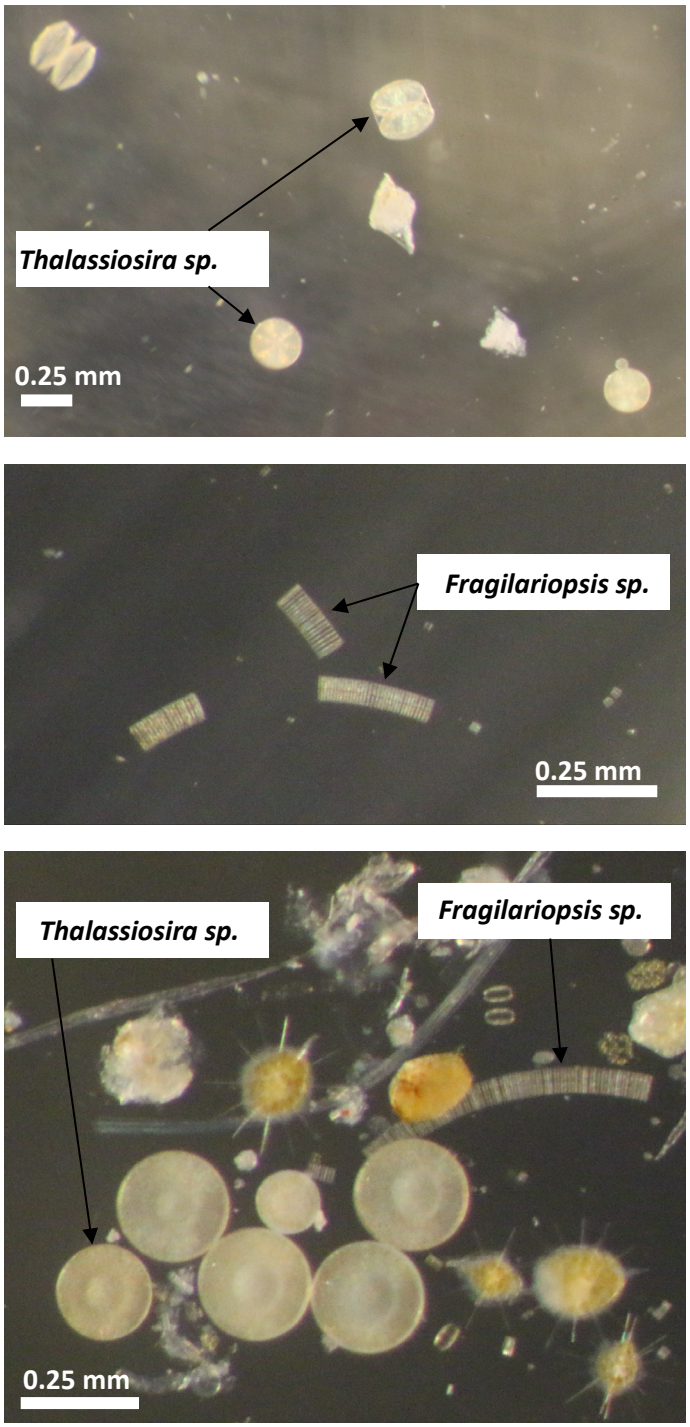


**Figure A-1: Light microscope imagery of phytoplankton cells collected in tray (fast-sinking fraction) of Marine Snow Catchers. Diatom species *Thalassiosira* and *Fragilariopsis* are labelled and scale bars of 0.25mm are shown for reference.**

# Appendix B Flow chamber experimental set up

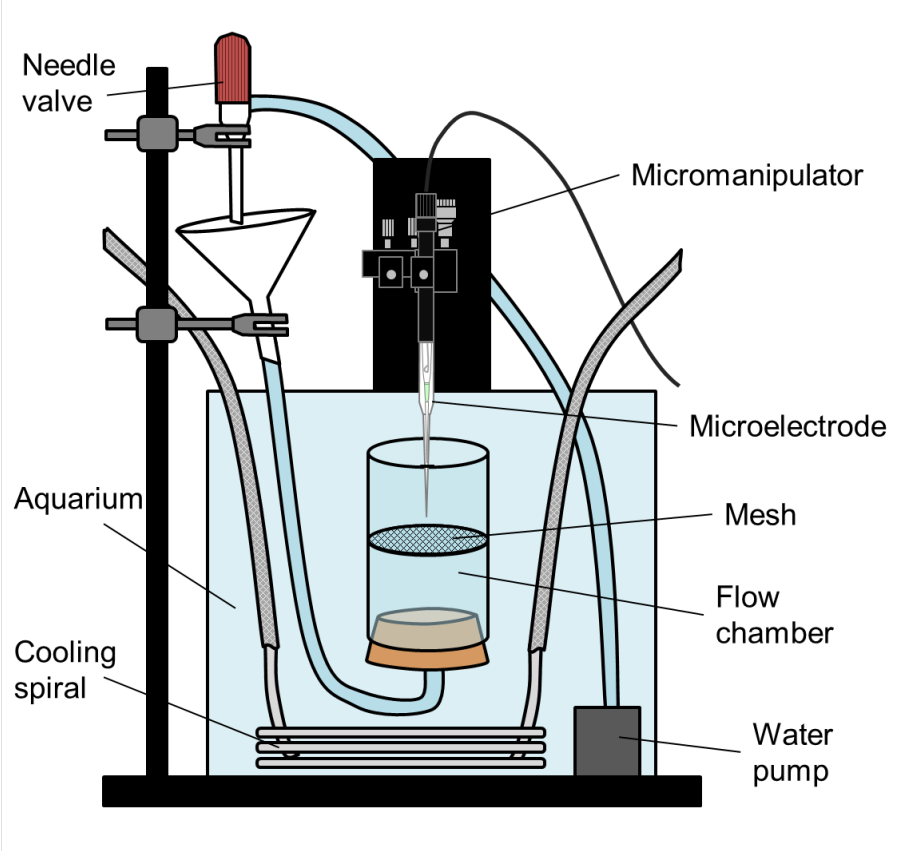


**Figure B-1: Schematic of flow chamber set up for measurement of particle-associated microbial respiration in particles using microelectrodes.**

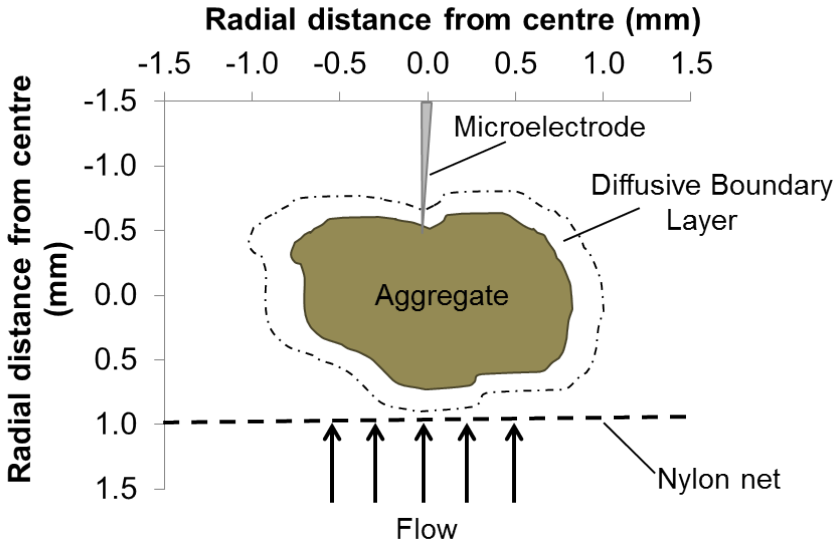


**Figure B-2: Schematic illustrating measurement of oxygen gradients within aggregates using microelectrodes. Adapted from Ploug et al. (1997).**

# Appendix C Krill faecal pellet production in the MIZ

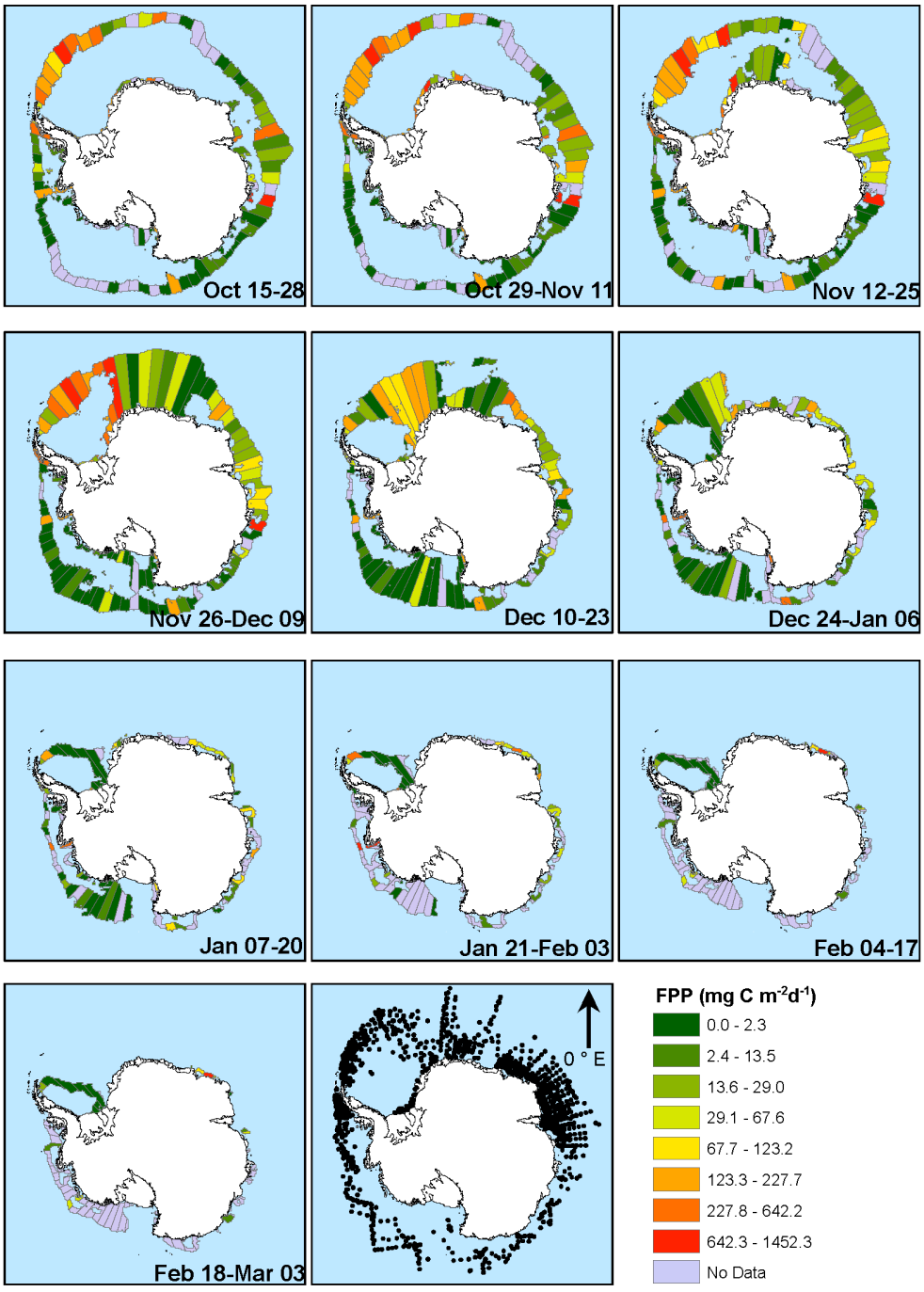


**Figure C-1: Estimated krill faecal pellet production (FPP) in the marginal ice zone (MIZ), Antarctica for the period 1980-1990. The MIZ, from fortnightly sea ice concentration data (15-80% ice cover), is divided into 5 ° zonal grids, and is coloured by FPP flux (mg C $m^{-2}$ $d^{-1}$) based on mean krill density measurements from pre 1990 KRILLBASE data (black dots) and literature krill FP production rates. Regions of the marginal ice zone where no KRILLBASE records occurred are coloured in grey.**

# List of References

Abramson, L., C. Lee, Z. Liu, S. Wakeham, and J. Szlosek. 2010. Exchange between suspended and sinking particles in the northwest Mediterranean as inferred from the organic composition of *in situ* pump and sediment trap samples. Limnol. Oceanogr. **55**: 725–739.

Accornero, A., C. Manno, F. Esposito, and M. C. Gambi. 2003. The vertical flux of particulate matter in the polynya of Terra Nova Bay . Part II . Biological components. Antarct. Sci. **15**: 175–188.

Alldredge, A. L. 1998. The carbon, nitrogen and mass content of marine snow as a function of aggregate size. Deep Sea Res. Part I Oceanogr. Res. Pap. **45**: 529–541.

Alldredge, A. L. 2000. Interstitial dissolved organic carbon (DOC) concentrations within sinking marine aggregates and their potential contribution to carbon flux. Limnol. Oceanogr. **45**: 1245–1253.

Alldredge, A. L., T. C. Granata, C. C. Gotschalk, and T. D. Dickey. 1990. The physical strength of marine snow and its implications for particle disaggregation in the ocean. Limnol. Oceanogr. **35**: 1415–1428.

Alldredge, A. L., and M. W. Silver. 1988. Characteristics, dynamics and significance of marine snow. Prog. Oceanogr. **20**: 41–82.

Alldredge, A. L., and M. J. Youngbluth. 1985. The significance of macroscopic aggregates (marine snow) as sites for heterotrophic bacterial production in the mesopelagic zone of the subtropical Atlantic. Deep Sea Res. **32**: 1445–1456.

Alonso-González, I. J., J. Arístegui, C. Lee, A. Sanchez-Vidal, A. Calafat, J. Fabrés, P. Sangrá, P. Masqué, A. Hernández-Guerra, and V. Benítez-Barrios. 2010. Role of slowly settling particles in the ocean carbon cycle. Geophys. Res. Lett. **37**: L13608.

Alonso-Sáez, L., J. M. Gasol, J. Arístegui, J. C. Vilas, D. Vaqué, C. M. Duarte, and S. Agustí. 2007. Large-scale variability in surface bacterial carbon demand and growth efficiency in the subtropical northeast Atlantic Ocean. Limnol. Oceanogr. **52**: 533–546.

Anderson, T. R., V. A. Ryabchenko, M. J. R. Fasham, and V. A. Gorchakov. 2007. Denitrification in the Arabian Sea: A 3D ecosystem modelling study. Deep. Res. Part I Oceanogr. Res. Pap. **54**: 2082–2119.

Anderson, T. R., and K. W. Tang. 2010. Carbon cycling and POC turnover in the mesopelagic zone

of the ocean : Insights from a simple model. Deep. Res. Part II **57**: 1581–1592.

Antezana, T., K. Ray, and C. Melo. 1982. Trophic behavior of Euphausia superba Dana in laboratory conditions. Polar Biol. **1**: 77–82.

Aristegui, J., C. M. Duarte, J. M. Gasol, and L. Alonso-Sáez. 2005. Active mesopelagic prokaryotes support high respiration in the subtropical northeast Atlantic Ocean. Geophys. Res. Lett. **32**, doi:10.1029/2004GL021863

Arístegui, J., J. M. Gasol, C. M. Duarte, and G. J. Herndl. 2009. Microbial oceanography of the dark ocean''s pelagic realm. Limnol. Oceanogr. **54**: 1501–1529.

Armstrong, R. A., C. Lee, J. I. Hedges, S. Honjo, and S. G. Wakeham. 2002. A new, mechanistic model for organic carbon fluxes in the ocean based on the quantitative association of POC with ballast minerals. Deep. Res. Part II Top. Stud. Oceanogr. **49**: 219–236.

Atkinson, A., K. Schmidt, S. Fielding, S. Kawaguchi, and P. A. Geissler. 2012. Variable food absorption by Antarctic krill: Relationships between diet, egestion rate and the composition and sinking rates of their fecal pellets. Deep Sea Res. Part II Top. Stud. Oceanogr. **59**–**60**: 147–158.

Atkinson, A., V. Siegel, E. A. Pakhomov, and P. Rothery. 2004. Long-term decline in krill stock and increase in salps within the Southern Ocean. Nature **432**: 100–103.

Atkinson, A., V. Siegel, E. A. Pakhomov, P. Rothery, V. Loeb, R. M. Ross, L. B. Quetin, K. Schmidt, P. Fretwell, E. J. Murphy, G. A. Tarling, and A. H. Fleming. 2008. Oceanic circumpolar habitats of Antarctic krill. Mar. Ecol. Prog. Ser. **362**: 1–23.

Aumont, O., and L. Bopp. 2006. Globalizing results from ocean in situ iron fertilization studies. Global Biogeochem. Cycles **20**: 1–15.

Azam, F., T. Frenchel, J. G. Field, J. S. Gray, L. A. Meyer-Reil, and F. Thingstad. 1983. The ecological role of water-column microbes in the sea. Mar. Ecol. Prog. Ser. **10**: 257–263.

Azam, F., and F. Malfatti. 2007. Microbial structuring of marine ecosystems. Nat. Rev Microbiol **5**: 782–91.

de Baar, H. J. W., J. T. M. de Jong, D. C. E. Bakker, B. M. Löscher, C. Veth, U. V. Bathmann, and V. Smetacek. 1995. Importance of iron for plankton blooms and carbon dioxide drawdown in the Southern Ocean. Nature **373**: 412–415.

Bakker, D. C. E., M. C. Nielsdóttir, P. J. Morris, H. J. Venables, and A. J. Watson. 2007. The island

mass effect and biological carbon uptake for the subantarctic Crozet Archipelago. Deep Sea Res. Part II Top. Stud. Oceanogr. **54**: 2174–2190.

Baltar, F., J. Arístegui, J. M. Gasol, and G. J. Herndl. 2010a. Prokaryotic carbon utilization in the dark ocean: Growth efficiency, leucine-to-carbon conversion factors, and their relation. Aquat. Microb. Ecol. **60**: 227–232.

Baltar, F., J. Aristegui, J. M. Gasol, E. Sintes, and G. J. Herndl. 2009. Evidence of prokaryotic metabolism on suspended particulate organic matter in the dark waters of the subtropical North Atlantic. Limnol. Oceanogr. **54**: 182–193.

Baltar, F., J. Arístegui, E. Sintes, J. M. Gasol, T. Reinthaler, and G. J. Herndl. 2010b. Significance of non-sinking particulate organic carbon and dark CO2 fixation to heterotrophic carbon demand in the mesopelagic northeast Atlantic. Geophys. Res. Lett. **37**, doi:10.1029/2010GL043105

Bathmann, U., G. Fischer, P. J. Müller, and D. Gerdes. 1991. Short-term variations in particulate matter sedimentation off Kapp Norvegia, Weddell Sea, Antarctica: relation to water mass advection, ice cover, plankton biomass and feeding activity. Polar Biol. **11**: 185–195.

Beaulieu, S. 2002. Accumulation and fate of phytodetritus on the sea floor. Oceanogr. Mar. Biol. Annu. Rev. **40**: 171–232.

Behrenfeld, M. J., and P. G. Falkowski. 1997. Photosynthetic rates derived from satellite-based chlorophyll concentration. Limnol. Oceanogr. **42**: 1–20.

Belcher, A., M. H. Iversen, C. Manno, S. A. Henson, G. A. Tarling, and R. Sanders. 2016. The role of particle associated microbes in remineralization of fecal pellets in the upper mesopelagic of the Scotia Sea, Antarctica. Limnol. Oceanogr. **61**: 1049–1064.

Berger, W. H. 1971. Sedimentation of planktonic foraminifera. Mar. Geol. **11**: 325–358.

Berggren, M., J.-F. Lapierre, and P. A. del Giorgio. 2012. Magnitude and regulation of bacterioplankton respiratory quotient across freshwater environmental gradients. ISME J. **6**: 984–93.

Biard, T., L. Stemmann, M. Picheral, N. Mayot, P. Vandromme, H. Hauss, G. Gorsky, L. Guidi, R. Kiko, and F. Not. 2016. In situ imaging reveals the biomass of giant protists in the global ocean. Nature **532**: 504–507.

Bidigare, R., L. Hanson, K. O. Buesseler, G. Wakeham, H. Freeman, R. D. Pancost, J. Millero, P.

Steinberg, N. Popp, M. Latasa, R. Landry, and A. Laws. 1999. Iron-stimulated changes in 13C fractionation and export by equatorial Pacific phytoplankton: Toward a paleogrowth rate proxy. Paleoceanography **14**: 589–595.

Bienfang, P. K. 1981. SETCOL- A technologically simple and reliable method for measuring phytoplankton sinking rates. Can. J. Fish. Aquat. Sci. **38**: 1289–1294.

Bochdansky, A. B., M. A. Clouse, and G. J. Herndl. 2016. Dragon kings of the deep sea : marine particles deviate markedly from the common number-size spectrum. Sci. Rep. **6**: 22633.

Bodungen, von B., G. Fischer, E. M. Nothing, and G. Wefer. 1987. Sedimentation of krill faeces during spring development of phytoplankton in the Bransfield Strait, Antarctica. Mitteilungen aus dem Geol. un Paläontologischen Inst. der Univ. Leipzig **62**: 243–235.

Bodungen, B. Von. 1986. Phytoplankton growth and krill grazing during spring in the Bransfield Strait, Antarctica - Implications from sediment trap collections. Polar Biol. **6**: 153–160.

Borrione, I., and R. Schlitzer. 2013. Distribution and recurrence of phytoplankton blooms around South Georgia, Southern Ocean. Biogeosciences **10**: 217–231.

Boyd, P., J. Laroche, M. Gall, R. Frew, and R. M. L. Mckay. 1999a. Role of iron , light , and silicate in controlling algal biomass in subantarctiv waters SE of New Zealand. J. Geophys. Res. **104**: 13395–13408.

Boyd, P. W., C. S. Law, C. S. Wong, Y. Nojiri, A. Tsuda, M. Levasseur, S. Takeda, R. Rivkin, P. J. Harrison, R. Strzepek, J. Gower, R. M. Mckay, E. Abraham, M. Arychuk, J. Barwell-clarke, W. Crawford, D. Crawford, M. Hale, K. Harada, K. Johnson, H. Kiyosawa, I. Kudo, A. Marchetti, W. Miller, J. Needoba, H. Saito, A. Sastri, N. Sherry, T. Soutar, S. E. Wong, and T. Yoshimura. 2004. The decline and fate of an iron-induced subarctic phytoplankton bloom. Nature **428**: 549–553.

Boyd, P. W., A. McDonnell, J. Valdez, D. Lefèvre, and M. P. Gall. 2015. RESPIRE: An in situ particle interceptor to conduct particle remineralization and microbial dynamics studies in the oceans' Twilight Zone. Limnol. Oceanogr. Methods **13**: 494–508.

Boyd, P. W., and P. P. Newton. 1999. Does planktonic community structure determine downward particulate organic carbon flux in different oceanic provinces? Deep Sea Res. Part I Oceanogr. Res. Pap. **46**: 63–91.

Boyd, P. W., N. D. Sherry, J. A. Berges, J. K. B. Bishop, S. E. Calvert, M. a. Charette, S. J. Giovannoni, R. Goldblatt, P. J. Harrison, S. B. Moran, S. Roy, M. Soon, S. Strom, D. Thibault, K. L. Vergin, F.

a. Whitney, and C. S. Wong. 1999b. Transformations of biogenic particulates from the pelagic to the deep ocean realm. Deep Sea Res. Part II Top. Stud. Oceanogr. **46**: 2761–2792.

Boyd, P. W., and T. W. Trull. 2007. Understanding the export of biogenic particles in oceanic waters: Is there consensus? Prog. Oceanogr. **72**: 276–312.

Briggs, N., M. J. Perry, I. Cetinic, C. Lee, E. D'Asaro, A. M. Gray, and E. Rehm. 2011. High-resolution observations of aggregate flux during a sub-polar North Atlantic spring bloom. Deep. Res. Part I Oceanogr. Res. Pap. **58**: 1031–1039.

Broecker, W. S., and T. H. Peng. 1974. Gas exchange rates between air and sea. Tellus **26**: 21–35.

Buesseler, K. O., A. N. Antia, M. Chen, S. W. Fowler, W. D. Gardner, O. Gustafsson, K. Harada, A. F. Michaels, M. Rutgers van der Loeff, M. Sarin, D. K. Steinberg, and T. Trull. 2007a. An assessment of the use of sediment traps for estimating upper ocean particle fluxes. J. Mar. Res. **65**: 345–416.

Buesseler, K. O., M. P. Bacon, H. D. Livingston, and K. Cochran. 1992. Carbon and nitrogen export during the JGOFS North Atlantic Bloom Experiment estimated from 234Th : 238U disequilibria. Deep Sea Res. Part A. Oceanogr. Res. Pap. **39**: 1113–1137.

Buesseler, K. O., L. Ball, J. Andrews, J. K. Cochran, D. J. Hirschberg, M. P. Bacon, a. Fleer, and M. Brzezinski. 2001. Upper ocean export of particulate organic carbon and biogenic silica in the Southern Ocean along 170°W. Deep Sea Res. Part II Top. Stud. Oceanogr. **48**: 4275–4297.

Buesseler, K. O., C. R. Benitez-Nelson, S. B. Moran, A. Burd, M. Charette, J. K. Cochran, L. Coppola, N. S. Fisher, S. W. Fowler, W. D. Gardner, L. D. Guo, Ö. Gustafsson, C. Lamborg, P. Masque, J. C. Miquel, U. Passow, P. H. Santschi, N. Savoye, G. Stewart, and T. Trull. 2006. An assessment of particulate organic carbon to thorium-234 ratios in the ocean and their impact on the application of 234Th as a POC flux proxy. Mar. Chem. **100**: 213–233.

Buesseler, K. O., and P. W. Boyd. 2009. Shedding light on processes that control particle export and flux attenuation in the twilight zone of the open ocean. Limnol. Oceanogr. **54**: 1210–1232.

Buesseler, K. O., C. H. Lamborg, P. W. Boyd, P. J. Lam, T. W. Trull, R. R. Bidigare, J. K. B. Bishop, K. L. Casciotti, F. Dehairs, M. Elskens, M. Honda, D. M. Karl, D. A. Siegel, M. W. Silver, D. K. Steinberg, J. Valdes, B. Van Mooy, and S. Wilson. 2007b. Revisiting Carbon Flux Through the Ocean's Twilight Zone. Science **316**: 567–570.

Buesseler, K. O., D. K. Steinberg, A. F. Michaels, R. J. Johnson, J. E. Andrews, J. R. Valdes, and J. F.

Price. 2000. A comparison of the quantity and composition of material caught in a neutrally buoyant versus surface-tethered sediment trap. Deep. Res. Part I Oceanogr. Res. Pap. **47**: 277–294.

Buesseler, K. O., T. W. Trull, D. K. Steinberg, M. W. Silver, D. A. Siegel, S.-I. Saitoh, C. H. Lamborg, P. J. Lam, D. M. Karl, N. Z. Jiao, M. C. Honda, M. Elskens, F. Dehairs, S. L. Brown, P. W. Boyd, J. K. B. Bishop, and R. R. Bidigare. 2008. VERTIGO (VERtical Transport In the Global Ocean): A study of particle sources and flux attenuation in the North Pacific. Deep Sea Res. Part II Top. Stud. Oceanogr. **55**: 1522–1539.

Burd, A. B., D. A. Hansell, D. K. Steinberg, T. R. Anderson, J. Arístegui, F. Baltar, S. R. Beaupré, K. O. Buesseler, F. Dehairs, G. A. Jackson, D. C. Kadko, R. Koppelmann, R. S. Lampitt, T. Nagata, T. Reinthaler, C. Robinson, B. H. Robison, C. Tamburini, and T. Tanaka. 2010. Assessing the apparent imbalance between geochemical and biochemical indicators of meso- and bathypelagic biological activity: What the @$♯! is wrong with present calculations of carbon budgets? Deep Sea Res. Part II Top. Stud. Oceanogr. **57**: 1557–1571.

Burd, A. B., and G. A. Jackson. 2009. Particle aggregation. Ann. Rev. Mar. Sci. **1**: 65–90.

Cadée, G. C. 1992. Organic carbon and its sedimentation during the ice retreat period in the Wedell-Scotia Sea, 1988. Polar Biol. **12**: 253–259.

Cadée, G. C., H. E. González, and S. B. Schnack-Schiel. 1992. Krill diet affects faecal string settling. Polar Biol. **12**: 75–80.

Carr, M. 2002. Estimation of potential productivity in Eastern Boundary Currents using remote sensing. Deep Sea Res. Part II Top. Stud. Oceanogr. **49**: 59–80.

Carr, M., M. A. M. Friedrichs, M. Schmeltz, M. Noguchi, D. Antoine, K. R. Arrigo, I. Asanuma, O. Aumont, R. Barber, M. Behrenfeld, R. Bidigare, E. T. Buitenhuis, J. Campbell, A. Ciotti, H. Dierssen, M. Dowell, J. Dunne, W. Esaias, B. Gentili, W. Gregg, S. Groom, N. Hoepffner, J. Ishizaka, T. Kameda, C. Le Que, T. E. Reddy, J. Ryan, M. Scardi, K. Moore, T. Smyth, K. Turpie, G. Tilstone, K. Waters, and Y. Yamanaka. 2006. A comparison of global estimates of marine primary production from ocean color. Deep Sea Res. Part I Oceanogr. Res. Pap. **53**: 741–770.

Carroll, M. L., J.-C. Miquel, and S. W. Fowler. 1998. Seasonal patterns and depth-specific trends of zooplankton fecal pellet fluxes in the Northwestern Mediterranean Sea. Deep Sea Res. Part I Oceanogr. Res. Pap. **45**: 1303–1318.

Cavalieri, D. J., C. L. Parkinson, P. Gloersen, and Z. H. 1996. Sea Ice Concentrations from Nimbus-7

SMMR and DMSP SSM/I-SSMIS Passive Microwave Data. Boulder, Color. USA. NASA Natl. Snow Ice Data Cent. Distrib. Act. Arch. Cent. , doi:http://dx.doi.org/10.5067/8GQ8LZQVL0VL

Cavan, E. L., S. A. Henson, A. Belcher, and R. Sanders. 2017. Role of zooplankton in determining the efficiency of the biological carbon pump. Biogeosciences **14**: 177–186.

Cavan, E. L., F. Le Moigne, A. J. Poulton, G. A. Tarling, P. Ward, C. J. Daniels, F. G, and R. J. Sanders. 2015. Attenuation of particulate organic carbon flux in the Scotia Sea, Southern Ocean, controlled by zooplankton fecal pellets. Geophys. Res. Lett. **42**: 821–830.

Cho, B. C., and F. Azam. 1988. Major role of bacteria in biogeochemical fluxes in the ocean's interior. Nature **332**: 441–443.

Ciais, P., C. Sabine, G. Bala, L. Bopp, V. Brovkin, J. Canadell, A. Chhabra, R. DeFries, J. Galloway, M. Heimann, C. Jones, C. Le Quéré, R. B. Myneni, S. Piao, and P. Thornton. 2013. Carbon and Other Biogeochemical Cycles, p. 465–570. *In* T.F. Stocker, D. Qin, G.-K. Plattner, M. Tignor, S.K. Allen, J. Boschung, A. Nauels, Y. Xia, V. Bex, and P.M. Midgley [eds.], Climate Change 2013 - The Physical Science Basis. Contribution of working group 1 to the fifth assessment report of the Intergovernmental Panel on Climate Change. Cambridge University Press.

Clarke, A., L. B. Quetin, and R. M. Ross. 1988. Laboratory and field estimates of the rate of faecal pellet production by Antarctic krill, Euphausia superba. Mar. Biol. **98**: 557–563.

Cnudde, C., C. Sanchez Clavano, T. Moens, A. Willems, and M. De Troch. 2013. Structural and functional patterns of active bacterial communities during aging of harpacticoid copepod fecal pellets. Aquat. Microb. Ecol. **71**: 25–42.

Collins, J. R., B. R. Edwards, K. Thamatrakoln, J. E. Ossolinski, G. R. Ditullio, K. D. Bidle, S. C. Doney, and B. A. S. Van Mooy. 2015. The multiple fates of sinking particles in the North Atlantic Ocean. Global Biogeochem. Cycles **29**: 1471–1494.

Dagg, M. J., J. Urban-Rich, and J. O. Peterson. 2003. The potential contribution of fecal pellets from large copepods to the flux of biogenic silica and particulate organic carbon in the Antarctic Polar Front region near 170°W. Deep Sea Res. Part II Top. Stud. Oceanogr. **50**: 675–691.

Dall'Olmo, G., and K. A. Mork. 2014. Carbon export by small particles in the Norwegian Sea. Geophys. Res. Lett. **41**: 1–6.

Devol, A. H., and H. E. Hartnett. 2001. Role of the oxygen-deficient zone in transfer of organic carbon to the deep ocean. Limnol. Oceanogr. **46**: 1684–1690.

Dilling, L., and A. L. Alldredge. 2000. Fragmentation of marine snow by swimming macrozooplankton: A new process impacting carbon cycling in the sea. Deep. Res. Part I Oceanogr. Res. Pap. **47**: 1227–1245.

Dubischar, C. D., and U. V. Bathmann. 2002. The occurrence of faecal material in relation to different pelagic systems in the Southern Ocean and its importance for vertical flux. Deep. Res. Part II Top. Stud. Oceanogr. **49**: 3229–3242.

Ducklow, H. W., D. L. Kirchman, and G. T. Rowe. 1982. Production and vertical flux of attached bacteria in the Hudson river plume of the New York Bight as studied with floating sediment traps. Appl. Environ. Microbiol. **43**: 769–776.

Dunbar, R. B. 1984. Sediment trap experiments on the Antarctic continental margin. Antarct. J. United States **19**: 70–71.

Dunne, J. P., R. A. Armstrong, A. Gnanadesikan, and J. L. Sarmiento. 2005. Empirical and mechanistic models for the particle export ratio. Global Biogeochem. Cycles **19**, doi:10.1029/2004GB002390

Dunne, J. P., J. G. John, S. Shevliakova, R. J. Stouffer, J. P. Krasting, S. L. Malyshev, P. C. D. Milly, L. T. Sentman, A. J. Adcroft, W. Cooke, K. A. Dunne, S. M. Griffies, R. W. Hallberg, M. J. Harrison, H. Levy, A. T. Wittenberg, P. J. Phillips, and N. Zadeh. 2013. GFDL's ESM2 global coupled climate-carbon earth system models. Part II: Carbon system formulation and baseline simulation characteristics. J. Clim. **26**: 2247–2267.

Dunne, J. P., J. L. Sarmiento, and A. Gnanadesikan. 2007. A synthesis of global particle export from the surface ocean and cycling through the ocean interior and on the seafloor. Global Biogeochem. Cycles **21**, doi:10.1029/2006GB002907

Durkin, C. A., M. L. Estapa, and K. O. Buesseler. 2015. Observations of carbon export by small sinking particles in the upper mesopelagic. Mar. Chem. **175**: 72–81.

Durkin, C. A., B. A. S. Van Mooy, S. T. Dyhrman, and K. O. Buesseler. 2016. Sinking phytoplankton associated with carbon flux in the Atlantic Ocean. Limnol. Oceanogr. **61**: 1172–1187.

Ebersbach, F., and T. W. Trull. 2008. Sinking particle properties from polyacrylamide gels during the Kerguelen Ocean and Plateau compared Study (KEOPS): Zooplankton control of carbon export in an area of persistent natural iron inputs in the Southern Ocean. Limnol. Oceanogr. **53**: 212–224.

Ebersbach, F., T. W. Trull, D. M. Davies, and S. G. Bray. 2011. Controls on mesopelagic particle

fluxes in the Sub-Antarctic and Polar Frontal Zones in the Southern Ocean south of Australia in summer — Perspectives from free-drifting sediment traps. Deep. Res. Part II **58**: 2260–2276.

Emerson, C., and J. Roff. 1987. Implications of fecal pellet size and zooplankton behaviour to estimates of pelagic-benthic carbon flux. Mar. Ecol. Prog. Ser. **35**: 251–257.

Le Fèvre, J., L. Legendre, and R. B. Rivkin. 1998. Fluxes of biogenic carbon in the Southern Ocean: Roles of large microphagous zooplankton. J. Mar. Syst. **17**: 325–345.

Field, C. B., M. J. Behrenfeld, J. T. Randerson, and P. G. Falkowski. 1998. Primary Production of the Biosphere: Integrating Terrestrial and Oceanic Components. Science **281**: 237–240.

Fielding, S., J. L. Watkins, M. A. Collins, P. Enderlein, and H. J. Venables. 2012. Acoustic determination of the distribution of fish and krill across the Scotia Sea in spring 2006 , summer 2008 and autumn 2009. Deep. Res. Part II **59–60**: 173–188.

Fielding, S., J. L. Watkins, A. Cossio, C. Reiss, G. Watters, L. Calise, G. Skaret, Y. Takao, X. Zhao, D. Agnew, D. Ramm, and K. Reid. 2011. The ASAM 2010 assessment of krill biomass for area 48 from the Scotia Sea CCAMLR 2000 synoptic survey.

Fielding, S., J. L. Watkins, P. Trathan, P. Enderlein, C. M. Waluda, G. Stowasser, G. A. Tarling, and E. J. Murphy. 2014. Interannual variability in Antarctic krill (Euphausia superba) density at South Georgia, Southern Ocean: 1997–2013. ICES J. Mar. Sci. **71**: 2578–2588.

Fischer, G., D. Fuetterer, R. Gersonde, S. Honjo, D. Ostermann, and G. Wefer. 1988. Seasonal variability of particle flux in the Weddell Sea and its relation to ice cover. Nature **335**: 426–428.

Fischer, G., and G. Karakas. 2009. Sinking rates and ballast composition of particles in the Atlantic Ocean : implications for the organic carbon fluxes to the deep ocean. Biogeosciences **6**: 85–102.

Fowler, S. W., and G. A. Knauer. 1986. Role of large particles in the transport of elements and organic compounds through the oceanic water column. Prog. Oceanogr. **16**: 147–194.

Francois, R., S. Honjo, R. Krishfield, and S. Manganini. 2002. Factors controlling the flux of organic carbon to the bathypelagic zone of the ocean. Global Biogeochem. Cycles **16**: 34-1-34–20.

Gehlen, M., L. Bopp, N. Emprin, O. Aumont, C. Heinze, and O. Ragueneau. 2006. Reconciling surface ocean productivity, export fluxes and sediment composition in a global

biogeochemical ocean model. Biogeosciences **3**: 521–537.

Giering, S. L. C., R. J. Sanders, A. P. Martin, S. A. Henson, J. S. Riley, C. M. Marsay, and D. Johns. 2017. Particle flux in the oceans: Challenging the steady state assumption. Global Biogeochem. Cycles , doi:10.1002/2016GB005424

Giering, S. L. C., R. J. Sanders, A. P. Martin, C. Lindemann, K. O. Moller, C. J. Daniels, D. J. Mayor, and M. St John. 2016. High export via small particles before the onset of the North Atlantic spring bloom. J. Geophys. Res. **121**: 6929–6945.

Giering, S. L. C., R. Sanders, R. S. Lampitt, T. R. Anderson, C. Tamburini, M. Boutrif, M. V Zubkov, C. M. Marsay, S. A. Henson, K. Saw, K. Cook, and D. J. Mayor. 2014. Reconciliation of the carbon budget in the ocean's twilight zone. Nature **507**: 480–483.

Giesecke, R., H. E. González, and U. Bathmann. 2009. The role of the chaetognath Sagitta gazellae in the vertical carbon flux of the Southern Ocean. Polar Biol. **33**: 293–304.

del Giorgio, P. A., and J. J. Cole. 2000. Bacterial energetics and growth efficiency, p. 289–325. *In* D.L. Kirchman [ed.], Microbial ecology of the oceans. Wiley.

Gleiber, M. R., D. K. Steinberg, and H. W. Ducklow. 2012. Time series of vertical flux of zooplankton fecal pellets on the continental shelf of the western Antarctic Peninsula. Mar. Ecol. Prog. Ser. **471**: 23–36.

Godlewska, M., and Z. Klusek. 1987. Vertical distribution and diurnal migrations of krill - Euphausia superba Dana - from hydroacoustical observations, SIBEX, December 1983/January 1984. Polar Biol. **8**: 17–22.

González, H. E. 1992. The distribution and abundance of krill faecal material and oval pellets in the Scotia and Weddell Seas (Antarctica) and their role in particle flux. Polar Biol. **12**: 81–91.

González, H. E., and V. Smetacek. 1994. The possible role of the cyclopoid copepod Oithona in retarding vertical flux of zooplankton faecal material. Mar. Ecol. Prog. Ser. **113**: 233–246.

Gordon, H. R., and W. R. McCluney. 1975. Estimation of the depth of sunlight penetration in the sea for remote sensing. Appl. Opt. **14**: 413.

Gorsky, G., M. D. Ohman, M. Picheral, S. Gasparini, L. Stemmann, J. B. Romagnan, A. Cawood, S. Pesant, C. García-Comas, and F. Prejger. 2010. Digital zooplankton image analysis using the ZooScan integrated system. J. Plankton Res. **32**: 285–303.

Gorsky, G., M. Picheral, and L. Stemmann. 2000. Use of the Underwater Video Profiler for the

Study of Aggregate Dynamics in the North Mediterranean. Estuar. Coast. Shelf Sci. **50**: 121–128.

Grossart, H. P., S. Hietanen, and H. Ploug. 2003. Microbial dynamics on diatom aggregates in Oresund, Denmark. Mar. Ecol. Prog. Ser. **249**: 69–78.

Grossart, H. P., K. W. Tang, T. Kiorboe, and H. Ploug. 2007. Comparison of cell-specific activity between free-living and attached bacteria using isolates and natural assemblages. FEMS Microbiol. Lett. **266**: 194–200.

Grossart, H., and H. Ploug. 2001. Microbial degradation of organic carbon and nitrogen on diatom aggregates. Limnol. Oceanogr. **46**: 267–277.

Grossart, H., and M. Simon. 1998. Bacterial colonization and microbial decomposition of limnetic oraganic aggregates (lake snow). Aquat. Microb. Ecol. **15**: 127–140.

Gruber, N., and J. L. Sarmiento. 2002. Large scale biochemical/physical interactions in elemental cycles, p. 337–399. *In* A.R. Robinson, J.J. McCarthy, and B.J. Rothschild [eds.], The Sea: biological-physical interactions in the oceans. John Wiley and Sons.

Guidi, L., S. Chaffron, L. Bittner, D. Eveillard, A. Larhlimi, S. Roux, Y. Darzi, S. Audic, L. Berline, J. Brum, L. P. Coelho, J. C. I. Espinoza, S. Malviya, S. Sunagawa, C. Dimier, S. Kandels-Lewis, M. Picheral, J. Poulain, S. Searson, T. O. Coordinators, L. Stemmann, F. Not, P. Hingamp, S. Speich, M. Follows, L. Karp-Boss, E. Boss, H. Ogata, S. Pesant, J. Weissenbach, P. Wincker, S. G. Acinas, P. Bork, C. de Vargas, D. Iudicone, M. B. Sullivan, J. Raes, E. Karsenti, C. Bowler, and G. Gorsky. 2016. Plankton networks driving carbon export in the oligotrophic ocean. Nature **532**: 465–470.

Guidi, L., G. A. Jackson, L. Stemmann, J. C. Miquel, M. Picheral, and G. Gorsky. 2008. Relationship between particle size distribution and flux in the mesopelagic zone. Deep. Res. Part I Oceanogr. Res. Pap. **55**: 1364–1374.

Guidi, L., L. Legendre, G. Reygondeau, J. Uitz, L. Stemmann, and S. A. Henson. 2015. A new look at ocean carbon remineralization for extimating deepwater sequestration. Global Biogeochem. Cycles **29**, doi:10.1002/2014GB005063

Guidi, L., L. Stemmann, G. A. Jackson, F. Ibanez, H. Claustre, L. Legendre, M. Picheral, and G. Gorsky. 2009. Effects of phytoplankton community on production, size, and export of large aggregates: A world-ocean analysis. Limnol. Oceanogr. **54**: 1951–1963.

Hamm, C., M. Reigstad, C. W. Riser, A. Mühlebach, and P. Wassmann. 2001. On the trophic fate of

Phaeocystis pouchetii. VII. Sterols and fatty acids reveal sedimentation of P. pouchetii-derived organic matter via krill fecal strings. Mar Ecol Prog Ser **209**: 55–69.

Hamner, W., P. Hamner, and B. Obst. 1989. Field observations on the ontogeny of schooling of Euphausia superba furciliae and its relationship to ice in Antarctic waters. Limnol. Oceanogr. **34**: 451–456.

Hansell, D. A., and H. W. Ducklow. 2003. Bacterioplankton distribution and production in the bathypelagic ocean: Directly coupled to particulate organic carbon export? Limnol. Oceanogr. **48**: 150–156.

Hansen, B., F. L. Fotel, N. J. Jensen, and S. D. Madsen. 1996. Bacteria associated with a marine planktonic copepod in culture. II. Degradation of fecal pellets produced on a diatom, a nanoflagellate or a dinoflagellate diet. J. Plankton Res. **18**: 275–288.

Hartman, S. E., Z.-P. Jiang, D. Turk, R. S. Lampitt, H. Frigstad, C. Ostle, and U. Schuster. 2015. Biogeochemical variations at the Porcupine Abyssal Plain sustained observatory in the northeast Atlantic Ocean, from weekly to inter-annual timescales. Biogeosciences **12**: 845–853.

Hartman, S. E., R. S. Lampitt, K. E. Larkin, M. Pagnani, J. Campbell, T. Gkritzalis, Z.-P. Jiang, C. A. Pebody, H. A. Ruhl, A. J. Gooday, B. J. Brett, D. S. M. Billett, P. Provost, R. McLachlan, J. D. Turton, and S. Lankester. 2012. The Porcupine Abyssal Plain fixed-point sustained observatory (PAP-SO): variations and trends from the Northeast Atlantic fixed-point time-series. ICES J. Mar. Sci. **69**: 776–783.

Hartman, S. E., K. E. Larkin, R. S. Lampitt, M. Lankhorst, and D. J. Hydes. 2010. Seasonal and inter-annual biogeochemical variations in the Porcupine Abyssal Plain 2003-2005 associated with winter mixing and surface circulation. Deep. Res. Part II Top. Stud. Oceanogr. **57**: 1303–1312.

Hebel, D. V., and D. M. Karl. 2001. Seasonal, interannual and decadal variations in particulate matter concentrations and composition in the subtropical North Pacific Ocean. Deep. Res. Part II Top. Stud. Oceanogr. **48**: 1669–1695.

Henderson, G. M., and O. Marchal. 2015. Recommendations for future measurement and modelling of particles in GEOTRACES and other ocean biogeochemistry programmes. Prog. Oceanogr. **133**: 73–78.

Henson, S. A., C. Beaulieu, and R. Lampitt. 2016. Observing climate change trends in ocean biogeochemistry: When and where. Glob. Chang. Biol. **22**: 1561–1571.

Henson, S. A., R. Sanders, and E. Madsen. 2012a. Global patterns in efficiency of particulate organic carbon export and transfer to the deep ocean. Global Biogeochem. Cycles **26**, doi:10.1029/2011GB004099

Henson, S. A., R. Sanders, E. Madsen, P. J. Morris, F. Le Moigne, and G. D. Quartly. 2011. A reduced estimate of the strength of the ocean's biological carbon pump. Geophys. Res. Lett. **38**: L04606.

Henson, S. A., A. Yool, and R. Sanders. 2015. Variability in efficiency of particulate organic carbon export: A model study. Global Biogeochem. Cycles **29**: 33–45.

Henson, S., R. Lampitt, and D. Johns. 2012b. Variability in phytoplankton community structure in response to the North Atlantic Oscillation and implications for organic carbon flux. Limnol. Oceanogr. **57**: 1591–1601.

Herndl, G. J., and T. Reinthaler. 2013. Microbial control of the dark end of the biological pump. Nat. Geosci. **6**: 718–724.

Hewitt, R. P., J. Watkins, M. Naganobu, V. Sushin, A. S. Brierley, D. Demer, S. Kasatkina, Y. Takao, C. Goss, A. Malyshko, M. Brandon, S. Kawaguchi, V. Siegel, P. Trathan, J. Emery, I. Everson, and D. Miller. 2004. Biomass of Antarctic krill in the Scotia Sea in January/February 2000 and its use in revising an estimate of precautionary yield. Deep Sea Res. Part II Top. Stud. Oceanogr. **51**: 1215–1236.

Hilton, J., J. P. Lishman, S. Mackness, and S. I. Heaney. 1986. An automated method for the analysis of "particulate" carbon and nitrogen in natural waters. Hydrobiologia **141**: 269–271.

Hofmann, E. E., and C. M. Lascara. 2000. Modeling the growth dynamics of Antarctic krill Euphausia superba. Mar. Ecol. Prog. Ser. **194**: 219–231.

Holeton, C. L., F. Nédélec, R. Sanders, L. Brown, C. M. Moore, D. P. Stevens, K. J. Heywood, P. J. Statham, and C. H. Lucas. 2005. Physiological state of phytoplankton communities in the Southwest Atlantic sector of the Southern Ocean, as measured by fast repetition rate fluorometry. Polar Biol. **29**: 44–52.

Honjo, S., R. Francois, S. Manganini, J. Dymond, and R. Collier. 2000. Particle fluxes to the interior of the Southern Ocean in the Western Pacific sector along 170°W. Deep. Res. Part II **47**: 3521–3548.

Honjo, S., S. J. Manganini, R. A. Krishfield, and R. Francois. 2008. Particulate organic carbon fluxes to the ocean interior and factors controlling the biological pump : A synthesis of global

sediment trap programs since 1983. Prog. Oceanogr. **76**: 217–285.

Huskin, I. 2004. Particle flux in the Subtropical Atlantic near the Azores: influence of mesozooplankton. J. Plankton Res. **26**: 403–415.

Ikeda, T. 1985. Metabolic rates of epipelagic marine zooplankton as a function of body mass and temperature. Mar. Biol. **85**: 1–11.

Ikeda, T., Y. Kanno, K. Ozaki, and A. Shinada. 2001. Metabolic rates of epipelagic marine copepods as a function of body mass and temperature. Mar. Biol. **139**: 1020–1020.

Ito, T., and M. J. Follows. 2005. Preformed phosphate, soft tissue pump and atmospheric CO2. J. Mar. Res. **63**: 813–839.

Iversen, M. H., N. Nowald, H. Ploug, G. A. Jackson, and G. Fischer. 2010. High resolution profiles of vertical particulate organic matter export off Cape Blanc, Mauritania: Degradation processes and ballasting effects. Deep Sea Res. Part I Oceanogr. Res. Pap. **57**: 771–784.

Iversen, M. H., and H. Ploug. 2010. Ballast minerals and the sinking carbon flux in the ocean: carbon-specific respiration rates and sinking velocity of marine snow aggregates. Biogeosciences **7**: 2613–2624.

Iversen, M. H., and H. Ploug. 2013. Temperature effects on carbon-specific respiration rate and sinking velocity of diatom aggregates - potential implications for deep ocean export processes. Biogeosciences **10**: 4073–4085.

Iversen, M. H., and L. Poulsen. 2007. Coprorhexy, coprophagy, and coprochaly in the copepods Calanus helgolandicus, Pseudocalanus elongatus, and Oithona similis. Mar. Ecol. Prog. Ser. **350**: 79–89.

Jing, H., L. Shek, W. Yung, X. Jin, and H. Liu. 2012. Dynamics of bacterial community composition during degradation of copepod fecal pellets. J. Plankton Res. **34**: 700–710.

Johnson, R., P. G. Strutton, S. W. Wright, A. McMinn, and K. M. Meiners. 2013. Three improved satellite chlorophyll algorithms for the Southern Ocean. J. Geophys. Res. Ocean. **118**: 3694–3703.

Jónasdóttir, S. H., A. W. Visser, K. Richardson, and M. R. Heath. 2015. Seasonal copepod lipid pump promotes carbon sequestration in the deep North Atlantic. Proc. Natl. Acad. Sci. U. S. A. **112**: 12122–6.

Jouandet, M. P., S. Blain, N. Metzl, C. Brunet, T. W. Trull, and I. Obernosterer. 2008. A seasonal

carbon budget for a naturally iron-fertilized bloom over the Kerguelen Plateau in the Southern Ocean. Deep Sea Res. Part II Top. Stud. Oceanogr. **55**: 856–867.

Jouandet, M. P., G. A. Jackson, F. Carlotti, M. Picheral, L. Stemmann, and S. Blain. 2014. Rapid formation of large aggregates during the spring bloom of Kerguelen Island: Observations and model comparisons. Biogeosciences **11**: 4393–4406.

Jumars, P. A., D. L. Penry, J. A. Baross, M. J. Perry, and B. W. Frost. 1989. Closing the microbial loop: dissolved carbon pathways to heterotrophic bacteria from incomplete ingestion, digestion and absorbtion in animals. Deep Sea Res. Part I Oceanogr. Res. Pap. **36**: 483–495.

Karl, D. M., G. A. Knauer, and J. H. Martin. 1988. Downward flux of particulate organic matter in the ocean: a particle decomposition paradox. Nature **332**: 438–441.

Kemp, A. E. S., J. Pike, R. B. Pearce, and C. B. Lange. 2000. The “Fall dump” - a new perspective on the role of a “shade flora” in the annual cycle of diatom production and export flux. Deep Sea Res. Part II Top. Stud. Oceanogr. **47**: 2129–2154.

Kiørboe, T. 2003. Marine snow microbial communities: scaling of abundances with aggregate size. Aquat. Microb. Ecol. **33**: 67–75.

Kiørboe, T., H.-P. Grossart, H. Ploug, and K. Tang. 2002. Mechanisms and rates of colonisation of sinking aggregates. Appl. Environ. Microbiol. **68**: 3996–4006.

Kiørboe, T., and G. A. Jackson. 2001. Marine snow, organic solute plumes, and optimal chemosensory behavior of bacteria. Limnol. Oceanogr. **46**: 1309–1318.

Kiørboe, T., and A. W. Visser. 1999. Predator and prey perception in copepods due to hydromechanical signals. Mar. Ecol. Prog. Ser. **179**: 81–95.

Klaas, C., and D. E. Archer. 2002. Association of sinking organic matter with various types of mineral ballast in the deep sea: Implications for the rain ratio. Global Biogeochem. Cycles **16**, doi:10.1029/2001GB001765

Knisely, K., and W. Geller. 1986. Selective feeding of four zooplankton species on natural lake phytoplankton. Oecologia **69**: 86–94.

Kobari, T., D. K. Steinberg, A. Ueda, A. Tsuda, M. W. Silver, and M. Kitamura. 2008. Impacts of ontogenetically migrating copepods on downward carbon flux in the western subarctic Pacific Ocean. Deep Sea Res. Part II Top. Stud. Oceanogr. **55**: 1648–1660.

Korb, R. E., M. J. Whitehouse, A. Atkinson, and S. Thorpe. 2008. Magnitude and maintenance of

the phytoplankton bloom at South Georgia: a naturally iron-replete environment. Mar. Ecol. Prog. Ser. **368**: 75–91.

Korb, R. E., M. J. Whitehouse, M. Gordon, P. Ward, and A. J. Poulton. 2010. Summer microplankton community structure across the Scotia Sea: implications for biological carbon export. Biogeosciences **7**: 343–356.

Korb, R. E., M. J. Whitehouse, P. Ward, M. Gordon, H. J. Venables, and A. J. Poulton. 2012. Regional and seasonal differences in microplankton biomass, productivity, and structure across the Scotia Sea: Implications for the export of biogenic carbon. Deep Sea Res. Part II Top. Stud. Oceanogr. **59–60**: 67–77.

Köster, M., G. A. Paffenhöfer, R. Schluter, and A. Meuche. 2014. Time-series observations of prokaryotic colonization of zooplankton fecal pellets. J. Plankton Res. **36**: 1461–1475.

Kwon, E. Y., and F. Primeau. 2008. Optimization and sensitivity of a global biogeochemistry ocean model using combined in situ DIC, alkalinity, and phosphate data. J. Geophys. Res. Ocean. **113**: 1–23.

Kwon, E. Y., F. Primeau, and J. L. Sarmiento. 2009. The impact of remineralization depth on the air–sea carbon balance. Nat. Geosci. **2**: 630–635.

De La Rocha, C. L., and U. Passow. 2007. Factors influencing the sinking of POC and the efficiency of the biological carbon pump. Deep Sea Res. Part II Top. Stud. Oceanogr. **54**: 639–658.

Lam, P. J., and J. K. B. Bishop. 2007. High biomass, low export regimes in the Southern Ocean. Deep Sea Res. Part II Top. Stud. Oceanogr. **54**: 601–638.

Lampitt, R. S., B. Boorman, L. Brown, M. Lucas, I. Salter, R. Sanders, K. Saw, S. Seeyave, S. J. Thomalla, and R. Turnewitsch. 2008. Particle export from the euphotic zone: Estimates using a novel drifting sediment trap, 234Th and new production. Deep Sea Res. Part I Oceanogr. Res. Pap. **55**: 1484–1502.

Lampitt, R. S., T. Noji, and B. Von Bodungen. 1990. What happens to zooplankton faecal pellets? Implications for material flux. Mar. Biol. **104**: 15–23.

Lampitt, R. S., I. Salter, B. A. de Cuevas, S. Hartman, K. E. Larkin, and C. A. Pebody. 2010. Long-term variability of downward particle flux in the deep northeast Atlantic: Causes and trends. Deep. Res. Part II Top. Stud. Oceanogr. **57**: 1346–1361.

Lampitt, R. S., K. F. Wishner, C. M. Turley, and M. V. Angel. 1993. Marine snow studies in the

Northeast Atlantic Ocean: distribution, composition and role as a food source for migrating plankton. Mar. Biol. **116**: 689–702.

Lancraft, T. M., T. L. Hopkins, J. J. Torres, and J. Donnelly. 1991. Oceanic micronektonic/macrozooplanktonic community structure and feeding in ice covered Antarctic waters during the winter (AMERIEZ 1988). Polar Biol. **11**: 157–167.

Lasbleiz, M., K. Leblanc, L. K. Armand, U. Christaki, C. Georges, I. Obernosterer, and B. Quéguiner. 2016. Composition of diatom communities and their contribution to plankton biomass in the naturally iron fertilized region of Kerguelen in the Southern Ocean. FEMS Microbiol. Ecol. **92**, doi:http://dx.doi.org/10.1093/femsec/fiw171

Laufkötter, C., M. Vogt, N. Gruber, L. Bopp, J. Dunne, J. Hauck, J. John, I. Lima, R. Seferian, and C. Volker. 2016. Projected decreases in future marine export production : the role of the carbon flux through the upper ocean ecosystem. Biogeosci. Discuss. **12**: 4023–4047.

Laurenceau-Cornec, E. C., T. W. Trull, D. M. Davies, S. G. Bray, J. Doran, F. Planchon, F. Carlotti, M. P. Jouandet, A. J. Cavagna, A. M. Waite, and S. Blain. 2015a. The relative importance of phytoplankton aggregates and zooplankton fecal pellets to carbon export: insights from free-drifting sediment trap deployments in naturally iron-fertilised waters near the Kerguelen Plateau. Biogeosciences **12**: 1007–1027.

Laurenceau-Cornec, E. C., T. W. Trull, D. M. Davies, C. L. De La Rocha, and S. Blain. 2015b. Phytoplankton morphology controls on marine snow sinking velocity. Mar. Ecol. Prog. Ser. **520**: 35–56.

Laws, E. A., P. G. Falkowski, W. O. Smith, D. Hugh, and J. J. Mccarthy. 2000. Temperature effects on export production in the open ocean. Global Biogeochem. Cycles **14**: 1231–1246.

Lehette, P., and S. Hernández-León. 2009. Zooplankton biomass estimation from digitized images: a comparison between subtropical and Antarctic organisms. Limnol. Oceanogr. Methods **7**: 304–308.

Logan, B. E., and D. B. Wilkinson. 1990. Fractal geometry of marine snow and other biological aggregates. Limnol. Ocean. **35**: 130–136.

Longhurst, A. R., and G. W. Harrison. 1988. Vertical nitrogen flux from the oceanic photic zone by diel migrant zooplankton and nekton. Deep Sea Res. **35**: 881–889.

Lutz, M., R. Dunbar, and K. Caldeira. 2002. Regional variability in the vertical flux of particulate organic carbon in the ocean interior. Global Biogeochem. Cycles **16**: 11–18.

Lutz, M. J., K. Caldeira, R. B. Dunbar, and M. J. Behrenfeld. 2007. Seasonal rhythms of net primary production and particulate organic carbon flux to depth describe the efficiency of biological pump in the global ocean. J. Geophys. Res. **112**: C10011.

MacCready, P., and P. Quay. 2001. Biological export flux in the Southern Ocean estimated from a climatological nitrate budget. Deep. Res. Part II Top. Stud. Oceanogr. **48**: 4299–4322.

Maiti, K., S. Bosu, E. J. D. Sa, P. L. Adhikari, M. Sutor, and K. Longnecker. 2016. Export fluxes in northern Gulf of Mexico - Comparative evaluation of direct , indirect and satellite-based estimates. Mar. Chem. **184**: 60–77.

Manno, C., G. Stowasser, P. Enderlein, S. Fielding, and G. A. Tarling. 2015. The contribution of zooplankton faecal pellets to deep-carbon transport in the Scotia Sea (Southern Ocean). Biogeosciences **12**: 1955–1965.

Manno, C., V. Tirelli, A. Accornero, and S. Fonda Umani. 2010. Importance of the contribution of limacina helicina faecal pellets to the carbon pump in terra nova bay (Antarctica). J. Plankton Res. **32**: 145–152.

Marinov, I., A. Gnanadesikan, J. L. Sarmiento, J. R. Toggweiler, M. Follows, and B. K. Mignone. 2008. Impact of oceanic circulation on biological carbon storage in the ocean and atmospheric pCO2. Global Biogeochem. Cycles **22**: 1–15.

Marinov, I., A. Gnanadesikan, J. R. Toggweiler, and J. L. Sarmiento. 2006. The Southern Ocean biogeochemical divide. Nature **441**: 964–967.

Marr, J. W. S. 1962. The natural history and geography of the Antarctic krill (Euphausia superba Dana). Discov. Reports **32**: 33–464.

Marra, J., C. Ho, and C. C. Trees. 2003. An alternative algorithm for the calculation of primary productivity from remote sensing data. LDEO Tech. Rep. 2003-1

Marsay, C. M., R. J. Sanders, S. A. Henson, K. Pabortsava, E. P. Achterberg, and R. S. Lampitt. 2015. Attenuation of sinking particulate organic carbon flux through the mesopelagic ocean. Proc. Natl. Acad. Sci. 201415311.

Martin, J. H., G. A. Knauer, D. M. Karl, and W. W. Broenkow. 1987. VERTEX: carbon cycling in the northeast Pacific. Deep Sea Res. Part I Oceanogr. Res. Pap. **34**: 267–285.

Martin, P., R. S. Lampitt, M. Jane Perry, R. Sanders, C. Lee, and E. D'Asaro. 2011. Export and mesopelagic particle flux during a North Atlantic spring diatom bloom. Deep. Res. Part I

Oceanogr. Res. Pap. **58**: 338–349.

Martinez-Garcia, S. 2017. Microbial respiration in the mesopelagic zone at Station ALOHA. Limnol. Ocean. **62**: 320–333.

Mayor, D. J., R. Sanders, S. L. C. Giering, and T. R. Anderson. 2014. Microbial gardening in the ocean's twilight zone: Detritivorous metazoans benefit from fragmenting, rather than ingesting, sinking detritus. BioEssays **36**: 1132–7.

McDonnell, A. M. P., P. W. Boyd, and K. O. Buesseler. 2015. Effects of sinking velocities and microbial respiration rates on the attenuation of particulate carbon fluxes through the mesopelagic zone. Global Biogeochem. Cycles **29**: 175–193.

McDonnell, A. M. P., and K. O. Buesseler. 2010. Variability in the average sinking velocity of marine particles. Limnol. Oceanogr. **55**: 2085–2096.

Mcgill, P. R., R. G. Henthorn, L. E. Bird, C. L. Huffard, D. V. Klimov, and K. L. Smith. 2016. Sedimentation event sensor: New ocean instrument for in situ imaging and fluorometry of sinking particulate matter. Limnol. Oceanogr. Methods **14**: 853–863.

Menden-Deuer, S., and E. J. Lessard. 2000. Carbon to volume relationships for dinoflagellates, diatoms, and other protist plankton. Limnol. Oceanogr. **45**: 569–579.

Miklasz, K. A., and M. W. Denny. 2010. Diatom sinking speeds: Improved predictions and insight from a modified Stokes' law. Limnol. Oceanogr. **55**: 2513–2525.

Miquel, J.-C., B. Gasser, J. Martín, C. Marec, M. Babin, L. Fortier, and A. Forest. 2015. Downward particle flux and carbon export in the Beaufort Sea, Arctic Ocean; the role of zooplankton. Biogeosciences **12**: 5103–5117.

Møller, E., P. Thor, and T. Nielsen. 2003. Production of DOC by Calanus finmarchicus, C. glacialis and C. hyperboreus through sloppy feeding and leakage from fecal pellets. Mar. Ecol. Prog. Ser. **262**: 185–191.

Monterey, G. I., and S. Levitus. 1997. Seasonal Variability of Mixed Layer Depth for the World Ocean. U.S. Gov. Printing Office.

Murphy, E. J., J. L. Watkins, P. N. Trathan, K. Reid, M. P. Meredith, S. E. Thorpe, N. M. Johnston, A. Clarke, G. A. Tarling, M. A. Collins, J. Forcada, R. S. Shreeve, A. Atkinson, R. Korb, M. J. Whitehouse, P. Ward, P. G. Rodhouse, P. Enderlein, A. G. Hirst, A. R. Martin, S. L. Hill, I. J. Staniland, D. W. Pond, D. R. Briggs, N. J. Cunningham, and A. H. Fleming. 2007. Spatial and

temporal operation of the Scotia Sea ecosystem: a review of large-scale links in a krill centred food web. Philos. Trans. R. Soc. B Biol. Sci. **362**: 113–148.

Nagata, T., C. Tamburini, J. Arístegui, F. Baltar, A. B. Bochdansky, S. Fonda-Umani, H. Fukuda, A. Gogou, D. A. Hansell, R. L. Hansman, G. J. Herndl, C. Panagiotopoulos, T. Reinthaler, R. Sohrin, P. Verdugo, N. Yamada, Y. Yamashita, T. Yokokawa, and D. H. Bartlett. 2010. Emerging concepts on microbial processes in the bathypelagic ocean - Ecology, biogeochemistry, and genomics. Deep. Res. Part II Top. Stud. Oceanogr. **57**: 1519–1536.

Najjar, R. G., and J. C. Orr. 1998. Design of OCMIP-2 simulations of chlorofluorocarbons, the solubility pump and common biogeochemistry, pg. 19.

Najjar, R. G., J. L. Sarmiento, and J. R. Toggweiler. 1992. Downward transport and fate of organic matter in the ocean: simulations with a general circulation model. Global Biogeochem. Cycles **6**: 45–76.

Nielsdóttir, M. C., T. S. Bibby, C. M. Moore, D. J. Hinz, R. Sanders, M. Whitehouse, R. Korb, and E. P. Achterberg. 2012. Seasonal and spatial dynamics of iron availability in the Scotia Sea. Mar. Chem. **130–131**: 62–72.

Nordhausen, W., and M. E. Huntley. 1990. RACER : Carbon egestion rates of Euphausia superba. Antarct. J. United States **25**: 161–162.

Orsi, H., T. Whitworth III, and W. D. Nowlin Jr. 1995. On the meridional extent and fronts of the Antarctic Circumpolar Current. Deep Sea Res. Part I Oceanogr. Res. Pap. **42**: 641–673.

Ortega-Retuerta, E., C. G. Fichot, K. R. Arrigo, G. L. Van Dijken, and F. Joux. 2014. Response of marine bacterioplankton to a massive under-ice phytoplankton bloom in the Chukchi Sea (Western Arctic Ocean). Deep Sea Res. Part II Top. Stud. Oceanogr. **105**: 74–84.

Pakhomov, E. A., R. Perissinotto, P. W. Froneman, and D. G. M. Miller. 1997. Energetics and feeding dynamics of Euphausia superba in the South Georgia region during the summer of 1994. J. Plankton Res. **19**: 399–423.

Parekh, P., S. Dutkiewicz, M. J. Follows, and T. Ito. 2006. Atmospheric carbon dioxide in a less dusty world. Geophys. Res. Lett. **33**: L03610.

Park, M. G., S. R. Yang, S. H. Kang, K. H. Chung, and J. H. Shim. 1999. Phytoplankton biomass and primary production in the marginal ice zone of the northwestern Weddell Sea during austral summer. Polar Biol. **21**: 251–261.

Passow, U., R. F. Shipe, A. Murray, D. K. Pak, M. A. Brzezinski, and A. L. Alldredge. 2001. The origin of transparent exopolymer particles (TEP) and their role in the sedimentation of particulate matter. Cont. Shelf Res. **21**: 327–346.

Picheral, M., L. Guidi, L. Stemmann, D. M. Karl, G. Iddaoud, and G. Gorsky. 2010. The Underwater Vision Profiler 5 : An advanced instrument for high spatial resolution studies of particle size spectra and zooplankton. Limnol. Ocean. Methods **8**: 462–473.

Ploug, H. 2001. Small-scale oxygen fluxes and remineralization in sinking aggregates. Limnol. Oceanogr. **46**: 1624–1631.

Ploug, H., and H.-P. Grossart. 2000. Bacterial growth and grazing on diatom aggregates: Respiratory carbon turnover as a function of aggregate size and sinking velocity. Limnol. Oceanogr. **45**: 1467–1475.

Ploug, H., H.-P. Grossart, F. Azam, and B. B. Jorgensen. 1999. Photosynthesis, respiration, and carbon turnover in sinking marine snow from surface waters of Southern California Bight: implications for the carbon cycle in the ocean. Mar. Ecol. Prog. Ser. **179**: 1–11.

Ploug, H., M. H. Iversen, and G. Fischer. 2008a. Ballast, sinking velocity, and apparent diffusivity within marine snow and zooplankton fecal pellets: Implications for substrate turnover by attached bacteria. Limnol. Oceanogr. **53**: 1878–1886.

Ploug, H., M. H. Iversen, M. Koski, and E. T. Buitenhuis. 2008b. Production, oxygen respiration rates, and sinking velocity of copepod fecal pellets: Direct measurements of ballasting by opal and calcite. Limnol. Oceanogr. **53**: 469–476.

Ploug, H., and B. B. Jorgensen. 1999. A net-jet flow system for mass transfer and microsensor studies of sinking aggregates. Mar. Ecol. Prog. Ser. **176**: 279–290.

Ploug, H., M. Kühl, B. Buchholz-Cleven, and B. B. Jergensen. 1997. Anoxic aggregates - an ephemeral phenomenon in the pelagic environment? Aquat. Microb. Ecol. **13**: 285–294.

Ploug, H., A. Terbruggen, A. Kaufmann, D. Wolf-gladrow, and U. Passow. 2010. A novel method to measure particle sinking velocity in vitro, and its comparison to three other in vitro methods. Limnol. Ocean. Methods **8**: 386–393.

Pollard, R. T., I. Salter, R. J. Sanders, M. I. Lucas, C. M. Moore, R. A. Mills, P. J. Statham, J. T. Allen, A. R. Baker, D. C. E. Bakker, M. a Charette, S. Fielding, G. R. Fones, M. French, A. E. Hickman, R. J. Holland, J. A. Hughes, T. D. Jickells, R. S. Lampitt, P. J. Morris, F. H. Nédélec, M. Nielsdóttir, H. Planquette, E. E. Popova, A. J. Poulton, J. F. Read, S. Seeyave, T. Smith, M.

Stinchcombe, S. Taylor, S. Thomalla, H. J. Venables, R. Williamson, and M. V Zubkov. 2009. Southern Ocean deep-water carbon export enhanced by natural iron fertilization. Nature **457**: 577–80.

Pomeroy, L. R., and W. J. Wiebe. 2001. Temperature and substrates as interactive limiting factors for marine heterotrophic bacteria. Aquat. Microb. Ecol. **23**: 187–204.

Poulsen, L., and M. H. Iversen. 2008. Degradation of copepod fecal pellets: key role of protozooplankton. Mar. Ecol. Prog. Ser. **367**: 1–13.

Poulsen, L., and T. Kiørboe. 2005. Coprophagy and coprorhexy in the copepods Acartia tonsa and Temora longicornis: clearance rates and feeding behaviour. Mar. Ecol. Prog. Ser. **299**: 217–227.

Poulsen, L., M. Moldrup, T. Berge, and P. Hansen. 2011. Feeding on copepod fecal pellets: a new trophic role of dinoflagellates as detritivores. Mar. Ecol. Prog. Ser. **441**: 65–78.

Prairie, J., K. Ziervogel, C. Arnosti, R. Camassa, C. Falcon, S. Khatri, R. McLaughlin, B. White, and S. Yu. 2013. Delayed settling of marine snow at sharp density transitions driven by fluid entrainment and diffusion-limited retention. Mar. Ecol. Prog. Ser. **487**: 185–200.

Primeau, F. W., M. Holzer, and T. DeVries. 2013. Southern Ocean nutrient trapping and the efficiency of the biological pump. J. Geophys. Res. **118**: 2547–2564.

Le Quéré, C., E. T. Buitenhuis, R. Moriarty, S. Alvain, O. Aumont, L. Bopp, S. Chollet, C. Enright, D. J. Franklin, R. J. Geider, S. P. Harrison, A. Hirst, S. Larsen, L. Legendre, T. Platt, I. C. Prentice, R. B. Rivkin, S. Sathyendranath, N. Stephens, M. Vogt, S. Sailley, and S. M. Vallina. 2016. Role of zooplankton dynamics for Southern Ocean phytoplankton biomass and global biogeochemical cycles. Biogeosciences **13**: 4111–4133.

Regaudie-De-Gioux, A., and C. M. Duarte. 2012. Temperature dependence of planktonic metabolism in the ocean. Global Biogeochem. Cycles **26**: 1–10.

Reigstad, M., C. W. Riser, and C. Svensen. 2005. Fate of copepod faecal pellets and the role of Oithona spp. Mar. Ecol. Prog. Ser. **304**: 265–270.

Reinthaler, T., H. Van Aken, C. Veth, J. Arı, C. Robinson, P. J. B. Williams, P. Lebaron, and G. J. Herndl. 2006. Prokaryotic respiration and production in the meso- and bathypelagic realm of the eastern and western North Atlantic basin. Limnol. Ocean. **51**: 1262–1273.

Rembauville, M., S. Blain, L. Armand, B. Quéguiner, and I. Salter. 2015a. Export fluxes in a

naturally iron-fertilized area of the Southern Ocean – Part 2: Importance of diatom resting spores and faecal pellets for export. Biogeosciences **12**: 3171–3195.

Rembauville, M., C. Manno, G. A. Tarling, S. Blain, and I. Salter. 2016. Strong contribution of diatom resting spores to deep-sea carbon transfer in naturally iron-fertilized waters downstream of South Georgia. Deep. Res. Part I **115**: 22–35.

Rembauville, M., I. Salter, N. Leblond, A. Gueneugues, and S. Blain. 2015b. Export fluxes in a naturally iron-fertilized area of the Southern Ocean – Part 1: Seasonal dynamics of particulate organic carbon export from a moored sediment trap. Biogeosciences **12**: 3153–3170.

Revsbech, N. P. 1989. An oxygen microsensor with a guard cathode. Limnol. Oceanogr. **34**: 474–478.

Ridgwell, A., J. C. Hargreaves, N. Edwards, J. D. Annan, T. M. Lenton, R. Marsh, A. Yool, and A. Watson. 2007. Marine geochemical data assimilation in an efficient Earth System Model of global biogeochemical cycling. Biogeosciences **4**: 87–104.

Riley, J. S., R. Sanders, C. Marsay, F. Le Moigne, E. P. Achterberg, and A. J. Poulton. 2012. The relative contribution of fast and slow sinking particles to ocean carbon export. Global Biogeochem. Cycles **26**, doi:10.1029/2011GB004085

Riser, C. W., P. Wassmann, K. Olli, and E. Arashkevich. 2001. Production, retention and export of zooplankton faecal pellets on and off the Iberian shelf, north-west Spain. Prog. Oceanogr. **51**: 423–441.

Robinson, C., D. K. Steinberg, T. R. Anderson, J. Arístegui, C. A. Carlson, J. R. Frost, J. F. Ghiglione, S. Hernández-León, G. A. Jackson, R. Koppelmann, B. Quéguiner, O. Ragueneau, F. Rassoulzadegan, B. H. Robison, C. Tamburini, T. Tanaka, K. F. Wishner, and J. Zhang. 2010. Mesopelagic zone ecology and biogeochemistry - A synthesis. Deep. Res. Part II Top. Stud. Oceanogr. **57**: 1504–1518.

Roca-Marti, M., V. Puigcorbé, M. H. Iversen, M. Rutgers van der Loeff, C. Klaas, W. Cheah, A. Bracher, and P. Masqué. 2015. High particulate organic carbon export during the decline of a vast diatom bloom in the Atlantic sector of the Southern Ocean. Deep Sea Res. Part II Top. Stud. Oceanogr. 1–14.

Roe, H. S. J., and D. M. Shale. 1979. A new multiple rectangular midwater trawl (RMT 1+8M) and some modifications to the institute of oceanographic sciences' RMT 1+8. Mar. Biol. **50**: 283–

288.

Roullier, F., L. Berline, L. Guidi, X. D. De Madron, M. Picheral, A. Sciandra, and S. Pesant. 2014. Particle size distribution and estimated carbon flux across the Arabian Sea oxygen minimum zone. Biogeosciences **11**: 4541–4557.

Russell, N. J. 1990. Cold adaption of microoganisms. Philos. Trans. R. Soc. B Biol. Sci. **326**: 595–611.

Saborowski, R., S. Bröhl, G. A. Tarling, and F. Buchholz. 2002. Metabolic properties of Northern krill, Meganyctiphanes norvegica, from different climatic zones. I. Respiration and excretion. Mar. Biol. **140**: 547–556.

Sampei, M., H. Sasaki, H. Hattori, M. Fukuchi, and B. T. Hargrave. 2004. Fate of sinking particles, especially fecal pellets, within the epipelagic zone in the North Water (NOW) polynya of northern Baffin Bay. Mar. Ecol. Prog. Ser. **278**: 17–25.

Sarmiento, J. L., N. Gruber, M. A. Brzezinski, and J. P. Dunne. 2004. High-latitude controls of thermocline nutrients and low latitude biological productivity. Nature **427**: 56–60.

Sarmiento, J. L., R. D. Slater, M. J. R. Fasham, H. W. Ducklow, J. R. Toggweiler, and G. T. Evans. 1993. A seasonal three-dimensional ecosystem model of nitrogen cycling in the North Atlantic Euphotic Zone. Global Biogeochem. Cycles **7**: 417–450.

Savoye, N., T. W. Trull, S. H. M. Jacquet, J. Navez, and F. Dehairs. 2008. 234Th-based export fluxes during a natural iron fertilization experiment in the Southern Ocean (KEOPS). Deep. Res. Part II Top. Stud. Oceanogr. **55**: 841–855.

Schlitzer, R. 2002. Carbon export fluxes in the Southern Ocean: results from inverse modeling and comparison with satellite-based estimates. Deep Sea Res. Part II Top. Stud. Oceanogr. **49**: 1623–1644.

Schmidt, K., A. Atkinson, H. J. Venables, and D. W. Pond. 2012. Early spawning of Antarctic krill in the Scotia Sea is fuelled by “superfluous” feeding on non-ice associated phytoplankton blooms. Deep. Res. Part II Top. Stud. Oceanogr. **59**–**60**: 159–172.

Schmidt, K., C. Schlosser, A. Atkinson, S. Fielding, H. J. Venables, C. M. Waluda, and E. P. Achterberg. 2016. Zooplankton Gut Passage Mobilizes Lithogenic Iron for Ocean Productivity. Curr. Biol. **26**: 2667–2673.

Schnetzer, A., and D. K. Steinberg. 2002. Natural diets of vertically migrating zooplankton in the

Sargasso Sea. Mar. Biol. **141**: 89–99.

Shek, L., and H. Liu. 2010. Oxygen consumption rates of fecal pellets produced by three coastal copepod species fed with a diatom Thalassiosira pseudonana. Mar. Pollut. Bull. **60**: 1005–1009.

Silver, M. W., and A. L. Alldredge. 1981. Bathypelagic marine snow: deep sea algal and detrital community. J. Mar. Res. **39**: 501–530.

Simon, M., H. Grossart, B. Schweitzer, and H. Ploug. 2002. Microbial ecology of organic aggregaes in aquatic ecosystems. Aquat. Microb. Ecol. **28**: 175–211.

Smayda, T. J. 1970. The suspension and sinking of phytoplankton in the sea. Oceanogr. Mar. Biol. Annu. Rev. **8**: 353–414.

Smayda, T. J. 1971. Normal and accelerated sinking of phytoplankton in the sea. Mar. Geol. **11**: 105–122.

Smetacek, V., P. Assmy, and J. Henjes. 2004. The role of grazing in structuring Southern Ocean pelagic ecosystems and biogeochemical cycles. Antarct. Sci. **16**: 541–558.

Smetacek, V., C. Klaas, V. H. Strass, P. Assmy, M. Montresor, B. Cisewski, N. Savoye, A. Webb, F. d'Ovidio, J. M. Arrieta, U. Bathmann, R. Bellerby, G. M. Berg, P. Croot, S. Gonzalez, J. Henjes, G. J. Herndl, L. J. Hoffmann, H. Leach, M. Losch, M. M. Mills, C. Neill, I. Peeken, R. Röttgers, O. Sachs, E. Sauter, M. M. Schmidt, J. Schwarz, A. Terbrüggen, and D. Wolf-Gladrow. 2012. Deep carbon export from a Southern Ocean iron-fertilized diatom bloom. Nature **487**: 313–319.

Smetacek, V. S. 1985. Role of sinking in diatom life-history cycles: ecological, evolutionary and geological significance. Mar. Biol. **84**: 239–251.

Smith, D. D., M. Simon, A. L. Alldredge, and F. Azam. 1992. Intense hydrolytic enzyme activity on marine aggregates and implications for rapid particle dissolution. Nature **359**: 139–142.

Smith, W. O., and D. M. Nelson. 1985. Phytoplankton Bloom Produced by a receding ice edge in the Ross Sea: Spatial coherence with the density field. Science **227**: 163–166.

Stamieszkin, K., A. J. Pershing, N. R. Record, C. H. Pilskaln, H. G. Dam, and L. R. Feinberg. 2015. Size as the master trait in modeled copepod fecal pellet carbon flux. Limnol. Oceanogr. **60**: 2090–2107.

Steinberg, D. K., C. A. Carlson, N. R. Bates, S. A. Goldthwait, L. P. Madin, and A. F. Michaels. 2000.

Zooplankton vertical migration and the active transport of dissolved organic and inorganic carbon in the Sargasso Sea. Deep Sea Res. Part I Oceanogr. Res. Pap. **47**: 137–158.

Steinberg, D. K., B. A. S. Van Mooy, K. O. Buesseler, P. W. Boyd, and D. M. Karl. 2008. Bacterial vs. zooplankton control of sinking particle flux in the ocean's twilight zone. Limnol. Oceanogr. **53**: 1327–1338.

Stemmann, L., G. A. Jackson, and G. Gorsky. 2004. A vertical model of particle size distributions and fluxes in the midwater column that includes biological and physical processes — Part II : application to a three year survey in the NW Mediterranean Sea. Deep Sea Res. **51**: 885–908.

Stemmann, L., M. Picheral, and G. Gorsky. 2000. Diel variation in the vertical distribution of particulate matter (>0.15 mm) in the NW Mediterranean Sea investigated with the Underwater Video Profiler. Deep Sea Res. Part I Oceanogr. Res. Pap. **47**: 505–531.

Stroeve, J. C., S. Jenouvrier, G. G. Campbell, C. Barbraud, and K. Delord. 2016. Mapping and Assessing Variability in the Antarctic Marginal Ice Zone, the Pack Ice and Coastal Polynyas. Cryosph. Discuss. 1–40.

Suess, E. 1980. Particulate organic carbon flux in the oceans - surface productivity and oxygen utilization. Nature **288**: 260–263.

Suzuki, H., H. Sasaki, and M. Fukuchi. 2001. Short-term variability in the flux of rapidly sinking particles in the Antarctic marginal ice zone. Polar Biol. **24**: 697–705.

Suzuki, H., H. Sasaki, and M. Fukuchi. 2003. Loss processes of sinking fecal pellets of zooplankton in the mesopelagic layers of the Antarctic marginal ice zone. J. Oceanogr. **59**: 809–818.

Svensen, C., N. Morata, and M. Reigstad. 2014. Increased degradation of copepod faecal pellets by co-acting dinoflagellates and Centropages hamatus. Mar. Ecol. Prog. Ser. **516**: 61–70.

Svensen, C., and J. C. Nejstgaard. 2003. Is sedimentation of copepod faecal pellets determined by cyclopoids? Evidence from enclosed ecosystems. J. Plankton Res. **25**: 917–926.

Svensen, C., C. Wexels Riser, M. Reigstad, and L. Seuthe. 2012. Degradation of copepod faecal pellets in the upper layer: role of microbial community and Calanus finmarchicus. Mar. Ecol. Prog. Ser. **462**: 39–49.

Taki, K., T. Hayashi, and M. Naganobu. 2005. Characteristics of seasonal variation in diurnal vertical migration and aggregation of antarctic krill (Euphausia superba) in the Scotia Sea, using Japanese fishery data. CCAMLR Sci. **12**: 163–172.

Tamburini, C., M. Boutrif, M. Garel, R. R. Colwell, and J. W. Deming. 2013. Prokaryotic responses to hydrostatic pressure in the ocean - a review. Environ. Microbiol. **15**: 1262–1274.

Tamburini, C., J. Garcin, G. Grégori, K. Leblanc, P. Rimmelin, and D. L. Kirchman. 2006. Pressure effects on surface Mediterranean prokaryotes and biogenic silica dissolution during a diatom sinking experiment. Aquat. Microb. Ecol. **43**: 267–276.

Tamburini, C., M. Goutx, C. Guigue, M. Garel, D. Lefe, M. L. Peterson, R. Sempe, S. Wakeham, and C. Lee. 2009. Effects of hydrostatic pressure on microbial alteration of sinking fecal pellets. Deep Sea Res. Part II Top. Stud. Oceanogr. **56**: 1533–1546.

Tarling, G. A., and S. Fielding. 2016. Swarming and behaviour in Antarctic krill, p. 279–319. *In* V. Siegel [ed.], Biology and ecology of Antarctic krill. Springer International Publishing.

Tarling, G. A., and M. L. Johnson. 2001. Satiation gives krill that sinking feeling. Curr. Biol. **16**: 83–84.

Taucher, J., L. T. Bach, U. Riebesell, and A. Oschlies. 2014. The viscosity effect on marine particle flux: A climate relevant feedback mechanism. Global Biogeochem. Cycles **28**: 415–422.

Thiele, S., B. M. Fuchs, R. Amann, and M. H. Iversen. 2015. Colonization in the photic zone and subsequent changes during sinking determines bacterial community composition in marine snow. Appl. Environ. Microbiol. **81**: 1–34.

Thor, P., H. Dam, and D. Rogers. 2003. Fate of organic carbon released from decomposing copepod fecal pellets in relation to bacterial production and ectoenzymatic activity. Aquat. Microb. Ecol. **33**: 279–288.

Thornton, D. C. O. 2002. Diatom aggregation in the sea: mechanisms and ecological implications. Eur. J. Phycol. **37**: 149–161.

Thorpe, S. E., K. J. Heywood, M. A. Brandon, and D. P. Stevens. 2002. Variability of the southern Antarctic Circumpolar Current front north of South Georgia. J. Mar. Syst. **37**: 87–105.

Tiselius, P., and T. Kiørboe. 1998. Colonization of diatom aggregates by the dinoflagellate Noctiluca scintillans. Limnol. Ocean. **43**: 154–159.

Toggweiler, J. R. 1994. The Ocean's Overturning Circulation. Phys. Today **47**: 45–50.

Treguer, P., D. M. Nelson, A. J. Van Bennekom, D. J. Demaster, A. Leynaert, and B. Queguiner. 1995. The Silica Balance in the World Ocean : A Reestimate. Science (80-. ). **268**: 375–379.

Trull, T. W., S. G. Bray, K. O. Buesseler, C. H. Lamborg, S. Manganini, C. Moy, and J. Valdes. 2008. In situ measurement of mesopelagic particle sinking rates and the control of carbon transfer to the ocean interior during the Vertical Flux in the Global Ocean (VERTIGO) voyages in the North Pacific. Deep Sea Res. Part II Top. Stud. Oceanogr. **55**: 1684–1695.

Turley, C. M., K. Lochte, and R. S. Lampitt. 1995. Transformations of biogenic particles during sedimentation in the northeastern Atlantic. Philos. Trans. R. Soc. B Biol. Sci. **348**: 179–189.

Turley, C. M., and E. D. Stutt. 2000. Depth-related cell-specific bacterial leucine incorporation rates on particles and its biogeochemical significance in the Northwest Mediterranean. Limnol. Oceanogr. **45**: 419–425.

Turner, J. T. 2002. Zooplankton fecal pellets, marine snow and sinking phytoplankton blooms. Aquat. Microb. Ecol. **27**: 57–102.

Turner, J. T. 2015. Zooplankton fecal pellets, marine snow, phytodetritus and the ocean's biological pump. Prog. Oceanogr. **130**: 205–248.

Urban-Rich, J. 1999. Release of dissolved organic carbon from copepod fecal pellets in the Greenland Sea. J. Exp. Mar. Bio. Ecol. **232**: 107–124.

Urban-Rich, J. 2001. Seston effects on faecal pellet carbon concentrations from a mixed community of copepods in Balsfjord, Norway, and the Antarctic Polar Front. ICES J. Mar. Sci. **58**: 700–710.

Urban-Rich, J., D. A. Hansell, and M. R. Roman. 1998. Analysis of copepod fecal pellet carbon using a high temperature combustion method. Mar. Ecol. Prog. Ser. **171**: 199–208.

Urban-Rich, J., E. Nordby, and I. Andreassen. 1999. Contribution by mezooplankton focal pellets to the carbon flux on Nordvestkbanken, north Norwegian shelf in 1994. Sarsia **84**: 253–264.

Urrere, M. A., and G. A. Knauer. 1981. Zooplankton fecal pellet flaxes and vertical transport of participate organic material in the pelagic environment. J. Plankton Res. **3**: 369–387.

Vandromme, P., S. Lars, C. Garcìa-Comas, L. Berline, X. Sun, and G. Gorsky. 2012. Assessing biases in computing size spectra of automatically classified zooplankton from imaging systems: A case study with the ZooScan integrated system. Methods Oceanogr. **1–2**: 3–21.

Viitasalo, M., M. Rosenberg, A.-S. Heiskanen, and M. Koski. 1999. Sedimentation of copepod fecal material in the coastal northern Baltic Sea: Where did all the pellets go? Limnol. Ocean. **44**: 1388–1399.

Volk, T., and M. I. Hoffert. 1985. Ocean Carbon Pumps: Analysis of relative strengths and efficiencies in ocean driven atmospheric CO2 changes, p. 99–110. *In* E.T. Sundquist and W.S. Broecker [eds.], The carbon cycle and atmospheric CO2:Natural variations Archean to Present. American Geophysical Union.

Waples, J. T., C. Benitez-Nelson, N. Savoye, M. Rutgers van der Loeff, M. Baskaran, and Ö. Gustafsson. 2006. An introduction to the application and future use of 234Th in aquatic systems. Mar. Chem. **100**: 166–189.

Ward, P., A. Atkinson, and G. Tarling. 2012a. Mesozooplankton community structure and variability in the Scotia Sea: A seasonal comparison. Deep Sea Res. Part II Top. Stud. Oceanogr. **59–60**: 78–92.

Ward, P., A. Atkinson, H. J. Venables, G. A. Tarling, M. J. Whitehouse, S. Fielding, M. A. Collins, R. Korb, A. Black, G. Stowasser, K. Schmidt, S. E. Thorpe, and P. Enderlein. 2012b. Food web structure and bioregions in the Scotia Sea: A seasonal synthesis. Deep Sea Res. Part II Top. Stud. Oceanogr. **59–60**: 253–266.

Wassmann, P., J. Erik, and A. Tselepides. 2000. Vertical flux of faecal pellets and microplankton on the shelf of the oligotrophic Cretan Sea ( NE Mediterranean Sea ). Prog. Oceanogr. **46**: 241–258.

Wassmann, P., K. Olli, C. Wexels Riser, and C. Svensen. 2002. Ecosystem function, biodiversity and vertical flux regulation in the twilight zone, p. 279–287. *In* G. Wefer, F. Lamy, and F. Mantoura [eds.], Marine science frontiers for europe. Springer Verlag.

Wefer, G., G. Fischer, D. Fuetterer, and R. Gersonde. 1988. Seasonal particle flux in the Bransfield Strait, Antarctica. Deep Sea Res. **35**: 891–898.

Wexels Riser, C., M. Reigstad, P. Wassmann, E. Arashkevich, and S. Falk-Petersen. 2007. Export or retention? Copepod abundance, faecal pellet production and vertical flux in the marginal ice zone through snap shots from the northern Barents Sea. Polar Biol. **30**: 719–730.

Wilson, S. E., H. A. Ruhl, and K. L. Smith. 2013. Zooplankton fecal pellet flux in the abyssal northeast Pacific : A 15 year time-series study. Limnol. Oceanogr. **58**: 881–892.

Wilson, S. E., D. K. Steinberg, and K. O. Buesseler. 2008. Changes in fecal pellet characteristics with depth as indicators of zooplankton repackaging of particles in the mesopelagic zone of the subtropical and subarctic North Pacific Ocean. Deep Sea Res. Part II Top. Stud. Oceanogr. **55**: 1636–1647.

Yool, A., A. P. Martin, C. Ferna, and D. R. Clark. 2007. The significance of nitrification for oceanic new production. Nature **447**: 999–1002.

Yool, A., E. E. Popova, and T. R. Anderson. 2011. MEDUSA-1.0: A new intermediate complexity plankton ecosystem model for the global domain. Geosci. Model Dev. **4**: 381–417.

Yool, A., E. E. Popova, and T. R. Anderson. 2013. MEDUSA-2.0: An intermediate complexity biogeochemical model of the marine carbon cycle for climate change and ocean acidification studies. Geosci. Model Dev. **6**: 1767–1811.

Yoon, W. D., S. K. Kim, and K. N. Han. 2001. Morphology and sinking velocities of fecal pellets of copepod, molluscan, euphausiid, and salp taxa in the northeastern tropical Atlantic. Mar. Biol. **139**: 923–928.